UNIVERSIDADE DE LISBOA
FACULDADE DE CIÊNCIAS
DEPARTAMENTO DE GEOLOGIA

Identification and characterization of fluid escape structures (pockmarks) in the Estremadura Spur, based on single-channel seismic reflection record

Mestrado em Geologia
Especialização em Estratigrafia, Sedimentologia e Paleontologia

Débora Filipa Pascoal Duarte

Dissertação orientada por:
Professor Doutor Pedro António Gancedo Terrinha
Doutor Vitor Hugo da Silva Magalhães

2015

“Olhando o mar, sonho sem ter de quê.

Nada no mar, salvo o ser mar, se vê.

Mas de se nada ver quanto a alma sonha!”

Fernando Pessoa

ABSTRACT

Located on the West Iberian margin, between Cabo Carvoeiro and Cabo da Roca, the Estremadura Spur is a trapezoidal promontory elongated in an east-west direction, extending until the Tore seamount. In 2011, during the scientific cruise 64PE332 (PACEMAKER project; Kim & the shipboard scientific party, 2011) a seismic reflection SPARKER survey discovered a field with more than 70 pockmarks in the NW region of the Estremadura Spur outer shelf (in the Lourinhã Monocline). Pockmarks are the seabed culminations of fluid migration through the sedimentary column and their characteristic seabed morphologies correspond to cone-shaped circular or elliptical depressions. Pockmarks have proven to be important seabed features that provide information about fluid flow on continental margins, being used by the oil and gas industry as an exploration tool and as an indicator of hydrocarbon sources for prospecting. These pockmarks and the associated fluid escape process are the main objectives of this work that aims to contribute to the characterization of the structures and to the understanding to their structural and stratigraphic control. In pursuing such objectives the following methodological approaches were used: 1) Seismic processing and interpretation of the high resolution 2D single-channel SPARKER seismic dataset acquired during the PACEMAKER cruise. In addition, it was done the interpretation of 2D multi-channel seismic lines from TGS-NOPEC, which provides information about the deep structure of this area; and 2) Bathymetric and Backscatter interpretation. During the EMEPC/PEPC/LUSO/2015 multi-beam bathymetry that complemented the PACEMAKER bathymetric coverage was acquired and were realized two dives using EMEPC Remotely Operated Vehicle (ROV) Luso. These dives allowed the direct observation of the seafloor and the recollection of push-core samples.

The analysis of the PACEMAKER high-resolution seismic allowed the identification of six seismic units, disturbed by the migration and accumulation of fluids. There was concluded that the Estremadura Spur outer shelf has been affected by several episodes of fluid migration and fluid escape during the Pliocene-Quaternary that are expressed by a vast number of seabed and buried pockmarks. At present the pockmarks are mainly inactive, as the seabed pockmarks are recovered by recent sediments.

The NW region of the Estremadura Spur outer shelf has been affected by several episodes of fluid migration and fluid escape that are expressed by a vast number of seabed and buried pockmarks. It was concluded that the migration of fluids to the seabed occurred

over the Pliocene-Quaternary, as indicated by the buried pockmarks at different depths. At present the pockmarks are mainly inactive, as the seabed pockmarks are recovered by recent sediments.

The stacking of various pockmarks suggests a cyclical fluid flow activity that can passably be the result of the eustatic sea level variations and the subsequent changes of the hydrostatic pressure. An alternative hypothesis can be considered assuming the episodes of intense fluid flow as being associated with the local seismicity. Precipitation of methane-derived authigenic carbonates (MDAC) inside the migration conduits that originate pockmarks can force the deactivation of the fluid migration pathways and, consequently, the deactivation of the related pockmarks and creation of new migration pathways.

Keywords: Pockmarks, Fluid migration, Estremadura Spur, West Iberian Margin, high-resolution seismic, seismic interpretation.

RESUMO

O Esporão da Estremadura é um promontório localizado na Margem Oeste Ibérica, entre o Cabo Carvoeiro e o Cabo da Roca. Apresenta uma forma trapezoidal com uma área de cerca de 3583 km^2, e prolonga-se desde a margem até às montanhas submarinas de Tore. O Esporão da Estremadura separa a Planície Abissal Ibérica, a norte, da Planície Abissal do Tejo, a sul. No ano de 2011, durante uma campanha oceanográfica do projeto PACEMAKER identificou-se, através dos dados sísmicos de reflexão, um conjunto de pequenas depressões no fundo do mar (pelo menos 70), reconhecidas como pockmarks. Este campo de pockmarks localiza-se entre os 240 e 350 m, na região NW da plataforma externa do Esporão da Estremadura, conhecida como Monoclinal da Lourinhã. Estas estruturas apresentam diâmetros que variam entre alguns metros a mais de 400 m e até cerca de 4 m de profundidade.

Os pockmarks são estruturas formadas pela libertação rápida e abrupta de fluidos, que migram através da coluna sedimentar, no fundo do mar. Foram descritos pela primeira vez por King & McLean (1970) na plataforma continental ao largo da Nova Escócia, Canadá. Apresentam topografia negativa e uma morfologia muito caraterística, sob a forma de depressão cónica circular ou elíptica, com flancos íngremes e fundo relativamente plano. Os pockmarks ocorrem em sedimentos finos e permeáveis, individualmente ou em grandes *clusters*, em variados ambientes geológicos como as plataformas continentais, os taludes continentais e nos fundos dos oceanos profundos. Encontram-se frequentemente associados a depósitos sedimentares com hidratos de gás nas margens continentais. A sua distribuição não ocorre de forma aleatória, estando frequentemente relacionados a estruturas da sub-superficie marinha, como falhas e zonas de maior permeabilidade, que servem de condutas para a migração de fluídos para a superfície. O estudo dos pockmarks é importante uma vez que estão muitas vezes relacionados com sistemas ativos de migração de hidrocarbonetos e portanto são estruturas de interesse para a indústria petrolífera. São também importantes devido ao perigo associado ao escape de gás do fundo do mar em zonas de exploração ou de transporte de petróleo e/ou gás.

A Margem Oeste Ibérica começou a desenvolver-se durante a abertura do Oceano Atlântico Norte. Este processo iniciou-se no Triásico Superior até ao momento de rutura continental entre as margens da Ibéria e da Terra Nova, no Cretácico Inferior. Existem na

margem, no *offshore* e também no *onshore*, diversas bacias sedimentares relacionadas com a abertura do Atlântico, como a Bacia Lusitânica. No Cenozoico a margem sofre uma fase de inversão tectónica generalizada, relacionada com as fases Pirenaica e Bética da Orogenia Alpina, o que levou ao soerguimento de algumas regiões da margem continental, como por exemplo o Esporão da Estremadura. O auge da deformação ocorreu no Miocénico, possivelmente durante o Tortoniano, com compressão máxima NW-SE.
Os pockmarks identificados no Esporão da Estremadura são a primeira evidência de processos de escape de fluidos identificados na Margem Oeste Ibérica e o presente trabalho é o primeiro estudo realizado sobre estas estruturas. As ocorrências escape de fluidas conhecidas, mais próximas da margem e portanto do Esporão da Estremadura, são a Ria de Vigo, o Estuário de Aveiro e o Golfo de Cádiz.

A principal motivação deste trabalho é o estudo das estruturas (pockmarks) e dos processos de escape de fluídos que ocorrem no fundo do mar do Esporão da Estremadura. Os principais objetivos podem resumidos nos seguintes tópicos: (1) Mapeamento batimétrico da área de estudo e, portanto do campo de pockmarks; (2) Descrição da morfologia e características do fundo do mar na área com pockmarks e na plataforma envolvente; (3) Caraterização estratigráfica e estrutural dos sedimentos Cenozoicos do Esporão da Estremadura e (4) Compreender a origem estratigráfica dos fluidos que dão origem aos pockmarks e o que controla a sua migração e escape no fundo do mar.

Para a realização deste estudo foram utilizados dados batimétricos, de refletividade do fundo do mar (*backscatter*), sísmica SPARKER 2D monocanal de alta resolução e observações diretas do fundo do mar, através de vídeos adquiridos em mergulhos com um submarino ROV (*Remotely Operated Vehicle*). Estes dados foram essencialmente obtidos durante a missão oceanográfica do projeto PACEMAKER (sísmica de alta resolução e batimetria), em colaboração com o projeto TOPOMED (TOPOEUROPE/0001/2007). Durante a campanha EMEPC/PEPC/LUSO/2015 (no âmbito do projeto PES – PTDC/GEO-FIQ/5162/2014) foram adquiridos novos dados de batimetria no Esporão da Estremadura, que complementaram os dados anteriores. Foram também realizados dois mergulhos com o ROV Luso em duas das depressões (pockmarks) identificadas no fundo marinho.

A partir dos dados batimétricos foram criados mapas batimétricos e de refletividade do fundo do mar, onde foram observadas depressões topográficas com formas circulares a alongadas e com *backscatter* elevado, interpretadas como pockmarks.

De modo a melhorar a qualidade dos dados sísmicos estes foram processados, através do *software* SPW (P*arallel Geoscience Corporation*). Foram realizados vários passos de processamento para as 14 linhas sísmicas PACEMAKER, como por exemplo, a aplicação de um filtro *butterworth*, correção do *swell* e das máres e migração *Stolt*. Os resultados do processamento foram considerados positivos, uma vez que a maioria do ruído que mascarava o sinal sísmico foi eliminado, sendo possível observar a sub-superficie do Esporão da Estremadura até cerca de 500 ms TWT.

Após o processamento sísmico foi realizada a interpretação dos perfis sísmicos no *software* SeisWorks da Landmark Graphic Corporation, sendo desenvolvido um modelo sísmostratigráfico. Foram identificadas seis unidades sísmicas (U1 a U6) separadas por horizontes (M a H4) que marcam importantes descontinuidades ou variações na fácies sísmica. A unidade sísmica mais antiga, U1, foi sujeita a uma intensa deformação dúctil, ao contrário das restantes unidades, pelo que a descontinuidade que separa U1 e U2 foi associada ao auge da deformação alpina, no Miocénico (Tortoniano). Assim, esta unidade sísmica U1 será anterior ao Tortoniano, provavelmente de idades do Miocénico inferior e médio. As restantes unidades sísmicas, U2 a U6, formam uma sequência sísmica de idades compreendidas entre o Pliocénico e o Holocénico.

No registo sísmico foram também identificadas várias evidências para a existência da migração e acumulação de fluidos. Além dos pockmarks, que já tinham sido identificados anteriormente, foram observados paleo-pockmarks (enterrados a varias profundidades), condutas de migração dos fluidos, zonas de transparência, turbidez e de *blanking* acústico. Deste modo, foi interpretado que os fluidos estão a migrar verticalmente e a acumular-se nas unidades sísmicas Plio-Quaternárias.

Os mergulhos com o ROV mostraram que, apesar da resposta de backscatter de alta refletividade associada aos pockmarks e das evidências para a existência de fluidos observadas na sísmica, no fundo do mar não se encontram evidências para a atividade atual do sistema de escape de fluidos. As depressões visitadas com o submarino mostraram que as estruturas estão cobertas por sedimentos arenosos e não foi observada fauna nem registado o borbulhar característico de *seeps* ativas.

Pode então ser concluído que na atualidade os fluidos não alcançam o fundo do mar, estando a acumular-se em zonas mais permeáveis dos sedimentos. Foram propostos dois modelos evolutivos, coexistentes no Esporão da Estremadura, para o sistema de migração de fluidos: (1) Atividade cíclica das *seeps* e (2) selagem do sistema pela precipitação de carbonatos autigénicos (MDAC). O primeiro baseia-se na observação de pockmarks "empilhados" (*stacked pockmarks*) no registo sísmico, o que sugere que a migração e escape dos fluidos é periódica, possivelmente condicionada pelas variações eustáticas do nível do mar. O segundo modelo consiste na descativação de condutas de migração de fluidos, pela precipitação de MDAC, o que causa o enterramento do pockmark alimentados por essas condutas. Posteriormente, ocorre a criação de novos caminhos de migração para os fluidos, que se acumulam em zonas permeáveis dos sedimentos até existir pressão suficiente para escaparem pelo fundo do mar.

Palavras-chave: Pockmarks, migração de fluidos, Esporão da Estremadura, Margem Oeste Ibérica, sísmica de alta-resolução, interpretação sísmica.

ACKNOWLEDGMENTS

This dissertation is the final outcome of a long project, it would have not been possible without the help and support of many people, who I grateful thank.

First, I thank my master supervisors, Prof. Dr. Pedro Terrinha and Dr. Vitor Magalhães, for their support along this last year. I am very grateful for their reviews of several versions of this thesis and discussions from which I learn a lot and help me improve this work. I am also thankful to Dr. Carlos Ribeiro for is patience, help and suggestions that help me immensely.

This work was carried out at the Marine Geology and Georesources Division of the Portuguese Sea and Atmosphere Institute (DivGM – IPMA) and partially in the framework of the PES project (PTDC/GEOFIQ/5162/2014) Pockmarks and fluid seepage in the Estremadura Spur: implications for regional geology, biology, and petroleum systems. To all the people in the Marine Geology division, not mentioned above, I am also very grateful for all the help, suggestions and motivation: Rui Quartau, João Noiva and Luis Batista (the Landmark masters), Marisa Loureiro, Susana Muiños, Sónia Silva, Margarida Henriques, Pedro Brito and Marta Neres. Cristiana Cunha and Sara Rodrigues, master students like me, at the DivGM, thank you for all the motivational talks and friendship.

My thanks to Kim Jung-Hyun (now at the Hanyang University, South Korea) and to Henko de Stigter (NIOZ - Royal Netherlands Institute for Sea Research) that allowed me the use of the sparker seismics and multibeam data acquired during the RV Pelagia cruise 64PE332 in the framework of the PACEMAKER project funded by the European Research Council.

I am also thankful to *Estrutura de Missão para a Extensão da Plataforma Continental* (EMEPC) for allowing me to participate in their 2015 scientific cruise and for letting me have access and use the data collected in the Estremadura Spur. A special thanks to Dra Cristina Roque, for all the productive talks and suggestions that help me improve this work.

I am grateful to Prof. Dr. Luis Menezes Pinheiro and Omar Benazzouz from the Geosciences Department of the University of Aveiro, for all the help and suggestions during the processing of the seismic data. The processing of the PACEMAKER seismic datased was carried out with a SPW software package license from the University of Aveiro. Prof. Dr. Luis Matias (from FCUL & IDL) and Henrique Duarte (from GeoSurveys) are also thanked for the help with SPW and for the fruitful discussions on the seismic processing.

I acknowledgment the support of the Landmark Graphic Corporation via the Landmark University Grant Program. I would also like to thank *Direção Geral de Energia e Geologia* (DGEG) for letting me have access and use data from industry wells of the Estremadura Spur and the TGS-NOPEC seismic dataset.

Finally, I would like to thank my closest family for their encouragement and support throughout my geological adventures. This journey began six years ago and since then many people have been by my side – João, Rosa, Ana, Sheyla. To Henrique, and Catarina, for always be present ("*however far away…*"). To Romeu and Carla for showing me that there are still good people in the world. To Miguel and Mr. R., for all the "study parties" and help with the GIS stuff. And to *tio* Ravana, Ana M. and Viri for all the bright moments.

TABLE OF CONTENTS

LIST OF FIGURES

LIST OF TABLES

ABBREVIATIONS

ES	Estremadura Spur
LM	Lourinhã Monocline
MDAC	Methane-derived authigenic carbonates
TWT	Two way time
TR	Traces
ms	Milliseconds
m	Meters
PM	PACEMAKER
LGM	Last Glacial Maximum
ROV	Remotely Operated Vehicle
WIM	West Iberian margin

CHAPTER 1

INTRODUCTION

The Estremadura Spur is a trapezoidal shape promontory, elongated in the east-west direction, located on the West Iberian margin (between the Cabo Carvoeiro and the Cabo da Roca), extending to the offshore until the Tore seamount (Figure 1). In 2011, under the scope of PACEMAKER project (Past continental climate change: temperatures from marine and lacustrine archives, ERC Advanced Grant, NIOZ, The Netherlands) and in collaboration with the TOPOMED project (TOPOEUROPE/0001/2007), a seismic reflection SPARKER survey detected an unknown field with more than 70 pockmarks in the Estremadura Spur (Kim & the shipboard scientific party, 2011). These pockmarks and the associated fluid escape process are the main objectives of this work that aims to contribute to the characterization of the structures and to the understanding to their structural and stratigraphic control. This master project was carried out partially in the framework of the PES project (PTDC/GEOFIQ/5162/2014) Pockmarks and fluid seepage in the Estremadura Spur: implications for regional geology, biology, and petroleum systems.

Pockmarks are seabed culminations of fluid (liquid or gas) migration through the sedimentary column and their escape to the seawater, which appear as cone-shaped circular or elliptical depressions (Judd & Hovland, 2007). Their distribution does not occur randomly and are often related to the subsurface geological structures, such as faults and weakness planes that serve as conduits for the migration of the fluids to the surface. These structures can also be related to the compaction of the sediments and flow straight upward to the venting sites. Pockmarks have proven to be important seabed features that provide information about fluid flow on continental margins, being used by the oil and gas industry as an exploration tool as an indicator of hydrocarbon sources for prospecting (Judd & Hovland, 2007).

The West Iberian margin (WIM), where the Estremadura Spur is located, began to develop during the opening stage of the North Atlantic Ocean, from the Late Triassic through the Early Cretaceous (Rasmussen *et al.*, 1998; Pinheiro *et al.*, 1996). The pre-Mesozoic rocks that form the basement of the WIM are part of the Hesperian Massif. During the Cenozoic the evolution of the WIM was characterized by periods of compression and tectonic inversion related to the Alpine orogeny (Pyrenean and Betic phases), leading to the uplift of some regions of the margin, such as the Estremadura Spur (ES). The peak of deformation, with maximum compression NW-SE, occurred in the Late-Miocene, possibly during Tortonian (Rasmussen *et al.*, 1998; Pinheiro *et al.*, 1996). Although fluid flow is a common process in passive continental margins and sedimentary basins, fluid escape processes were not previously identified on the WIM. The above mentioned pockmarks and associated fluid escape processes, which are the focus of this thesis, are the first fluid seepage system identified in the WIM and in which no investigation was previously done. To our best knowledge the nearest occurrences of fluid seepage in the offshore of the West Iberia Margin are found only in the estuarine environments of the Ria de Vigo (García-García *et al*., 1999; 2003; 2004; Judd and Hovland, 2007; Martínez-Carreño and García-Gil, 2013), the Aveiro Estuary (Duarte *et al.* 2007; Duarte, 2009), and in the Gulf of Cadiz (Pinheiro *et al.*, 2003; Magalhães, 2007; Magalhães *et al.*, 2012; León *et al*., 2010).

In the onshore portion of the WIM many cases of oil and gas seeps in outcrops are known (e.g. Montejunto Fm; Pena dos Reis and Pimentel, 2010; 2014) in the regions of Torres Vedras, Leiria and Paredes da Vitória (where a mine that explored oil sand existed). This suggests the existence of active hydrocarbon migration in the Lusitanian basin.

1.1 Previous work on the Estremadura Spur

The WIM has been the subject of many studies over the past decades. The 'Groupe d'Étude de la Marge Continentale' of the Rennes University was among the first groups to study the geological aspects of the Portuguese continental shelf, publishing many important works in the 70s. The thesis of Musselec (1974) and Mougenot (1976) presented the geomorphology, structure, and geological evolution of the Portuguese continental shelf including the Estremadura Spur area, based on seismic reflection profiles and samples of seabed sediments. These two works kept their great importance and are still used major references for the Western Iberian margin geology.

Vanney & Mougenot (1981) did a bathymetric and geomorphological characterization of the continental shelf, based on bathymetric (single beam) and reflection seismic surveys. The bathymetric analysis was subsequently revised and updated by Mougenot (1989). More recently, Badagola *et al*. (2006) compiled a bathymetric map of the continental shelf and the upper slope of the Estremadura Spur, based on the existing bathymetric single and multibeam data, characterizing, in detail, the geomorphology of the area. In 2008, Badagola updated and detailed the continental shelf morpho-tectonic evolution and the geologic structures of the Estremadura Spur. In this work he mapped the rocky outcrops and characterize the composition and age of the seabed outcrops.

The Meso-Cenozoic tectono-sedimentary evolution of the WIM was studied by Alves *et al.* (2002; 2003 and 2006), focusing on the structures observed in the Lusitanian and Peniche basins. Canérot *et al*. (1995) studied the geological evolution of the Caldas de Rainha sector of the WIM, allowing a more detailed interpretation of the tectonic evolution of the area. The Paleogene and Neogene evolution of the western Iberia was compiled by Pais *et al*., (2012), specifically the geology and tectonic setting of the new basins formed during the Cenozoic. The study of the WIM's surface sedimentary deposits was made by Dias *et al*. (1980a and 1980b), who identified the gravel and sand outcrops along the margin. More recently, Balsinha *et al*. (2014) characterized the patterns of sediment transport on the Estremadura Spur continental shelf. The evolution of the coastal morphology of the WIM, since the Last Glacial Maximum, was synthesized by Dias *et al*. (2000) and Rodrigues *et al*. (2000).

1.2 Study Area

The study area of this project is located in the NW region of the Estremadura Spur outer shelf (Lourinhã Monocline; Figure 1[1]. The Estremadura Spur (ES) is a trapezoidal promontory, elongated in an east-west direction with an area of about 3583 km2, located on the continental shelf off Portugal, between Cabo Carvoeiro (39º21'37.62"N) and Cabo da Roca (38º46'49.0"N) and extending from the Portuguese coast line (9º25'02.4"W) until the Tore seamounts (10º29'09.9"W) (Figure 1). It separates the Iberian Abyssal Plain (at north) from the Tagus Abyssal Plain (at south).

The Estremadura Spur is part of the WIM, where a series of onshore and offshore sedimentary sub-basins, related to the opening of the North Atlantic Ocean, formed from

[1] All the maps presented in this work are projected in the coordinate system UTM WGS84 (zone 29N).

the Triassic through the Cretaceous. The onshore and shelf basins are usually grouped under the domain of the Lusitanian Basin. The ES was uplifted during the Cenozoic collision of Africa and Eurasia as part of the Alpine Orogeny. Badagola *et al.* (2006) sustains that in the Lourinhã Monocline region, where the ES pockmarks occur, sedimentary basins are established and filled with up to 40 meters of Pliocene and Quaternary sediments.

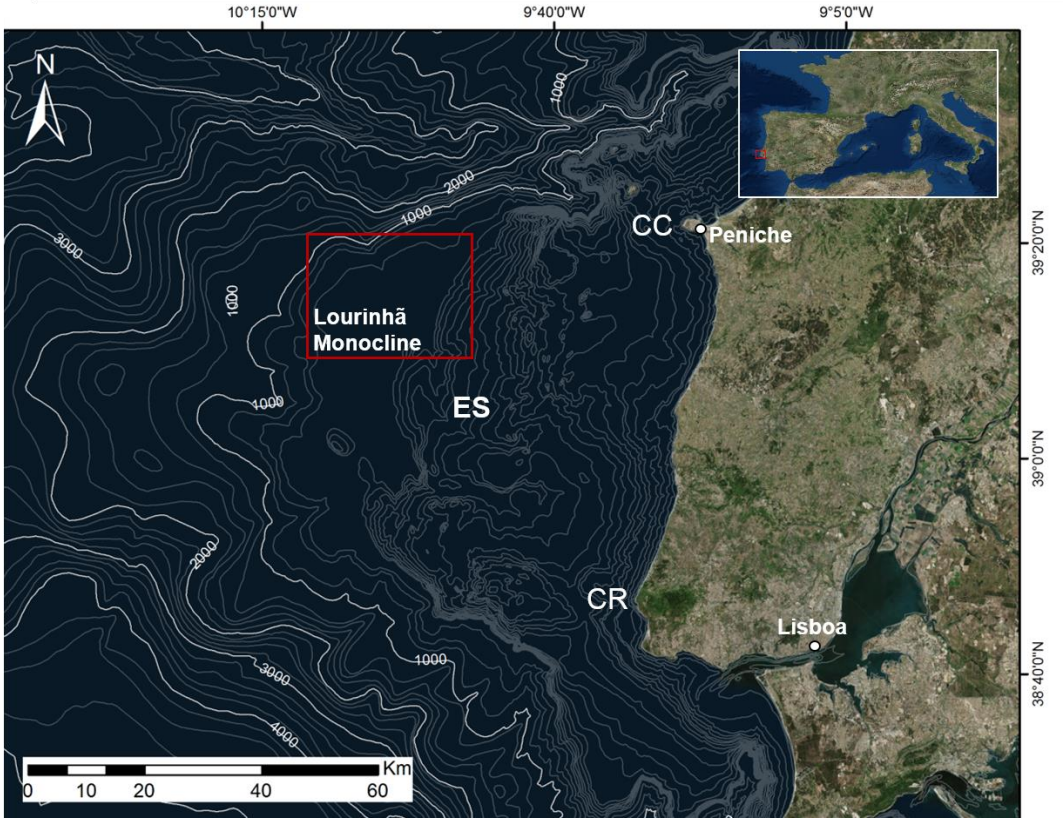

Figure 1 Geographic location of the Estremadura Spur (ES) with the indication of the Lourinhã Monocline pockmark field (red rectangle); CC – Cabo Carvoeiro; CR – Cabo da Roca.

In the north the continental shelf of the ES is bounded by the upper and middle sectors of the Nazaré Canyon (Vanney & Mougenot, 1990) and in the south it is limited by a slope widely carved by straight and parallel gullies, oriented ENE-WSW to NE-SW (Alves *et al.*, 2003). In the west the continental shelf is delimited by a smooth uniform slope, with the base defined around the depth of -3000 m.

According to Vanney & Mougenot (1981) the continental shelf in the ES region, is divided in two distinct sectors, the internal sector, from the coastline to 120-130 m below the sea level (bsl) and the external sector down to 500 m bsl (Figure 2). The internal sector is marked by two large plateaus the Costeiras Pêro da Covilhã (CPC) and the Montanha de

Camões (MC) separated by a large basin, the Mar da Ericeira (ME), where occurs the deposition of fine-grain sediments. In the external sector of the platform, west of the CPC, there is a shallow dipping surface, the Lourinhã Monocline (LM), where Pliocene-Quaternary sediments lie unconformably on top of folded Mesozoic and Neogene basement. In the southern region of the Spur two ridges with NW – SE strike are found (PDG – Planalto Diogo Gomes and PGZ – Pico Gonçalves Zarco) separated by a linear depression.

The pockmark field discovered in the Estremadura Spur, during the PACEMAKER seismic survey, was found on the external sector of the continental shelf, in the Lourinhã Monocline region.

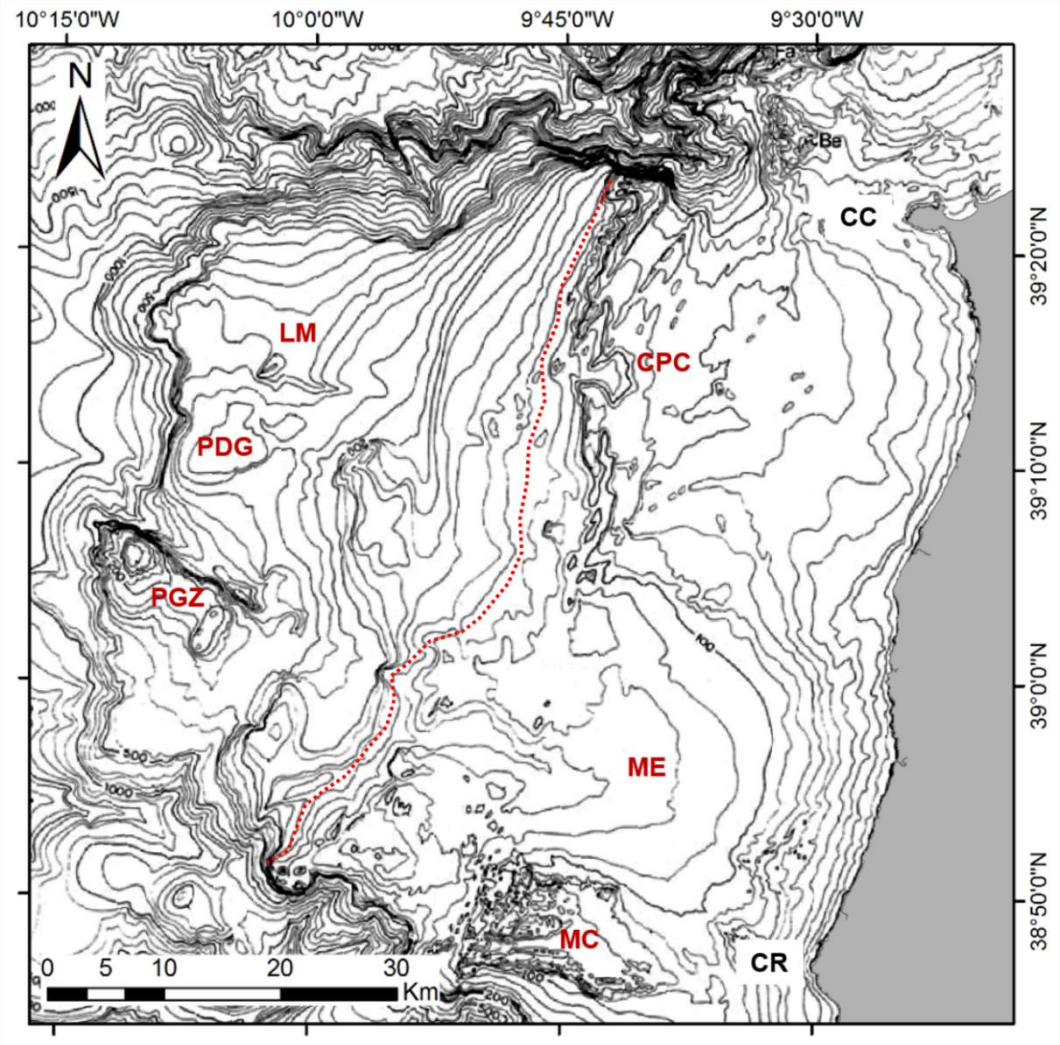

Figure 2 Estremadura Spur's bathymetric map with reference to the different morphologic units (adapted from Mougenot, 1989): LM – Lourinha Monocline; PDG – Planalto Diogo Gomes; PGZ – Pico Gonçalves Zarco; CPC – Costeiras Pêro da Covilhã; ME – Mar da Ericeira; MC – Montanha de Camões. Bathymetry contour intervals, 10m. **Red dotted line:** separation of the inner shef (from the shore to the line) and external shelf (from the line until 500 m bsl).

1.3 Research objectives

The motivation of this work is the study of the fluid escape structures in the Estremadura Spur. It aims to contribute to a better understanding of the structural control and the characteristics of the fluid escape structures in the Estremadura Spur, both at the seafloor and in the subsurface. The main objectives can be outlined as follows:

(1) Bathymetric mapping of the area and of the pockmarks field;
(2) Description of the morphology and characteristics of the seabed in the pockmarks area and surrounding shelf;
(3) Stratigraphic and structural characterization of the Cenozoic sediments of the Estremadura Spur region;
(4) Understanding the stratigraphic source of the fluids and the control of their migration and seepage.

1.4 Thesis outline

This dissertation is organized in the following eight chapters:

- Chapter 1 – Introduction

In this chapter the nature and the aims of this research are presented, the objectives described, as well as the database and the methodologies used. A brief description of the thesis outline and their content is also include.

- Chapter 2 – Pockmarks: an evidence of Seabed Seepage

In the second chapter the focus is on the characteristics and importance of the fluid flow systems and of the fluid escape processes and manifestations (seepages) on the seabed at continental margins. Special importance is given to the possible relation between fluid escape structures, like pockmarks, and the existence of structural pathways.

- Chapter 3 – Geological Setting

In this chapter the geomorphological, tectonic and stratigraphic settings of the study area, and its geodynamic evolution is presented.

- Chapter 4 – Data and Methods

This chapter lists the different datasets used in the work, referring their provenance. It is also made a description of the different types of data (such as bathymetry, seafloor reflectivity and seismic profiles), followed by an explanation of the methods and procedures used to prepare the data for interpretation.

- Chapter 5 – Geomorphologic Analysis of the Seafloor

In this chapter the interpretation of the bathymetric and backscatter data acquired in the study area is presented. It is also described the visual observations of the seafloor from the ROV dives in two different locations. Then, the surface evidences of fluid seepage are discussed, based on the previous data interpretation.

- Chapter 6 – Seismic Data Processing

In the sixth chapter the data acquisition and its parameters are described. Then, it is presented a brief summary of the theoretical concepts employed for the processing of the seismic data, the flowchart of the sequence of the several processing steps applied to the PACEMAKER seismic dataset and the results obtained along each steps. The parameterization of each processing step and the comparison of the different and equivalent steps are tested and discussed.

- Chapter 7 – Seismic Interpretation

In this section the interpretation of the seismic data acquired in the Lourinhã Monocline region is presented. A total of eight 2D high-resolution seismic profiles were interpreted, featuring a detailed seismic-chronostratigraphic model, structures interpretation and isobaths and isopachs maps. A general interpretation of the low-resolution and high penetration TGS-NOPEC seismic was carried out to provide an overview of the prominent structures present in the deeper subsurface. Seismic evidences of fluid flow are also discussed.

- Chapter 8 – Discussion and Conclusions

In this last chapter the main interpretations and conclusions that resulted from this study are presented. Also possible research lines for future works is summarized.

CHAPTER 2

POCKMARKS: AN EVIDENCE OF SEABED SEEPAGE

Seabed fluid[2] flow is of fundamental importance in the geological, chemical and biological cycles of the marine environment and also influences the composition of the atmosphere (Judd and Hovland, 2007).

2.1 Seabed Fluid Seepage

Within the sedimentary basins, fluids migration towards the seabed may result in seafloor seepage where fluids are released into the water column. Seabed seepages occur in a wide variety of geological environments: in the continental shelf, slope and rise. The intensity of the fluid flow in seepages range between the slow diffuse, inter-granular, 'micro-seepage' and the vigorous focused flow, with sometimes violent eruptions of gas (Judd, 2003; Talukder, 2012). Their activity is in general episodic, with short periods of activity intercalated with long periods of dormancy.

The seeping fluids can be gaseous or aqueous solutions rich in hydrocarbons (in general dominated by methane) or can be groundwater more or less modified by the water-rock interaction processes (Judd and Hovland, 2007). The seeping fluids do not have a significant temperature anomaly (and therefore called "cold seeps") relatively to the seepage setting (sediments and seawater), in opposite to the hydrothermal or volcanic origin fluids that define the Hot or Hydrothermal Vents. Regarding the cold seep gases, methane is the biggest contributor to seeping gases by volume (Judd and Hovland, 2007). Minor quantities of other hydrocarbon gases such as ethane, butane, pentane, and CO_2 can also occur in conjunction with methane (Judd and Hovland, 2007; McGinnis *et al.*, 2011). The Hydrothermal Vents are places occurring/located mostly along oceanic spreading centers where high-temperature fluids (heated in the close vicinity of magma

[2] In marine geology and geophysics the term fluid refers both to liquid and gas.

chambers) escape from the seafloor. On the contrary, cold seeps (Figure 3) are defined as sites where low-temperature fluids and/or gas escape from the seafloor (Talukder, 2012).

2.1.1 Cold Seeps

As stated above, Cold Seeps are structures where the fluids that escape to the seabed are characterized by low temperatures, i.e., temperatures similar to the bottom sea water. Examples for active cold seepage in continental margins can be found in many areas of the world (Figure 4).

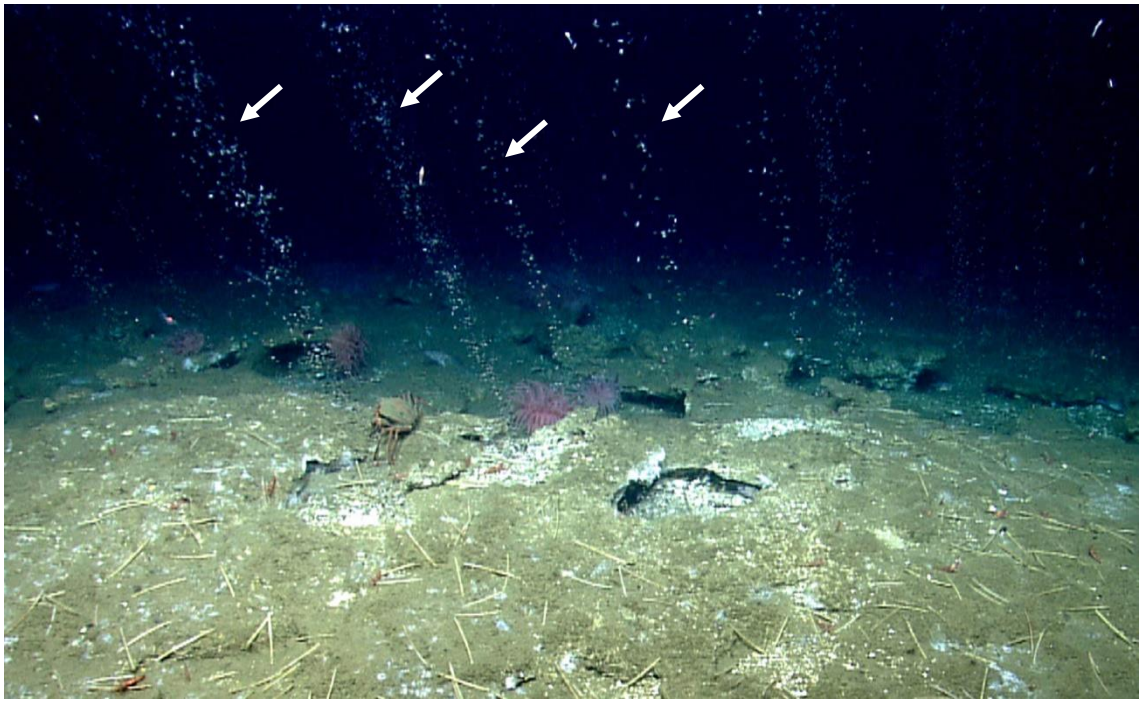

Figure 3 Figure: Gas plumes (white arrows) emanating from the seabed at a cold-seep site on water depths less than 500 meters (http://soundwaves.usgs.gov/2014/10/).

Most seepage of low temperature fluids that occurs on passive continental margins (Figure 4) are related to high sedimentary input associated with high fluxes of accumulation of organic matter and associated with basins with active petroleum systems. The joint effect of thick sedimentary successions, continuous sediment burial, diagenesis and maturation of organic matter promotes the widespread occurrence of fluid seepage in these geological settings. Examples for passive margins cold seepage occur in the Gulf of Mexico (Joye *et al*., 2004; Roberts and Aharon, 1994), in the Gulf of Cadiz (Léon *et al*., 2006; Niemann *et al*., 2006; Magalhães *et al*., 2012) or in the western African margin (Gay *et al*., 2005 and 2007).

The morphological expression of seepage include a wide variety of features (Judd and Hovland, 2007); the two most common are mud volcanoes and pockmarks.

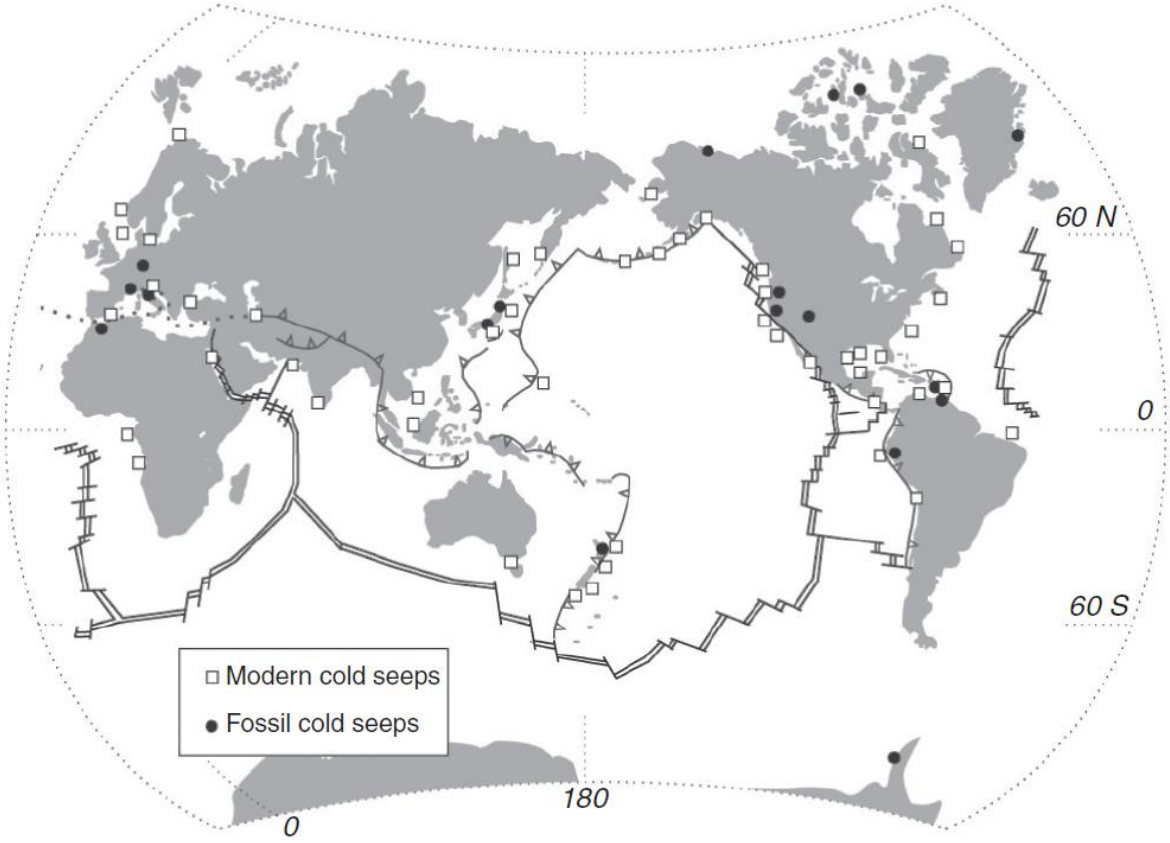

Figure 4 World-wide distribution of modern and ancient cold seeps (adapted from Campbell *et al*., 2002).

2.1.2 Methane formation and Gas Hydrates

Methane seepage occurs if organic matter contents in the sediments are sufficient to allow the generation of high volumes of methane within the sedimentary column and if geological features (such as fractures) that facilitate the methane migration towards the seafloor are present. The escape of fluids, such as methane from the seafloor is a consistent feature throughout geologic time as documented by seismic surveys and seepage outcrops.

Methane, being highly abundant in the earth's crust, is often found to be related with fluid flow features and gas hydrate formation. In seabed sediments there are three possible sources of methane: microbial, thermogenic and abiogenic (Judd, 2003).

Microbial methane is originated by the microbial activity during the decomposition of organic matter at small burial depths under low temperature and pressure conditions

(Moore and Wade, 2013). The primary producers contribute to most of the organic matter available in the oceans that is generated through photosynthesis and, after the dead of the organisms, settles through the water column. It is oxidized in the uppermost oxygen-rich layer of the sedimentary column (the top few millimeters or centimeters of the sediments) as long as oxygen is available. In the anoxic environment immediately below the oxygen-rich zone, oxidation stops and the organic matter is buried and may be decomposed anaerobically. This is a very complex process and the final steps of it may be summarized by the following equation representing the formaldehyde decomposition into methane and carbon dioxide by the action of methanogenic microbes:

$$2CH_2O \rightarrow CH_4 + CO_2 \qquad \text{Equation 1}$$

The organic matter that is not degraded by methanogenic microbes within the top 1000 m of the sedimentary column is buried and can be degraded by thermocatalystic processes, forming thermogenic methane. The organic matter which survives the burial is transformed into kerogen (amorphous organic matter), under the influence of increasing temperature and pressure (Judd, 2001). As burial increases kerogen undergoes thermal cracking which leads to the formation of various hydrocarbons compounds with solid, liquid and gaseous fractions. Methane is the most abundant hydrocarbon molecule formed, and the most mobile since it has the simplest and the smallest molecule size, therefore it's the most prone to migrate to the seabed.

Abiogenic methane is formed through inorganic reactions. The most frequently invoked reaction for abiotic hydrocarbons generation are the Fischer–Tropsch type reactions (e.g. Potter *et al*., 2004 and 2013; Cao *et al*., 2014), that converts CO_2 to hydrocarbon gas by reacting it with H_2:

$$nCO_2 + (3n+1)H_2 \rightarrow C_nH_{2n+2} + 2_nH_2O \qquad \text{Equation 2}$$

Methane (CH_4) is produced when $n = 1$:

$$CO_2 + 4H_2 \rightarrow CH_4 + 2H_2O \qquad \text{Equation 3}$$

One of the possible origins of the H_2 required for the reaction is the hydrothermal alteration of Fe-rich minerals, at temperatures above 200ºC (Potter *et al*., 2004; Tassi *et*

al., 2012). These processes occurs during serpentinization processes, during the magma cooling and, more commonly in hydrothermal systems during water–rock interactions (Lollar *et al*., 2002). It is also been claimed that abiogenic methane can have a primary mantle origin, emanating from the deep of the Earth and being incorporated into magmas (Gold and Soter, 1985). Hence, abiogenic methane may be of magmatic or hydrothermal origin and is usually observed in oceanic lithosphere instead of passive continental margins.

Gas hydrates are ice-like crystalline solid structures consisting of a rigid cage of water molecules that entrap hydrocarbon and non-hydrocarbon gas by hydrogen bonds, forming clathrates (Sloan and Koh, 2007). They occur naturally in the pore space of different types of marine and lacustrine sediments and permafrost, where appropriate pressure, temperature and salinity (PTS) conditions, and sufficient supplies of gas (mainly methane) and water exist. Due to these requirements oceanic gas hydrates are only stable in the upper few hundred meters of the sediments on the continental margins. This zone is called the gas-hydrate stability zone (GHSZ) (Figure 5). The base of the GHSZ represents the phase boundary between stable gas hydrates and free gas below. This phase boundary is dependent on the geothermal gradient, bottom water temperature, pressure, gas composition, pore water salinity and the physical and chemical properties of the host rock (Bünz *et al*., 2003). When the amount of free gas within the sediments bellow the GHSZ is sufficient, then the base of the GHSZ is distinctly marked on the seismic reflection profiles by a bottom simulation reflection called BSR.

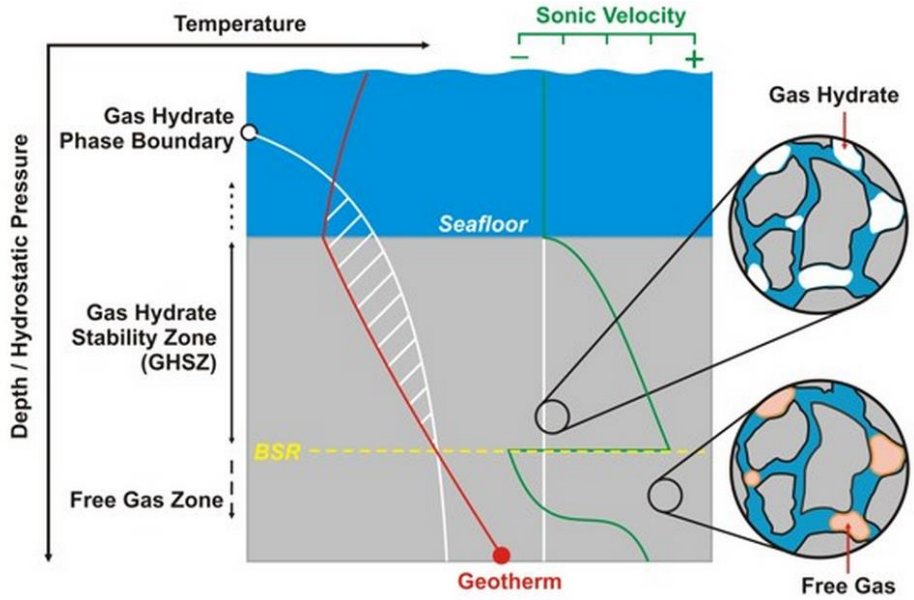

Figure 5 Gas-hydrate stability zone in sub-surface sediments (adapted from Clennell, 1999).

The BSR are high amplitude and reversed polarity reflector on the seismic records that are sub-parallel to the seafloor (Figure 6) and that are due to an acoustic impedance contrast between the hydrate-bearing sediments and free gas trapped in the sediments beneath the gas hydrates at the base of the GHSZ (BGHSZ). Hydrate-bearing sediments may not have BSR associated if the amount of free gas present underneath the base of the GHSZ is not sufficient to produce a significant density/acoustic impedance contrast between the hydrate cemented sediments within the GHSZ and the free gas hosting sediments below the BGHSZ (Chand and Minshull, 2003; Bünz *et al*., 2003).

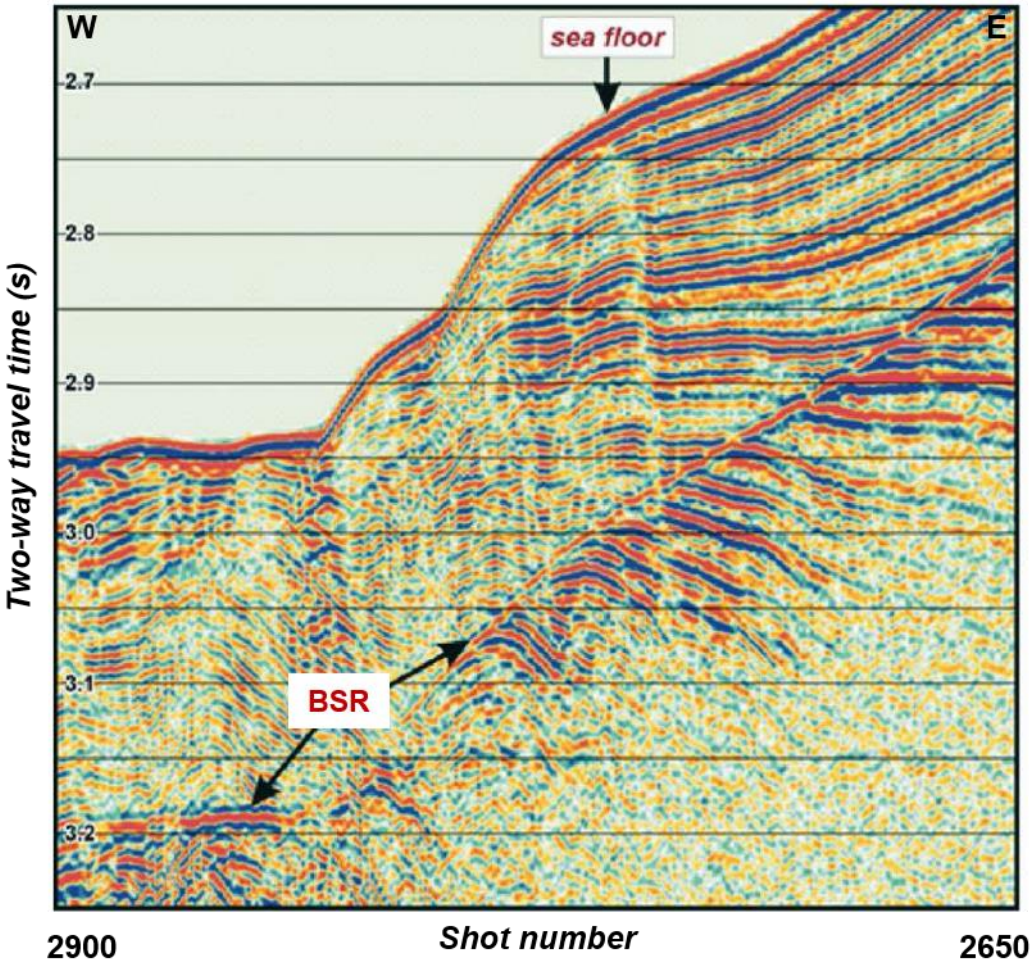

Figure 6 Seismic expression of a BSR in the western Svalbard margin (Vanneste *et al*., 2005).

2.1.3 Migration Pathways

Pore fluids, generated at depth or entrapped during sedimentation, escape to the seafloor through migration pathways. The existence of migration pathways are determined by the

interrelationship of sediment permeability/porosity, sedimentation rate, rock deformation and flow rates (Hindle, 1997).

Fluids within sedimentary basins migrate due to pressure gradients, to variations in the existent excess pore water pressures and due to the buoyancy diferentials within the sedimentary basins (England *et al*., 1987). The density and pressure gradients between sedimentary layers play a major role in the rate of fluid migration. In porous media, the rate of fluid flow is controlled by the intrinsic permeability of the medium, fluid viscosity and the pressure gradient, as stated by the Darcy's law. Low-permeability formations can, thus, inhibit the flow of fluids, leading to local pore pressure build-up. In unconsolidated sediments when the pore fluid pressure exceeds the lithostatic pressure, mechanical failure of the low-permeability formation occurs (Clennell *et al*., 1998) resulting in the formation of new pathways which allows the escape of the pore fluids, until the pressure is reduced to the hydrostatic values (Roberts and Nunn, 1995). Fluid escape into the low-pressure areas, usually towards the surface. However, this can be precluded by impermeable layers acting as sealing or trap structures.

In non-porous media, vertical fluid migration occurs as a result of either capillary seal breaking or permeability enhancement usually related with faults, diapirs or pipes (Cartwright *et al*., 2007). The most important external triggers for fluid migration, as enumerated by Talukdar (2012), are the following:

1. Tectonics (faults and fractures): Faults are the most important conduits for fluid flow in sedimentary basins, especially at depths where the sediments are consolidated or completely lithified (Ligtenberg, 2005). Faults zones may provide permeable vertical pathways through the otherwise impermeable strata (Çifçi *et al*., 2003; Gay *et al*., 2006 and 2007; Ostanin *et al*., 2012) and may contain large interconnected fractures that act as good pathways for fluid flows.
2. Erosion of overburden rocks: Overburden erosion, caused for example by landslides, reduces the lithostatic pressure. Consequently, entrapped fluid overpressure can easily overcome the lithostatic pressure, causing the ascent of mud and fluids.
3. Earthquakes: Onshore and offshore increased fluid venting and seepage, as also mud volcano eruptions are frequently related to moderate and strong seismicity events. When earthquake waves pass through water-saturated and confined unconsolidated sediments it can lead to localized pore fluid pressure increases,

exceeding the lithostatic pressure and the cohesion of the overlying sediments will cause sediments liquefaction and fluid ascent injections.

4. Tides and eustatic sea level changes: the decrease of the hydraulic pressure by low tides or, on a longer time scale by a sea level drop, can trigger the rise of fluid flow.

2.2 Seismic Indicators of Fluid Flow

Hydrocarbon seepage can often be recognized on seismic data, because it causes a diagenetic mechanical change or compositional variability in the geological sequences that can produce a detectable acoustic anomaly. Indications for fluid and seepage are expressed in characteristic seepage features both at seabed and in the subsurface. Evidences for the presence of gas in the sedimentary sequence and fluid flow is inferred by the observation of geophysical indicators, such as acoustic turbidity, enhanced reflections, intrasedimentary doming, reflectors pulldown, gas chimneys and bright spots in the seismic data (Judd and Hovland, 2007; Duarte *et al*., 2007). Often, these indicators are observed in association with other resulting from the presence of gas in the water column like acoustic plumes (flares), cloudy turbidity and acoustic turbidity near the seabed.

Acoustic turbidity (AT) appears on shallow seismic reflection profiles as a disturbance on the seismic record obliterating all seismic reflections of the deeper layers (Figure 7–A). Sometimes, coherent reflections can still be followed inside AT zones, despite the reduced amplitude of the acoustic turbidity areas. This effect is caused by the fact that in the sediments with high gas contents, the majority of the acoustic energy is being attenuated by the gas bubbles, causing chaotic reflections. Acoustic turbidity is most common is soft, fine-grained sediments, but similar effects may also be caused by gravel beds, shell beds and peat layers (Ligtenberg, 2005; Judd and Hovland, 2007; Duarte *et al*., 2007).

Enhanced reflections (ER) are characterized by a marked lateral increase in the amplitude of coherent reflectors (Figure 7–B). They are interpreted as indicating an increase of the gas contents in relatively porous horizons, generally at the top of a sediment bed, or at an angular truncation overlain by a dominantly impermeable muddy sequence. The enhanced reflections can also be produced by the presence of diagenetically cemented sections of layers, such as the presence of methane-derived

authigenic carbonates that occur bellow cold seeps (Ligtenberg, 2005; Judd and Hovland, 2007; Duarte *et al*., 2007). They can also be caused by lateral facies variations, with no relation to gas bearing sediments. Enhanced reflections are observable in shallow high-resolution seismic profiles and are the equivalents of the 'bright spots' which occur in greater depths (only visible in deep seismic profiles).

Acoustic blanking (AB) is defined by a transparent or signal-starved domain in the seismic profile, topped either by an enhanced reflection or by acoustic turbidity (Figure 7–C). Acoustic blanking is often close to the seabed, usually develops vertically (Judd and Hovland, 2007). It is interpreted as the result of the weakening of the acoustic signal caused by gas accumulations in the sediments (Ligtenberg, 2005; Judd and Hovland, 2007; Duarte *et al*., 2007).

Gas chimneys (Figure 7–D) are vertical to near-vertical zones associated with upward fluid migration. The shape of the gas chimneys can vary from diffuse shadows, funnels or pipes. Their appearance can be explained by the transport of gas from a reservoir and into the cap rock through a connected fracture network also associated with some lateral diffusion. The gas in the sediments causes fluctuations in the compressional velocity field which again cause scattering and deterioration of a passing seismic wave. The general texture of the internal structure of gas chimneys shows a chaotic reflection pattern of low energy. Gas chimneys often terminate in the shallower stratigraphy, topped by a strong reflection at the water-sediment interface, and are associated with acoustic evidence of gas accumulations (Ligtenberg, 2005; Judd and Hovland, 2007; Duarte *et al.*, 2007).

Intrasedimentary doming can appear beneath pockmarks in seismic profiles and are characterized by the upwards doming of individual reflectors (Figure 7–E). These features are considered artifacts caused by the difference in the seismic velocity at sediments containing indurated sediments associated with the migration or presence of free gas, in relation with the similar contiguous sediments with no gas (Ligtenberg, 2005; Judd and Hovland, 2007; Duarte *et al*., 2007). Unaffected reflections are often observed above the intrasedimentary doming, indicating the some of these features are genuine, most probably resulting from the upward grow of sedimentary layers due to increased pore pressure in some way related to vertical gas migration.

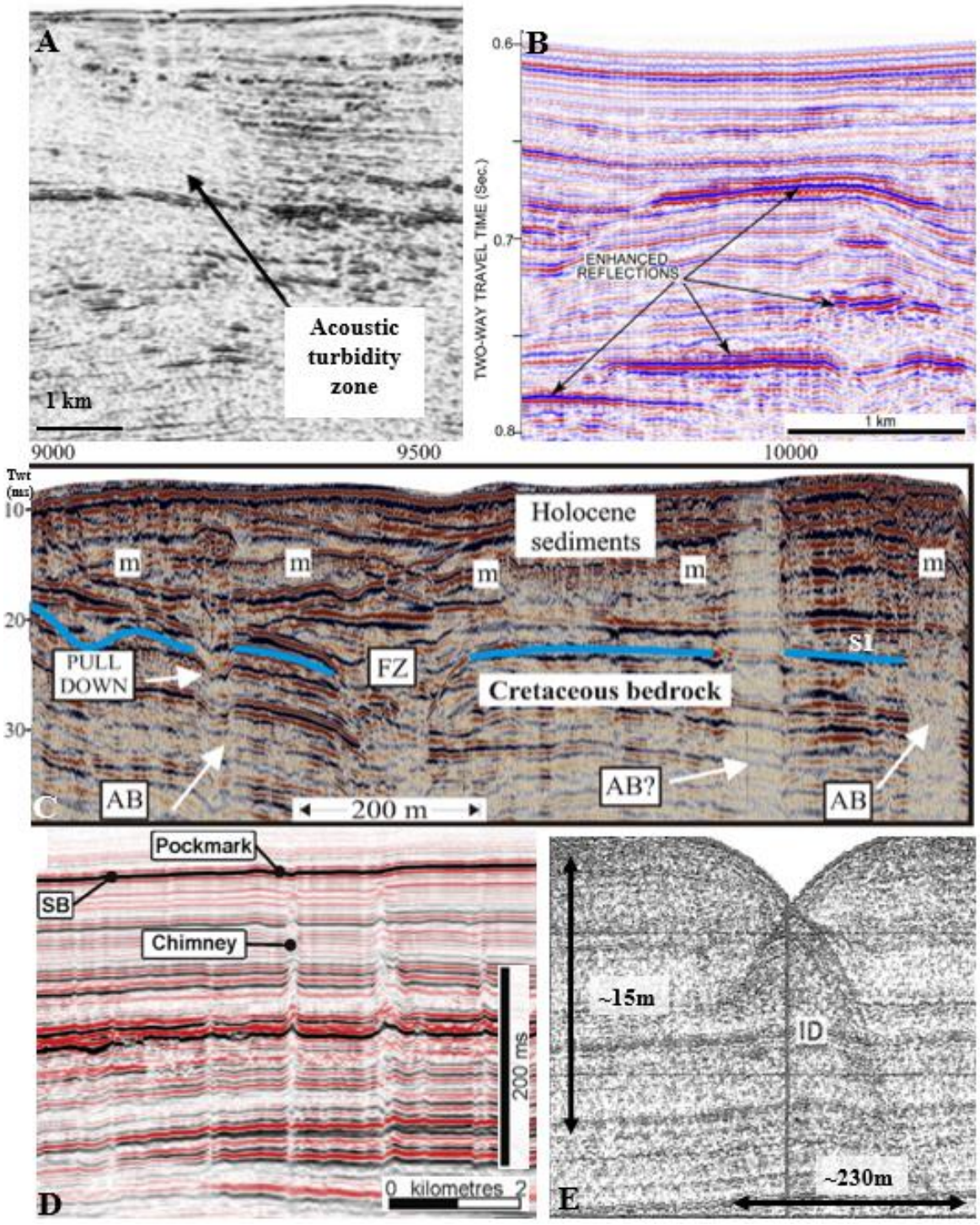

Figure 7 Geophysical indicators of the presence of gas and fluid flow in seismic data. **A** – Acoustic turbidity zone (from Ligtenberg, 2005*);* **B** – Seismic profile showing enhanced reflections, characterized by very high-amplitude positive polarity reflectors (from Cukur *et al*., 2013*);* **C** –Examples of acoustic blanking (AB) and a Pull Down from the Ria de Aveiro. FZ: fault zone; S1 – erosive horizon; m –seafloor multiple (adapted from Duarte *et al*., 2007)*;* **D** – Profile showing several chimneys with loss of coherence and subtle convex upwards deformation, from offshore Norway *(*Hustoft *et al*., 2010*);* **E** – Intrasedimentary doming (ID) beneath a seabed pockmark (Judd and Hovland, 2007).

Pull down of reflectors (Figure 7.c) correspond to coherent reflections depressed in relation to their lateral setting, located below units of gas-charged sediments. The pull down reflectors are interpreted as the result of the decrease in seismic velocity at sediments containing small amounts of free gas. If the gas-charged zone is thick enough this effect gives the impression that the sediments are sagging, due to a longer time travel of the seismic waves. The opposite effect, a pull up, would be caused by the presence of a high-velocity zone (Ligtenberg, 2005; Judd and Hovland, 2007; Duarte *et al.*, 2007).

2.3 Morphological expressions of Fluid Seepage

The morphological expression of seepage include a wide variety of features (Judd and Hovland, 2007), the two most common being the mud volcanoes and the pockmarks. These features are described in more details below.

2.3.1 Mud volcanoes

Mud volcanoes are defined as conical shape positive morphological features (Figure 8.a) formed as a result of the emission of semi-liquid material on the seafloor or on land (Milkov, 2000; Kopf, 2002; Dimitrov, 2002). The material extruded is a fluidized mixture of sediments dominated by clays (Magalhães, 2007). Usually this mixture includes rock fragments dragged from the sedimentary units crossed during the upward flow. The extruded material forms characteristic circular to elongated features that varies in shape and size, characterized by elevation of a conical shape structure from some centimeters to hundreds of meters high or by negative funnel-shaped forms (mud pools). In passive margins, such as the WIM, these structures occurs generally associated with thick sedimentary sequences composed of soft and fine-grained sediments at great depths that are moved upwards together with ascending fluids and expelled at the surface (Judd and Hovland, 2007; Magalhães, 2007; Talukder, 2012).

Mud volcanoes were described onshore and offshore in many places on Earth. Until the 1970s these structures were only recognized on land and in adjacent very shallow waters (Jakubov *et al.*, 1971 and Ali-Zade *et al.,* 1984 *in* Dimitrov, 2002). Examples of onshore mud volcanoes can be observed in Azerbaijan (e.g. Mazzini *et al.*, 2009; Bonini *et al.*, 2013; Antonielli *et al.*, 2014) and in Italy (Giammanco *et al.*, 2007; Heller *et al.*, 2012; Rainone *et al.*, 2015). With the development of equipment for underwater research, many mud volcanoes have been discovered on the sea floor in water depths between 500 and

5000 m, in regions like the Gulf of Cadiz (e.g. Somoza *et al*., 2003; Pinheiro *et al*., 2003; Medialdea *et al*., 2009; Palomino *et al*., 2015) and the Black Sea (e.g. Ivanov *et al*., 1996; Stadnitskaia *et al*., 2008; Xing and Spiess, 2015).

These features can be easily detected in reflection seismic profiles (Figure 8.b), when the host is a well stratified sedimentary sequence and with more difficulty in accretionary and overthrust complexes (Dimitrov, 2002). Their identification is based on the characteristic bathymetric positive expression at the seabed and on the existence of vertical, narrow zone lacking reflections or of chaotically disrupted, short reflections on the sub-seabed, beneath the seabed topographic high (Dimitrov, 2002; Magalhães, 2007).

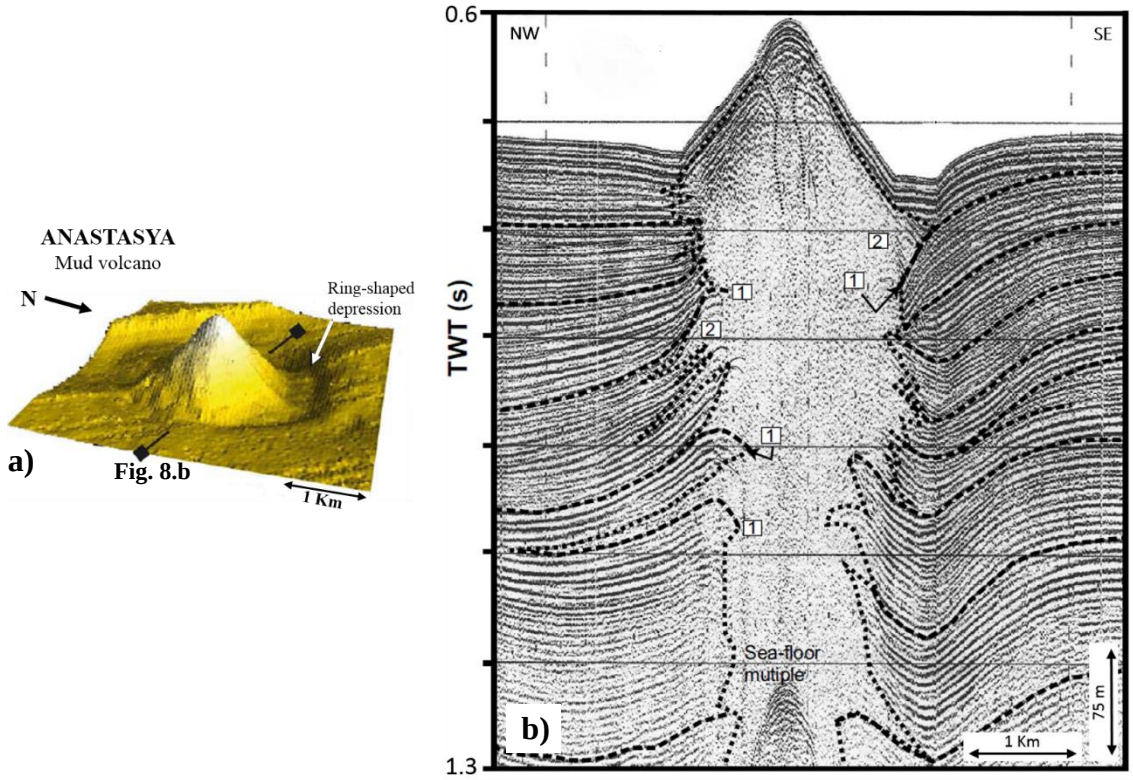

Figure 8 Anastasya mud volcano: **a)** multibeam bathymetry 3D image and **b)** single-channel sparker seimic profile (Somoza *et al*., 2003). **1**: Downward bending of reflectors; **2**: transparent facies.

2.3.2 Pockmarks

Pockmarks are crater like negative topographic features at the seabed (Figure 9.a) with a round to oval shape which vary in diameter from few meters to over 1 km (Judd and Hovland, 2007) and vary in depth between <1 m and up to 100 m. Pockmarks occur mostly in soft, low permeable fine-grained sediments, in large clusters or individually, in a wide variety of geological settings: continental shelves, slopes, rises and in the deep

ocean (Judd, 2003; Judd and Hovland, 2007). The pockmarks can be clearly distinguished on the seabed in high resolution seismic reflection profiles (Ligtenberg, 2005), as illustrated in Figure 9.b.

Pockmarks were first described by King and MacLean, 1970 on the continental shelf off Nova Scotia, Canada and then observed in many places all over the world (e.g. Judd and Hovland, 2007), in various depositional systems at water depths ranging from 30 m to over 3000 m (Gay *et al*., 2007).

Pockmarks are formed by the expulsion of fluids through the seabed, when the flux is rapid and abrupt (Talukder, 2012). Since the generation of fluids and its migration towards the seabed occur over geological time periods, fluids escape and, consequently, the pockmarks formation are either continuous or intermittent over extended periods of time. It is therefore frequently to find buried pockmarks in the seismic profiles, occurring vertically stacked or isolated, as in the Turkish shelf of the Black Sea (Çifçi *et al*., 2003) and in the slope of the Gulf of Cadiz (Baraza and Ercilla, 1996) suggesting that the migration of fluids is intermittent and periodically repeated in the geological time scale. Several reasons for the periodic interruption and reactivation of fluids seeping can be invoked, such as periodic sea-level changes, seismologically driven periodical overpressure conditions or cycles of fluid pressure build up under a sedimentary impermeable layer.

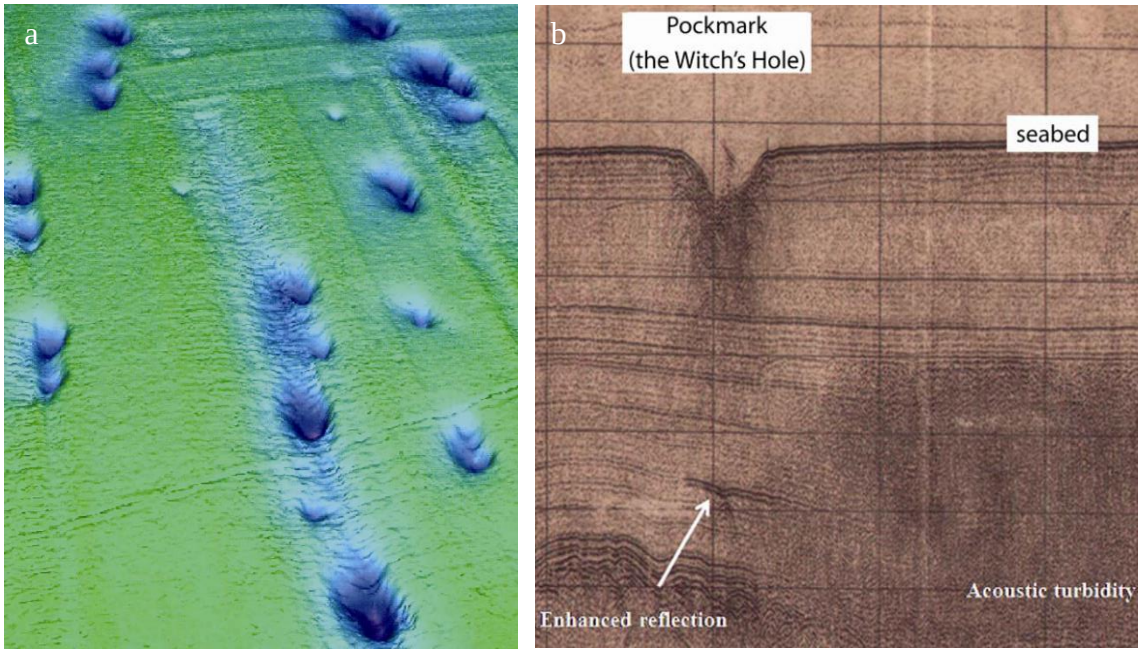

Figure 9 Appearance of pockmarks on the seabed, as imaged with multibeam bathymetry (**a**) and on a high resolution seismic reflection profile (**b**) (Judd and Hovland, 2007).

Çifçi *et al*. (2003) classified the pockmarks into four categories, according to their stage of formation (Figure 10). In the first stage, the gas accumulation in the uppermost sedimentary sequence under overpressure conditions causes an expulsion, in a single event, which fluidizes the sediments and lifts it into the water column forming a depression on the seabed. The fine-grained sediments are suspended in the water and drift away in the current leaving behind the coarse sediment that fall back to the seafloor. In the second stage, the lose sediment expulsion ceased and recent sediments started filling the depression formed in the previous first stage. In the third stage, the depression is completely filled by the sediments and the pockmark is buried. In the fourth stage, the gas expulsion is reactivated so that a new pockmark is formed in the seabed. Judd (2001) described an earlier stage to the abrupt expulsion of fluids, the accumulation of these fluid beneath the seabed. Where the gas accumulates close to the seabed, the excess pore fluid pressure may inflate the sediments to form a seabed dome.

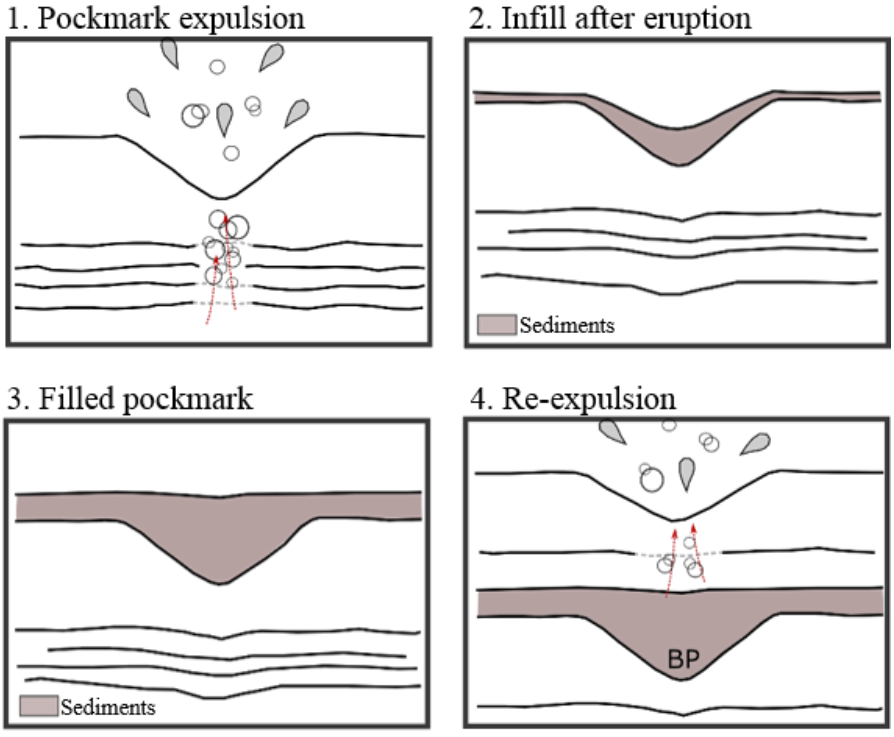

Figure 10 Schematic illustration for the evolution of vertically stacked pockmarks (adapted from Çiçfi *et al*., 2003). **Circles** and **drops** symbolize the fluids and the **red arrows** the fluid migration; **BP**: buried pockmark.

CHAPTER 3

GEOLOGICAL SETTING OF THE ESTREMADURA SPUR

The Estremadura Spur is a structural high with trapezoidal shape that is bounded by two deep canyons systems, the Nazaré and Lisbon (Mougenot, 1989; Badagola, 2008). It is the result of the overlay of the various tectonic cycles that affect the WIM since the Late Paleozoic until the present.

The Estremadura Spur is a positive relief with a triangular shape that lies offshore the central part of the Lusitanian Basin that resulted from the various continental rifting stages that led to the opening of the Atlantic ocean from Triassic through Early Cretaceous times and formation of the West Iberia passive Margin in the Late Cretaceous (Figure 11) (Pinheiro *et al*., 1996; Kullberg *et al*., 2013). The positive relief results from perpendicular tectonic inversion of the LB in Cenozoic times with respect to the direction of opening of the rift. The rifting and inversion tectonics reactivated deep seated faults that were inherited from the Paleozoic Variscan orogeny.

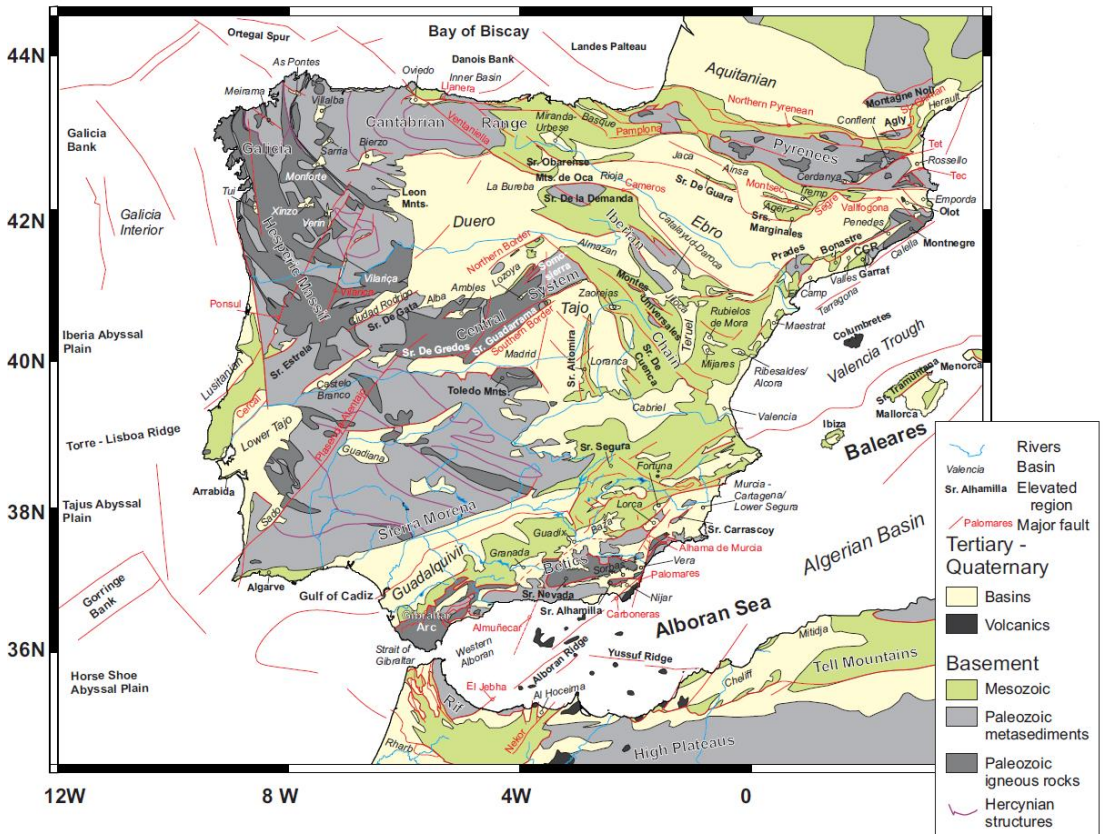

Figure 11 Iberian Peninsula and western Mediterranean schematic geological map (Andeweg, 2002).

3.1 Geodynamic evolution of the Western Iberian Margin

The WIM began to develop during the early stages of continental rifting that led to the opening of the North Atlantic Ocean, from the Triassic through the Early Cretaceous (Rasmussen *et al.*, 1998; Pinheiro *et al.*, 1996). The rocks that form the basement of the WIM are part of the Hesperian Massif, which incorporate Precambrian and Paleozoic rocks. Since the beginning of the Cenozoic the evolution of WIM was characterized by periods of compression and tectonic inversion related to the Alpine orogeny (Pyrenean and Betic phases), resulting in the uplift of some regions of the margin, such as the ES.

3.1.1 The Late Paleozoic and Mesozoic Evolution

The Variscan Orogeny

The rocks that form the basement of the WIM are part of the Hesperian Massif, a segment of the Variscan Orogenic Belt that extends all over Europe. This orogenic belt resulted from the convergence and collision of two major continents, Laurasia and Gondwana, during the Late Paleozoic (Devonian-Permian) Variscan Orogeny, which led to the formation of the supercontinent Pangea. The deformed rocks that constitute the WIM

basement are from Upper Proterozoic to Carboniferous age and are often metamorphosed and intruded by different types of granitoids (Ribeiro, 2013a).

Opening of the North Atlantic

During the Mesozoic the evolution of West Iberia was controlled by the opening of the North Atlantic Ocean. Throughout the Triassic, the supercontinent Pangea began fracturing, leading to the formation of epicontinental seas, first by the thinning of the continental lithosphere (the continental rifting created graben and half-graben structures where continental deposits and evaporates sedimented) followed by whole lithospheric rupture that accommodated the initial formation of oceanic lithosphere and subsequently by the formation and development of the West Iberia passive margin.

The western Iberia Atlantic margin evolved as the conjugate of the Grand Banks area after four distinct phases of rifting during Late Triassic, Lower Jurassic, Upper Jurassic and Early Cretaceous (Pinheiro *et al.*, 1996; Rasmussen *et al.*, 1998; Kullberg *et al*., 2013). The continental stretching led to the oceanization of the North Atlantic and the process of continental breakup progressively migrated from the south to the north, along the margin (Pinheiro *et al*., 1996; Alves *et al.* 2006). The complete separation of the Iberian margin from North America in the late Aptian (Driscoll *et al*., 1995; Pinheiro *et al.*, 1996) was followed by the development of a separate micro-plate successively attached to Eurasia and Africa – the Iberian plate (Sibuet *et al*., 2007; Soares *et al*., 2012; Ribeiro, 2013b). This micro-plate is limited by four major lithospheric structures: the Charlie Gibbs Fracture Zone in the north, the Açores-Gibraltar Fracture Zone in the south, the Atlantic Rift to the west and the Tethyan Rift in the south and southeast. The continued northward migration of seafloor spreading drove the ocean opening in the Bay of Biscay, in the Late Cretaceous and the counter-clockwise and southeast motion of the Iberian plate, from the Late Cretaceous to Paleogene (Pinheiro *et al*., 1996).

In the WIM, several extensional basins evolved during the Mesozoic; they are, from south to north, the Alentejo Basin, the Lusitanian Basin, the Peniche Basin, the Porto Basin and the internal and external Galicia basins (Pais *et al*., 2012; Kullberg *et al*., 2013; Figure 12). The formation and evolution of western basins were mainly controlled by deep normal faults oriented NNE–SSW to N–S and NW–SE, corresponding to the reactivations of inherited Variscan faults. The basins are separated by major transfer faults oriented from NE–SW to ENE–WSW (from north to south: the Aveiro Fault, the Nazaré Fault and

the Arrábida Fault; Figure 12) that played important roles during the Alpine compression. Most of the Mesozoic basins are located offshore in the present day, with the exception of about a third of the Lusitanian Basin that crops out in the central part of the West Iberia Margin as a result of tectonic inversion in Cenozoic times.

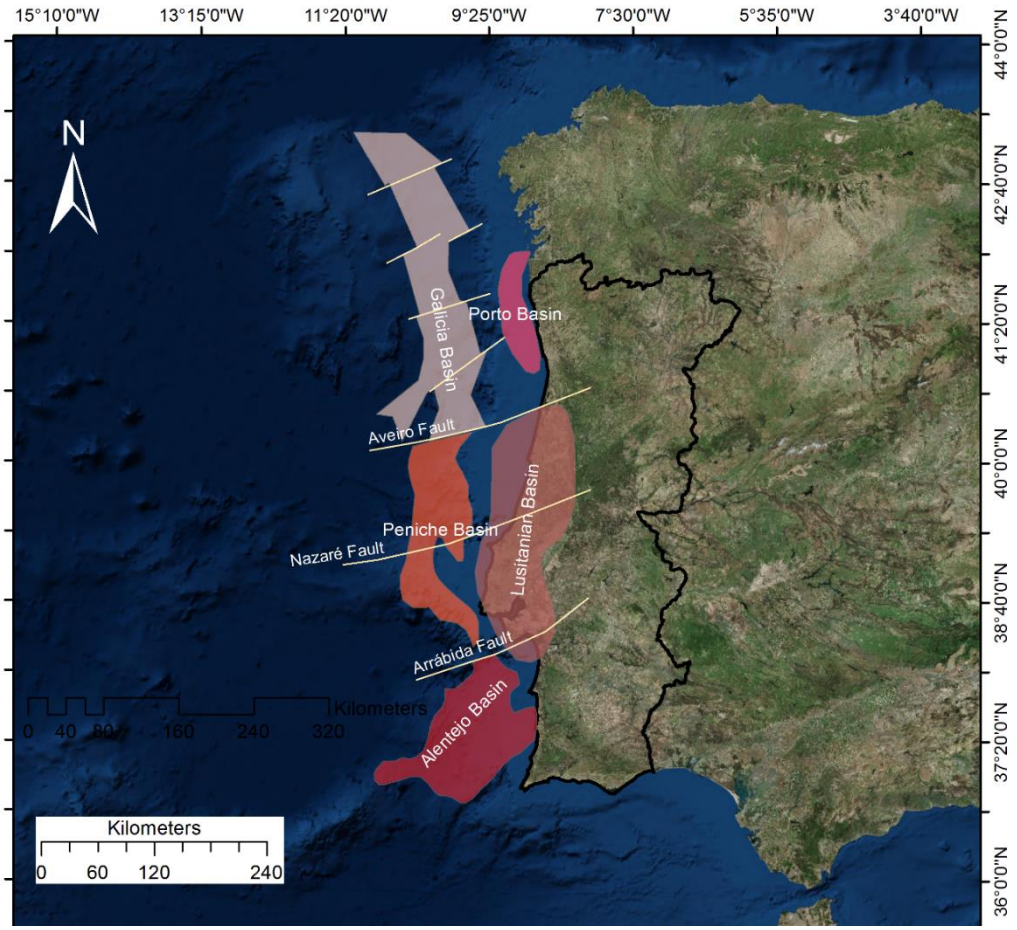

Figure 12 Geographic localization of the WIM Portuguese sedimentary basins and major faults (adapted from Kullberg *et al*., 2013).

3.1.2 The Cenozoic Alpine Orogeny

The Cenozoic evolution of Iberia was marked by the Alpine compressional phases that affected all of southern Eurasia. At the end of the Cretaceous, the Iberian Peninsula was subjected to a compressive tectonic regime, as a result of the counter-clockwise and southeast motion of the Iberian plate. This led to the tectonic inversion of the structures formed during the Mesozoic extensional periods. The orientation of the maximum compression was oriented N–S to NNE–SSW from the Late Cretaceous until the Paleogene (Kullberg *et al*., 2013). During the Miocene the compression direction changed to NNW–SSE, evolving to NW–SE to WNW–ESE in the Pliocene-Quaternary (Ribeiro

et al., 1996; Cunha *et al*., 2012). The tectonic inversion occurred in two main phases: the Pyrenean (Late Cretaceous – Late Eocene) and the Betic (Oligocene – Late Miocene) phase.

In the Pyrenean phase the Iberian micro-plate moved, along with the African plate, northward against the Eurasian Plate. As a consequence of the convergence between Iberia and Europe, the southern margin of the Bay of Biscay become active, the Cantabrian subduction zone formed with northwards subduction of oceanic crust that led ultimately to the continental collision and formation of the Pyrenees. This caused the inversion and shortening of some extensional structures. The crustal shortening and subsequent intense intraplate deformation were responsible for a drastic change in the continental topography of the Iberian plate (Casas-Sainz and De Vicente, 2009; De Vicente *et al.* 2011). The peak of compression occurred in the middle Eocene, with the formation of the Pyrenees collisional chain with E–W oriented mountain belts rising to approximately 2000 m (De Vicente *et al.* 2011).

In the Betic phase, the Iberian microplate started to move along with the Eurasia plate. Consequently, Iberia converged with the African plate (maximum compression N–S with the paroxysm in the Tortonian) in the southern border of Iberia (Açores-Gibraltar Fracture Zone). During the Betic phase a large-scale shortening of Iberia occurred that caused lithospheric folding (e.g. De Vicente *et al.* 2011). As a result of this compressional phase the Betic chain formed in southeastern Iberia. This collisional mountain chain trends in ENE–WSW orientation and rises to around 700 m (Casas-Sainz and De Vicente, 2009).

The evolution of the Betic-Rif orogen is intimately related to the mostly northwards subduction of the Tethyan ocean, continental collision and development of back-arc basins in the West Mediterranean. As a consequence the Betic-Rif arc formed, possibly underplating and mantle exhumation and thrusting occurred (Ronda peridotite massif) and the a remnant of the Jurassic ocean rolled back into the Atlantic Ocean forming the Gibraltar orogenic arc and the Gulf of Cadiz Accretionary Wedge (Gutscher *et al*., 2002, Gutscher *et al*., 2012, Terrinha *et al*., 2009; Duarte *et al*., 2013). The last mountain building phases of this processes apparently strongly diminished at the end of the Miocene and deformation concentrated in the oceanic domain of the Africa-Iberia tectonic boundary (Zittellini *et al*., 2009).

Throughout the Pliocene there has been some tectonic stability (Pais *et al*., 2012). In the Late Pliocene and Quaternary, the tectonic regime became compressive with maximum compression of NW–SE to WNW–ESE probably due to changes of the Açores-Gibraltar

tectonic regime (Terrinha *et al.* 2009). During the Cenozoic many basins with different dimensions developed, bordered by topographic highs related to thrusts or strike-slip faults (De Vicente *et al*., 2011). In the central area of Iberia, the main uplifted zones are the Iberian Chain and the Central System (Estrela-Seia-Lousã and Aire-Candeeiros-Montejunto) that extends westwards to the Estremenho Massif and the Estremadura Spur in the WIM offshore.

The WIM was deformed by the compressional Alpine tectonics principally during the Betic phase during Miocene times (Pais *et al*., 2012). The two Cenozoic compressional episodes effects on the margin was the formation of folds and the reactivation of old Variscan structures (also reactivated onshore). The WIM and its onshore extension were differentiated into a series of uplifted blocks (like the Estremadura Spur and its onshore prolongation) and areas of subsidence (e.g. Lower Tagus Basin) (Mougenot, 1989; Rasmussen *et al*., 1998). The tectonic inversion is registered in the Lusitanian Basin, where the maximum compression has a NW–SE direction (Kullberg *et al.*, 2000). The inverted structures in the basin are anticlines associated with thrust faults. These faults were Late Variscan strike-slip faults, striking between ENE–WSW and NE–SW that were reactivated as reverse faults with NW and SE verging thrusts. The inversion is better expressed in the onshore sector of the basin, since the sedimentary record and tectonic structures are almost non-existent due to an important and long lasting uplift of the entire region. Cenozoic sub-basins developed in the inverted areas of the Lusitanian Basin generally conditioned by local halokinesis triggered in different times by different processes, including Cenozoic compression or by thin-skinned structures. The organization of these dispersed basins is here simplified since most of the basins are, in fact, sub-basins of larger basins that were exhumed presumably from the Late Neogene to the Present.

3.2 Stratigraphy

The WIM sedimentary fill is composed of Mesozoic and Cenozoic deposits that rest over a Variscan deformed and metamorphosed basement, like in the onshore equivalent. During the inversion of the tectonic regime in the Cenozoic the basin was uplifted, which lead to the erosion of the emerged areas. As a result, the Cenozoic sedimentary sequence in the onshore only occurs in small basins, where the erosion was less intense. Contrariwise, in the offshore the Cenozoic sedimentation has a significant thickness and

lateral continuity of the deposits. *Shell Prospex Portuguesa* drilled two wells (17 C-1 and 20 B-1) in the Estremadura Spur (Figure 13) in the late 70s, which allowed to know the Mesozoic stratigraphy of this offshore region of WIM with more detail (the wells sequence stratigraphy is summarized in Table 1 and Table 2). It was also used the onshore sedimentary sequence as an analogue.

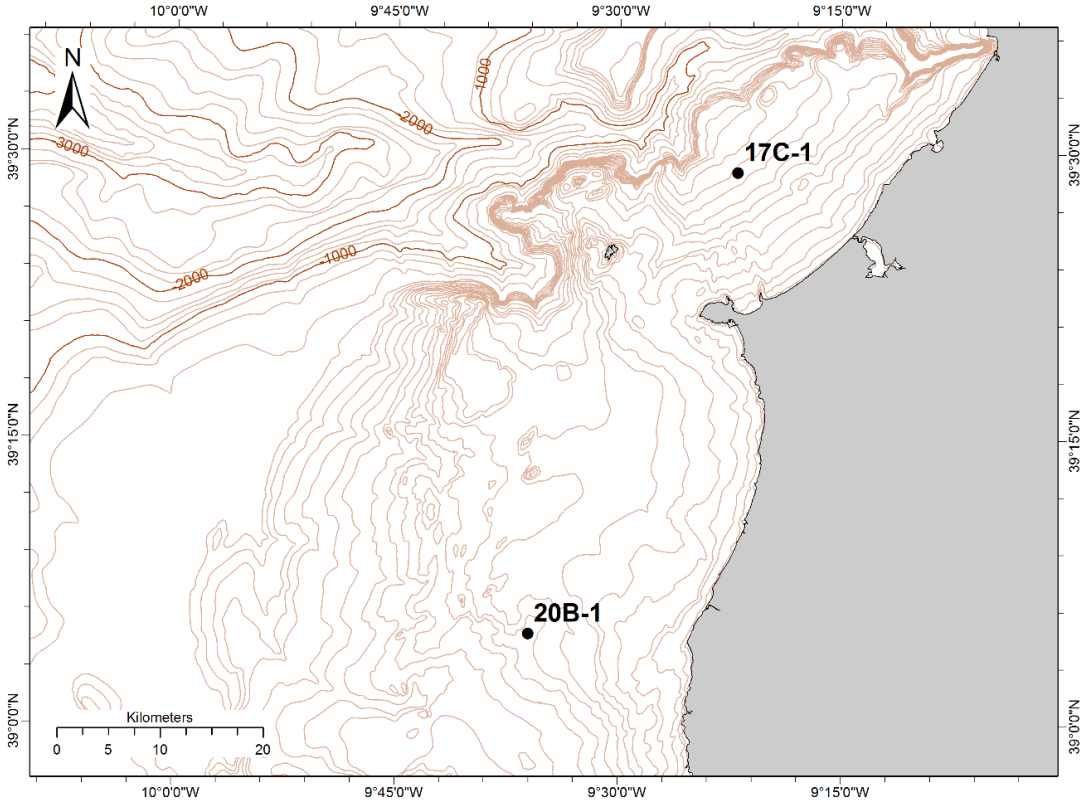

Figure 13 Localization of the exploration wells drilled in the Estremadura Spur region, 17C-1 and 20B-1. Equidistance: 10 m (between 0 and 200 m); 200 m (below 200 m).

Table 1 Formations drilled by well 17 C-1.

Depth (mbsf)	Formation/Member	Age
Seabed - 376	Alcobaça Fm	Kimmeridgian
-	unconformity	-
376 - 1058	Brenha Fm	Callovian – Upper Sinemurian
1058 – 1230	Coimbra Fm	Sinemurian
1230 – 1481	Dagorda Fm, Dol. Mbr	Hettangian
1481 – 1799	Dagorda Fm, Salt-Dol Mbr	Early Lower Jurassic –

1799 - 2148	Dagorda Fm, Massive Salt mbr Equ	Upper Triassic
2148 – 2195	Silves Fm, Shale-Lst Mbr	Upper Triassic
2195 – 2308	Silves Fm	Triassic
-	unconformity	-
2308 – 2402 (T.D.)	Basement	Pre-Mesozoic

Table 2 Formations drilled by well 20 B-1.

Depth (mbsf)	Formation	Age
Seabed - 181	-	Valanginian
-	disconformity	-
181 - 793	Candeeiros Fm	Bathonian – Callovian
793 - 2285	Brenha Fm	Pliensbachian – Bajocian
2288 – 2541 (TD)	Coimbra – Dagorda Fm	(?) Hettangian – Sinemurian

3.2.1 Paleozoic

The Paleozoic units represented in the area are igneous (leucogranite) and metasedimentary (gneiss and micaschist) rocks, found at the islands of Berlenga and Farilhões, respectively. These islands are the only vestige of the Variscan basement, which underlay the Mesozoic and Cenozoic units, that outcrops at the surface. In the well 17 C-1 it was encountered rocks that constitute the pre-Mesozoic basement: tectonized granite, which was alike to the granite that forms the Berlenga Islands (Shell Prospex Portuguesa, 1976a).

3.2.2 Mesozoic

Mesozoic sediments constitute the foundations of the margin and correspond to the offshore part of the Lusitanian basin (Alves *et al*., 2003). During Upper Triassic coarse arkoses and sub-arkoses were deposited followed by sandy-pelitic and laminated pelitic with carbonate fragments and arkosandstones from the Conraria Formation. From Upper Triassic to Lower Jurassic evaporitic rocks were deposited, in the deeper regions of the margin (graben and half-graben structures). In well 17 C-1 was observed that these deposits covers unconformably the underlying Paleozoic basement. It was identified the

Silves Formation, which consists of clay and claystone interbedded with small salt stringers. The Silves Formation is overlain by a sequence of salt with dolomitic, calcareous, anhydritic and argillaceous stringers, which is the Salt Member of the Dagorda Formation. In the earliest Lower Jurassic occurred fault controlled regional subsidence (Rasmussen *et al*., 1998). This marks the beginning of a marine transgression, that lead to the deposition of dolomitic lime-mudstone grading to interbedded dolomite and anhydrite and then to anhydrite with argillaceous stringers (in wells 17 C-1 and possibly 20 B-1) that corresponds to the Dagorda Marls (Dolomite Member of the Dagorda Formation). This sequence is overlain by compacted and cemented lime-mudstones, which occasionally grade to packstone and grainstones (Shell Prospex Portuguesa, 1976a; 1976b), belonging to the Coimbra Formation (observed in both wells). In 20B-1 this formation showed minor gas readings, but further studies did not indicate the presence of hydrocarbons. The transgression initiated in the Lower Jurassic continues during the Middle Jurassic (Rasmussen *et al*., 1998), but it does not affect the entire region of the Estremadura Spur (Figure 14); the area between Cabo Raso and Ericeira was emerged during much of the Middle Jurassic (Berthou, 1973 in Badagola, 2008).

The Brenha Formation was observed in both wells, formed by argillaceous limestone interbedded with marlstones and claystones deposited in the Lower-Middle Jurassic (Upper Sinemurian – Callovian in well 17 C-1; Pliensbachian – Bajocian in well 20 B-1). In the well 17 C-1, located in the area north to Peniche, this deeper shelf facies sequence constitute the majority of the Middle Jurassic sedimentary deposits, but in the well 20 B-1 that is located in the middle of the Estremadura Spur, a large portion of the Middle Jurassic (Bathonian – Callovian) consists of carbonate platform sediments of the Candeeiros Formation: particle supported limestone of a shallow marine, mainly high energy depositional environment.

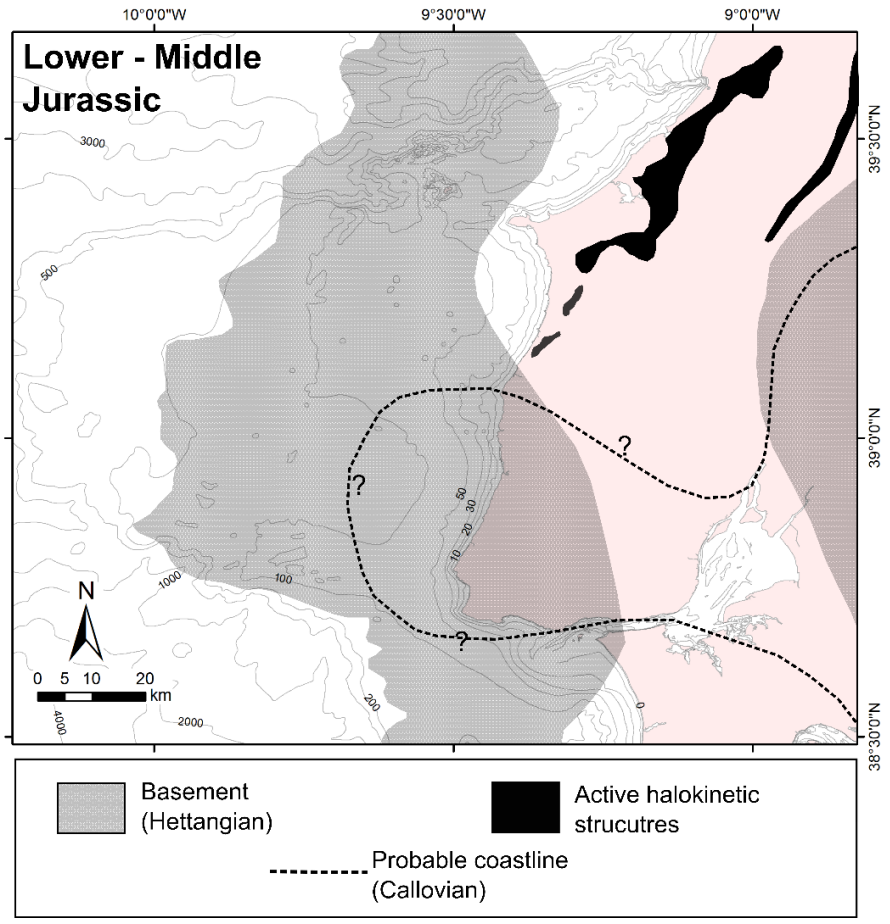

Figure 14 Paleogeographic scheme of the Estremadura region (off- and onshore) during the Lower and Middle Jurassic (adapted from Mougenot, 1976 *in* Badagola, 2008).

The base of Upper Jurassic is marked by an important unconformity, due to the occurrence of a marine regression. The sedimentary hiatus of the Upper Callovian – Lower Oxfordian is associated with an important episode of crustal uplift (Kullberg, 2000; Terrinha *et al*., 2002), which was followed by a strong subsidence of the basin. In the Kimmeridgian occurred the deposition of a detritic series (Figure 15) consisting of sandstone, clay and conglomerates, characteristic of a sedimentary environment of shallow depth shelf (Grés Superiores Formation). This evidenced the resuming of marine conditions in the Late Oxfordian. In the well 17 C-1 it was observed a sequence of conglomerates with abundant igneous and metamorphic rock fragments, limestone pebbles, some red clay and limestone intercalations, interpreted as belonging to the Alcobaça Formation (or Grés Superiores Formation).

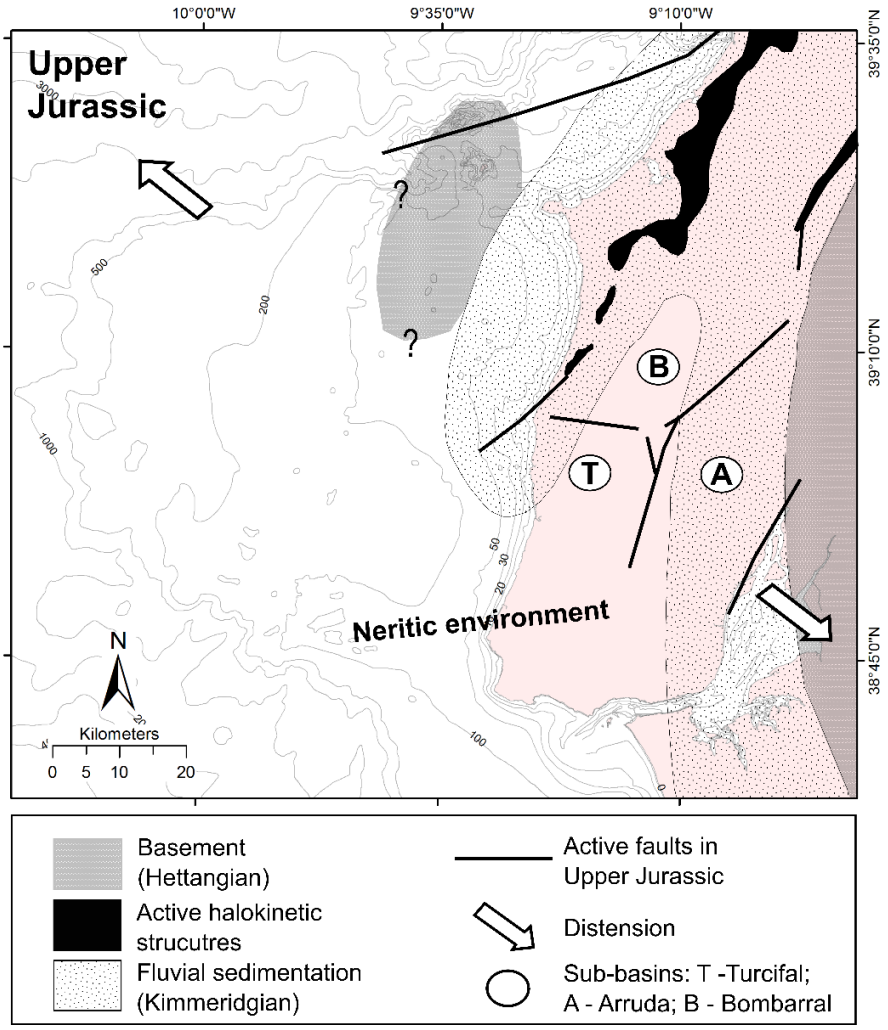

Figure 15 Paleogeographic scheme for the Estremadura region (off- and onshore) during the Upper Jurassic (adapted from Mougenot, 1976 *in* Badagola, 2008).

The lowermost Cretaceous sedimentary sequence is missing in most of the Lusitanian Basin (Rasmussen *et al*., 1998, Dinis *et al*., 2008). From the Valanginian to the Early Aptian occurred the deposition of fluvial sediments of the Torres Vedras Formation. In the 20 B-1 well a sequence of lime mudstones and marls of the Valanginian, overlay unconformably the Alcobaça Formation. The sedimentation sequence of the Lower Cretaceous was dominated by mixed carbonate-siliciclastic systems (Rasmussen *et al.,* 1998): such systems were characterized by the deposition of shallow carbonates on topographic highs, shifting laterally to fluvial-deltaic siliciclastic deposits near the shore and to marine shale and limestone towards the deeper parts of the basin (e.g. Wilson, 1988; Rasmussen *et al.,* 1998). During this period there are several transgressive-regressive shifts with a regressive maximum in the Barremian (causing the emersion of the area that corresponds to the actual continental territory) and other important regional

event of erosion in the upper Aptian (Kullberg *et al*., 2013). It was marked by the influx of high-energy clastic material and the installation of fluvial deposits system throughout the basin (Figure 16).

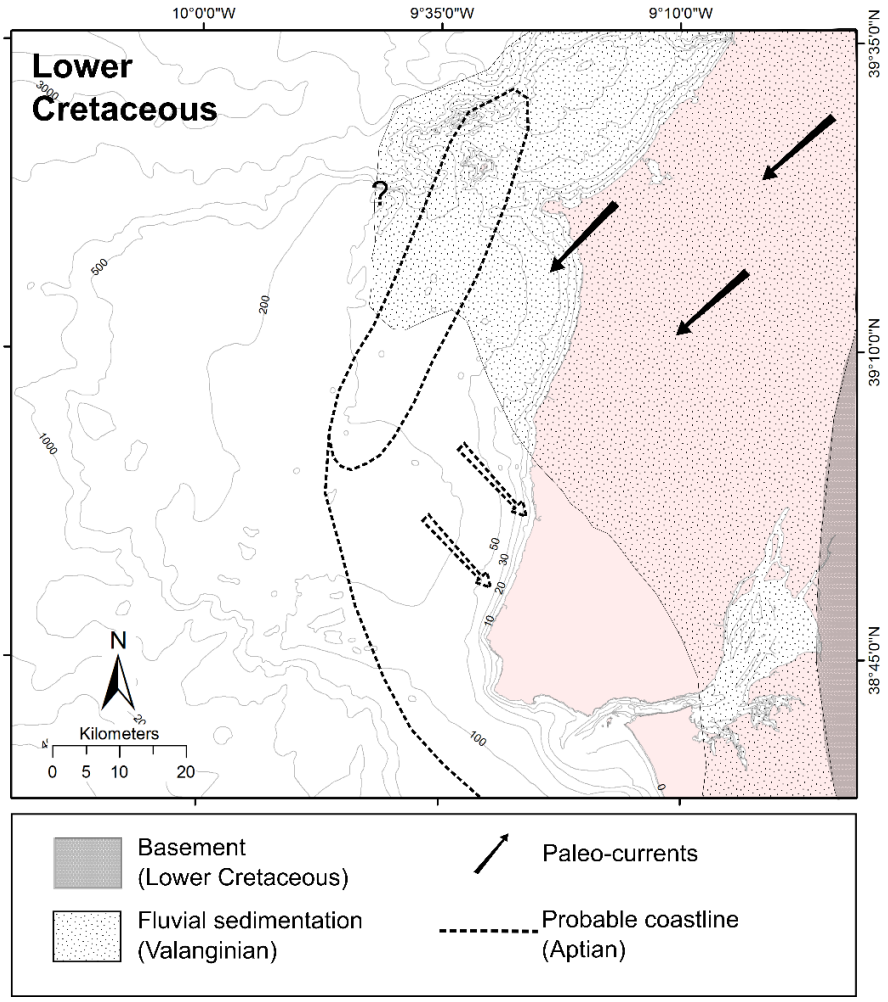

Figure 16 Paleogeographic scheme for the Estremadura region (off- and onshore) during the Lower Cretaceous (adapted from Mougenot, 1976 *in* Badagola, 2008).

In the beginning of the Late Cretaceous the sea level rose again until the Late Cenomanian, causing the expansion of the carbonate platform towards north and east (Kullberg *et al*., 2013) and the retraction of the adjacent clastic systems (Figure 17). In the end of Cenomanian the Nazaré Fault was reactivated causing the uplift of areas to the south of this fault, causing a northward displacement of marine sedimentation (Berthou, 1973; Berthou and Lauverjat, 1979; Boillot *et al.* 1972; 1975 *in* Pinheiro *et al*., 1996).

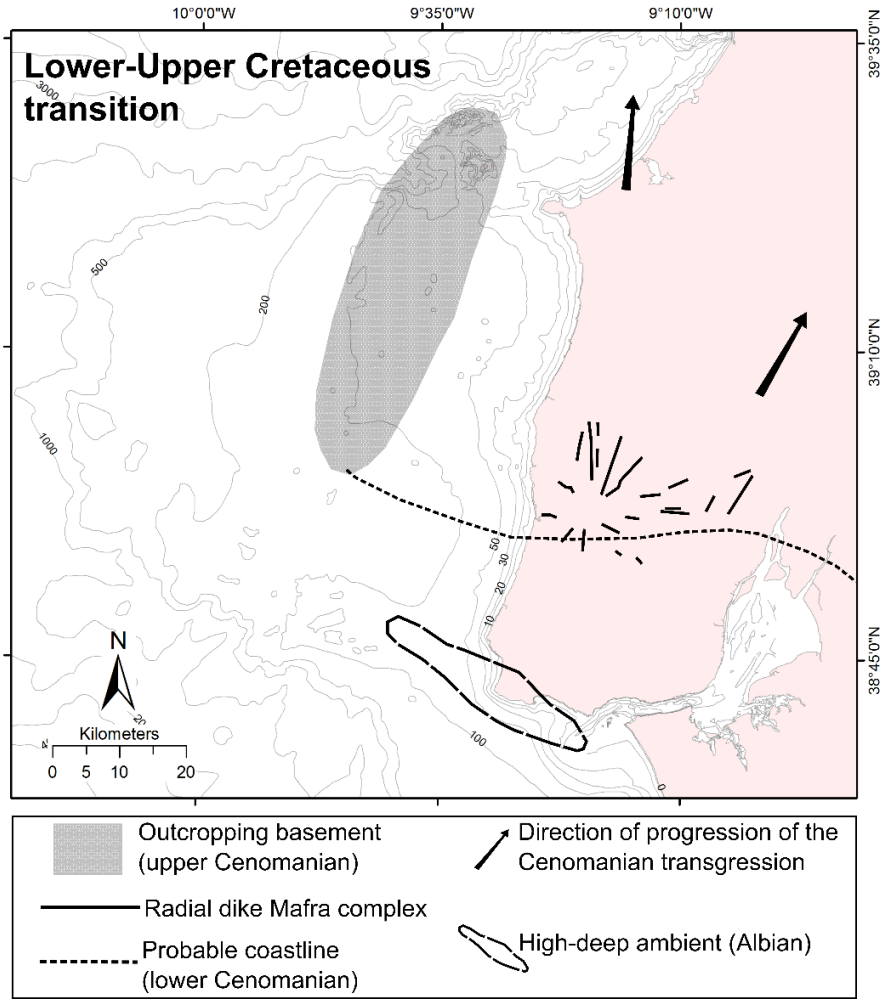

Figure 17 Paleogene scheme for the Estremadura region (off- and onshore) during the transition of Lower to Upper Cretaceous (adapted from Mougenot, 1976 *in* Badagola, 2008).

The Cenomanian-Turonian boundary is marked by an unconformity and associated karstifications (Kullberg *et al.*, 2013). In the Late Campanian-Maastrichtian (probably during the middle Campanian) occurred the principal phase of the Nazaré Fault reactivation as a thrust verging to NW (Cunha and Pena dos Reis, 1994 and Pinheiro *et al.*, 1996) that led to the uplift and sub-aerial exposure of the Estremadura region and of an important portion of the continental shelf establishing in the Cretaceous–Paleogene transition (Figure 18), a forced regressive cycle.

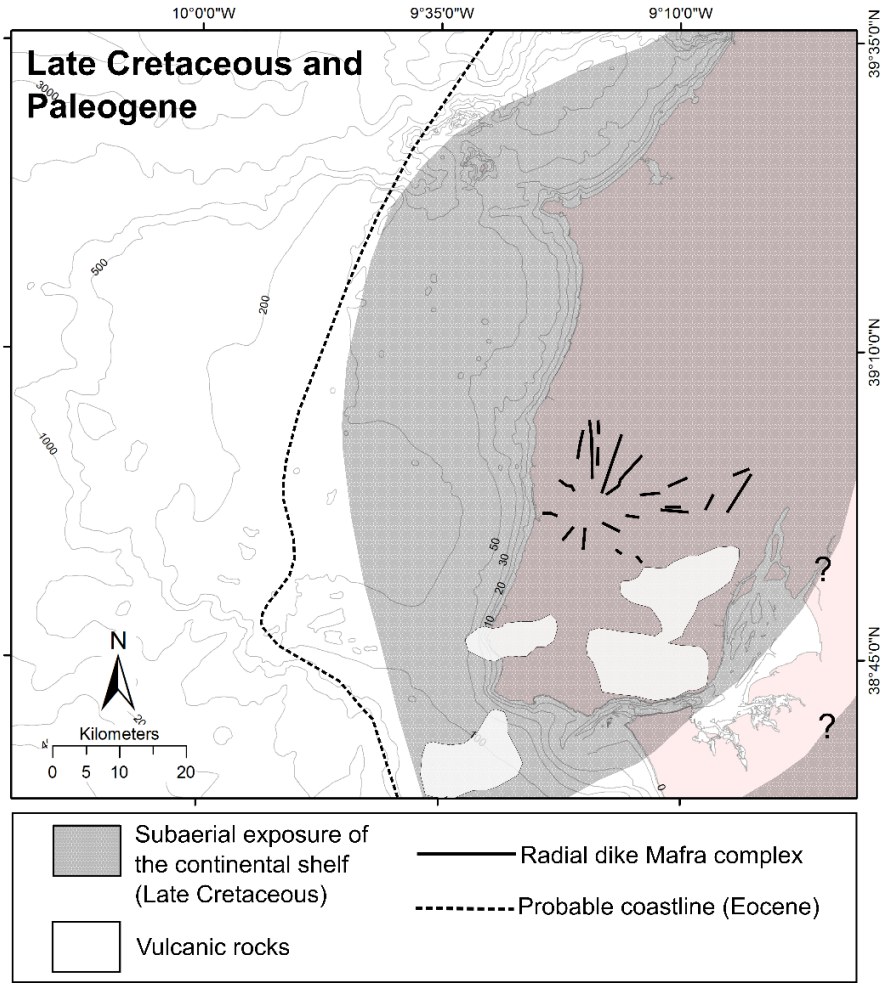

Figure 18 Paleogeographic scheme of the Estremadura region (off- and onshore) during the Late Cretaceous and Paleogene (adapted from Mougenot, 1976 *in* Badagola, 2008).

3.2.3 Cenozoic

During the beginning of the Cenozoic occurred the events of tectonic inversion related to the Pyrenean phase of the Alpine orogeny. Therefore, the Paleogene deposits are rare on the onshore sector of central Portugal, were the tectonic inversion is more intense (Mougenot, 1989; Pais *et al*., 2012) being only deposited in local sub-basins. Sedimentation of the continental sequences of Grés do Buçaco (siliciclastic sediments predominantly of granitic origin, with common clasts of quartz, quartzite and schist) and Benfica Complex (shallow limestones deposited during the Eocene and shallow marine sands, conglomerates and red marls during the Oligocene). In the offshore the Paleogene deposits are represented north of the Nazaré Canyon and appear locally south of the canyon (Musellec, 1974; Mougenot, 1976; 1989). Clastic deposition continued during the Neogene, with thick sedimentary sequences deposited in local basins (Rasmussen *et al.*, 1998), controlled by various phases of tectonic deformation. In the Miocene occurred the

sedimentation of fine sand, lacustrine and shallow marine clastic and carbonate deposition (Pinheiro *et al.*, 1996) and the Pliocene and Quaternary was marked by the deposition of siliciclastic sediments associated to transgression and regression cycles, which led to the formation of several generations of protofluvial deltas and prograding wedges truncated by ravinement surfaces (Mougenot, 1989). An important hiatus separates the Eocene–Miocene succession from the Pliocene–Pleistocene succession. It is associated with the compressional movements that began in the Middle Miocene, related to the Betic phase of the Alpine orogeny.

Since the Upper Pliocene new tectonic pulses and various glacio-eustatic variations led to the erosion and overprint of the Neogene sedimentary sequence (Vanney and Mougenot, 1981; Cachão and Silva, 2000). These variations had several effects on the WIM, such as continental shelf and coastal areas were eroded, sedimentary bodies advanced towards the shelf and upper slope and occurred the incision of major submarine canyons and gullies on the continental slope (Mougenot, 1988; Dias *et al.*, 2000). The stratigraphic structures observed in the Quaternary consist of progradational wedges, eroded at the top, and paleo-valleys in the continental shelf (Lobo *et al.*, 2015). Associated with the sea-level regression stages occurred a profound erosion in the inner continental shelf and continental slope. The most recent lowstand stage is related to the last glacial maximum (LGM) that occurred at ~18 ka BP (Dias *et al.*, 2000; Rodrigues *et al.*, 2000). At that time the sea-level was below 140 m depth (Figure 19) and the inner part of the continental shelf was enduring subaerial exposure (Dias, 1987).

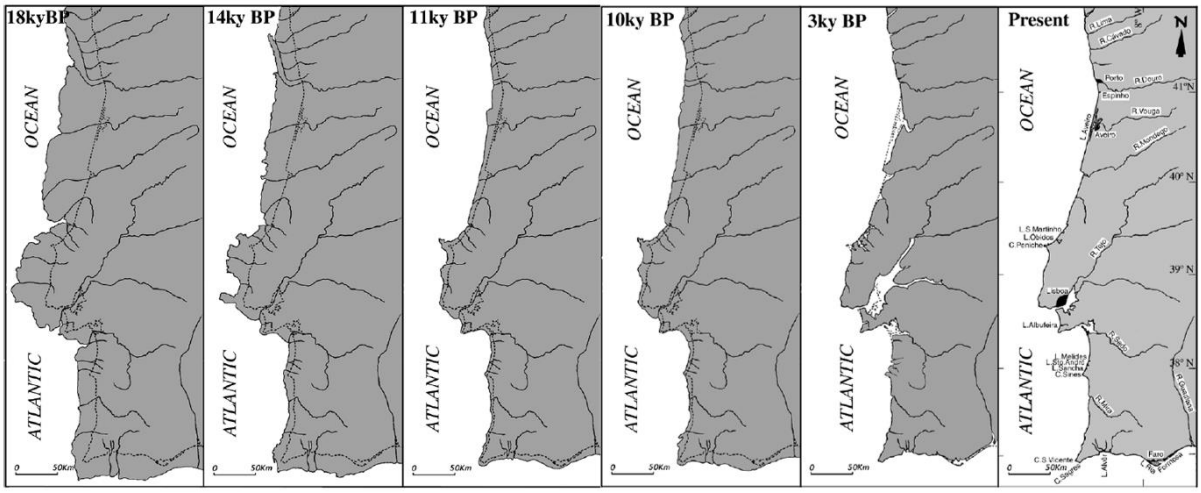

Figure 19 Evolution of the Portuguese coastline since the LGM (Dias *et al.*, 2000).

With the end of this glacial period in the Late Pleistocene (13–11 ka), the sea-level started to rise leading to the eastwards migration of the coastline (Lobo *et al*., 2015; Figure 19). The continental shelf exposed during the LGM become submerged and the sediments started to accumulate in the shelf (filling of valleys and canyons formed during the LGM). This tendency was disturbed by a rapid and drastic climate crisis (Younger Dryas; 11 ka), attributed to the massive inflow of ice meltwaters into the Atlantic Ocean (Dias *et al*., 2000). This crises interrupted the thermohaline circulation and led to a global cooling and to the development of more ice masses to each is associated a sea-level fall of about 60 m below its actual level. In response to the lowering of the sea-level renewed river erosion of the sedimentary infill of estuaries occurred, leading to massive influx of terrigenous sediments (coarse-grained sand and gravel) on the shelf (Dias *et al.,* 2000), deposited in thick shore bars. The finer material was transported by shelf currents to greater depths (Rodrigues et al., 2000). During the Holocene the sea-level rise rapidly between 10 and 8 ka (Figure 19) and reached its present level between 5 to 2.5 ka (Figure 19), when the rates of the sea-level rise were attenuated (Dias, 1987). These transgression spread throughout the margin and was responsible for the formation of progradational coastal sand bodies on the continental shelf (Dias *et al*., 2000).

3.2.4 Magmatism

Between the Nazaré Fault and the north of Lisbon, two important phases of igneous activity in the Lusitanian Basin were recognized (Miranda *et al*., 2009; Kullberg *et al*., 2013). The first phase occurred from at least 148 to 140 Ma (Mata *et al*., 2015) and was characterized by its transitional geochemistry (mildly alkaline magmas). This phase is associated with the late stages of the extensional regime associated with the Iberia-Newfoundland rifting, during the Jurassic-Cretaceous transition.

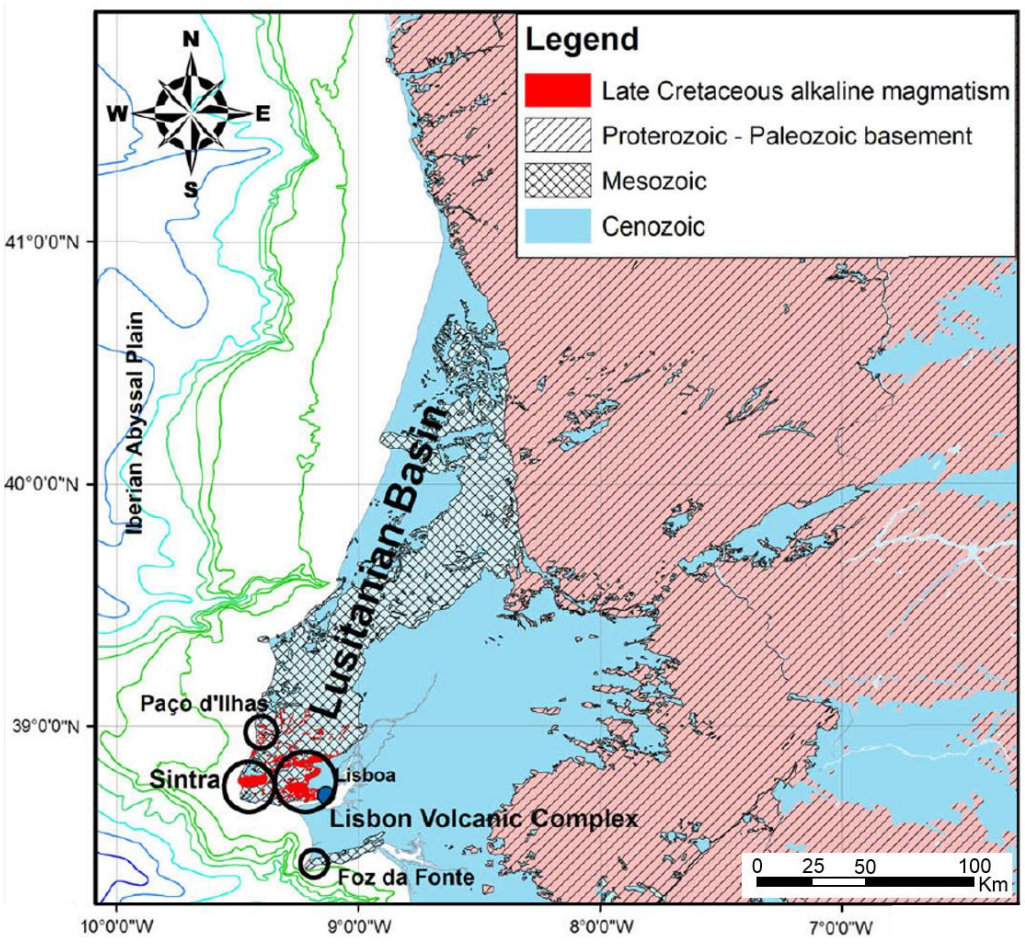

Figure 20 Main magmatic occurrences in the Lusitanian Basin (adapted from Miranda *et al*., 2009).

In the Late Cretaceous (Figure 20), from 94 to 69 Ma, another important phase of igneous activity was recognized in the Estremadura Spur. This episode is characterized by the alkaline chemical signature bodies that can be found in the Tore-Madeira Rise and in the Estremadura Spur (Neres *et al*., 2014), related with the Sintra Intrusive Complex, the Radial Dyke swarm of Mafra Complex and the basaltic Lisbon Volcanic Complex.

3.3 Estremadura Spur

3.3.1 Geological Evolution

The morpho-tectonic evolution of the ES continental shelf (Figure 21) was studied in detail by Badagola (2008) who concluded that the tectonic regime was the main conditioner for the evolution of the ES continental shelf. The same author established four important phases to the Neogene and Quaternary geological evolution of the ES shelf, as follows below.

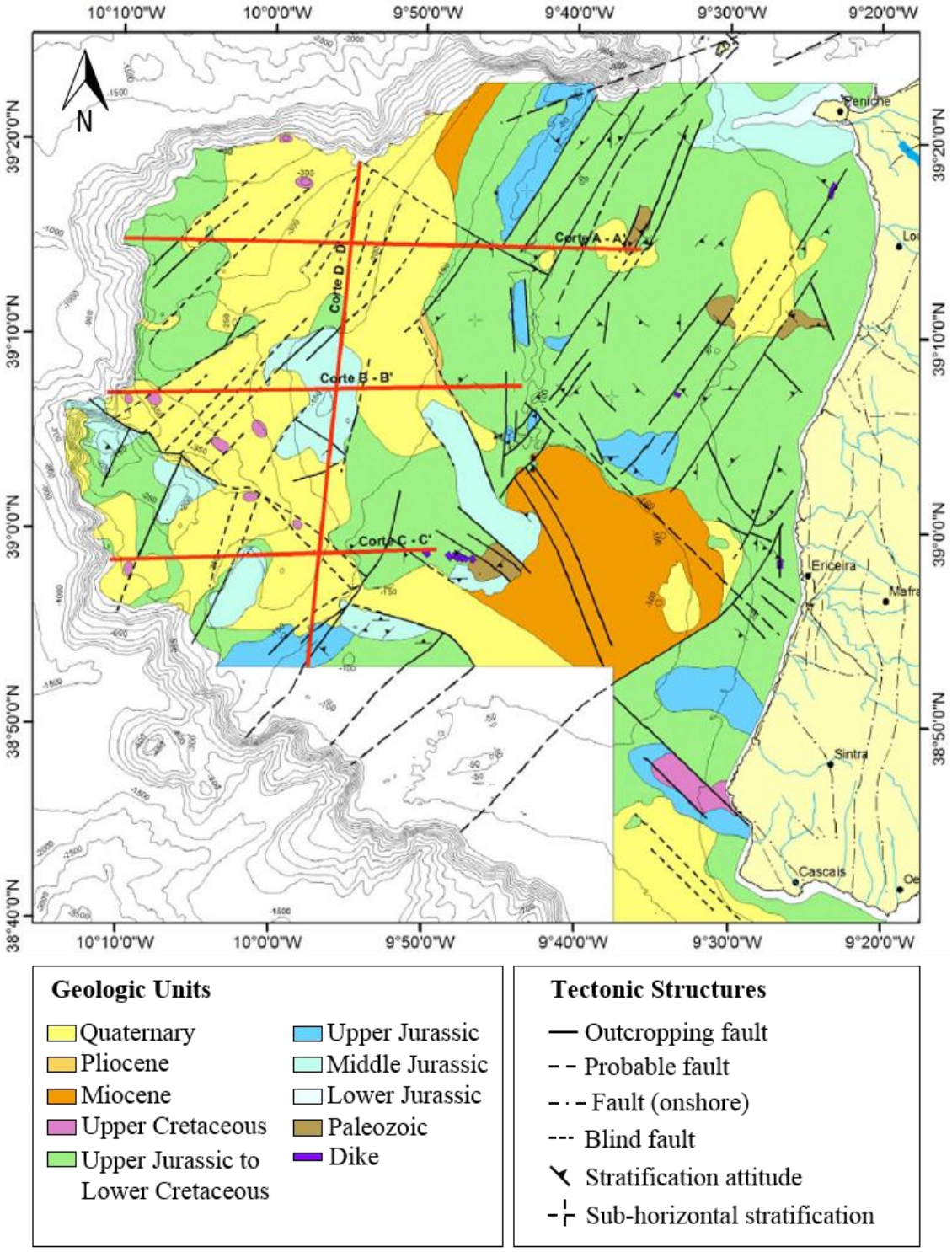

Figure 21 Geological map of the Estremadura Spur shelf (Badagola, 2008).

In the transition from the Paleogene to the Neogene two thirds of the continental shelf were uplifted and exposed sub-aerially. A transgressive cycle occurred during the late Chattian and Aquitanian with a maximum in the Langhian. This led to the formation of two gulfs in the middle shelf, the Lourinhã Basin and the Ericeira Sea (Figure 22). During the Langhian, localized subsidence of some areas of the outer shelf, led to the formation of various sub-basins with ~40m of sediment deposition (e.g. the Lourinhã Monocline basin in Badagola *et al*. 2006b; Figure 22).

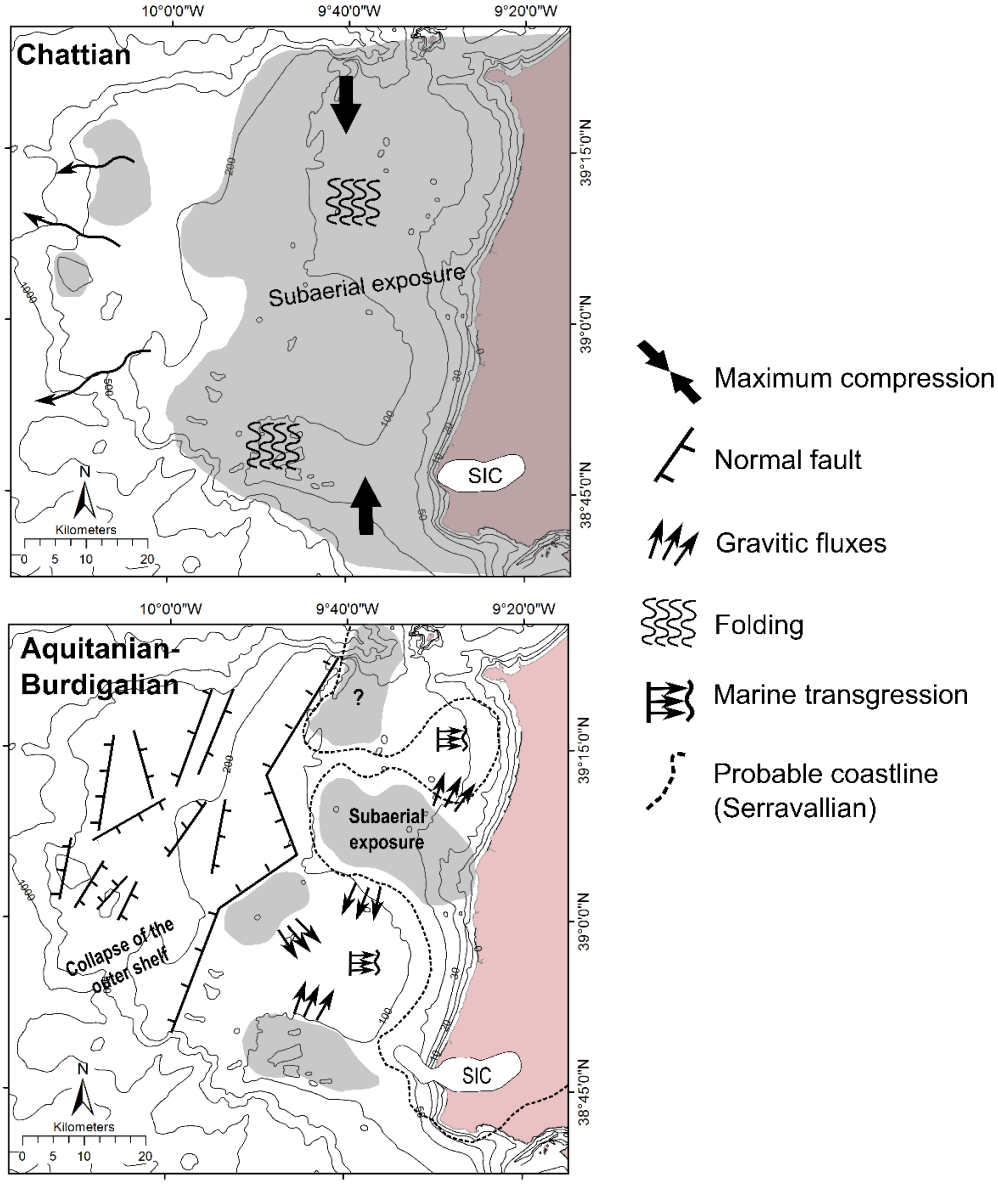

Figure 22 Estremadura Spur evolution during Chattian and Aquitanian-Burdigalian (adapted from Badagola, 2008). **SIC** - Sintra Intrusive Complex; **Gray areas** – Subaerial exposure of the continental shelf.

The Miocene tectonic inversion in the WIM led to shoreline setback exposing again a

significant area of the inner and middle shelf (Figure 23). Faults with NNE-SSW direction were reactivated as thrusts with folding of the basement and sedimentary cover, creating or accentuating reliefs, such as the Pico Gonçalves Zarco and the Costeiras Pêro da Covilhã. After the tectonic inversion, during the Pliocene-Quaternary (Figure 23), the deposition of predominant siliciclastic sediments filled paleo-valleys and depressions on the continental shelf (especially in the outer shelf).

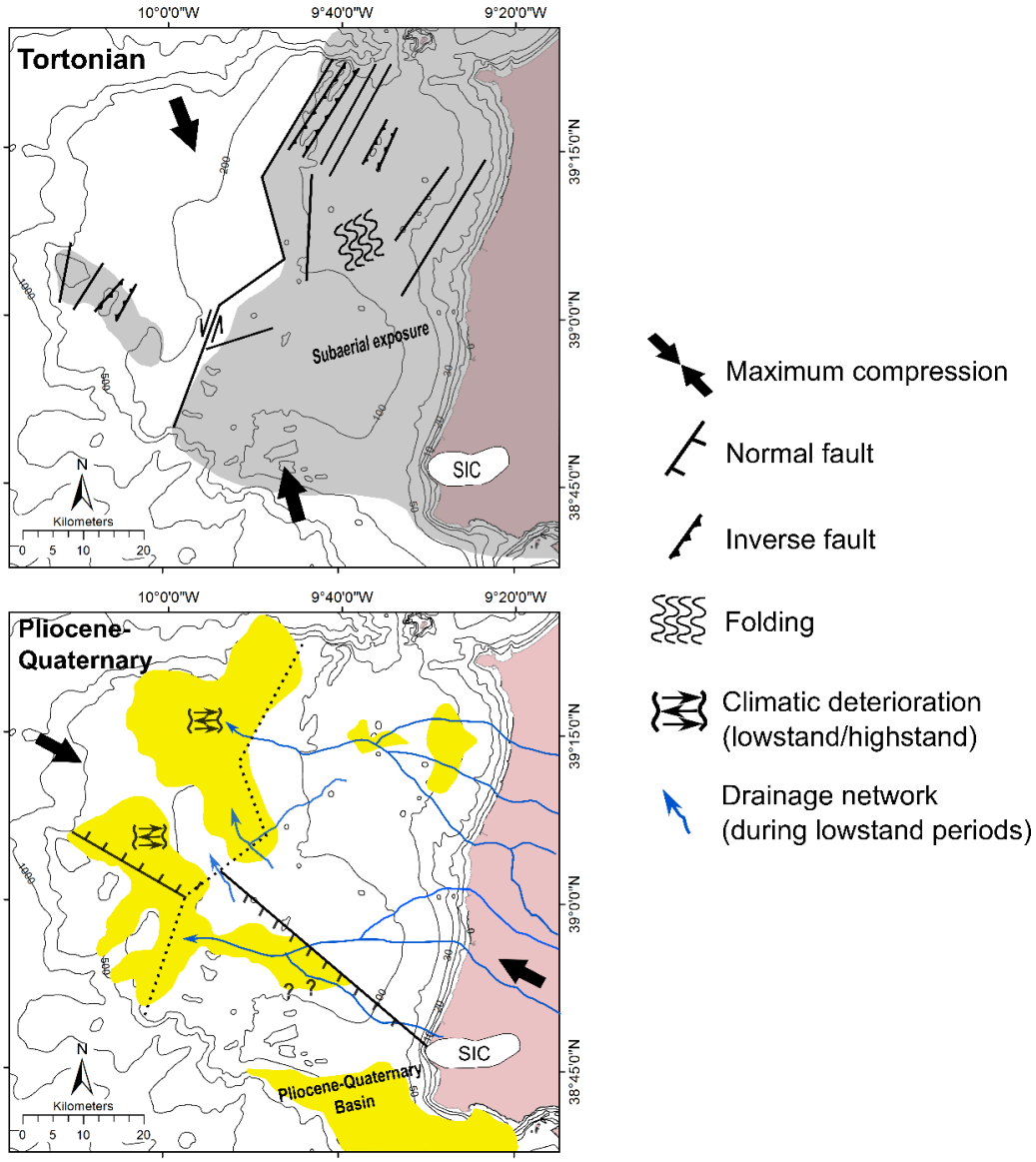

Figure 23 Estremadura Spur geologic evolution during the Tortonian (Miocene) and Pliocene-Quaternary (adapted from Badagola, 2008). **SIC** - Sintra Intrusive Complex; **Gray areas** - subaerial exposure of the continental shelf; **Yellow areas** - sub-basins formed during the Pliocene-Quaternary.

3.3.2 Shelf geomorphology and sedimentary deposits

The continental shelf of the ES reaches 400 m depth, being abnormally extensive (Vanney and Mougenot, 1981). The ES continental shelf has slopes between 0.1 and 5%, being the strongest slopes associated with the limit of the shelf (continental slope), associated with rocky outcrops (Figure 24) or associated with some well-developed morphological units (Balsinha, 2008).

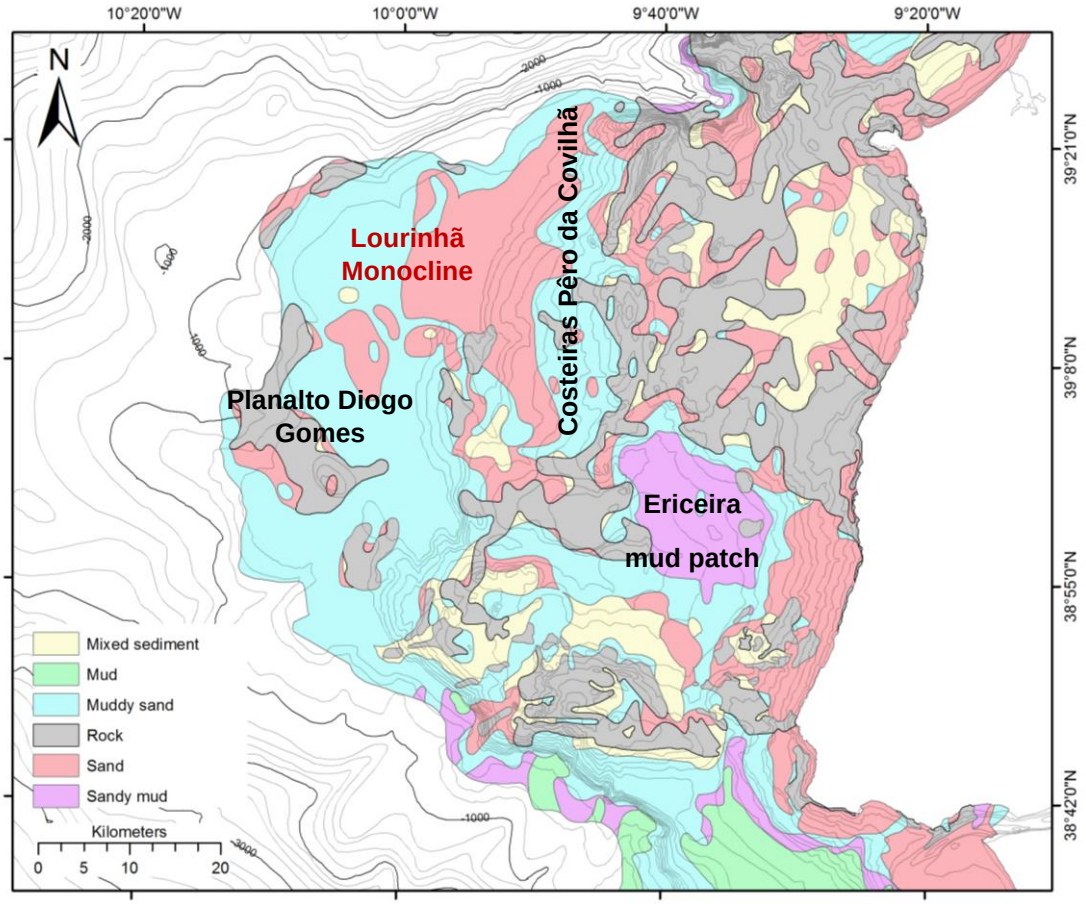

Figure 24 Map of rocky outcrops (in gray) and seafloor sediments (adapted from Folha 4 da Carta dos Sedimentos Superficiais da Plataforma Continental Portuguesa, 2010).

The sedimentary cover of the ES continental shelf is characterized by its wide variability, due to the morphological diversity and local heterogeneities and was described by Balsinha *et al*. (2014). The deposited sediments are essentially of terrigenous origin (detritic particles transported by local rivers, cliff and submarine outcrop erosion), but with a significant contribution of biogenic particles, particularly near the main rocky outcrops and autigenic particles, which abundance tends to increase with depth (Balsinha, 2008). The sediments that predominate in the inner shelf are well sorted fined grained

littoral sands. In the northern part of the mid shelf (until ~120 m depth) the sedimentary cover is made of coarse particles (sandy gravel) and in the southern part is covered by finer sediments with a nucleus of sandy mud at 115m (Ericeira mud patch; Figure 24). The outer shelf is dominated by deposits of sand and muddy sand.

The LM is a flat area delimited by the Nazaré canyon at north and by the PDG ridge at south. In the west the continental shelf is bounded by the continental slope (the ES west border) and in the east by the CPC plateau (Figure 24).

CHAPTER 4

DATA AND METHODOLOGY

The following data were used during this study: bathymetry, seafloor reflectivity (backscatter), seismic profiles and direct observations of the seafloor, in order to reach the proposed objectives of this research. Processing and interpretation of these data were done. The used dataset, followed by a brief explanation of the methods and the softwares employed for the processing and the interpretation are presented.

4.1 Dataset

The data used for this thesis was collected essentially in the scientific cruise 64PE332 with RV Pelagia (Kim & the shipboard scientific party, 2011), within the PACEMAKER (in collaboration with the TOPOMED project –TOPOEUROPE/0001/2007) and during the EMEPC/PEPC/LUSO/2015 cruise onboard the NRP Gago Coutinho, within the PES project (PTDC/GEO-FIQ/5162/2014). In addition to this, seismic data from TGS and exploration wells (courtesy of DGEG) were used.

4.1.1 PACEMAKER survey

During the PACEMAKER (PM) cruise a dataset was collected in the northern and central WIM, including high-resolution 2D single-channel seismic lines with a 1 kJ SPARKER seismic reflection system and bathymetry using a Kongsberg EM300 multibeam sea bathymetry system of RV Pelagia. For this dissertation only 30 km of high-resolution seismic data and multibeam bathymetry acquired simultaneously in Estremadura Spur was utilized (Figure 25).

4.1.2 EMEPC Cruise

During the EMEPC/PEPC/LUSO/2015 (27.05.2015 – 03.06.2015), in the Estremadura Spur region, multi-beam bathymetry (Figure 26) that complemented the PACEMAKER bathymetric grid was acquired. Two dives were done in the Estremadura Spur region using EMEPC Remotely Operated Vehicle (ROV) Luso (Figure 26).

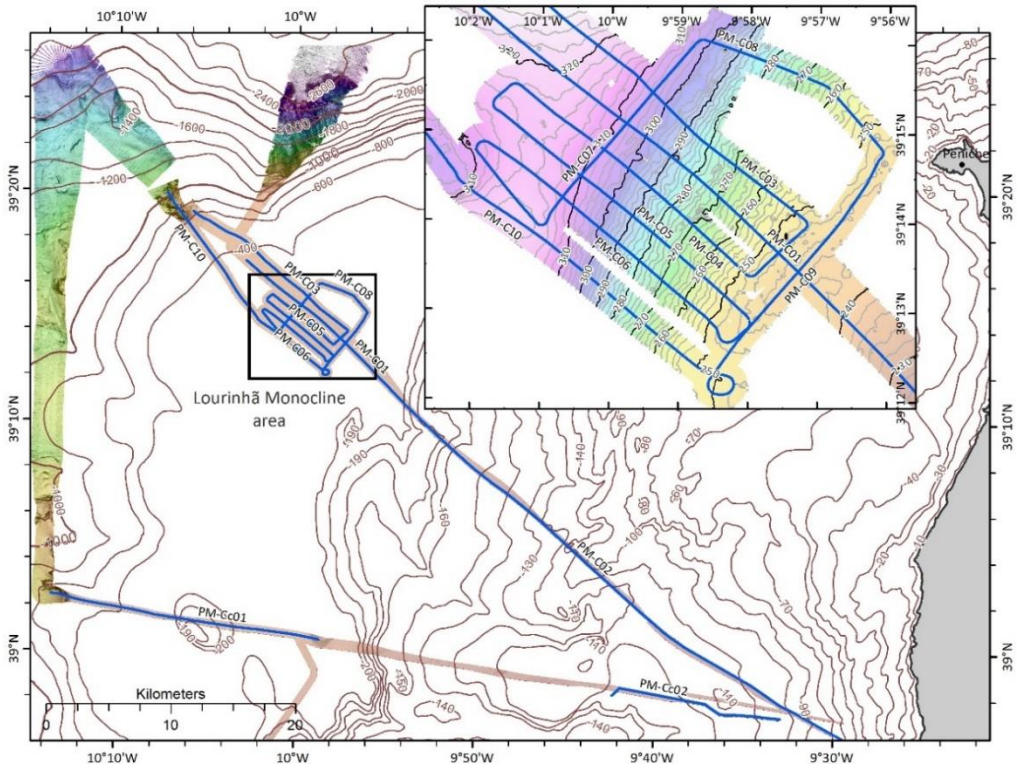

Figure 25 Seismic and bathymetric data acquired during the PM survey. Equidistance: 10 m (between 0 and 200 m); 200 m (below 200 m).

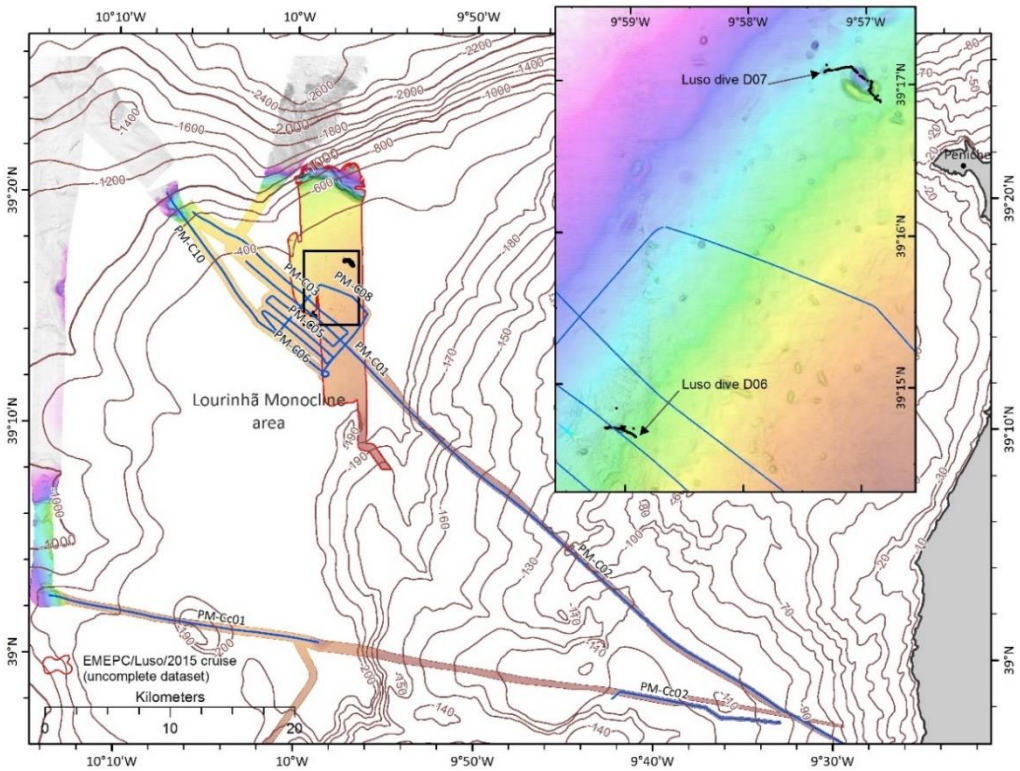

Figure 26 Bathymetric data acquired during the EMEPC/Luso/2015 cruise, to complement the PM grid (transparent in this figure) and the location and transects of the ROV Luso dives. Equidistance: 10 m (between 0 and 200 m); 200 m (below 200 m).

4.1.3 TGS-NOPEC seismic data

Low-resolution 2D multi-channel seismic data acquired during the PD-00 survey by TGS-NOPEC (www.tgs.com), in the Estremadura Spur region (Figure 27) was also used as a courtesy of DGEG.

4.1.4 Wells

As part of their Portuguese continental shelf research program the Shell Prospex-Sacorex association conducted two exploration wells on the Estremadura Spur shelf (Figure 27), 17C-1 (39º29'01.8''N, 09º22'00.2''W) in the concession area no. 17 'Chicharro' and 20B-1 (39º04'48''N, 09º36'02''W) in the concession no. 20 'Safio' that provided data on the lithostratigraphy of the Estremadura Spur. These oil exploration wells reports offshore Portugal was also presented as a courtesy of DGEG.

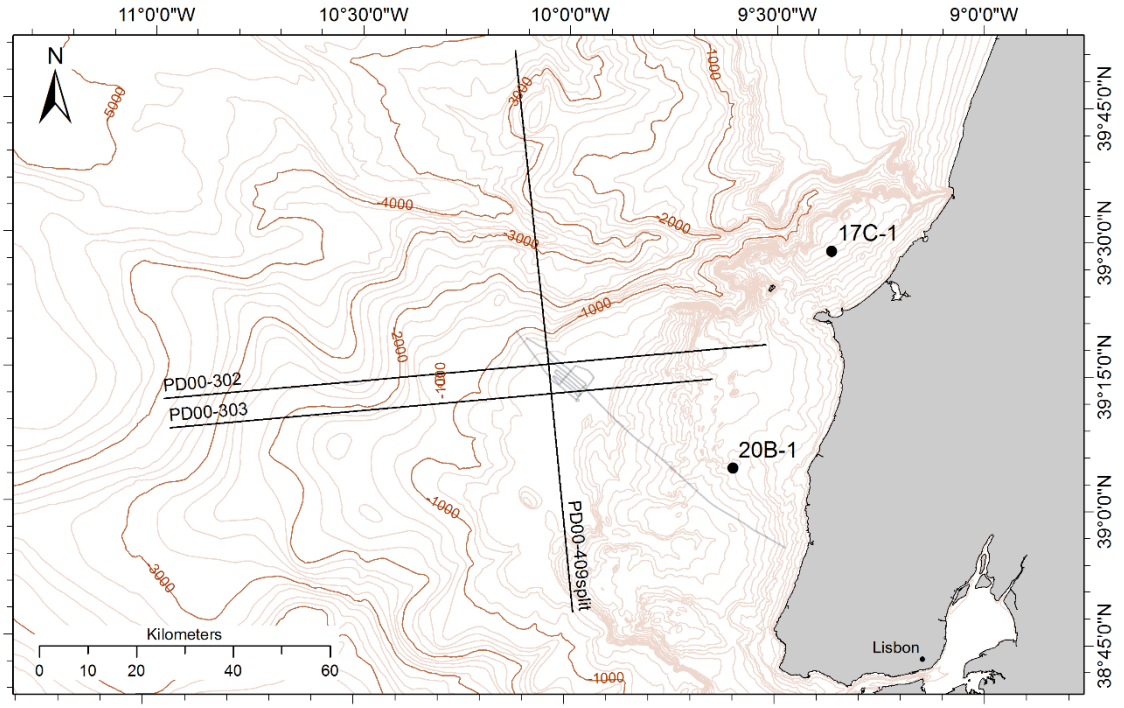

Figure 27 Localization of the TGS-NOPEC 2D seismic profiles (PD00-302, PD00-303 and PD00-409split) and of the two exploration wells drilled in the Estremadura Spur region, 17C-1 and 20B-1.

4.2 Methodology

The pockmark field was studied using geophysical acoustic methods and direct observations using ROV. These methods are an essential tool for investigation of the seafloor morphology and the subsurface geology.

The interpretation of the multibeam bathymetry and backscatter data was done in order

to characterize the seafloor geomorphology and to identify the pockmarks herein. The seabed backscatter from the swath-bathymetry echo sounder was used to characterize the nature of the seabed, mapping of different reflections' sedimentary deposits and identification of rocky outcrops or carbonate hardgrounds. The interpretation of the seismic reflection datasets provides the stratigraphic and structural characterization of the Pliocene-Quaternary sediments and of the basement of the Estremadura Spur region. The PM high resolution 2D single-channel seismic dataset was processed using Seismic Processing Workshop (SPW) to improve the quality of the seismic lines for the interpretation (see detailed description and processing in Chapter 6). After that, the single-channel seismic dataset, as well, as the multi-channel seismic from TGS-NOPEC were interpreted with the Landmark software. The interpretation of the high-resolution 2D single-channel seismic provided information on the shape, stratification and structural control of the Estremadura Spur pockmarks. The interpretation of the low-resolution 2D multi-channel seismics provided information about the basement structure.

4.2.1 Multibeam Sonar Method

Imaging the seabed using sonars is widely used in the marine environment. The multibeam sonar system permits the full coverage of bathymetric data along a corridor on the seafloor, thus, creating an altimetric map of the seabed. The system comprises two transducers: a transmitter and a receiver. The transmitter is composed of several high-precision echo-sensors that produce multiple acoustic beams, arranged in a fan shape so as to cover a determined seafloor's band. The size of this band varies according to the angle formed between the beams and water depth. The receiver obtains the echo of the emitted waves and calculates the time between the emission and reception for the various beams, thus determining the water depth for the central footprint of each seafloor area imaged by each beam,

The PM dataset was acquired with Kongsberg-Simrad EM300 multibeam sonar system. This system is designed to do seafloor mapping from 10m depth down to more than 5000m depth with swath widths up to about 5000m. The technical specifications of EM300 system are enumerated in Table 3.

Table 3 EM300 technical specifications (from Kongsberg Technical Manual 2003).

Main operational frequency	30 kHz
Angular coverage sector	up to 150º
Number of beams	135
Beam width	Simultaneous 1x1º, 1x2º, 2x2º or optionally 2x4º
Range sampling interval	17 m (variable with depth)
Beam spacing	Normally equidistant
Pulse length	0.7, 2 or 15 ms (variable with depth)
Peak power	4.5 or 9 kW
Depth range	10 m to >5000 m
Maximum swath width	>5000 m

During the EMEPC/PEPC/LUSO/2015 onboard the RV Gago Coutinho was used the Kongsberg-Simrad EM710 multibeam. The technical specifications of EM710 system are enumerated in Table 4.

Table 4 EM710 technical specifications (from Kongsberg Technical Manual 2014).

Frequency range	40 to 100 kHz
Angular coverage sector	up to 140º
Number of beams	up to 400 or 200 soundings per swath
Beam width	0.5x1º,1x1º, 1x2º or 2x2º
Range sampling interval	17 m (variable with depth)
Beam spacing	Equidistant, equiangular, high density
Pulse length	max. 120 ms
Depth range	3 m (below transducers) to max. >3000 m
Maximum swath width	max. >3000 m

4.2.2 Backscatter analysis method

The collected depth data from each sounding also contains the amplitude of the return sound pulse. This information is called backscatter data. The backscatter signal depends on the physical nature of the seafloor, orientation of the illuminate surface and the frequency and angle used. Acoustic backscatter data are used for classifying seafloor characteristics. In simplified terms: a weak return signal (low amplitude) indicates a soft bottom substrate and a strong return signal (high amplitude) indicates a hard bottom substrate.

The acoustic reflectivity response of the seafloor is affected by three factors: geometry of the sensor-target system (e.g. local slope, local angle of incidence), the intrinsic nature of the surface (e.g. composition, density) and the physical characteristics of the surface (roughness, sound speed, etc.).

Both chemosynthetic cold seep communities (supported by the expulsion of methane and sulfide-rich fluids from the seafloor) and authigenic carbonate (precipitated from the bacterial oxidation of methane) may cause higher acoustic reflectance and roughness than occur in the surrounding seafloor. Therefore, acoustic backscatter data can be used to identify the distribution of potential seeps sites (Orange *et al*., 2002; Gay *et al*., 2007; Naudts *et al.,* 2008). The distribution of anomalous reflectivity can be used to constrain the area of the seafloor characterized by venting, both active (cold seep communities and carbonate) and dormant (carbonate).

Gay *et al*. (2007) developed a model, based on observations in the Lower Congo Basin (Western African margin), that correlated the seafloor backscatter response with chemo-biological facies that occur in the seabed associated with fluid seep activity (Figure 28). This model sustains that both active and recently active and buried under 10 m of sediments seep sites may create anomalies of high backscatter. The increase in surface roughness (Figure 28–B and C) when compared to the surrounding smooth seafloor of fine-grained hemipelagic sediments (Figure 28–A) leads to an increase in the seafloor acoustic reflectivity response, i.e. higher backscatter facies. The diminution of seepage sites activity can also be inferred from the backscatter data, since the burial of seepage related features leads to a decrease in acoustic reflectivity response of the seafloor (Figure 28–D and E).

Then, according to this model, a high backscatter anomaly indicates that fluid expulsion is active (chemosynthetic fauna and/or carbonate buildups present at the seabed; Figure 28 –B and C) or has been recently active (dead or dormant site characterized by buried chemosynthetic fauna and/or carbonate buildups within the upper 10 m; Figure 28–D).

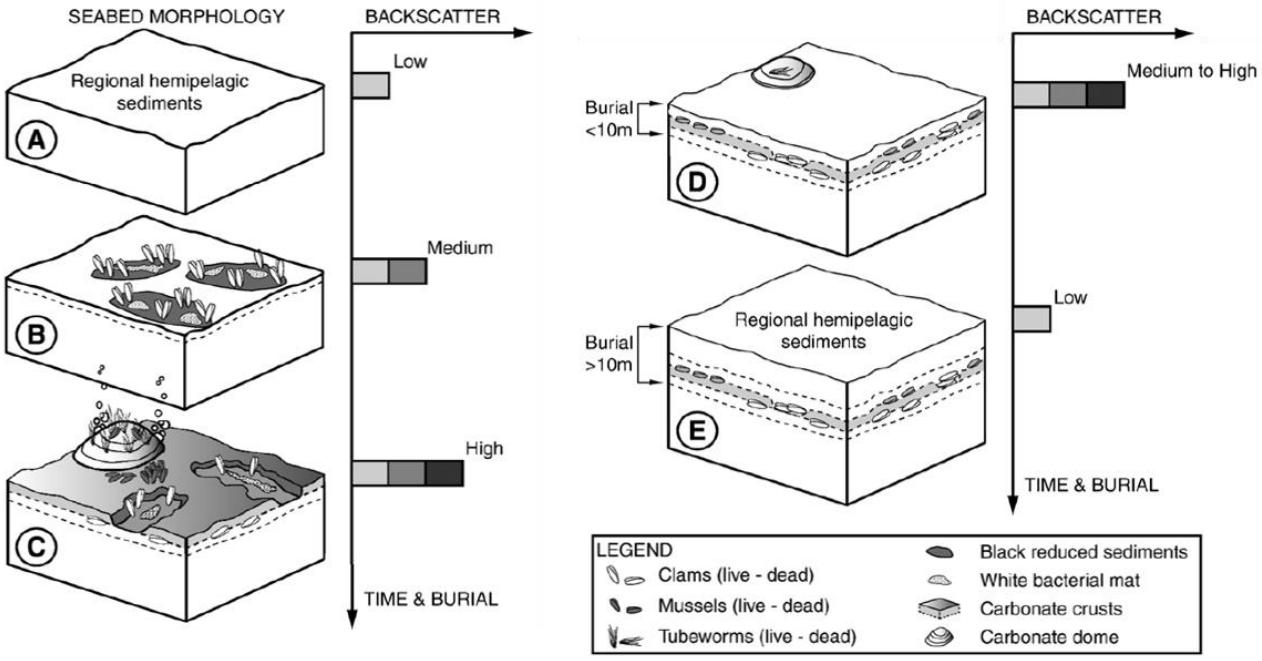

Figure 28 Correlation between backscatter response and seafloor chemo-biological facies chemo-biological, associated with fluid seep activity (from Gay *et al*., 2007).

4.2.3 Seismic Reflection Method

Seismic reflection is a geophysical method used to get an acoustic vertical 2D image of the structure and the stratigraphic layers under the seabed. This method depends on the generation and detection of acoustic waves that are mechanically generated. In shallow-marine seismic profiling, the acoustic source generates a short pulse of sound (shot) which travels through the water and into the rock layers (Figure 29). Some part of this energy is reflected back to the surface from different layers of rocks beneath, due to acoustic impedance ($I = velocity \times density$) contrasts generally occurring where the lithology changes. The reflected energy is recorded by seismic receivers (hydrophone). These recordings are processed (see Chapter 6), and the data are transformed into visual images that give a picture of the subsurface geology in the survey area.

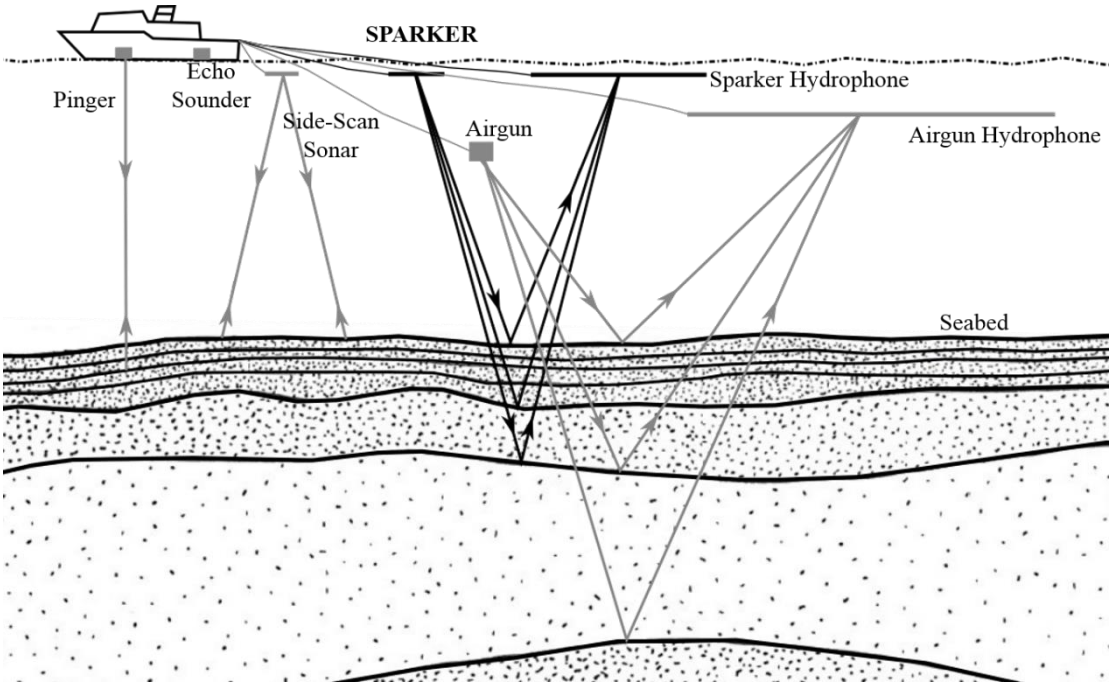

Figure 29 Configuration of a shallow single-channel seismic survey (adapted from Stoker *et al*., 1997).

Since the target zone for the seismic survey was located in the continental shelf at relatively shallow depths and the aim was to study the cover sediments a high-resolution single-channel seismic was used. The seismic profiles processed and interpreted in this work were acquired with a SPARKER seismic reflection system from Geo-Marine Systems (www.geomarinesurveysystems.com).

This system consists of a catamaran mounted Geo-Source 200 multi-tip sparker source, a 1 kJ Geo-Spark high voltage power supply unit, 2 Geo-Sense mini streamers of different lengths, with 3.5 and 6.8 m long active sections. The technical specifications of Geo-Spark system are enumerated in Table 5.

Table 5 Geo-Source 200 Light Weight technical specifications (adapted from GEO Marine Survey Systems Technical Manual).

Water depths	2 to 500 m
Penetration	200 to 300 ms below seabed
Vertical resolution	up to 20-30 m
Streamer lengths	3.5 and 6.8 m
Effective source depth	15-20 cm below the surface
Electrode modules	Two, spaced in a planar array of 0.50 m x 1.00 m 100 tips each; 10 J per tip

Energy output for highest resolution	< 400 J

4.2.4 Seismic Interpretation

Interpretation of seismic data usually consists of a seismic stratigraphic interpretation as much as possible calibrated by chronologic information/data. Structural and tectonic interpretation complements this interpretation and stratigraphic models are produced. The data was interpreted using the concepts of seismic stratigraphy that is essentially a geologic approach to the stratigraphic interpretation of seismic data, in other words, is the application of geologic concepts of physical stratigraphy on the seismic data. This method of seismic interpretation was developed by R. Mitchum, P. Vail and associates in the 70s (Mitchum *et al*., 1977a, 1977b and 1977c). This methodology is focused in the interpretation of seismostratigraphic surfaces, allowing the extraction of geological information related to tectonic and/or sedimentary events and eustatic variations, from the seismic profiles.

The interpretation of seismic stratigraphy is based on the identification of seismic sequences. Stratigraphic analysis involves the subdivision of seismic sections into sequences of reflections, which are interpreted as a seismic expression of genetically related sedimentary sequences, termed depositional sequences (Figure 30). A **depositional sequence** is defined as a stratigraphic unit composed of a relatively conformable succession of genetically related strata (numbers in Figure 30), bounded by unconformities or correlative conformities (surfaces A and B – Figure 30) in their top and base (Mitchum *et al*., 1977a and 1977b). An **unconformity** has an associated hiatus and is itself a surface generated by erosion and/or non-deposition that separates rocks of different ages. A hiatus is a time interval that is not represented in a geological record, if the time interval is significant at a geological scale then the surface it originates is defined as an unconformity. A **conformity** is a surface that separates strata of different ages but where no physical evidence of erosion and/or non-deposition can be identified and no significant hiatus is identifiable.

A **seismic sequence** is a depositional sequence identifiable on the seismic record; it is made up by seismic units and bounded by discontinuities. **Seismic units** are tri-dimensional bodies made up by sets of reflectors (interpreted as genetically related strata) whose parameters and configuration differ from the ones in the adjacent units. A sequence

has to be bounded by unconformities associated with erosion or nondeposition, which can, however, laterally pass onto conformities.

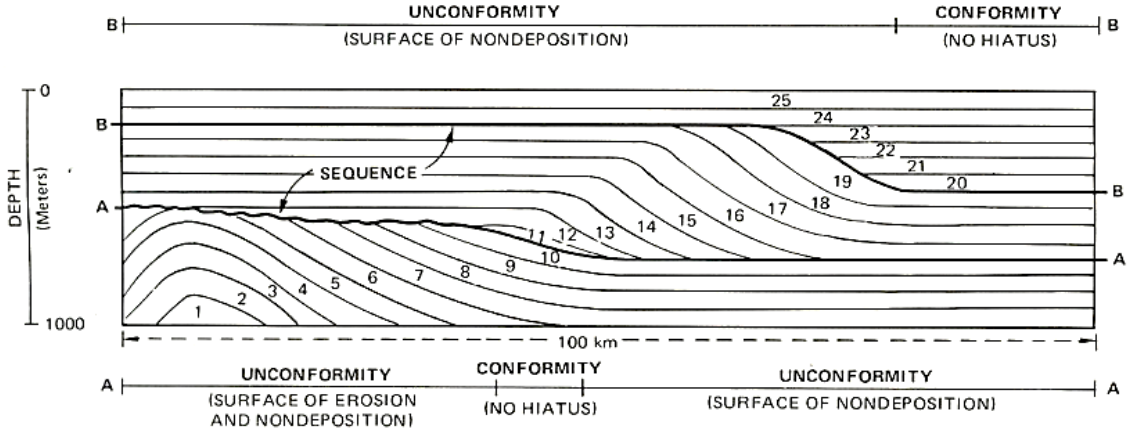

Figure 30 Basic concept of depositional sequence, limited by bounded unconformities and their relative conformities (surfaces A and B) and termination of reflectors (from Mitchum *et al*., 1977b).

Seismic facies can be defined as a set of seismic and geometric parameters that allow characterizing a seismic unit and that distinctly differ from those of other facies. These parameters are configuration, amplitude, continuity, interval velocity and frequency. Seismic facies analysis consists in the identification of the following characteristics: type of reflection terminations, characteristics of the reflections patterns, types of internal reflections patterns and external shape and reflection configuration patterns (Mitchum *et al*., 1977c).

(1) Reflection terminations

The geometry and the type of reflection terminations allowed the identification of the limits of seismic upper and lower units. It is possible to distinguish five types of reflections with respect to their terminations: onlap, downlap, toplap, truncation and conformity (Figure 31).

Conformity can be used both in relation to the upper and lower sequence boundaries and are characterized by the parallelism of reflections. It indicates that the depositional conditions remained unchanged in what regards the control on the local strata geometry.

Top-discordant relations include truncation or toplap. **Truncation** (erosional and structural) can be characterized by the abrupt lateral ending of the reflectors against a discordant surface. It can be generated by tectonic tilting of a sequence followed by

erosion over large areas or confined to the flanks of submarine channels. **Toplap** is the termination of reflections interpreted as strata against an overlying surface. This type of termination forms as a result of non-deposition hiatus and minor erosion.

Base-discordant relations include seismic onlap and downlap. **Onlap** is a relation in which seismic reflections are interpreted as initially horizontal strata terminating progressively on top of a dipping surface, or as initially inclined strata terminating progressively updip against a surface of higher dip. This termination can be associated with seafloor irregularities, caused by non-depositional hiatus or by deposition on tilted blocks. **Downlap** is a relation in which seismic reflections are interpreted as initially dipping strata terminating downdip against an initially dipping or horizontal surface. It is caused by non-depositional hiatus.

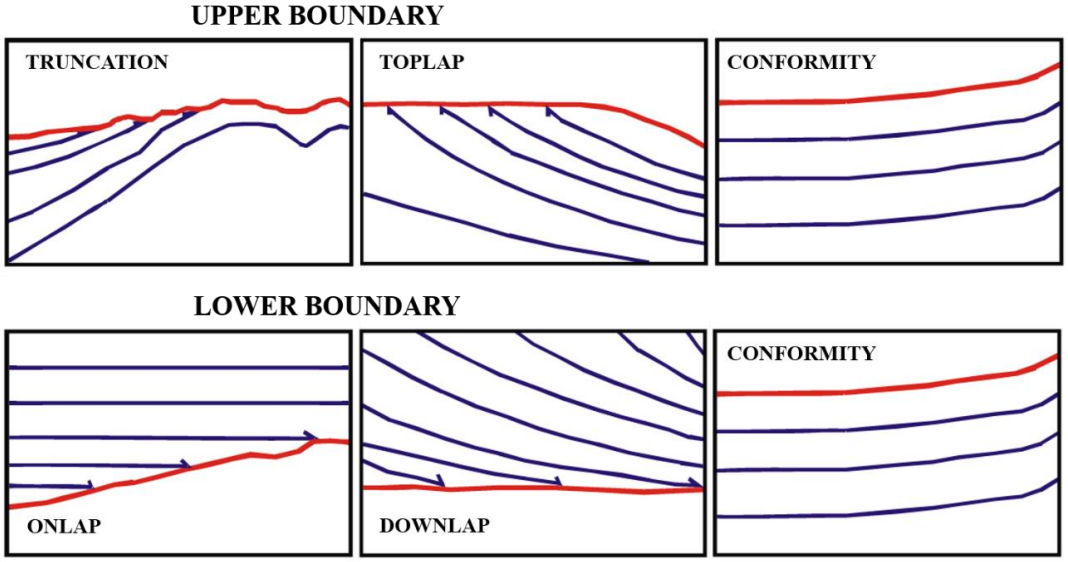

Figure 31 Seismic reflection terminations according to Mitchum *et al*., 1977b (from Roque, 2007).

(2) Characteristics of the reflection patterns

The characteristics of the reflections can provide information on the lithologies that constitute the seismic sequences (Mitchum *et al*., 1977c). Thus, several seismic parameters are studied, as reflection signature, continuity, amplitude and frequency.

Reflection signature consists of the particular characteristics of a single reflector and can give useful information about the stratification patterns and consequently more information on the depositional processes, erosion, paleotopography and fluid presence.

Reflection continuity corresponds to the lateral juxtaposition of successive reflections of the same horizon and is related to the physical continuity of the strata. Thus, continuous

reflections suggest widespread, uniformly stratified deposits. Continuity of a given horizon is interpreted as preservation of the depositional conditions with no main changes in the energy of the environment.

Reflection amplitude is related to the maximum amplitude of the reflected wave which is dependent on the velocity and density contrasts through each individual interface and the spacing between interfaces (high amplitudes reflect high acoustic impedance). Fluid content in the sediments can have an influence in the reflections amplitude. Usually, if a high amplitude reflection diminishes rapidly it indicates a high energy depositional environment and the opposite suggests a large continuity of the formations and a stable depositional environment.

Reflection frequency is the time interval between two successive reflections. It reflects the instrumental seismic characteristics but it is also influenced by other factors such as the presence of fluids and by the thickness of the layered deposits. There is an inverse relation between strata thickness and reflection frequency: high frequencies correspond to thin strata.

(3) Configuration of internal reflection patterns

The geometric relations between the internal reflections of a seismic sequence often allows to assigning specific seismic facies to the depositional processes, erosion, paleotopography or the presence of fluids (Mitchum *et al*., 1977c). Various types can be distinguished as follows.

Parallel and **subparallel** patterns, even or wavy, refer to high amplitude, continuous and parallel reflections (Figure 32). These patterns suggest uniform rates of deposition in a steady subsiding shelf or a stable basin environment.

Divergent pattern is characterized by a wedge-shaped sequence of seismic horizons (Figure 32). It is associated with lateral variations of the deposition rate, to the progressive tilting of the depositional surface and syn-rift sequences.

Chaotic pattern refers to discontinuous, discordant and disordered reflections (Figure 32), characterized by high frequencies. This pattern is associated with a high energy environment with large variability of the depositional conditions and it is commonly found in slumps, erosion derived deposits, cut-and-fill channel bodies and on high energy zones affected by faults or folds.

Transparent pattern is characterized by the total or partial absence of reflections or by lack of lateral continuity. This pattern is related to homogeneous rocks (with low acoustic impedance contrasts), highly deformed or metamorphosed rocks, evaporites or igneous bodies. Rapidly deposited large sequences of pelitic rocks can also give a transparent acoustic response.

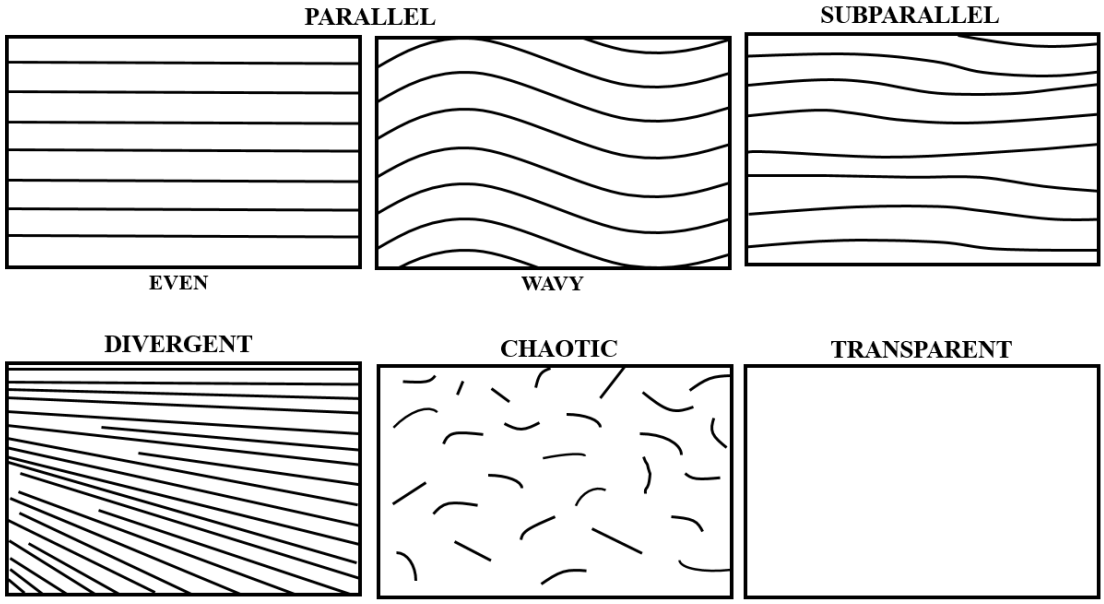

Figure 32 Seismic internal reflection patterns (from Mitchum *et al*., 1977c).

Prograding clinoforms configurations are packages of oblique to sigmoidal shaped reflections. They are interpreted as strata where the main deposition occurred by the prograding or lateral sedimentation outbuilding. Several sub-types of prograding configurations can be identified (Figure 33), such as sigmoid, oblique (tangential and parallel), sigmoid-oblique, shingled and hummocky. These configurations result from variations of deposition rate and water depth and are formed in a wide variety of environments.

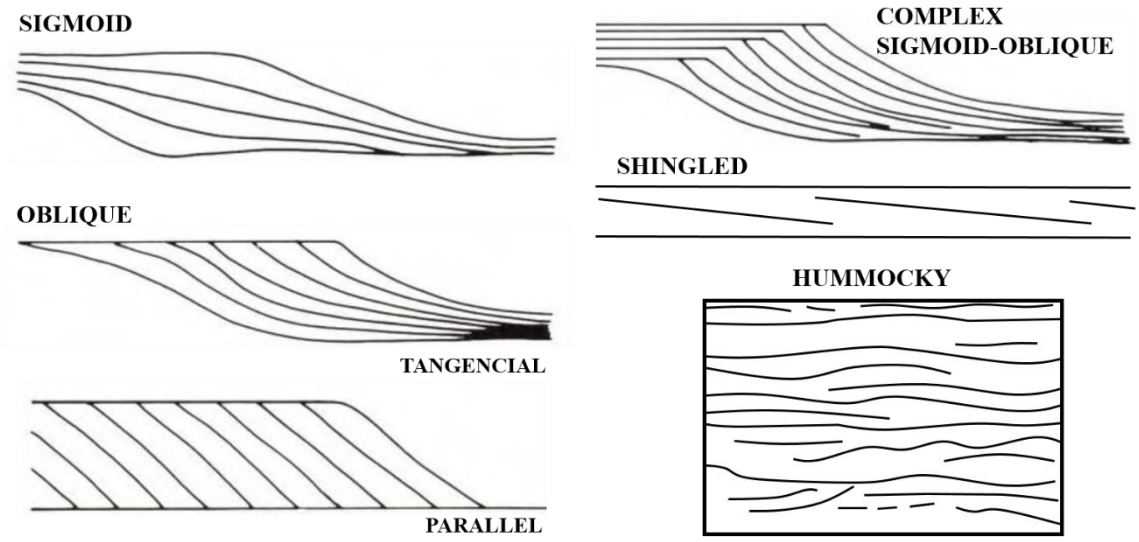

Figure 33 Seismic internal reflection patterns of prograding clinoforms (from Mitchum *et al*., 1977c).

Sigmoid progradational configuration is an S-shaped clinoform with thin, shallow dipping strata at the top and base and a thicker, steeper intermediate sector. They are characteristic of a low energy environment with a low sediment supply, rapid basin subsidence and/or rapid sea level rise.

Oblique configuration is interpreted as a prograding clinoform pattern of steep dipping strata with a toplap termination at a horizontal or subhorizontal boundary and a downlap termination at the bottom boundary. Due to the foreset steepness, the new strata builds almost laterally. In the tangential oblique pattern the dip diminishes gradually in the foreset generating a concave-upward architecture that passes onto a gently dipping bottomset. Towards the bottom the strata become thinner with downlap terminations. In the parallel oblique configuration the foreset maintain its strong dip from the top to the bottom where it has a downlap termination at a high angle with the lower boundary. The oblique progradational configuration owes its formation to high energy sedimentary regime characterized by a high sedimentary supply, slow to none basin subsidence or a stillstand of the sea level to allow sediment bypass and scouring of the upper depositional surface.

The **complex sigmoid-oblique** configuration is a complex prograding clinoform made up of a combination of variably alternating sigmoid and oblique progradational configurations. Within the same seismic unit. This architecture suggests an alternate history of upbuilding and depositional bypass on a high energy environment.

Singled configuration is a thin prograding pattern, commonly with parallel top and bottom boundaries and with gently dipping parallel internal reflectors oblique to these boundaries that terminate with apparent toplap and downlap. This configuration is generally interpreted as prograding seismic units formed in shallow water.

The **hummocky** clinoform consists of irregular and subparallel reflection segments forming a somewhat irregular pattern marked by non-systematic termination and splits. This pattern is interpreted as the strata forming small, interfingering clinoforms lobes forming in a shallow water prodelta or interdeltaic environment.

(4) External shape and reflection configuration patterns

The classification of the external form patterns is used to identify and individualize a seismic unit in relation to the adjacent units and it is also used to infer the type of depositional environment. The external shape of a seismic unit is dependent, among other factors, on the geometry of the surface on which it lies on. Various types of external shapes can be distinguished, such as sheet, sheet drape, wedge, bank, lens, mound and fill (Figure 34).

External shapes as **sheets**, **wedge**, **lens** and **bank** can reach over large areas, are commonly associated with shelf deposits and can display internal configurations as parallel, divergent or prograding. **Sheet drape** shapes are usually associated with pelagic or hemiplegic sediments deposited in a low energy or deep environments. **Mound** shapes can be of different origins, such as carbonate edifications and diapirs, and their dimensions are usually small, the configuration of their internal reflections is varied and when associated with detrital deposits it reflects a high energy event. **Fill** type deposits like the mound type ones can have different configurations (e.g. onlap, chaotic, prograding, divergent), however these deposits may reach over larger areas (from meters to kilometers) when in a basin context or can be smaller (from centimeters to meters) when in the dependency of a channel.

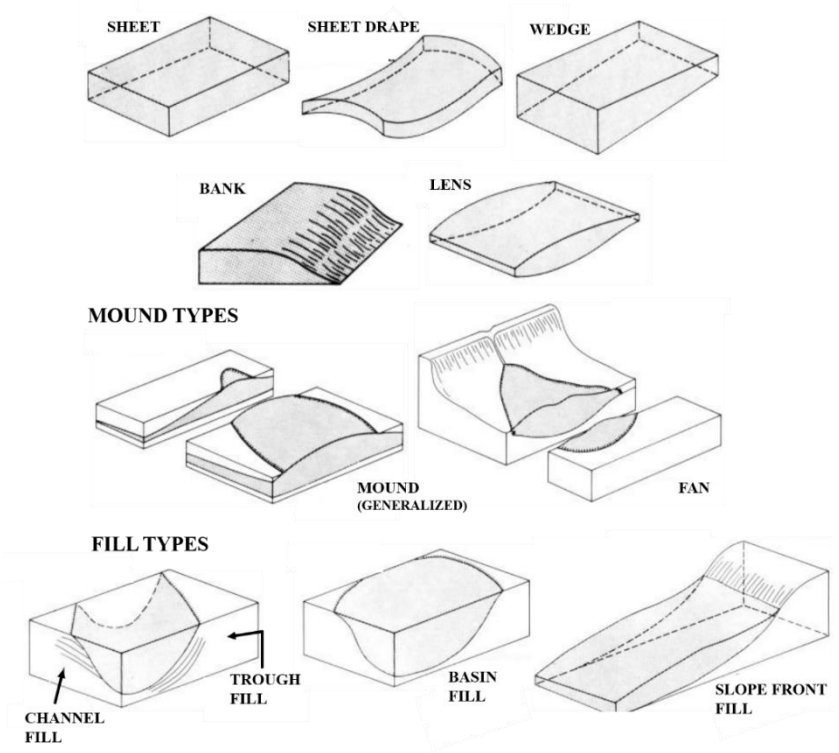

Figure 34 External forms of seismic facies units (from Mitchum *et al*., 1977c).

4.4 Software

During this work several software packages were used in order to process, view and/or interpret the data. The used programs are listed below:

4.4.1 Seismic Processing Workshop

The Seismic Processing Workshop (SPW) by Parallel Geoscience Corporation (http://www.parallelgeo.com/), was the software used to perform the processing of the seismic data from the PACEMAKER project. It was used the SPW version 3, which Flowchart allowed the creation of a project (in which all the data and processing is organized), building processing flows and the display of the seismic profiles.

4.4.2 SeiSee

SeiSee developed by Dalmorneftegeophysica Company (DMNG) was also used in the seismic processing, to have a first view of the seismic data and its properties and to edit the Trace Headers (coordinate correction).

4.4.3 Landmark

Landmark from Landmark Graphic Corporation was used for the interpretation of the seismic profiles. *SeisWorks* and *Power View* tools were utilized. *SeisWorks* was used to viewing and interpret the seismic data, allowing the mapping of seismic horizons and faults. *Power View* was used to create isobath maps, that show the spatial distribution of the selected horizons depth and isopach maps that represent the spatial variation of the unities thickness.

4.4.4 ArcGIS

ArcGIS is a geographic information system (GIS) from ESRI. In this work, it was used the main component of this software package, the ArcMap, to compile all the available data and to create the maps presented in this thesis.

CHAPTER 5

GEOMORPHOLOGIC ANALYSIS OF THE SEAFLOOR

During the PACEMAKER cruise the Estremadura Spur was surveyed simultaneously with multibeam and sparker seismics and a more detailed survey was done at the Lourinhã Monocline region (Figure 35), where pockmarks were identified. In May – June 2015, during the EMEPC/PEPC/LUSO/2015 cruise, onboard the NRP Gago Coutinho the area previously surveyed during the PACEMAKER cruise was enlarged showing a larger area comprising the pockmarks (Figure 35). In this chapter the characterization and interpretation of the Lourinhã Monocline seabed morphology as well as its composition (classification of the sedimentary cover and identification of rocky outcrops or carbonate hardgrounds) is presented.

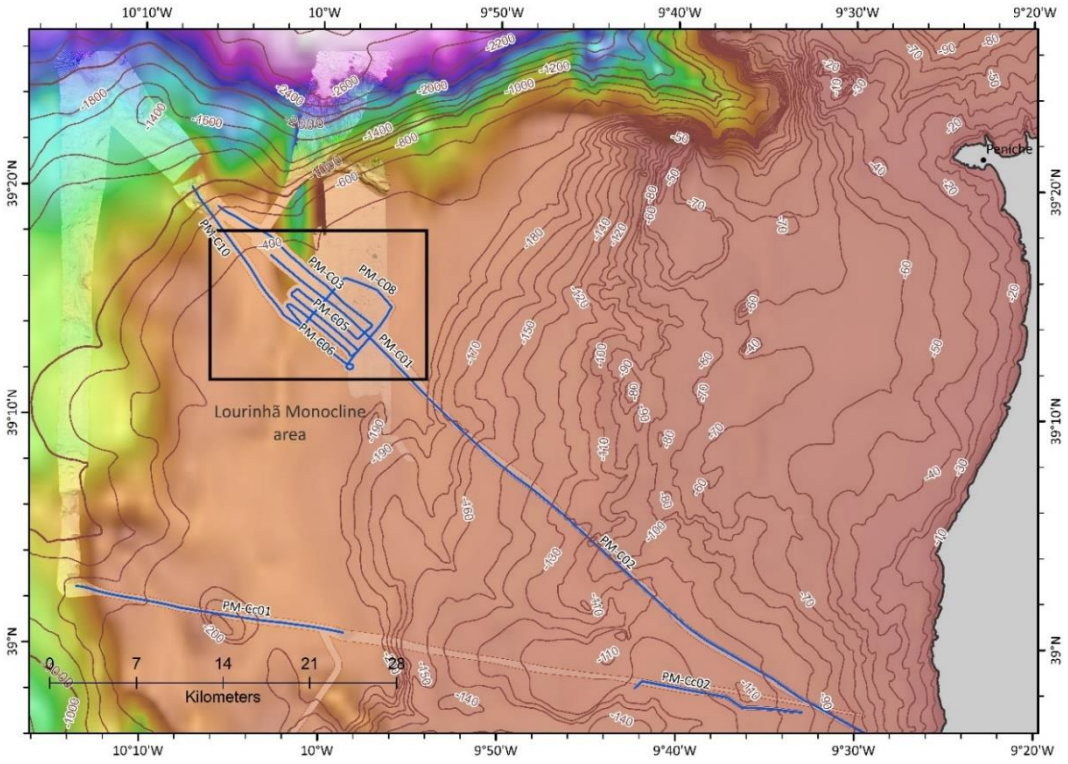

Figure 35 Estremadura Spur with the PACEMAKER seismic lines and the PACEMAKER and EMEPC/LUSO survey multibeam coverage. Equidistance: 10 m (between 0 and 200 mbsl); 200 m (below 200 mbsl).

5.1 Seabed morphology

The Estremadura Spur continental shelf is unusually large, with an area of 4.760 km^2 (Vanney and Mougenot, 1981; Badagola, 2008), reaching water depths of 500 m. Badagola (2008) enumerated the principal characteristics of the ES continental shelf, according to Table 6:

Table 6 Estremadura Spur continental shelf parameters (from Badagola, 2008).

	Minimum	Maximum	Average
Width (km)	38	79	60
Length (km)	14	70	52
Shelf break (m)	70	440	264
Slope (º)	0.1	29	

The pockmark field is located in the Lourinhã Monocline, on the NW edge of the Estremadura Spur outer shelf (Figure 35), at water depths between 240 and 350 m (Figure 36). This morphology is described in detail below.

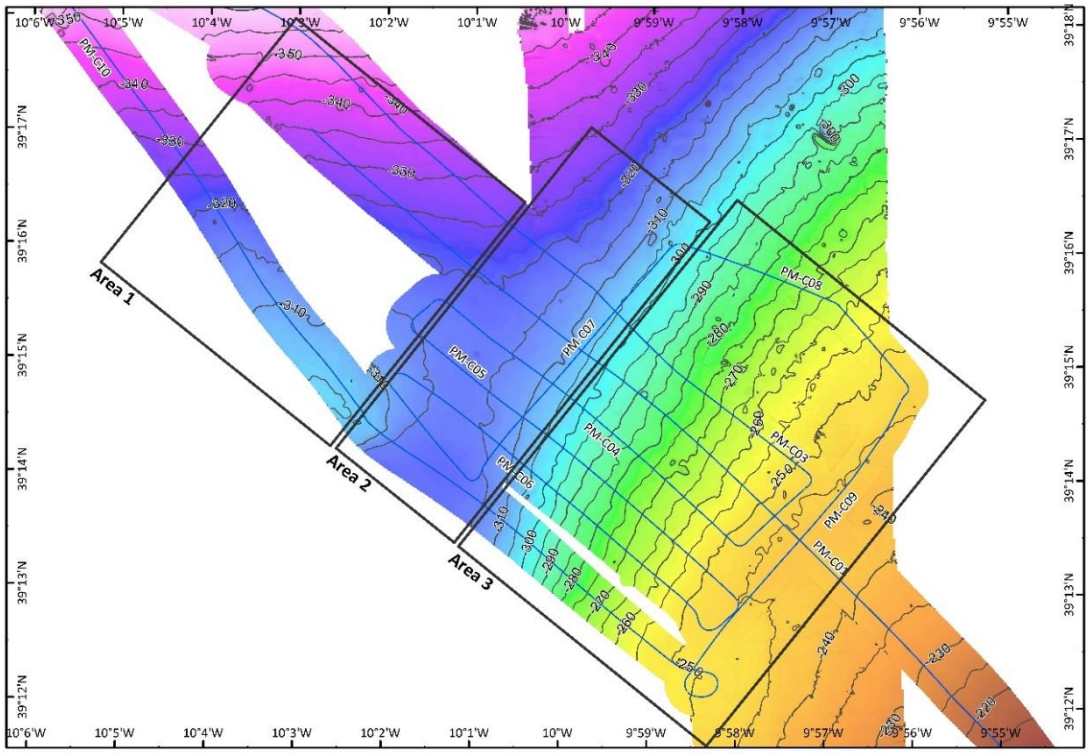

Figure 36 The Lourinhã Monocline area of the Estremadura Spur with the PACEMAKER seismic lines and the PACEMAKER and EMEPC/LUSO survey multibeam coverage. Equidistance: 5 m.

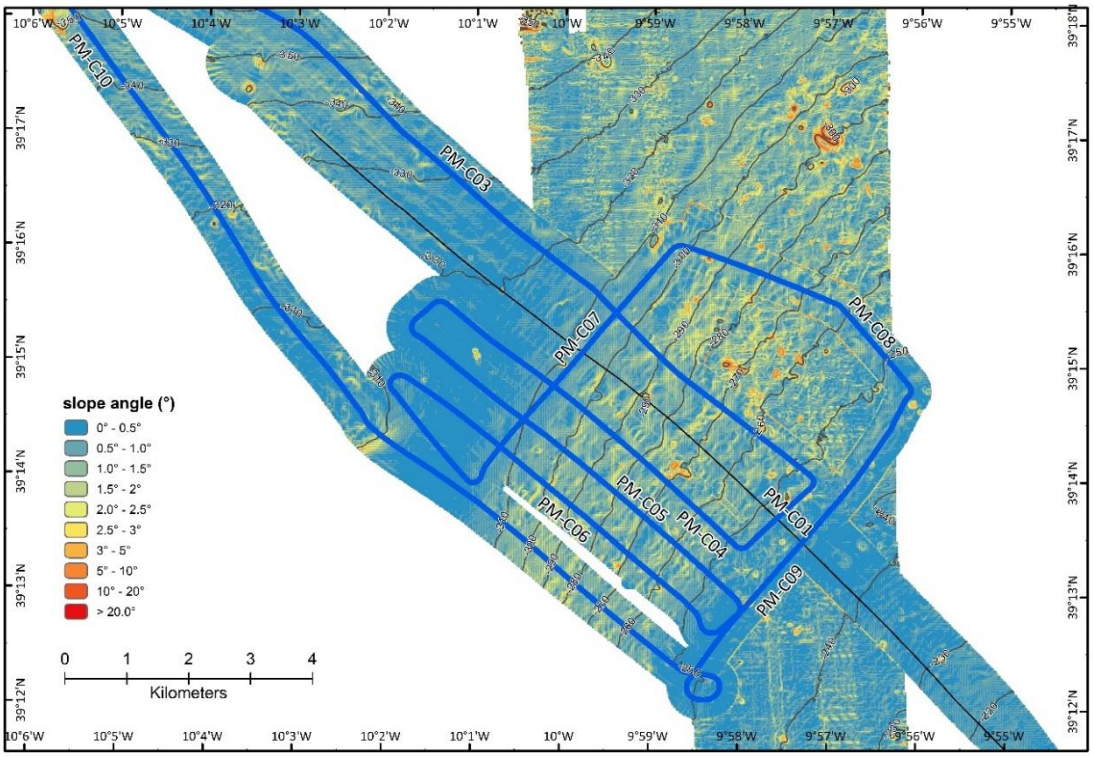

Figure 37 Slope map of the Lourinhã Monocline region obtained from the multibeam bathymetry. Equidistance: 10 m.

In general, a more or less flat and featureless seabed with a gentle slope is observed (Figure 37), until the shelf edge, where the slope increases abruptly (from 400 to more than 2000 m depth, in about 20 km). The mean slope angle of the Lourinhã Monocline is less than 0.65°.

To facilitate the description of the studied sector, the LM zone was subdivided in three different areas (Figure 36) based on their morphological characteristics, each being interpreted in more detail below. Area 1, located in the western part of the LM, is limited at the W by the shelf break defined in this region by the 400 m bathymetric curve. The outstanding morphological feature of this area is an elevated region with circular shape (305 m in the top; Figure 36). Area 2 corresponds to a smooth and flat region, dipping < 0.50° to the NNW, with maximum depths of about 330 m. Area 2 also displays an elongate moat-like depression parallel to the general trend of the isobaths. A view at the low resolution bathymetry suggests this trend can vary from NNW-SSE to N-S in the central part of the LM (Figure 35). The eastern zone, Area 3, exhibits bathymetric contours with sub-parallel orientation to the present shoreline, dipping 0.75° - 2° to the NNW, with depths ranging between 240 and 300 m.

In the PACEMAKER surveyed region, 76 shallow round depressions were identified in the bathymetry, occurring mainly in Area 3 (Figure 38). These depressions have depths of 2-17 m, with respect to the local sea floor, with diameters ranging from 30 m up to 400 m and slopes of more than 3º. In plan-view they have circular, sub-circular and elliptical shapes, while in cross-sections they have 'U' and 'V' shaped profiles (Figure 38).

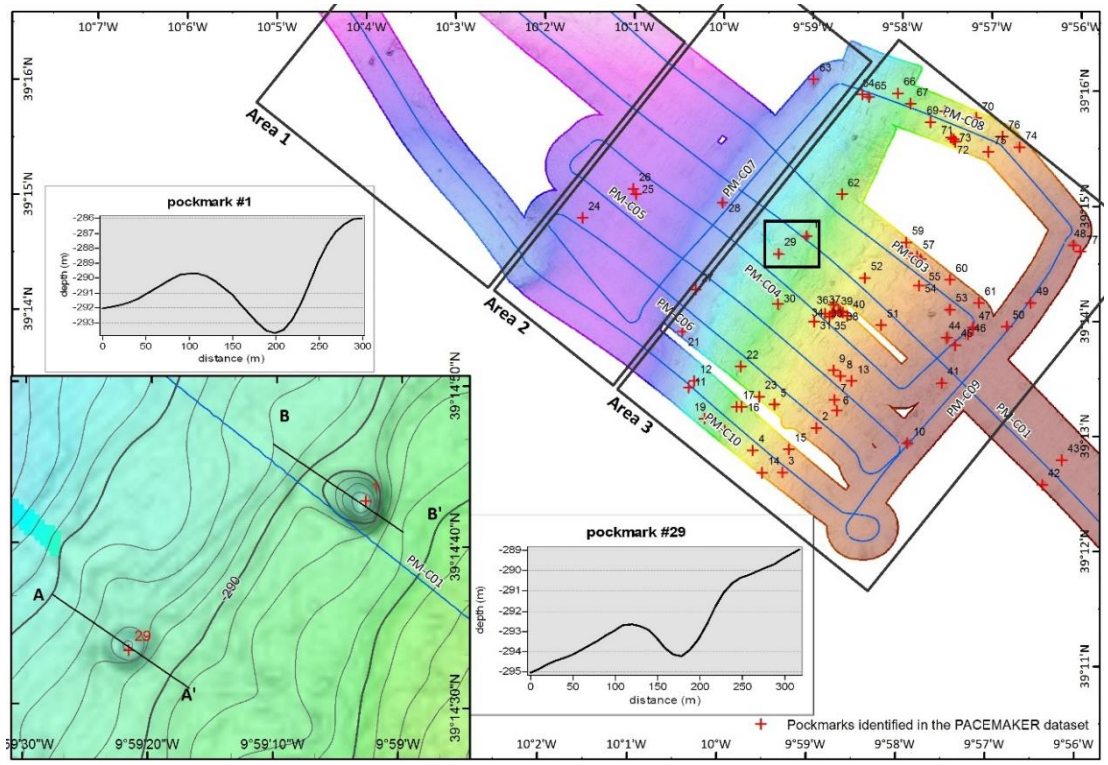

Figure 38 Detail of the seafloor bathymetry in a region with two depressions and topographic profiles of these features. Vertical exaggeration of profiles is approximately 25x.

Besides these negative round morphologic features, one topographically positive mound-like structure was mapped in the northwest of Area 1 (Figure 39). This feature has vertical relief of about 4 m and 200 m of diameter.

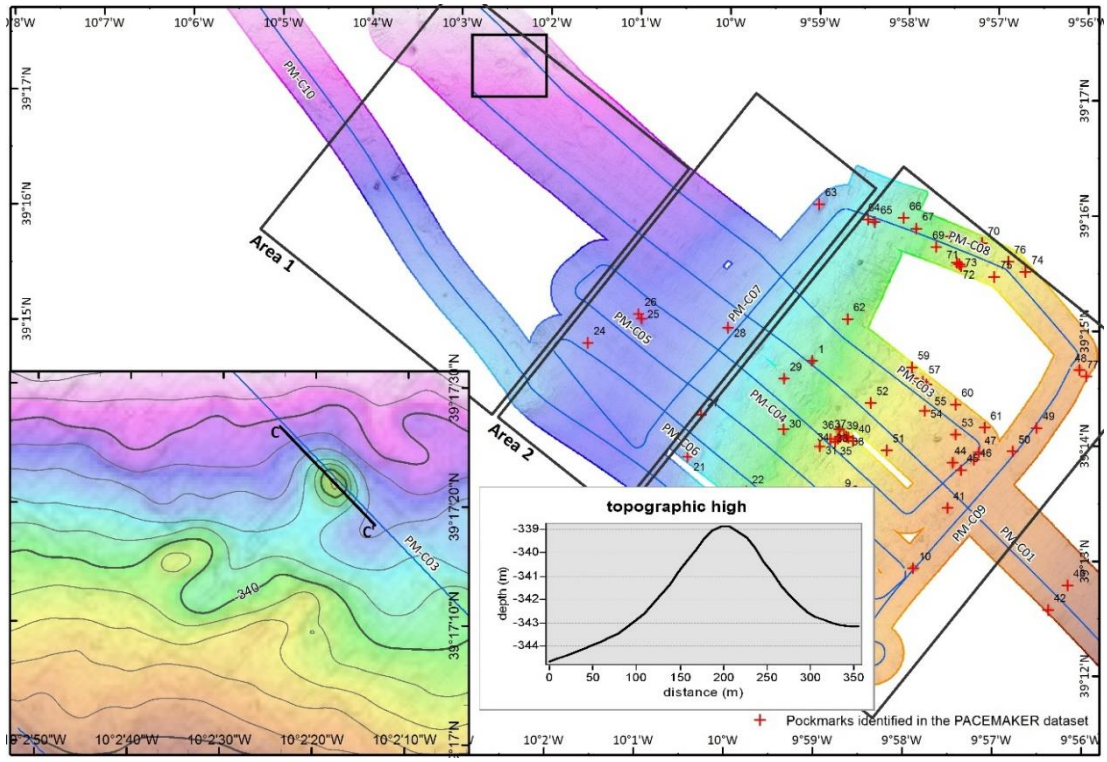

Figure 39 Detail of the seafloor bathymetry in the area with the positive relief and topographic profile of this high. Vertical exaggeration of profile ~25x. Slope of the flanks ~2º.

5.2 Backscatter analysis

The multibeam-derived backscatter images (Figure 40) shows different patterns for the Areas 1, 2 and 3. Area 2 display a monotonous low backscatter pattern with occasional intermediate intensity spots, separating Areas 1 and 3 that show a spotted backscatter pattern. The western region of Lourinhã Monocline, Area 1, is marked by a wide variation of backscatter intensity, with predominant low-backscatter areas and the high-backscatter facies appearing as spot clusters with a high concentration at the north-west edge of the covered area. In the eastern region of the Lourinhã Monocline, Area 3 a spotted backscatter pattern is observed, but as opposed to Area 1, this zone is characterized by the prevalence of high-backscatter facies.

Balsinha *et al*. (2014) characterized the sedimentary deposits of the outer shelf of the Estremadura Spur as dominated by sand and muddy sand sediments. In Sheet 4 of the Superficial Sediments Map (Figure 24 in Chapter 3) the seafloor sediments of the Lourinhã Monocline is also described, being this region mostly composed by sandy mud, but also by sand and some mixed sediments. Thus, the low acoustic seafloor reflectivity can be a consequence of the presence of these fine-grain sediments. The high-backscatter

facies, on the other hand, was interpreted as a consequence of the occurrence of coarser sediments or even exposed rocky outcrops, in areas of increased topographic relief (like the circular relief in Area 1, Figure 36, and the general higher slope angle in Area 3, Figure 36).

Some of the round depressions that have been observed in the bathymetry (Figure 38) are also visible in the backscatter imagery, being characterized by high-backscatter signal in the central part the depressions. Closer inspection of the image shows that the high backscatter spot can have a round (spot-like) shape, linear or wriggly.

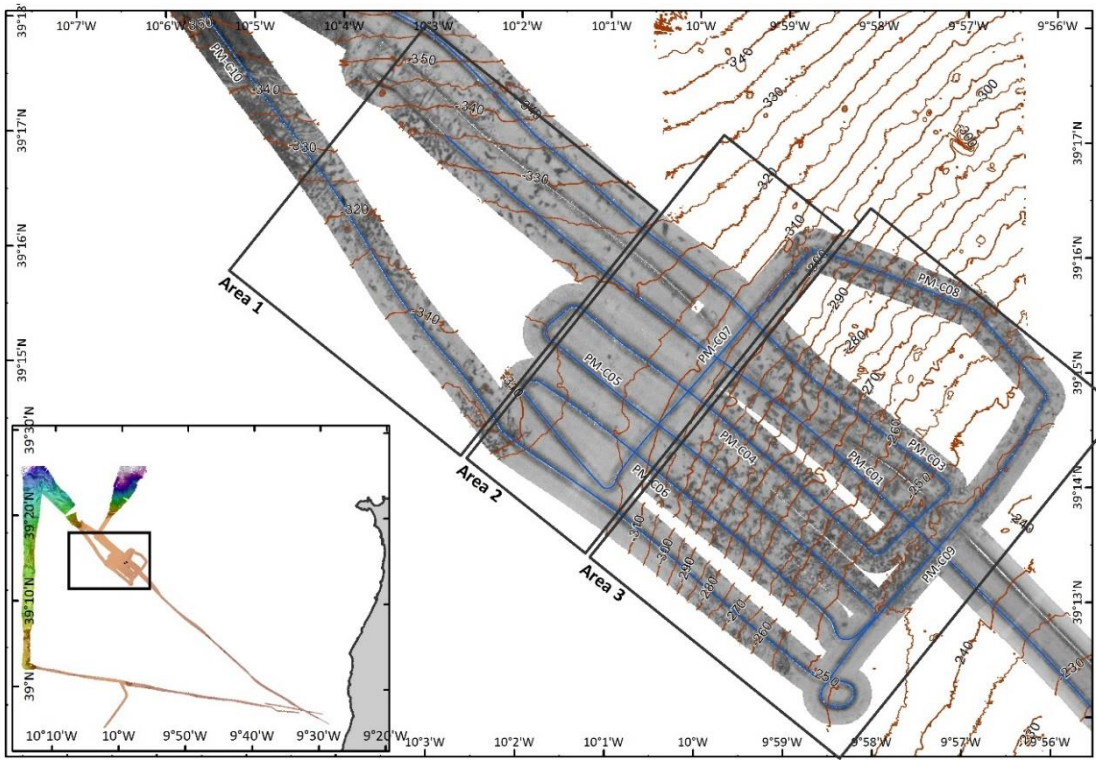

Figure 40 The Lourinhã Monocline area of the Estremadura Spur with the PACEMAKER Multibeam-derived backscatter imagery (lighter grey: low backscatter; darker grey: high backscatter). Equidistance: 5 m.

In Areas 2 and 3 six linear low-backscatter anomalies were identified, approximately with a NNE–SSW to N–S direction (Figure 40), that are oblique to the ship tracks, indicating that they are not artifacts resulting from data acquisition. These features were interpreted as the possible morphological expression of faults affecting the Lourinhã Monocline.
In Figure 41 it is observed the offset of the high backscatter facies (at SE) separated by one of these lineaments (red lines), suggesting a sinistral strike-slip component.

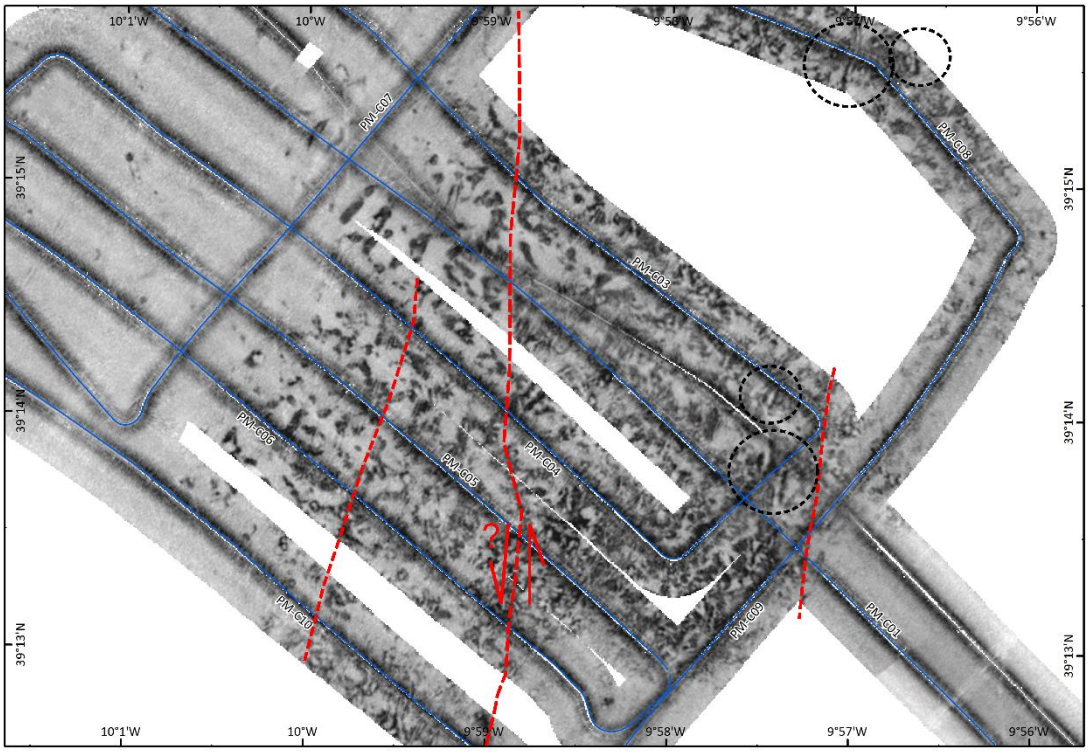

Figure 41 Detail of the Multibeam-derived backscatter imagery from the PACEMAKER survey in Area 2 and 3 (lighter grey: low backscatter; darker grey: high backscatter). **Red lines**: strike-slip faults; **Black circles**: icebergs ploughmarks. Equidistance: 5 m.

Other lineaments of smaller lengths and with various orientations are observed in Figure 41 (marked by black dotted circles), and have morphologies similar to the icebergs ploughmarks observed in the Norway offshore (Hovland, 2008). Both the faults and ploughmark-like have a small morphological expression and are not evident in the bathymetric map (Figure 36) due to their small depth.

5.3 ROV dives

During the research cruise EMEPC/PEPC/LUSO/2015, onboard the NRP Gago Coutinho, two dives with the EMEPC ROV Luso were carried out in the Lourinhã Monocline region (Figure 42). These dives, D06 and D07, allowed the direct observation of the seafloor and the recollection of push-core samples inside 3 of the rounded depressions.

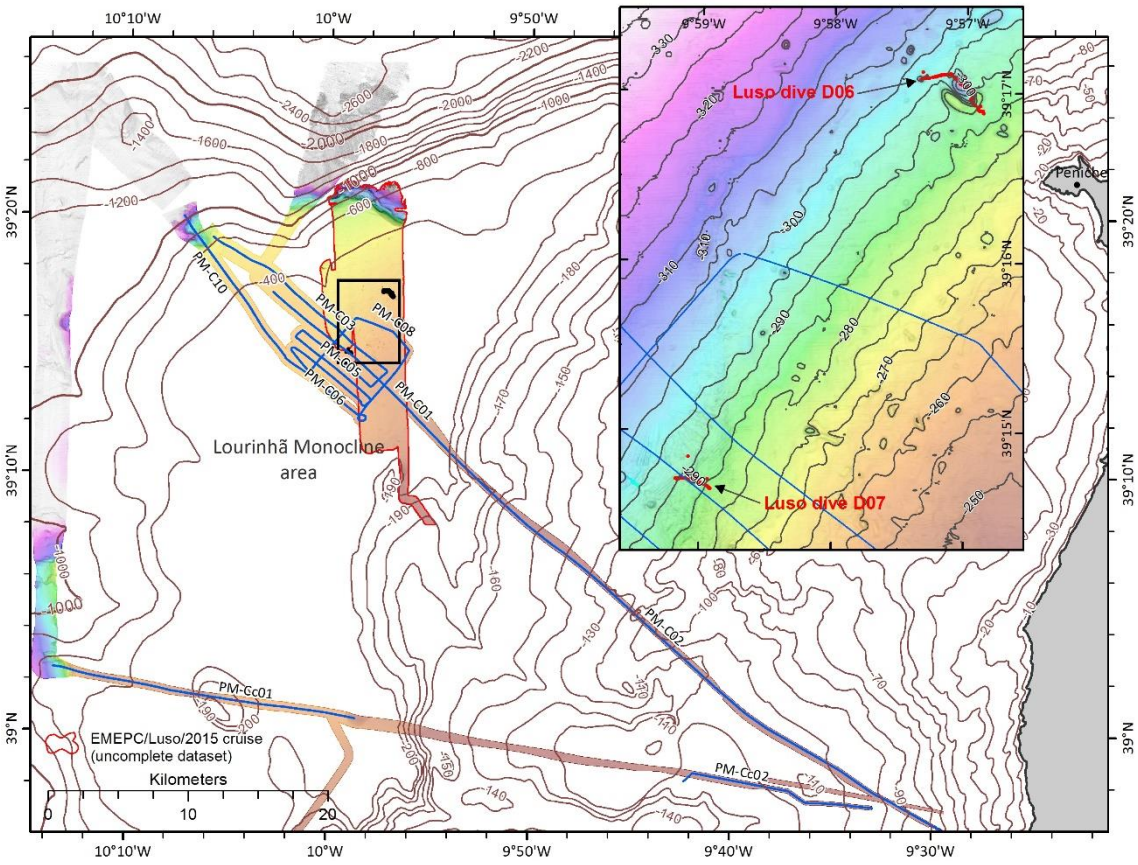

Figure 42 Location of the ROV Luso dives D06 and D07.Equidistance 5 m (between 0 and 200 mbsl); 200 m (below 200 mbsl).

5.3.1 ROV dive D06

Two of the depressions, located at 284 m water depth, were inspected (Figure 42) during this dive. The ROV was piloted along SE–NW and ENE–WSW transects. The first depression, L15D06.1, corresponds to the largest structure identified in the available multibeam dataset, it is elliptical with the big axis trending NW-SE, a maximum length of 400 m and a minimum of 230 m, and a depth of 17 m. The second structure, L15D06.2, is located W of the previous one. This feature has a circular shape, a diameter of about 85 m and height of 6 m. The seafloor, both outside and inside the depressed areas, is composed of a fine to coarse sandy non-consolidated sediment (Figure 43-A,C,D,E) rich in heavy minerals with very well consolidated rock clasts dispersed at the seafloor in small clusters (Figure 43-A,B,F). These rock clasts are more frequent along the slopes of the depressions and preliminary hand speciems observations indicate that they are composed by black colored breccias formed by sedimentary and igneous clasts, with quartz and bioclasts.

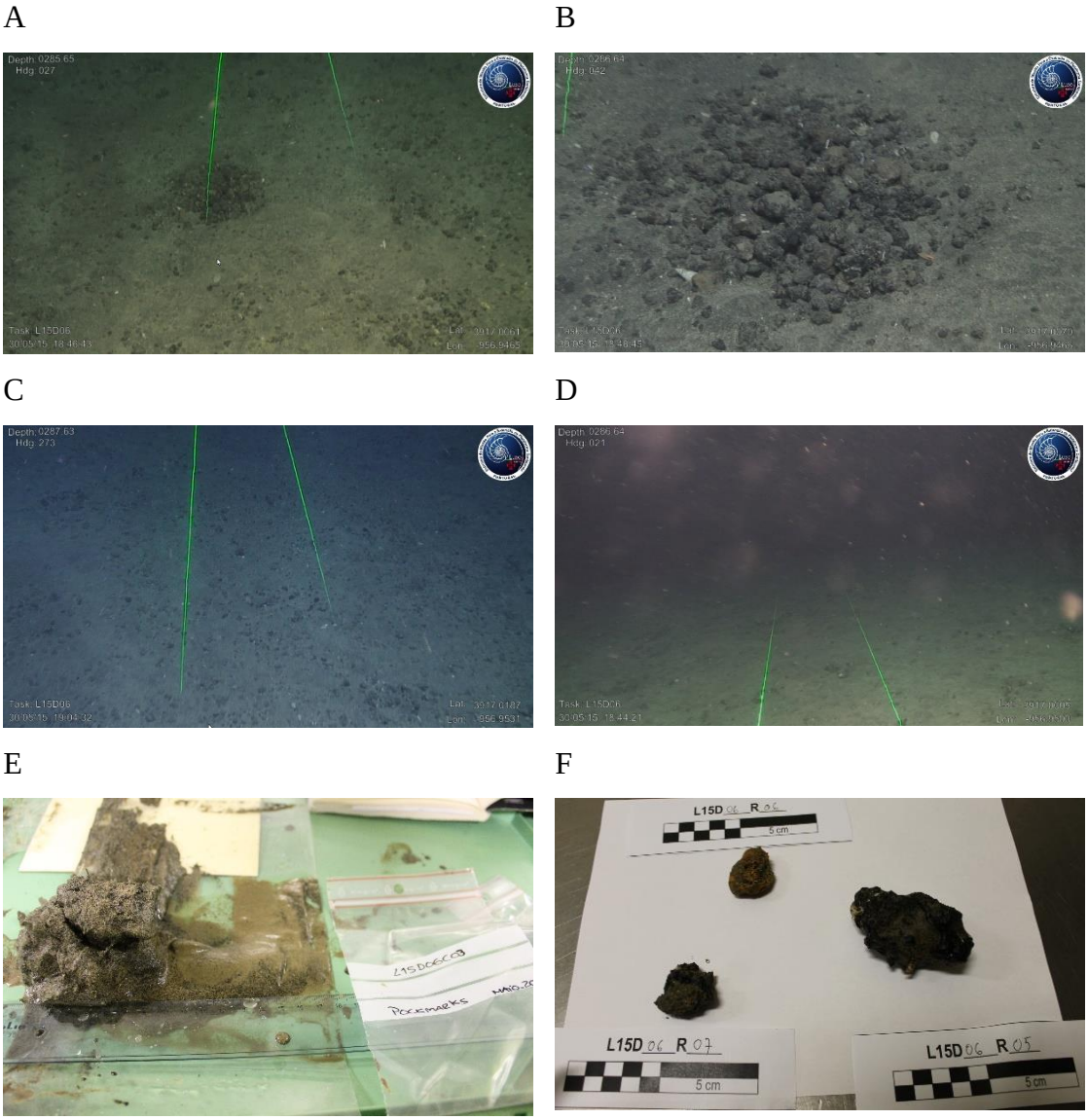

Figure 43 Photographs and samples collected during ROV/LUSO dive L15D06. Distance between lasers is 80 cm. (**A**-**D**) Seafloor aspects observed during the dive: (**A**) fine to coarse sandy sediment with a rock clasts cluster; (**B**) detail of a rock clasts (breccia) cluster; (**C**) and (**D**) general aspect of the sedimentation in the seafloor; (**E**) push-core recollected during the dive, showing fine to coarse sands, rich in heavy minerals and (**F**) rock clasts (breccia with heavy minerals) also recollected during the dive (courtesy of EMEPC).

5.3.2 ROV dive D07

This dive, carried out along a SE–NW transect, aimed to investigate one pockmark like feature (Figure 42), located at 300 m water depth, selected because it presented a high backscatter signature at its interior. This structure has a diameter of 120 m and 4 m depth. It started at 150 m SE of the structure, in an area of medium to high backscatter, corresponding to sandy sediments with some dispersed rock clasts (Figure 44-A, B, D) and sometimes small negative reliefs (20 to 50 cm in diameter and 10-20 cm depth)

(Figure 44-C), frequently filled by rock clasts of 2-10 cm in size (Figure 44-E, F). The flanks and base of the depressed structure had similar characteristics as the observed outside of the depression, but with a strong increase in the rock clasts density and a significant increase in the frequency of the small depressions filled with rock clasts. The lithology of these rock clasts is the same of the rock clasts observed in the dive D06, black colored breccias.

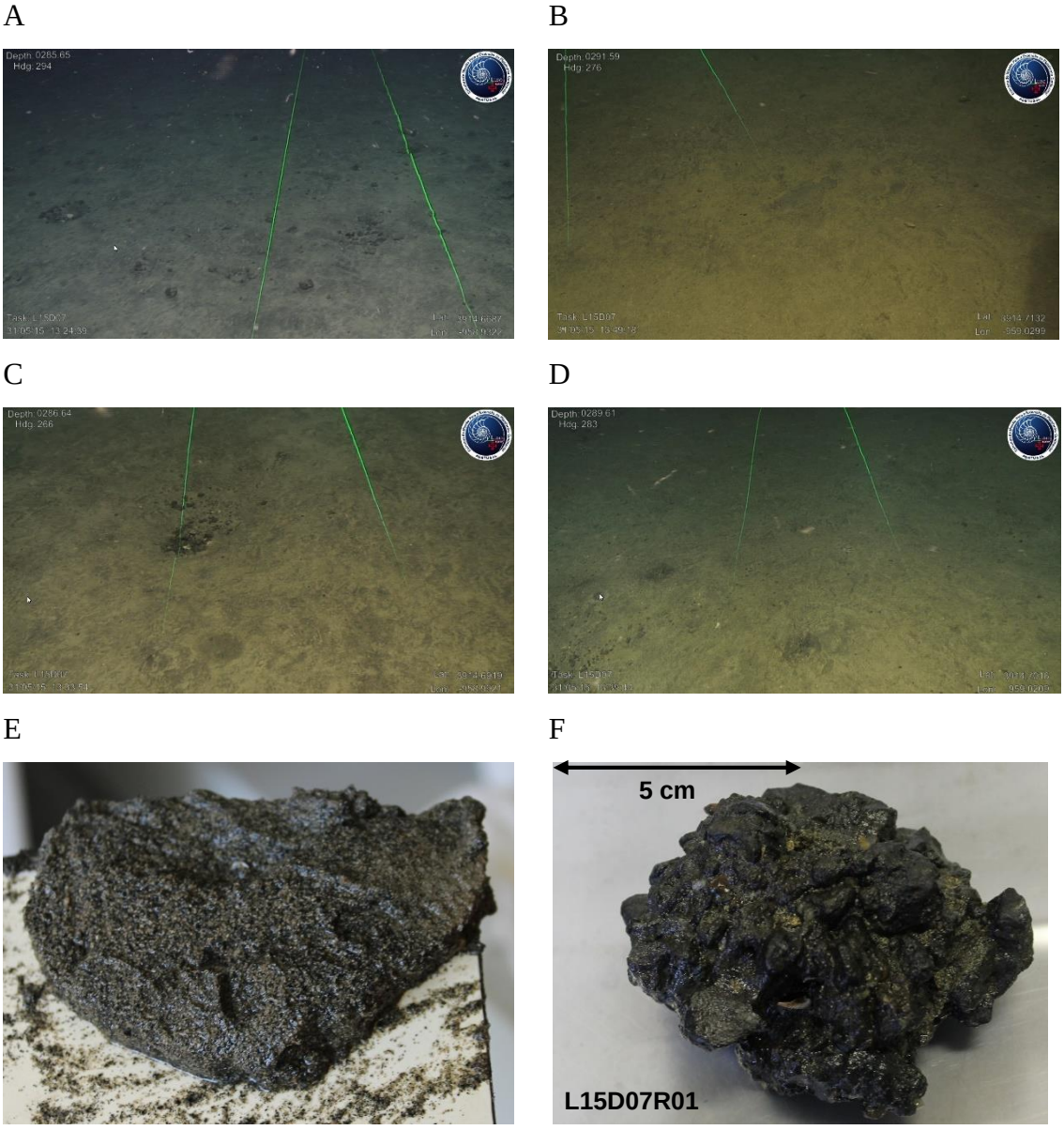

Figure 44 Photographs and samples collected during ROV/LUSO dive L15D07. Distance between lasers is 80 cm. (**A-D**) Seafloor sedimentation is mainly composed by fine to coarse sandy sediment with punctual rock clasts clusters, as seen in (**C**); (**E**) sediment recollected during the dive (push-core): fine to coarse sands, rich in heavy minerals and (**F**) rock clasts (breccia with heavy minerals) also recollected during the dive (courtesy of EMEPC).

These direct observations of the Lourinhã Monocline seafloor confirm the composition of the sedimentary deposits that occur in this region of the Estremadura Spur outer shelf. The black breccia clasts found dispersed at the seafloor in small clusters (e.g. Figure 43–B) appears to be an exotic lithology in this region, associated with the small depressions (20 to 50 cm in diameter and 10-20 cm depth) observed in the seafloor (Figure 44–C), especially within the depressed areas with low backscatter response.

5.4 Surface indications for fluids seepage from the seafloor

Multibeam and side-scan sonar surveys distinguish variations in the seafloor morphology, which can mark the location of fluid seeps (Judd and Hovland, 2007). The topographic expression of fluid expulsion at the seafloor commonly includes depressions, such as pockmarks and buildups, such as mud volcanoes. Commonly associated with these features exist chemosynthetic communities and authigenic carbonates that may cause higher acoustic impedance and roughness than in the surrounding seafloor (Orange *et al*., 2002 and Klaucke *et al*., 2006), making possible the recognition of these features by the effects they cause on the acoustic properties of near-surface sediments and the seafloor physiography.

The topographic depressions with circular to elongated shapes are interpreted as pockmarks, caused by the fluid escape at the seabed, based on their morphology, dimensions and for having high-backscatter response in their central part. The high acoustic seafloor reflectivity are, most probably, associated with the presence of hard-grounds of methane-derived authigenic carbonates. Although the existence of high-backscatter anomalies could be observed in several features in the Estremadura Spur, the seafloor observations during the ROV dives, has provided no evidences for seepage activity at present-day. The structures observed during the dives were found to be covered with sandy sediments and no carbonates were found. Also, neither bubbling nor characteristic fauna were observed and the seafloor in these sites.

Gay *et al*. (2007) sustains that seep sites, both active and recently active but currently inactive and buried under 10 m of sediments, may create anomalies on the backscatter signal (described in Chapter 4; Figure 28).

CHAPTER 6

SEISMIC DATA PROCESSING

The aim of the seismic data processing, is to increase the signal-to-noise ratio and to improve the vertical resolution of the individual seismic traces. The main types of waveform manipulation are frequency filtering and inverse filtering (deconvolution). Frequency filtering can improve the signal-to-noise ratio, but it damages the vertical resolution, conversely the inverse filtering improves the resolution, but decreases the signal to noise ratio (Kearey *et al*., 2002). The processes of seismic data processing used in this work are presented in this chapter as well as a brief explanation of the basic theoretical concepts involved and the results of each process in the seismic data.

6.1 Data Acquisition Parameters

The processed seismic data consist of 14 single-channel high-resolution 2D seismic profiles acquired during the PACEMAKER survey, with a sparker source, during the Cruise 64PE332 aboard the RV Pelagia in March 2011.

The PM seismic dataset was acquired with 1000 J of energy except PM-C01, which was obtained with 300 J and the lines PM-C02 and PM-C02pt1, obtained with 500 J. In Table 7 a portion of the log book from the campaign is presented where the different acquisition parameters and characteristics are listed as well as some other relevant informations. The sparker seismic profiles had an average signal penetration of 100 ms below the seafloor, with coherent signal being observed at more than 150 ms below seafloor.

Table 7 Log book of the PM survey for Estremadura Spur seismic lines.

Line	Power	Trigger	Active Section Length	Number of Hydrophones	Record Length	Sample Interval	Sample Format	Hardware Gain	SoL	EoL	Shots	Average Speed	observations
PM-C01	300 J	700	3.5 m	4	650	0.1ms	4byteInt	24db	03h37-21Mar11	05h28-21Mar11	9561	5knts	lower energy and speed for piston site survey
PM-C02	500 J	500	3.5 m	4	450	0.1ms	4byteInt	24db	05h29-21Mar11	06h55-21Mar12	10239	8knts	
PM-C02-Part01	500 J	500	3.5 m	4	450	0.1ms	4byteInt	24db	06h55-21Mar11	08h14-21Mar11	9498	5knts	
PM-C03	1000 J	1000	3.5 m	4	950	0.1ms	4byteInt	24db	22h30-21Mar11	00h12-22Mar11	6291	5knts	
PM-C04	1000 J	1000	3.5 m	4	950	0.1ms	4byteInt	24db	00h13-22Mar11	01h03-22Mar11	3045	5knts	
PM-C05	1000 J	1000	3.5 m	4	950	0.1ms	4byteInt	24db	01h03-22Mar11	01h54-22Mar11	3091	5knts	
PM-C06	1000 J	1000	3.5 m	4	950	0.1ms	4byteInt	24db	01h55-22Mar11	02h45-22Mar11	2962	5knts	
PM-C07	1000 J	1000	3.5 m	4	950	0.1ms	4byteInt	24db	02h45-22Mar11	03h31-22Mar11	2803	5knts	Change in survey plan due to fishing traffic
PM-C08	1000 J	1000	3.5 m	4	950	0.1ms	4byteInt	24db	03h31-22Mar11	04h11-22Mar11	2311	5knts	
PM-C09	1000 J	1000	3.5 m	4	950	0.1ms	4byteInt	24db	04h11-22Mar11	04h52-22Mar11	2489	5knts	
PM-C10	1000 J	1000	3.5 m	4	950	0.1ms	4byteInt	24db	04h52-22Mar11	07h36-22Mar11	9838	5knts	
PM-Cc01	1000 J	1000	3.5 m	4	950	0.1ms	4byteInt	24db	04h13-23Mar11	07h47-23Mar11	9248	5knts	Lost GPS signal at from trace 8953 to 9248 end of the line
PM-Cc02	1000 J	1000	3.5 m	4	950	0.1ms	4byteInt	24db	07h51-23Mar11	09h42-23Mar11	10239	5knts	No GPS signal until trace 8557
PM-Cc02-part-01	1000 J	1000	3.5 m	4	950	0.1ms	4byteInt	24db	09h42-23Mar11	10h32-23Mar11	3012	5knts	

6.2 Processing Steps

A total of fourteen seismic profiles from the PACEMAKER data set were processed. A seismic processing flow chart was developed (Figure 45), based in the basic processing of high resolution seismic data. The processing steps and their results are here illustrated for the line PM-C07. The geometry have been already corrected onboard, thus it was not necessary to perform this step.

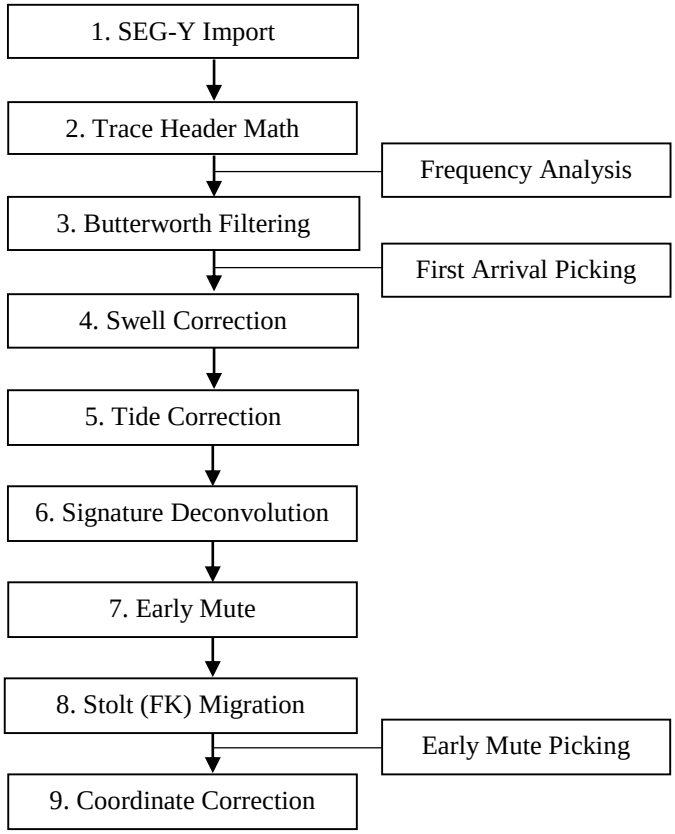

Figure 45 Processing steps of seismic data.

6.2.1 SEG-Y Import

The first step of the processing sequence was the import of the seismic raw data (Figure 46) in SEG-Y format into SPW. This was done using the SEG-Y Import function (*Processing Categories > Seismic Data > SEGY Import*). Since SPW uses SEG-Y as its internal processing file format, this step was done to create an index file for each SEG-Y file (*Build Index*). The index files contain the necessary information (trace header fields) to perform the processing and are required to be present for the display of the data.

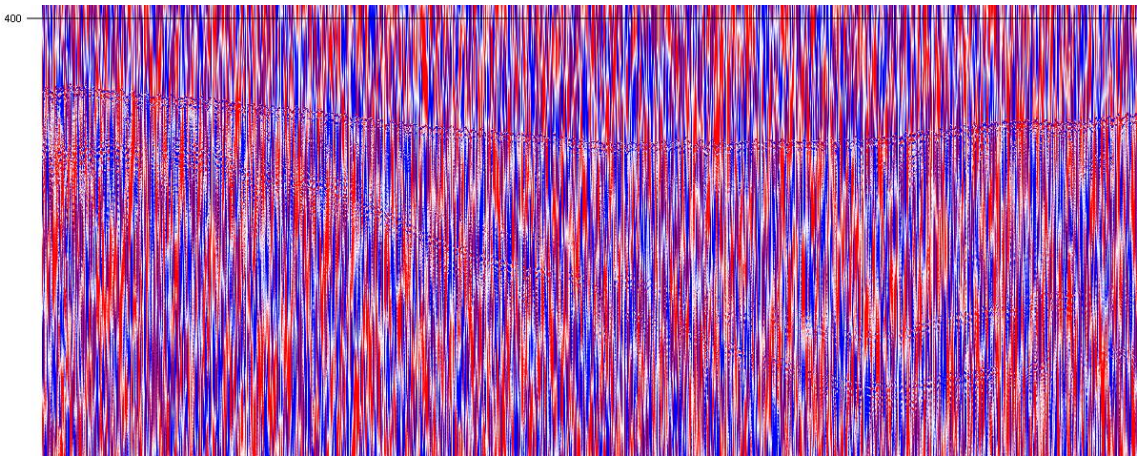

Figure 46 PM-C07 raw data.

6.2.2 Trace Header Math

To perform the picking of the seafloor reflection and for muting the noise present in the water column it is necessary that each trace data is sorted according with its offset (therefore, the sort keys must be displayed according to common shot). To be able to sort the keys according to the shot order, the trace headers fields: Source Line, Source Location and Offset were edited (with the function *Trace Header Math*, from *Processing Categories* > *Editing*). The Source Line field was calculated as equal to the Channel field value (which was a constant value, as the data is single-channel), the Source Location was also filled with a constant value (in this case: 13), and the Offset header (that was absent) was calculated as being equal to the Field File multiplied by 2.

6.2.3 Butterworth Filtering

Unwanted frequency bands are removed from the seismic data preserving the frequency band that contains the relevant information. In other words, before the filter application it is advisable to limit the frequency band of the data, in order to remove components that are usually classified as noise, such as the low frequencies (produced by ocean waves for example).

The application of frequency-filtering requires the display of the data in the frequency domain (amplitude as a function of frequency), which is achieved using the Fourier transform. The most common types of filters in the processing are Band-pass, High-pass and Low-pass filters.

To select the most appropriate filter to this dataset we first analyzed the amplitude spectra of the seismic lines (*Data and Display Tools > Calculate Spectra in a Rectangular Window* in the *Seismic Display Control Panel*), and then select a trace/time window for which we calculate the amplitude spectra. According to the amplitude spectra of the PM-C07 seismic line, the predominant band of frequencies was located between 450 Hz and 2000 Hz (Figure 47).

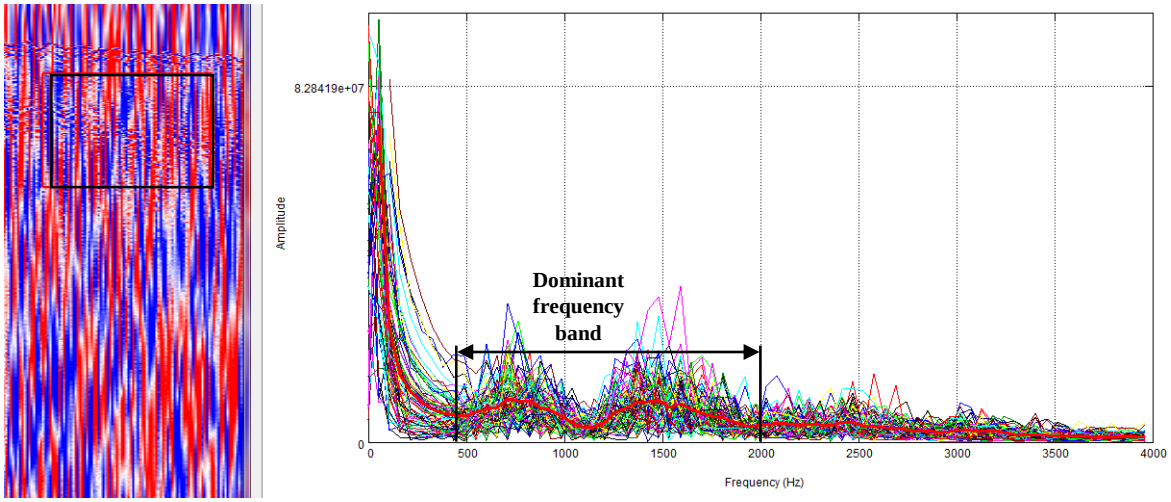

Figure 47 Amplitude spectra of PM-C07 seismic profile. The predominant signal frequency are located between 450 and 2000 Hz. **Black box:** sampled area; **Red line**: frequency mean.

To decrease the level of low-frequency noise, various hypotheses were tested (Table 8) to find the right parameters for the filtering the seismic raw data (Figure 48 – A).

Table 8 Parameters used in the Butterworth band-pass filter tests.

Low cut (Hz)	High cut (Hz	Attenuation ramp (dB/octave)	Figure
200	1500	18/18	Figure 48 – B
500	**2100**	**18/18**	**Figure 48 – C**
800	3000	18/18	Figure 48 – D

According to the tests, the best results were obtained with the cut-off values defined in the 500 and 2100 Hz domain, and the attenuation ramp set for 18 dB/ octave in both (Figure 48– C). After the application of the filter some noise is still observed in the upper part of the seismic data. Considering the characteristics of the equipment used for the acquisition and the amplitude spectrum of this noise, one can assign it to the direct waves, i.e., seismic waves that have traveled directly from the transmitter to the receiver. This

noise was not eliminated in this processing step because since its frequency band is similar to the signal's band its elimination would lead to signal loss.

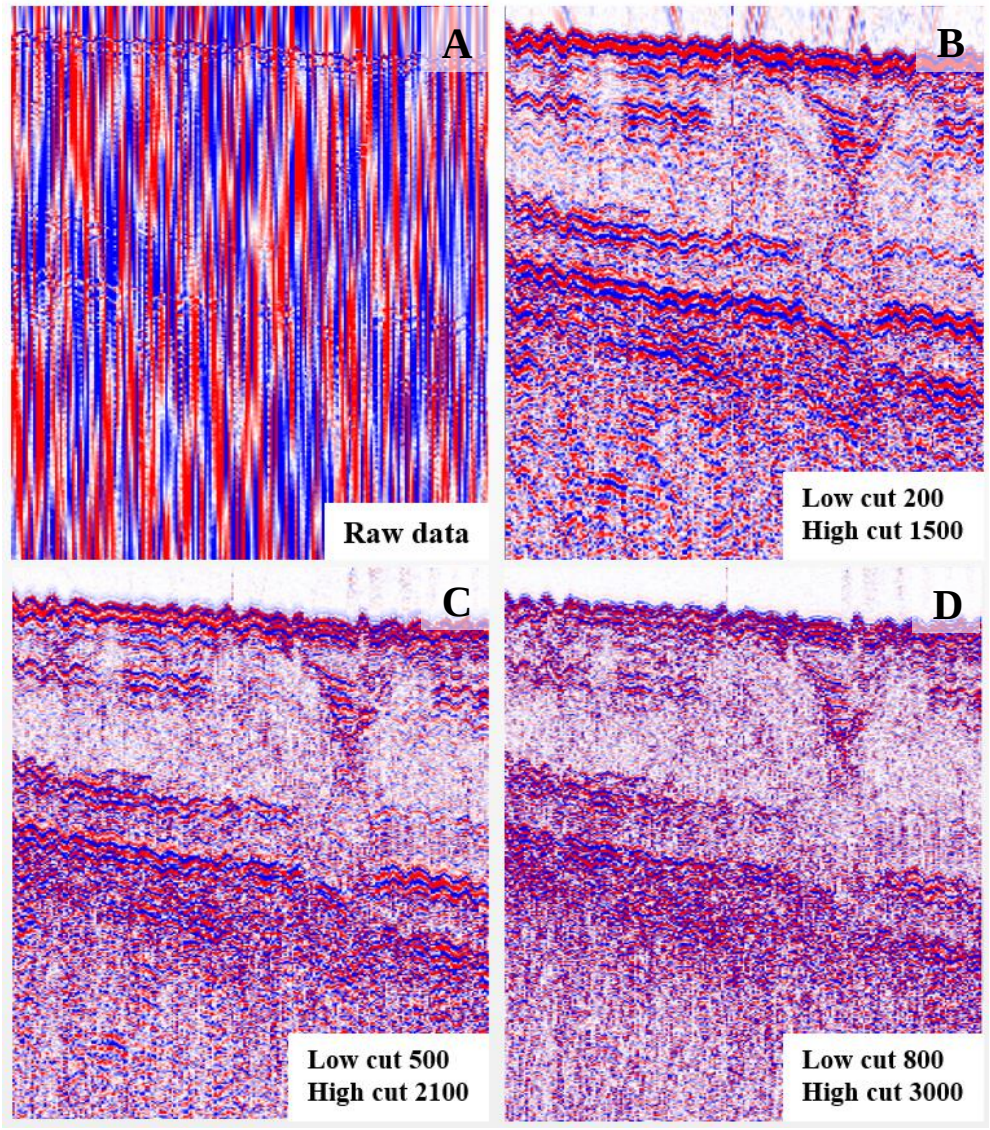

Figure 48 Butterworth band-pass filter test. The best results were acquired with the low-cut of 500, high-cut of 2100 and an attenuation ramp set for 18 dB/ octave (**C**).

6.2.4 Swell Static Correction

The swell filter refers to the static correction that restores the coherence of a high resolution seismic profile. High-resolution marine seismic surveys, such as this dataset, are used to detail image subsurface geology. During the seismic data acquisition, the sea swell condition influence quality of the data, not only the signal/noise ratio, but also the sea swell, leads to a loss of lateral coherence of the reflectors. The application of the swell filter minimizes the positioning errors of the seismic traces from the seismic profile. The

swell filter is a static correction applied to each trace, according to a sinusoidal function with a height and wave length defined by the user that will compensate the vertical shift of each trace during the acquisition due to the sea swell.

To correct the swell it was first necessary to pick the seafloor reflection on each trace and save it in a card data: this was done by applying a first arrival picking detection algorithm to detect the sea floor and then a manual adjustment was done to accurate the picking.

After doing that, the SPW's Swell Statics function (*Survey* > *Marine Statics*) was used, and the statics shifts caused by the ocean swell was corrected, by applying a filter to the file resulting from the seabed picking. Various hypotheses were tested for finding the right filter length, as shown in Figure 49. These were the filter lengths tested: 15, 25 and 35 traces with the maximum shift of 10 ms.

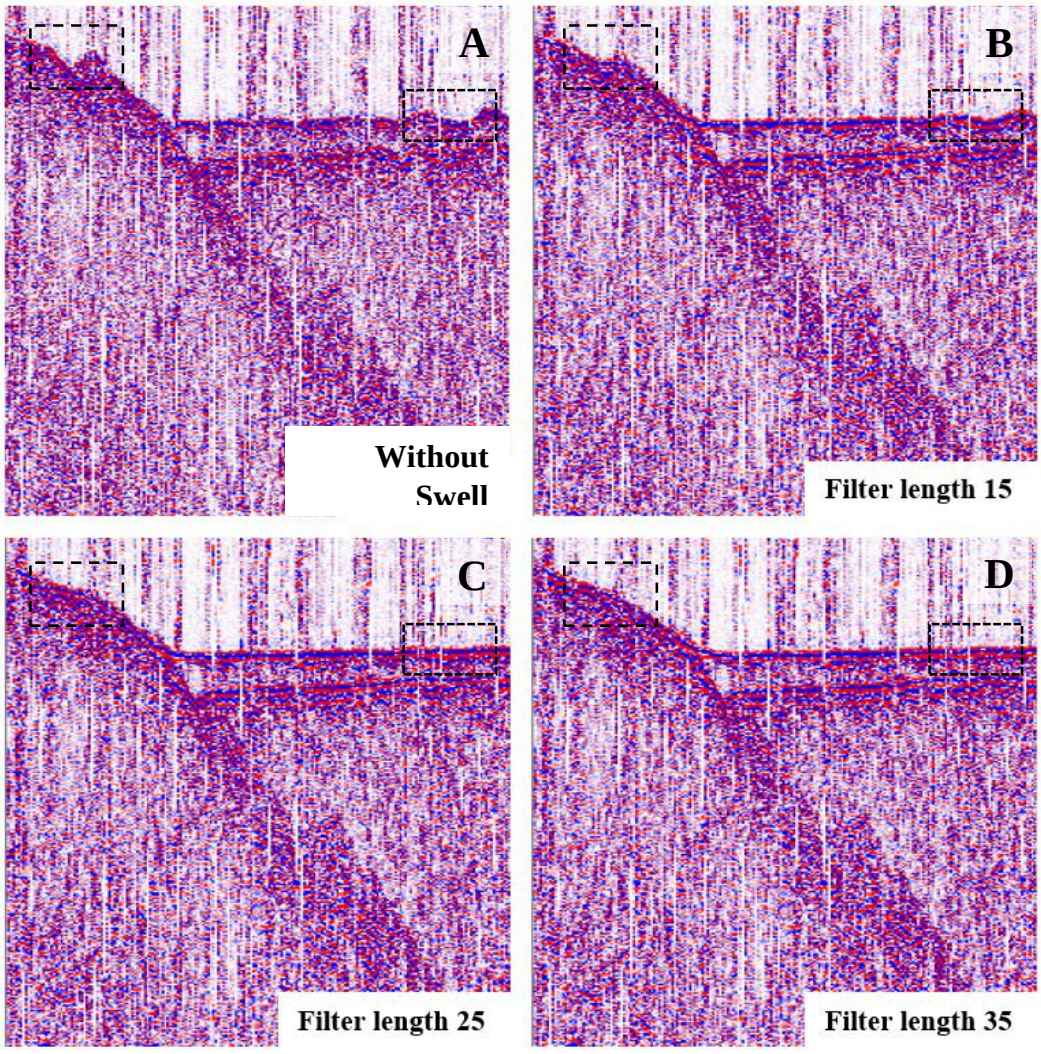

Figure 49 Swell filter length test in seismic line PM-C02. **A**: data without the swell correction; **B**, **C** and **D**: filter length of 15, 25 and 35, respectively. **Black rectangles** shown differences in the attenuation of the seabed caused by the different filter lengths.

It was chosen the filter length of 25 traces because although it soothes the seabed surface and corrects the swell effect, it keeps the small variations of this reflector that may be related to its geological structure or real morphology (Figure 49– black rectangle).

Finally, this file was loaded into a trace statics card file (*Processing Categories > Auxiliary Data R-Z > Trace Statics*) and a Statics Shift was applied, based on this file (*Processing Categories > Statics > Apply Statics Shift*). The final result of this step is shown in the Figure 50.

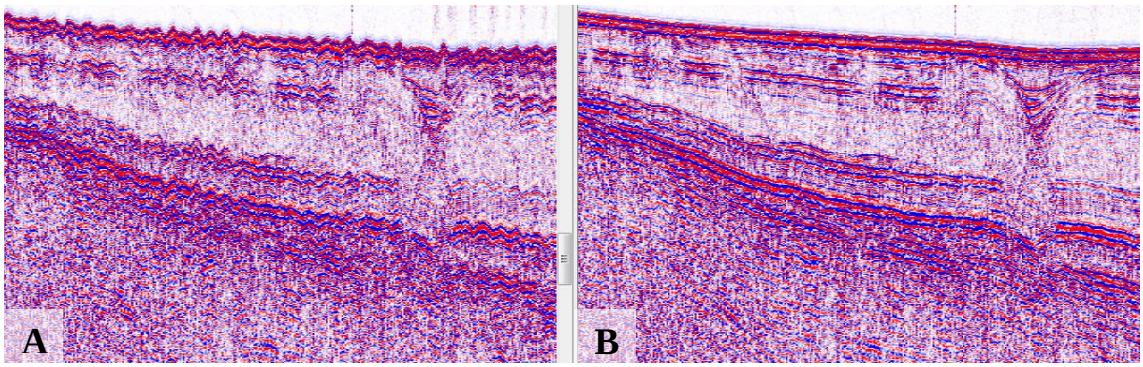

Figure 50 Detail of PM-C07 line before (**A**) and after (**B**) the swell correction

6.2.5 Tide Static Correction

In seismic data processing, tidal static corrections are important to determine the reflection arrival times that would have been observed if data had been recorded on a flat reference datum. The level of the ocean as well as its physical properties varies with tides, currents or seasonal changes. Tide variations will affect the water depth, whereas changes in salinity or temperature will result in a change of seismic velocity. As marine data were acquired in a group of seismic lines that were shot in different days, or in different phases of the tide cycles, this will induce lateral discontinuities between the different seismic lines. So, it's important to correct these variations before the seismic lines are imported into an interpretation software, so the interception of the different seismic lines will not show any vertical lags or discontinuities.

To make the correction of the tidal statics tide tables were used, even though their accuracy can be questioned. The tide tables from Instituto Hidrográfico were used (www.hidrografico.pt*/previsao-mares.php*), measured in Peniche in the days of seismic lines acquisition (21, 22 and 22 March 2011). After getting the tide level data (values of

high tide and low tide) these values were linearly interpolated for all Trace Numbers of each seismic line. Linear interpolation is a method to estimate the value of a function between two known values using the equation of the straight line. The calculation of the tide level was done using Excel, following these steps:

- Tide level interpolation for certain time intervals in order to know the tide level when the line was started (SoL) and finished (EoL);
- Interpolation of the tide level for each Trace Number, to know the height of the tide in each shot of lines;
- Conversion from depth (m) to time (twt in ms), using a reference value of 1500 m/s (sound velocity in salt water).

Linear interpolation involves estimation of a new value by connecting two adjacent known values with a straight line. The equation of linear interpolation for the interval (x_0, x_1) is (solving it for y, which is the unknown value at x),

$$y = y_0 + (y_1 - x_0)\frac{x - x_0}{x_1 - x_0} \qquad \text{Equation 4}$$

To convert the tide level from depth to time the following conversion was made,

$$twt = (tide\ level/1.5) \times 2. \qquad \text{Equation 5}$$

Then the values were copied (trace number and tide level in two way time) for a Trace Static card file (*Processing Categories > Auxiliary Data R-Z > Trace Statics*). Finally the file was loaded into a trace statics card file (*Processing Categories>Auxiliary Data R-Z> Trace Statics*) and a Statics Shift was applied, based on the tidal values file (*Processing Categories> Statics> Apply Statics Shift*). This step is important since when the seismic lines were imported to the interpretation software, the points where the lines intersect show a good coincidence and the vertical displacement between the lines is minimal.

6.2.6 Deconvolution

Deconvolution is an inverse filter used to improve seismic data since it removes the adverse filtering effects encountered by seismic waves as they pass through the ground. It is applied to increase the temporal or vertical resolution of seismic traces and can also remove reverberations and contributes to the attenuation of multiple reflections. This filter should be able to provide the impulse response of the earth (reflectivity function) when applied to the seismic trace.

It was chosen to apply a Signature Deconvolution to the data (*Processing Categories* > *Wavelet Shaping* > *Signature Deconvolution*), which filters the data with the seismic signature inverse. This signature is supplied from the selected data traces. The seafloor reflection was used to estimate the trace signature since the direct wave signal was affected by the swell and didn't provide enough quality to choose the parameters.
A set of parameters need to be defined for the signature deconvolution application, such as pre-whitening, inverse filter length, signature input start time and the input signature length. Three different combinations of parameters (values) were tested for the implementation of the deconvolution in the seismic data (Table 9; Figure 51).

Table 9 Parameters combination tested for Signature Deconvolution.

Pre-whitening	**Inverse Filter Length**	**Signature Input Start Time**	**Input Signature Length**	**Figure**
0.10 %	2.5 ms	415 ms	5 ms	Figure 51 – B
0.10 %	**5 ms**	**415 ms**	**10 ms**	**Figure 51– C**
0.10 %	7.5 ms	415 ms	15 ms	Figure 51– D

The test that presented better results was the one that defined the inverse filter length in 5 ms and the signature input start time in 415 ms with a length of 10 ms, where it was observed a slight improvement in the resolution of the signal. Despite this, it was not noticed any great improvements in seismic signal from the application of this processing step.

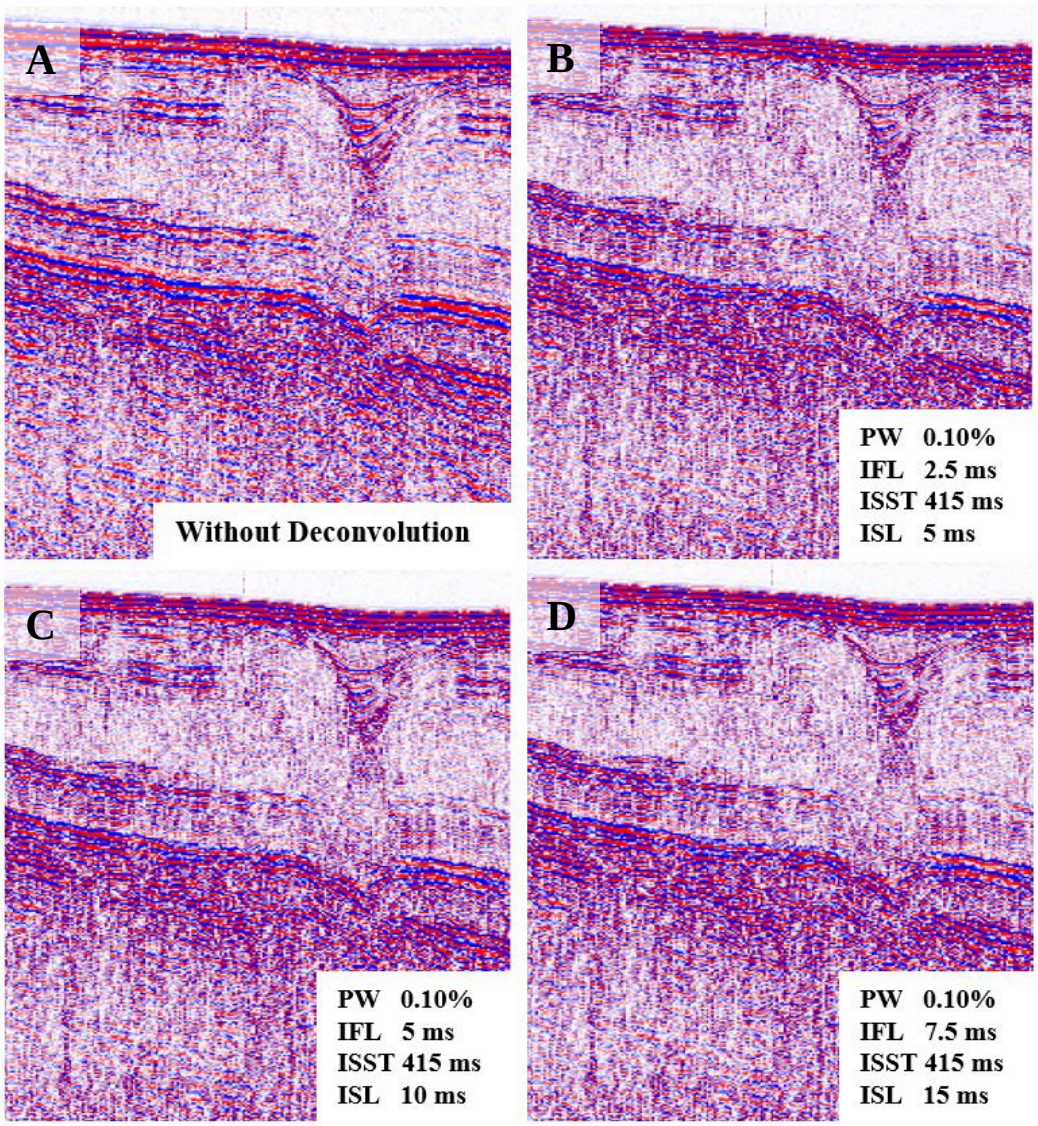

Figure 51 Deconvolution parameters test. **A**: data before the deconvolution was applied. **B**, **C** and **D**: tests with the deconvolution parameters pre-whitening (PW), inverse filter length (IFL), input signature start time (ISST) and input signature length (ISL). The parameters defined in **C** were those with the best results.

6.2.7 Early Mute

To apply the mute, it was first necessary to pick the seismic lines just a little above the seabed reflector, in order to cut the whole area above, and save it in a card data (*Seismic Picker > Mutes: Early Mute*). Then, all traces were muted between 0 ms and the seafloor reflector (Figure 52), in order to eliminate the relative contributions of the direct arrivals and the noise present in the water column (*Processing Categories > Mutes > Apply Early Mute*).

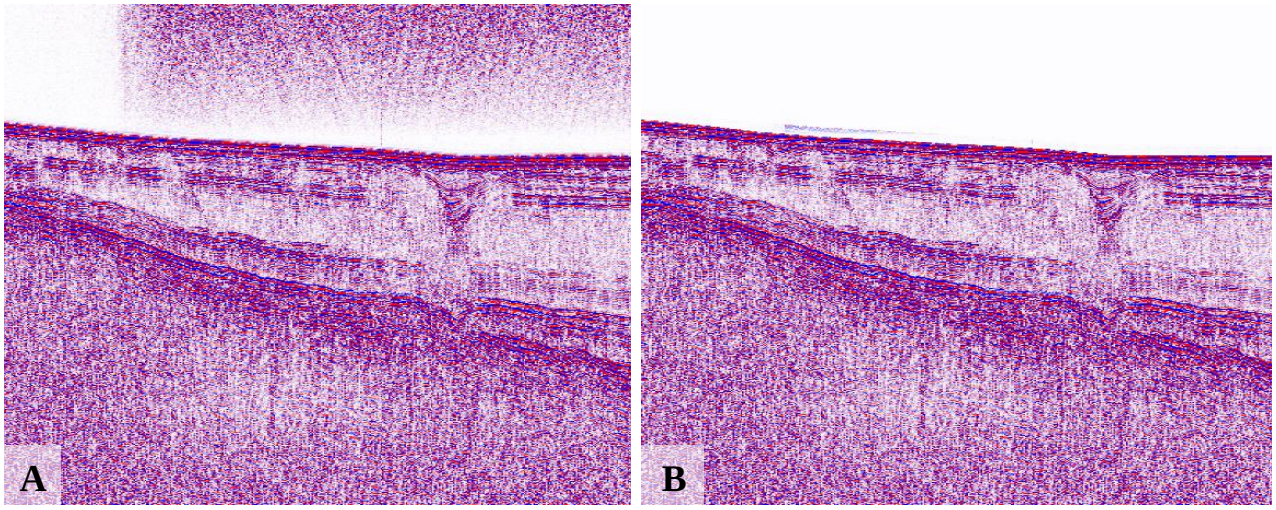

Figure 52 PM-C07 seismic line before (**A**) and after (**B**) the application of early mute.

6.2.8 Migration

Migration is one of the key steps in seismic data processing. Migration is a process in which a seismic section is reconstructed, so that all the seismic events are repositioned to their correct subsurface location with a corrected vertical reflection time. The process of migration also improves the resolution of the seismic section by focusing all the energy spread over the Fresnel zone and collapses diffractions, thereby delineating subsurface features, such as fault planes, with increased detail.

A Stolt (2D) migration was performed (*Processing Categories> Migration*), with a constant velocity of 1500 m/s (sound velocity in sea water) and the maximum frequency to migrate defined in 2100 ms (the high-cut frequency of the Butterworth filter). It was also defined the true trace spacing of 2.2 m. The result of this processing step is observed in Figure 53.

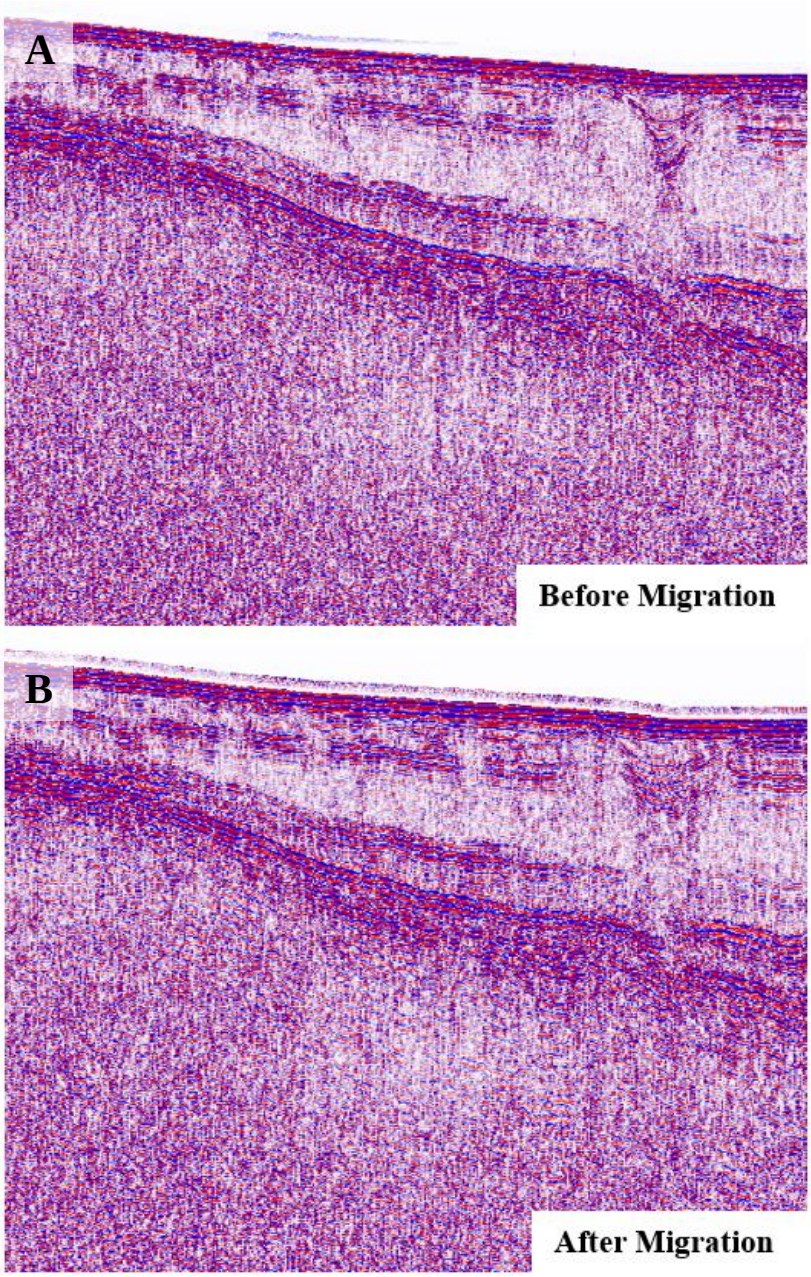

Figure 53 Detail of PM-C07 seismic line before (**A**) and after (**B**) migration.

6.2.9 Coordinates Correction

The last step in the processing flow was the correction of the location or coordinates of the seismic lines. It was done in SeiSee software. First, the geographic coordinates were converted to Universal Transverse Mercator (UTM). Then, in SeiSee the trace headers of the seismic data were exported as an ASCII file. The headers were edited, modifying the columns from SAC, SRCX and SRCY (scale factor and coordinate values). Finally, the changed files were imported back into the SeiSee (*Import Trace Headers from ASCII files*).

The final result of the processing flow was considered positive, since most of the noise that were masking the seismic signal was eliminated. Thus, (e.g. PM-C07; Figure 54) the structure of the ES subsurface can be effectively observed in the seismic profiles, to about 500 ms TWT.

6.3 Seismic Resolution

Seismic resolution is the ability to distinguish between two features in seismic data. It refers to the necessary minimum distance between these features such that is possible to distinguish that these are two features rather than one (Sheriff and Geldart, 1995). In reflection seismic data, the depth is normally measured in two-way travel time in milliseconds or seconds. This is the time that the sound waves takes since they leave the seismic source until they hit the reflector and return to the seismic receiver. With the increase in depth, the frequency of the signal will decrease while the velocity and wavelength will increase. This means that with the increase in depth, the seismic resolution decreases. The high frequencies are preferentially reflected from the shallower reflectors, while the low frequencies can reach further down in the sedimentary column. The velocity of the sound increases with increasing depth as the sediments are gradually more compacted with increasing depth and therefor denser. The seismic resolution can be characterized in two types, vertical resolution and horizontal resolution.

6.3.1 Vertical resolution

The smallest distance, in time or depth, between two layers appearing as separate reflections is called vertical resolution. The vertical resolution is dependent on the wavelength of the sound waves and the layers can be discerned when their thickness is more than 1/4 of the dominant wavelength. For two reflections, the limit for how close they may be is calculated by the Yilmaz (2001) expression:

$$Vertical\ Resolution\ = \lambda/4 = ({}^{v}/_{f})/4 \qquad \text{Equation 6}$$

where $\boldsymbol{\lambda}$ the dominant wavelength, $\boldsymbol{v}$ is the seismic velocity and $\boldsymbol{f}$ is the seismic frequency. A spectrum analysis was performed to calculate the frequency spectrum and the dominant frequencies of the PACEMAKER dataset (third topic of the Processing Steps - Butterworth Filtering). As shown in Figure 47, the predominant band of frequencies are located between 450 Hz and 2000 Hz, and the dominant frequency is 700 Hz. For the

sound wade velocity value it was considered the velocity of the sound in water, 1500 m/s and therefore the seismic vertical resolution is approximately 50 cm.

$$\lambda = v/f$$

$$\lambda = 1500/700$$

$$\lambda = 2.14$$

$$Vertical\ Resolution = 1/4\ \lambda$$

$$Vertical\ Resolution\ = 0.5\ m^3$$

6.3.2 Horizontal resolution

Horizontal resolution is the minimum distance between two reflection points that will give two separate reflections. It depends on the frequency and on the velocity of the seismic waves (Yilmaz, 2001) and is determined by the width of the first Fresnel Zone on the non-migrated seismic sections. The Fresnel Zone is a function of the signal frequency and of the distance between the reflector and the signal source (Equation 4). When the reflector dimensions are smaller than this zone, their response is that of a diffraction point (Sheriff and Geldart, 1995).

$$r\ =\ v/2\ \sqrt{t/f} \qquad \text{Equation 7}$$

Where ***r*** is the radius of the 1º Fresnel zone, ***v*** is the average sound velocity, ***t*** the depth in time and ***f*** the signal frequency. Using the parameters of the PACEMAKER acquisition the horizontal resolution can be calculated as follows:

$$r\ =\ 1500/2\ \sqrt{0.42/700}$$

$$r\ =\ 750\ \sqrt{0.0006}$$

$$r\ =\ 18.37\ m$$

$$Horizontal\ Resolution =\ 18.37\ m, \text{for } 420 \text{ ms depth.}$$

[3] The calculated value is in disagreement with the values from the Technical Manual in Chapter 4.

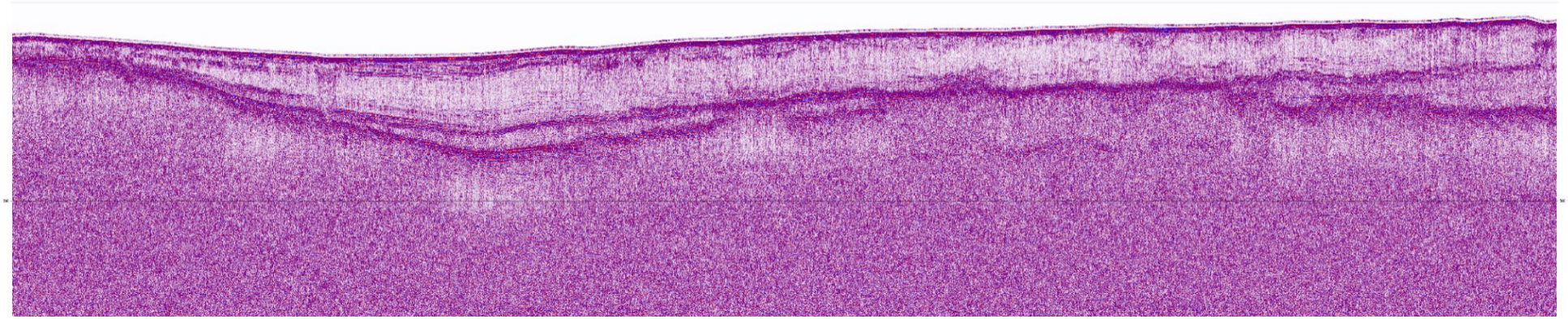

Figure 54 Seismic line PM-C07 after the application of all processing steps (The aspect of the seismic data before the processing application

CHAPTER 7

SEISMIC INTERPRETATION

7.1 Seismic-stratigraphic model

Seismic reflection profiles acquired during the PACEMAKER survey (PM–C03, PM–C04, PM–C05, PM–C06, PM–C07, PM–C08, PM–C09 and PM–C10) were interpreted using the seismic-stratigraphic methodology, allowing the identification of several seismic units with evidence of the occurrence of fluids or fluid flow (Figure 55). The remaining seismic profiles (PM–C01, PM–C02, PM–C02pt1, PM–Cc01, PM–Cc02 and PM–Cc02pt1) do not display sufficient quality to attain these objectives. The criteria used in the identification and definition of seismic units are enumerated in Chapter 4.

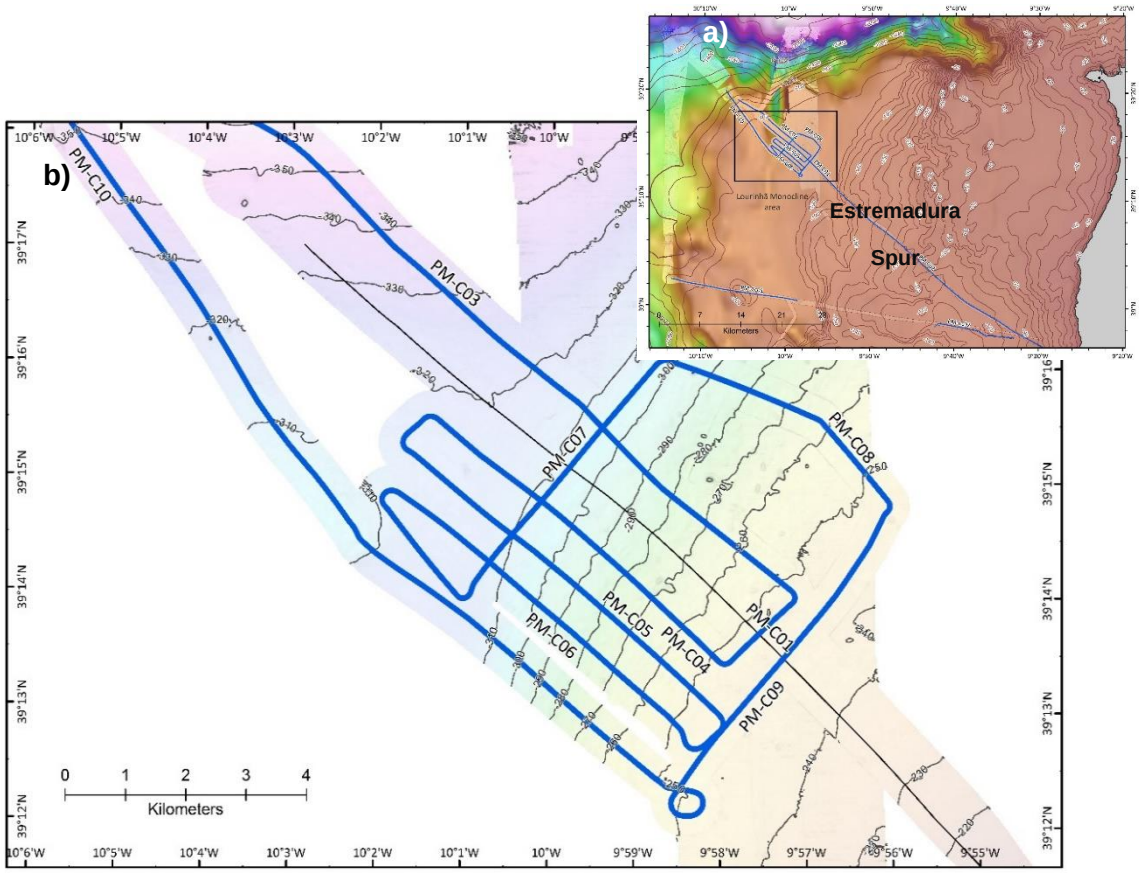

Figure 55 Location of the PACEMAKER 2D high-resolution seismic profiles in the Estremadura Spur (**a**) and location of the interpreted seismic profiles in the Lourinhã Monocline (**b**).

Using this set of high-resolution seismic six seismic units (U1 to U6) delimited by horizons (M to H4) were identify. These horizons mark the main geologic discontinuities or variations in seismic facies (e.g. PM-C05 – Figure 58, PM-C10 – Figure 63). Their characteristics are described below:

- Horizon M discontinuity is the deepest horizon identified in this area with this dataset, overlying a set of well layered reflections, but discontinuous and poorly imaged on the majority of the seismic profiles. This horizon is characterized by a high amplitude reflector with good lateral continuity that marks a major discontinuity in the sedimentary sequence: an erosive unconformity that truncates a folded unit (U1) overlain by a seismic sequence of quasi-conformable units, U2 to U6 (e.g. Figure 58 and Figure 63).
- Horizon H1 tops seismic unit U2 that fills depocentres located above synclines of unit U1. Horizon amplitude varies laterally as it tops an acoustically heterogeneous unit U2 separating it from a more homogeneous unit U3 unit. This horizon either truncates or toplaps reflections of unit U2 and is usually conformable with reflections of the overlying unit U3.
- Horizon H2 is a coherent seismic reflection with good lateral continuity. It is outlined by a high amplitude reflection and by truncations topping the underlying unit U3; it is usually covered by shallow dipping downlap or onlap terminations of U4 unit reflections.
- Horizon H3 separates unit U4 and U5 unit usually eroding the underlying unit U4 sediments. It does not have a good lateral continuity because in some places these units do not have contrasting reflections packages. At places (e.g. PM-C05; Figure 56) it constitutes an unconformity truncating folded unit U4 reflections.
- Horizon H4 has good lateral continuity in the depocentre of the study area, usually separating underlying low amplitude reflections of unit U5 from higher amplitude reflections of unit U6. Usually these reflections lie conformable on top of unit H4 or at a very shallow angle, while unit U5 sediments are generally toplapped or truncated.

The identification of these seismic discontinuities permitted the individualization of six seismic units, U1 to U6 from bottom to top, described in the following table (Table 10).

Table 10 Principal features of the seismic units identified in the PACEMAKER dataset (the red lines mark discontinuities in the seismic sequence).

Seismic Unit	Thickness (twt)	Internal Characteristics	Probable Age
U6	± 15 ms	Characterized by high amplitude, continuous and parallel reflections that are only locally disturbed, defining a stratified configuration. This unit is restricted to the basin area and has a lenticular shape. It is possible to subdivide unit U6 into sub-units, since in this interior is possible to identify reflections with toplap and onlap terminations, marking local discontinuities.	Upper Pleistocene-Holocene
U5	± 16 ms	Characterized by chaotic to transparent facies, locally with some lateral continuity.	Lower-Middle Pleistocene (Gelasian-Middle)
U4	± 10 ms	It shows seismic facies similar to unit U3, with continuous and parallel reflections but with lower amplitude and with lower lateral continuity. In shallow areas unit U4 has a chaotic character.	
U3	± 5 ms	Internal reflections show good continuity, high amplitude and parallel configuration. Occasionally, this unit seems to lose its lateral continuity due to semi-transparent reflections.	
U2	± 10 ms	This unit has a lens shape pinching out laterally onlapping horizon M, i.e. U2 fills in the main depocentre above unit U1. Internally, it consists mainly of a whole thickness semi-transparent body within which thick segments of well bedded high amplitude can occur. The semi-transparent facies are made up of discontinuous non-parallel low amplitude reflections.	Pliocene (Piacenzian)
U1	> 15 ms	This unit, topped by horizon M, is characterized by coherent high amplitude, continuous and parallel reflections. It constitutes the deepest imaged signal of seismic record, and it is not include in the seismic sequence developed above horizon M.	Lower-Middle Miocene

The exact ages of the seismic units have not been determined, since there are no wells in the study area, therefore it was not possible to carry out the chronostratigraphic calibration of the interpreted seismic units and horizons. However, a chronostratigraphic constrain is proposed for the seismic sequence based on its acoustic characteristics and the regional geology.

As previously mentioned, unit U1 underwent an intense ductile deformation, which can be associated with the peak of the alpine compression (Tortonian) in the Western Iberian Margin. This reasoning suggests that the seismic horizon M marks the Miocene discontinuity (related to the compression peak at Middle Miocene; Rasmussen *et al*., 1998), thus allowing constraining of the age of the unit U1 consists of Lower to Middle Miocene age sediments.

As in the overlying 50.4 ms (approx. 38 m) thick seismic sequence (units U2 to U6) it is not observed a deformation of intensity similar to the one observed in unit U1, therefore is reasonable to interpret that the age of these units as corresponding to the deposits of Late Pliocene and Quaternary age. The seismic unit U2 was considered as of Late Pliocene (Piacenzian) age, due to the fact that in the region of Lisbon no sedimentation occurs during the Zanclean (Pais, 2002). This seismic unit is separated from U3 by a discontinuity possibly related to a sea-level low-stand in the Pliocene-Pleistocene transition (Haq *et al*., 1987). Therefore, seismic units U3, U4 and U5 were considered of Lower and Middle Pleistocene age (Gelasian-Middle). The most recent seismic unit (U6) is separated from U5 by other discontinuity and was considered to be of upper Pleistocene (Upper)-Holocene age, since the discontinuity was possible related to the LGM (~18 ka BP).

7.2 Faults

The poor quality of the seismic data (partially as result of the accumulation of fluids in the seismic sequence - discussed in 7.5) difficult the identification and interpretation of faults. Despite that, some probable fault planes were identified (black and black dotted lines in Figure 56 to Figure 63) in all the PACEMAKER seismic profiles.

In the NW – SE seismic profiles (*e.g.* PM–C05, PM–C06 and PM–C10) the seismic unit U1 and the Pliocene-Quaternary units occur laterally and the sequence ends at the northwest segment of the profiles with onlap terminations against horizon M (e.g. PM-C10; Figure 63). This may be caused by the deposition of the more recent units in the

synform folds of U1, meaning that the displacement of the horizon M is a consequence of the ductile deformation suffered by this unit.

Mapping this discontinuity (onlap termination against the top of U1) in profiles PM – C10, PM – C06, PM – C05, PM – C04 and PM – C03 (Figure 55) it is oriented along a NNE – SSW direction, which is the orientation of the strike-slip faults orientation previously mapped by Badagola (2008) in the Estremadura Spur. The displacement of the top of U1 is maximum in PM-C10 (Figure 63), where the horizon M depth changes from 419 to 468 ms, a difference of 49 ms (approx. 37 meters), in approximately 1 kilometer along strike.

Despite no fault plane reflections are evident in the seismic data, the orientation of this feature and the displacement of U1, was interpreted as being the result of the activity of a near vertical strike-slip fault (F1), with NNE-SSW orientation and a minor dip-slip component during the Pliocene-Quaternary. Based on the present day NW-SE orientation of the maximum horizontal stress (Ribeiro *et al*., 1998, Cunha *et al*., 2011), the NNE-SSW faults in the Estremadura Spur have a sinistral strike-slip component. The position and kinematics of these faults agree with the similar interpretations proposed by Badagola (2008). Besides this, the backscatter data interpreted in this study (Chapter 5) also support this interpretation (Figure 41).

Approximately 2.5 kilometers southeast of F1, the Pliocene-Quaternary units were displaced, being noticed the deepening of the northwest segment, which indicate the presence of a NNE – SSW important normal fault (F2), also identified in the backscatter map (Figure 41).

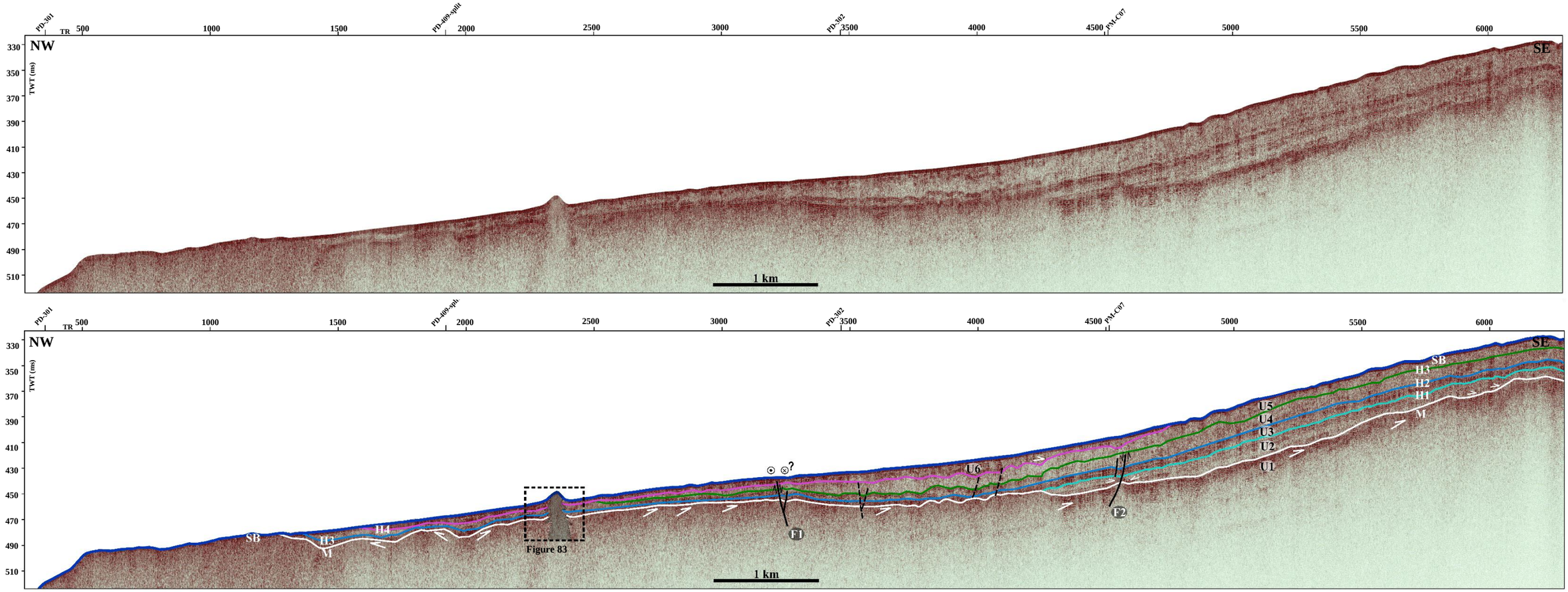

Figure 56 Interpretation of seismic profile PM-C03. **Black letters:** seismic units; **White letters and colorful lineaments:** Seismic horizons. **Black and black dotted lines:** faults and possible fault planes. **White arrows:** onlap and toplap terminations. **Shaded area:** christmas-tree structure. TR: traces; TWT (ms): two-way time in ms (Location in Figure 55).

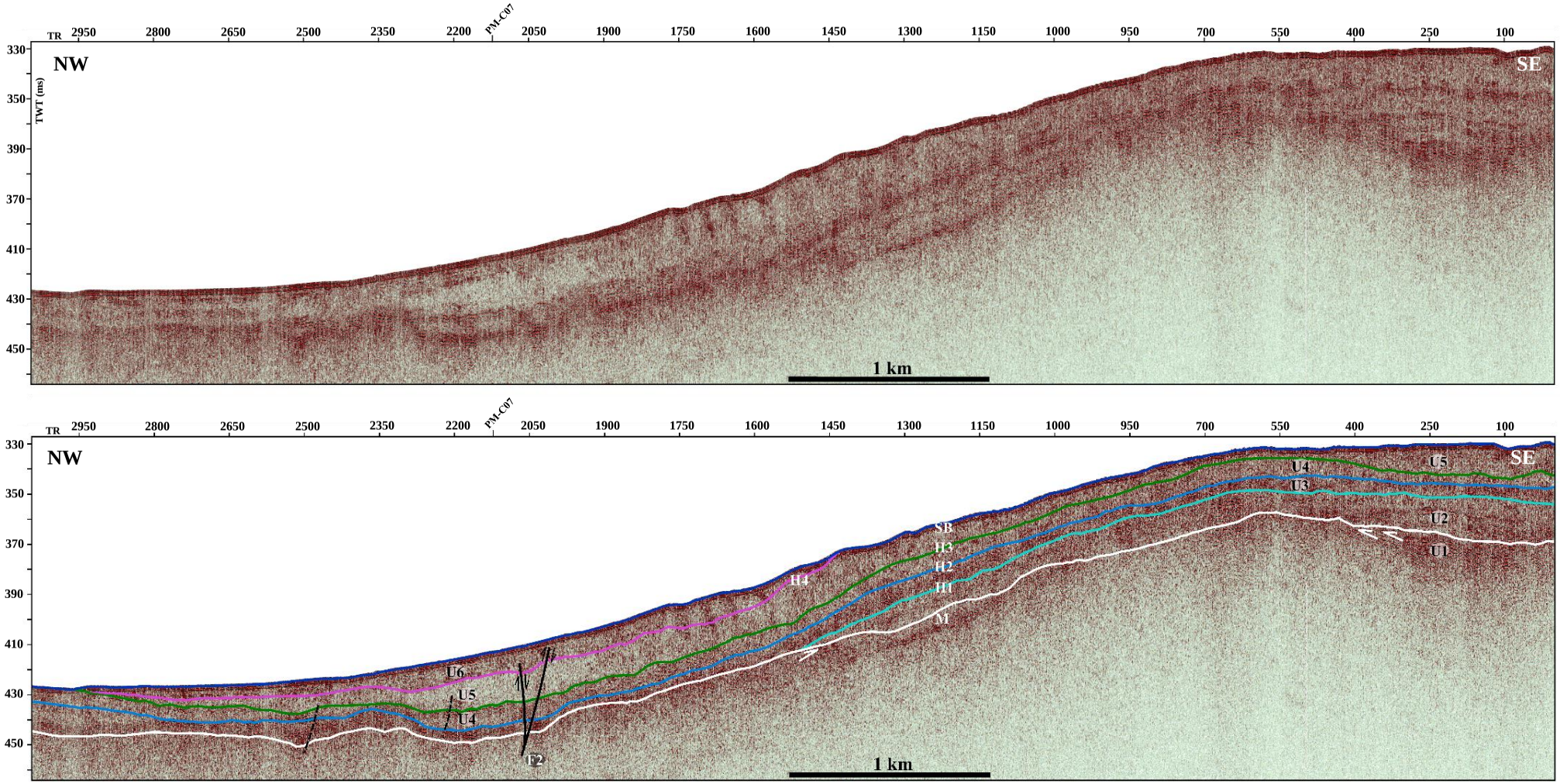

Figure 57 Interpretation of seismic profile PM-C04. **Black letters:** seismic units; **White letters and colorful lineaments:** Seismic horizons. **Black lines:** faults. **White arrows:** toplap terminations. TR: traces; TWT (ms): two-way time in ms (Location in Figure 55).

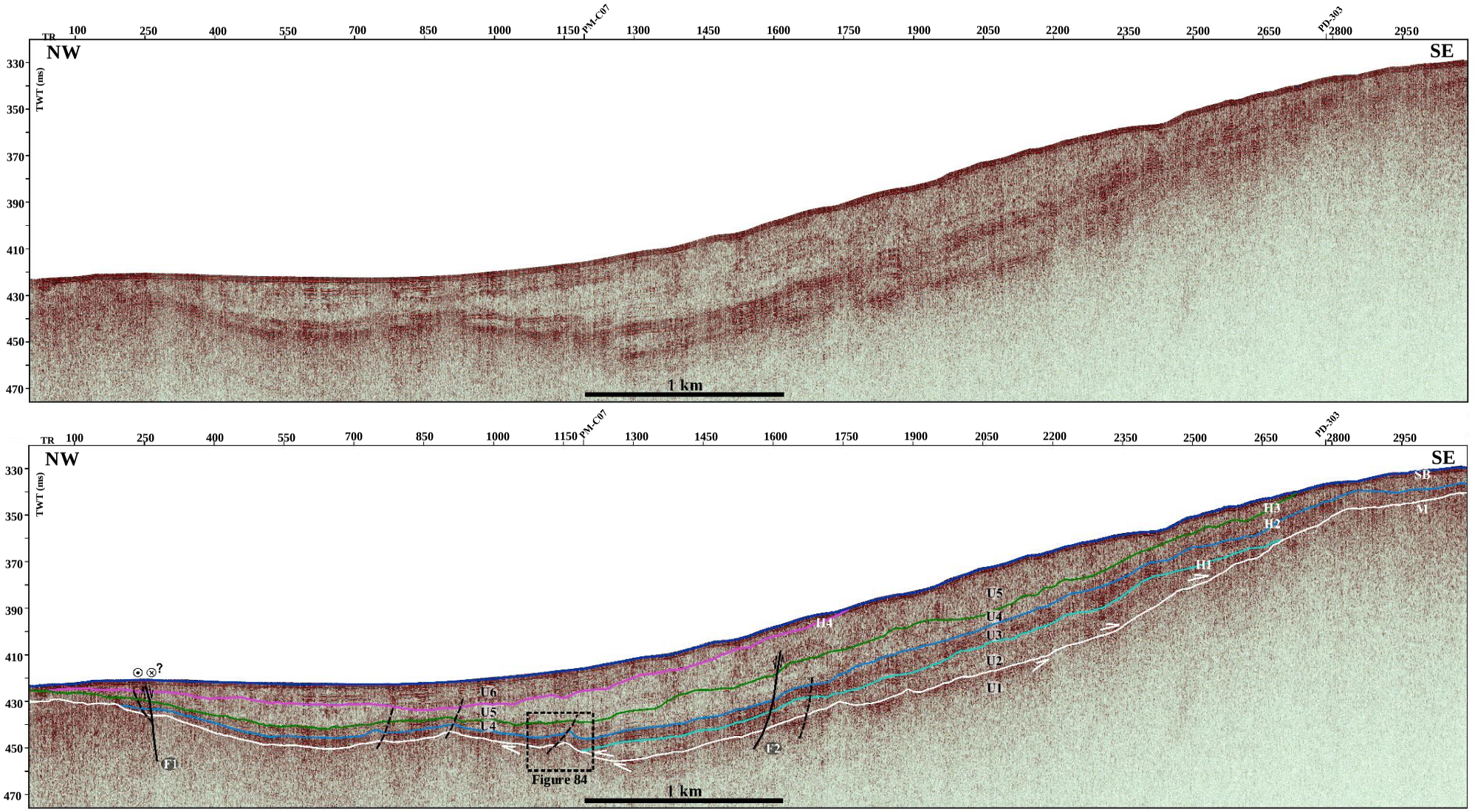

Figure 58 Interpretation of seismic profile PM-C05. **Black letters:** seismic units; **White letters and colorful lineaments:** Seismic horizons. **Black and black dotted lines:** faults and possible fault planes. **White arrows:** onlap and toplap terminations. TR: traces; TWT (ms): two-way time in ms (Location in Figure 55).

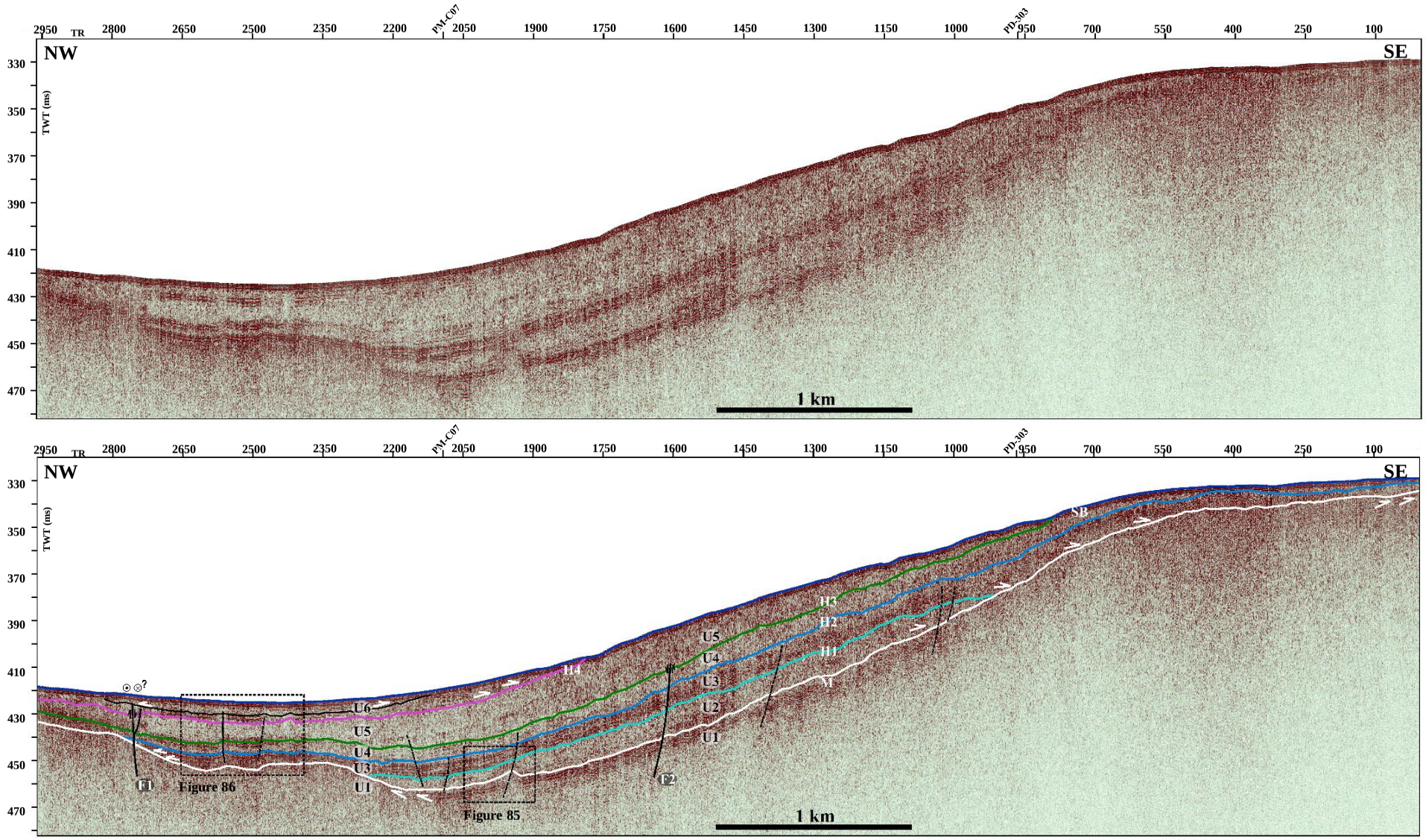

Figure 59 Interpretation of seismic profile PM-C06. **Black letters:** seismic units; **White letters and colorful lineaments:** Seismic horizons. **Black and black dotted lines:** faults and possible fault planes. **White arrows:** onlap and toplap terminations. TR: traces; TWT (ms): two-way time in ms (Location in Figure 55).

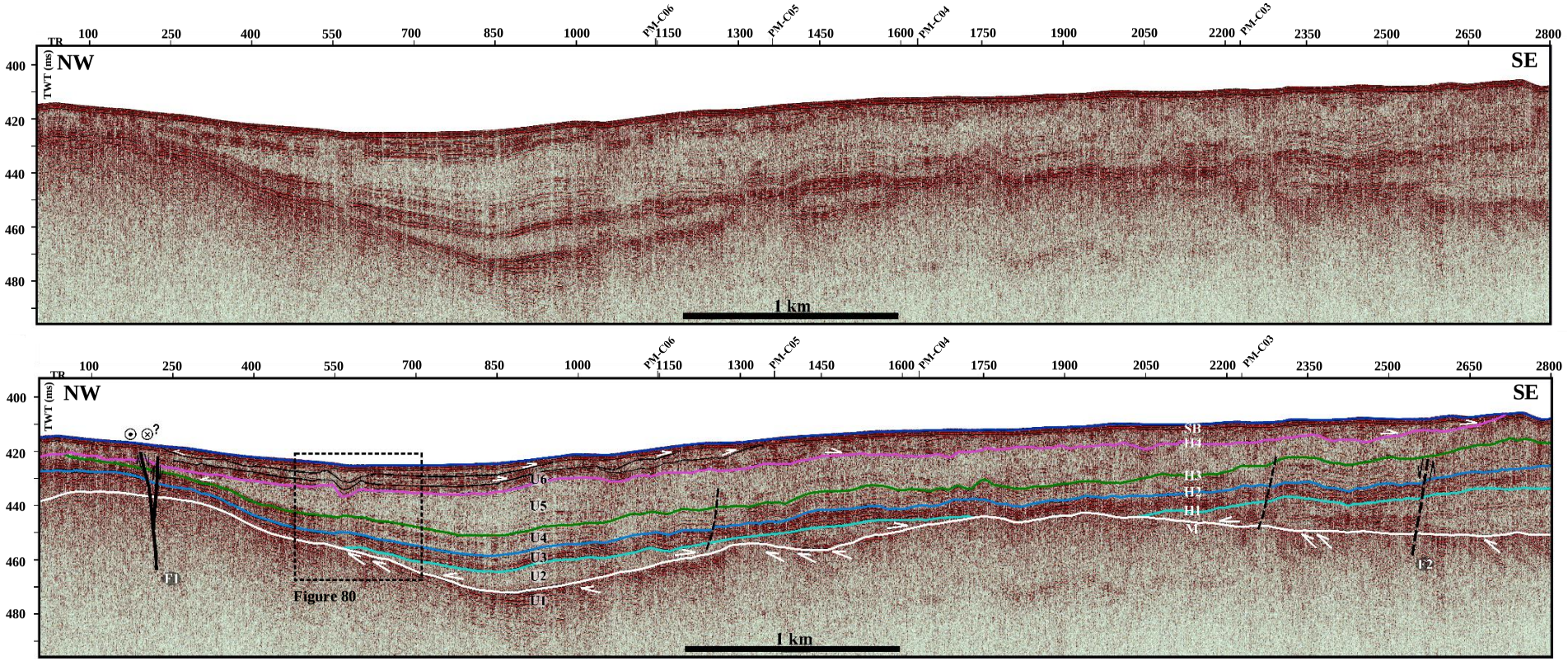

Figure 60 Interpretation of seismic profile PM-C07. **Black letters:** seismic units; **White letters and colorful lineaments:** Seismic horizons. **Black and black dotted lines:** faults and possible fault planes. **White arrows:** onlap and toplap terminations. . TR: traces; TWT (ms): two-way time in ms (Location in Figure 55).

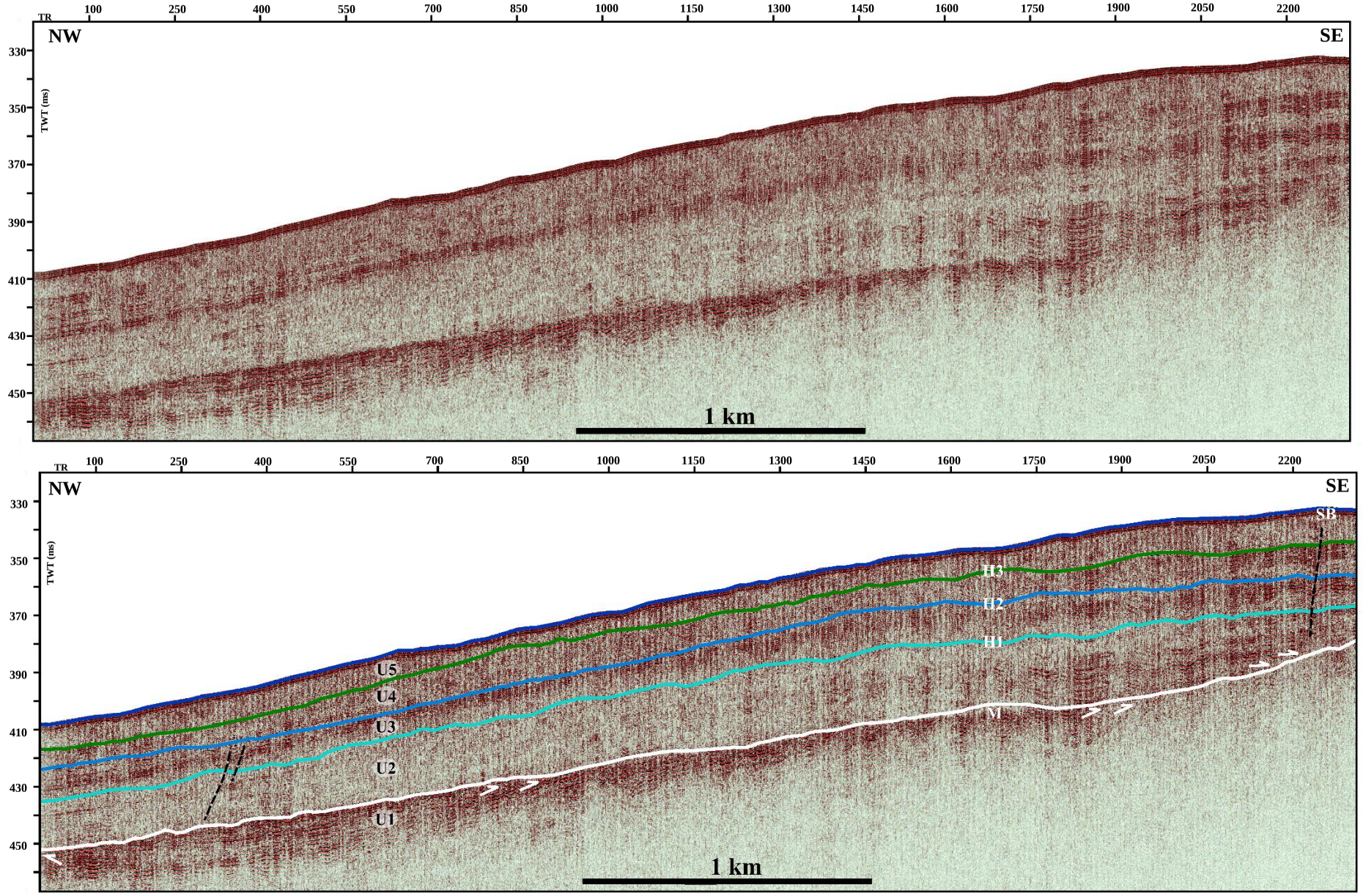

Figure 61 Interpretation of seismic profile PM-C08. **Black letters:** seismic units; **White letters and colorful lineaments:** Seismic horizons. **Black dotted lines:** possible fault planes. **White arrows:** onlap and toplap terminations. TR: traces; TWT (ms): two-way time in ms (Location in Figure 55).

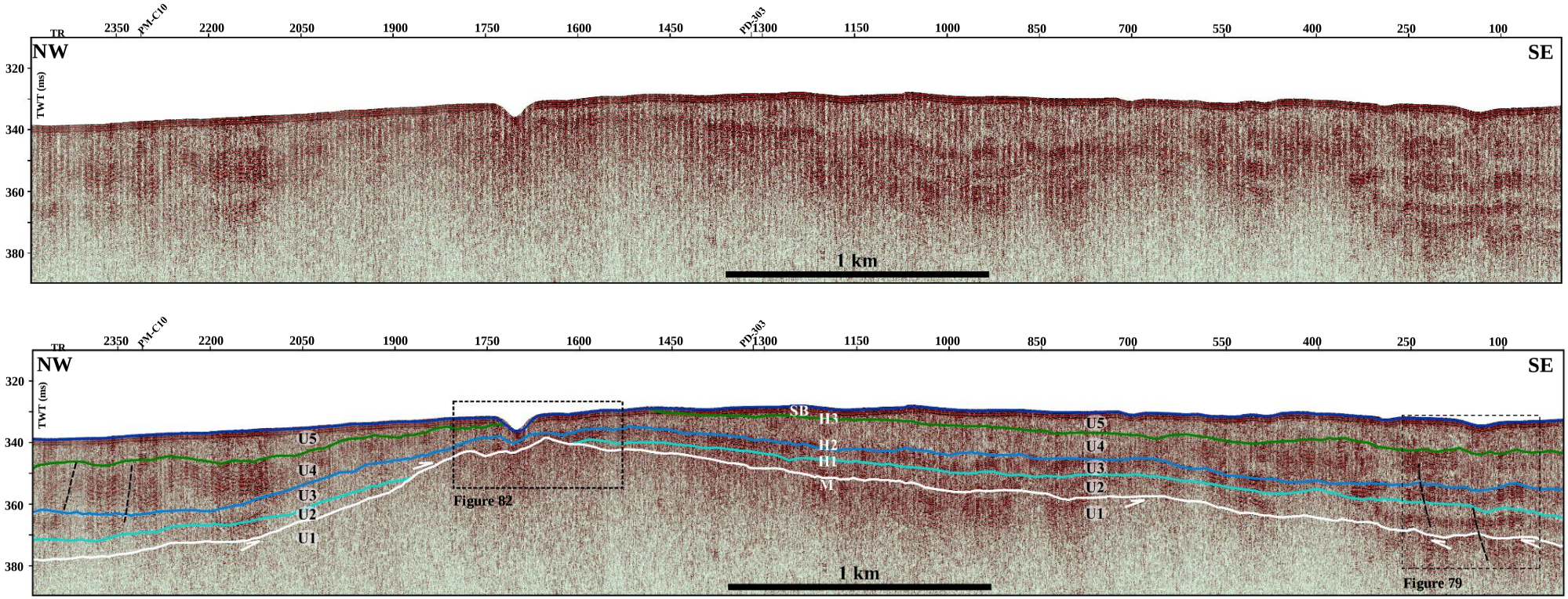

Figure 62 Interpretation of seismic profile PM-C08. **Black letters:** seismic units; **White letters and colorful lineaments:** Seismic horizons. **Black dotted lines:** possible fault planes. **White arrows:** onlap and toplap terminations. TR: traces; TWT (ms): two-way time in ms (Location in Figure 55).

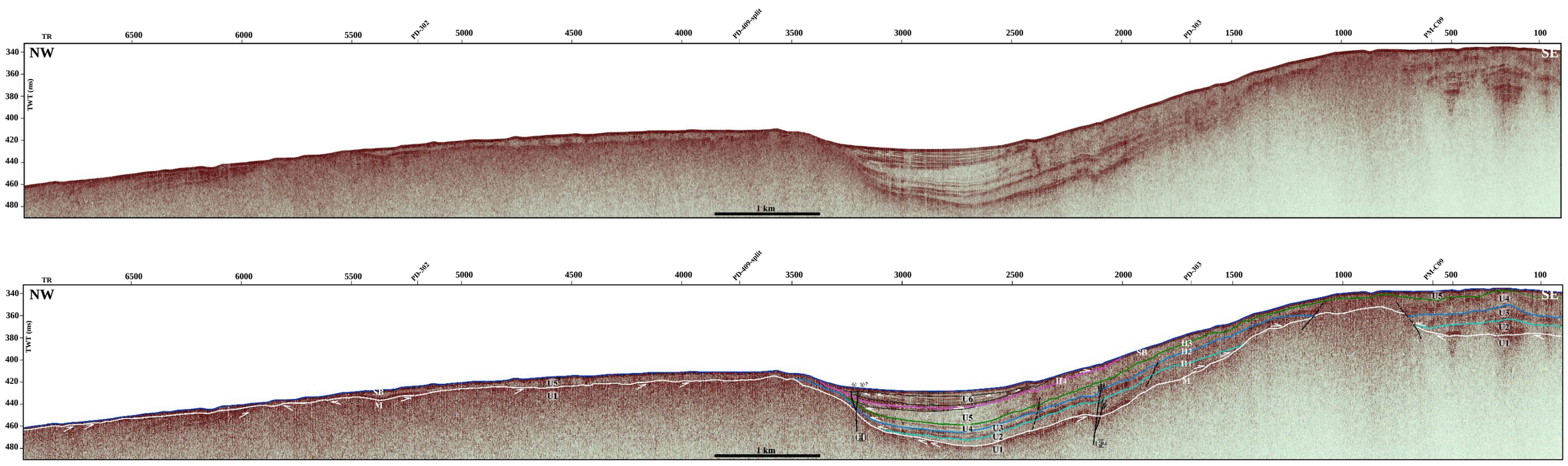

Figure 1 Interpretation of seismic profile PM-C10. **Black letters:** seismic units. **White letters and colorful lines:** seismic horizons. **Black and black dotted** lines: possible fault and fault planes. **White arrows:** toplap and onlap terminations. TR: traces; TWT (ms): two-way time in ms (Location in Figure 55).

7.3 TGS–NOPEC Seismic Segments

To better understand the deep structure of the subsurface of the Lourinhã Monocline, three sections of 2D multichannel low-resolution and high-penetration seismic profiles of TGS-NOPEC were used. These profiles allowed the visualization of the subsurface at depths greater than 500 ms TWT, the range of the PACEMAKER seismic data. The three seismic profiles crossing the study area are: PD00–302, PD00–303 and PD00–409_split (Figure 64).

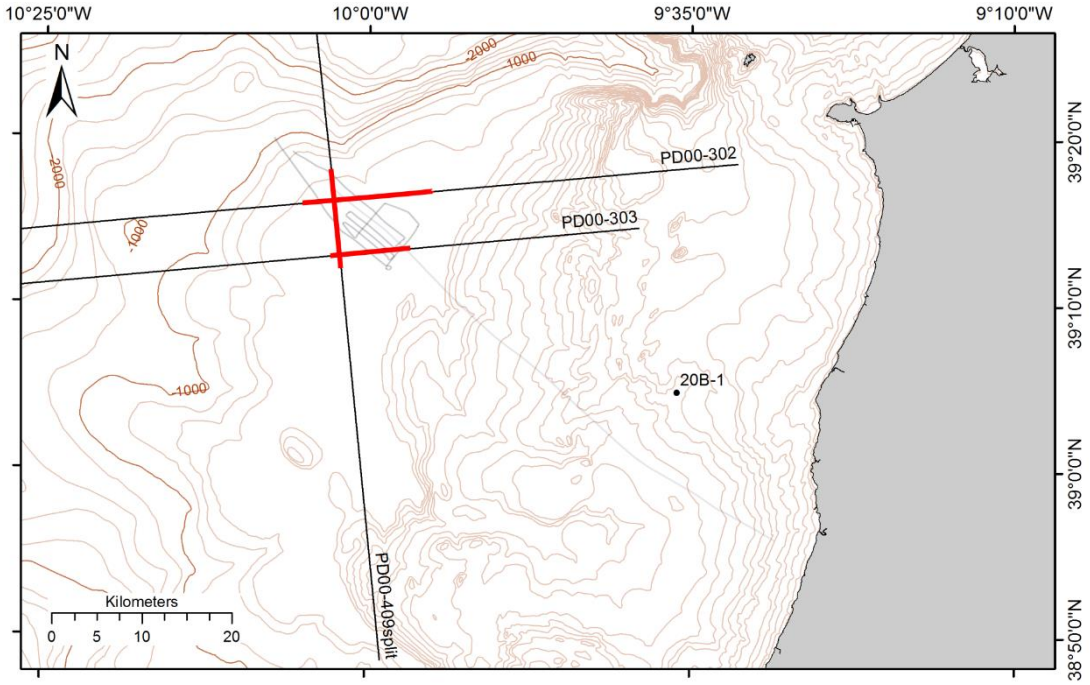

Figure 64 Localization of TGS-NOPEC seismic lines PD00-302, PD00-303 and PD00-409-split. The red lines represent the interpreted segments in this study.

Four seismic units were observed in this dataset (S1 to S4) separated by reflections that mark major discontinuities in the seismic stratigraphy, T1 to T3 and M (Figure 65, Figure 66 and Figure 67). Seismic horizon M was considered as corresponding to the horizon that marks the base of the Pliocene-Quaternary seismic sequence (the base of U2) observed in the PACEMAKER seismic profiles.

7.3.1 Seismic profile PD00 – 302

Seismic profile PD00-302 (Figure 65) trends W–E and shows a slightly folded pre-Neogene sediments, with at least three major discontinuities in the upper 1200 ms. The Pliocene-Quaternary sequence has a thickness of less than 500 ms, without any

observable internal structures. A sinistral strike-slip fault (near trace number 6800) was interpreted as being the F1 fault of the PACEMAKER profiles (Figure 56 to Figure 63).

7.3.2 Seismic profile PD00 – 303

Seismic profile PD00-303 (Figure 66) has a W–E and is located 6 km south of profile PD00-302. In both profiles it is also observed a folded basement with at least three major discontinuities in the upper 1000 ms TWT. The depocenter of the Pliocene-Quaternary sequence is located between traces 6600 and 6750, and reaches 1.6 km long and a maximum thickness of about 120 ms. Onlap and toplap terminations of their internal reflections against the basin walls and the top reflection (seismic horizons M and SB) are observed. The presence of the strike-slip fault (near trace 6600), corresponding to the sinistral strike-slip fault F1 identified in the PACEMAKER profiles was also registered.

7.3.3 Seismic profile PD00 – 409_split

This profile strikes N-S and crosses profiles PM-C10 and PM-C03 (Figure 67). In this deep seismic section is possible to observe the deformation of the basement (unit U1) and the three major discontinuities located above 1300 ms. The Pliocene-Quaternary sub-basin was observed between traces number 4000 and 3850, with maximum thickness of about 120 ms and with 2 km in length. The depositional sequence that infills this basin presents reflections with onlap and toplap terminations against seismic horizons M and SB. In the vicinities of trace 4200, a thrust-fault is observed, which evolves upwards into a strike-slip fault, interpreted as F1 in the PACEMAKER seismic profiles (Figure 56 to Figure 63).

These high-penetration seismic sections show that the Pliocene-Quaternary sub-basin thickens towards the SW. In the section PD00 – 302, that is located further north the Pliocene-Quaternary sub-basin is almost absent and in the sections that cross the sub-basin at the south (PD00 – 303 and PD00 – 409) it exhibits a greater thickness (about 3x higher). This is consistent with the observations done in the PACEMAKER seismic profiles.

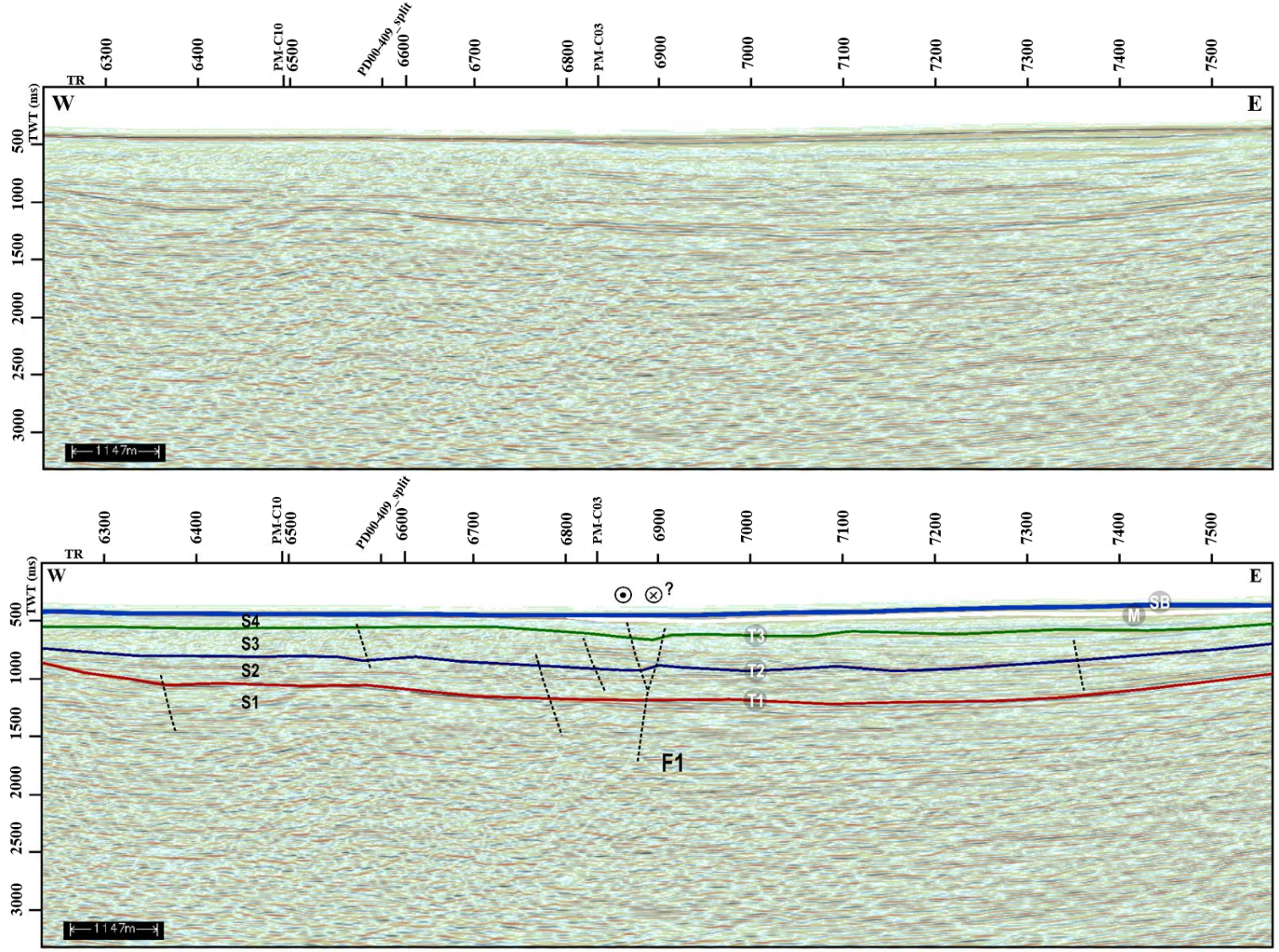

Figure 65 Interpretation of the PD00–302 seismic segment. It is possible to observe a sinistral strike-slip fault, interpreted as corresponding to F1 fault defined in the PACEMAKER seismic profiles. Location of this section if given in **Figure 64**. **SB** – Seafloor reflection; **M** – Miocene disconformity (the same observed in the PM seismic profiles); **T1**, **T2** and **T3** – seismic reflectors interpreted in the TGS-NOPEC seismic data, that separate four seismic units from Lower Jurassic to Middle Miocene (**S1** to **S4**).

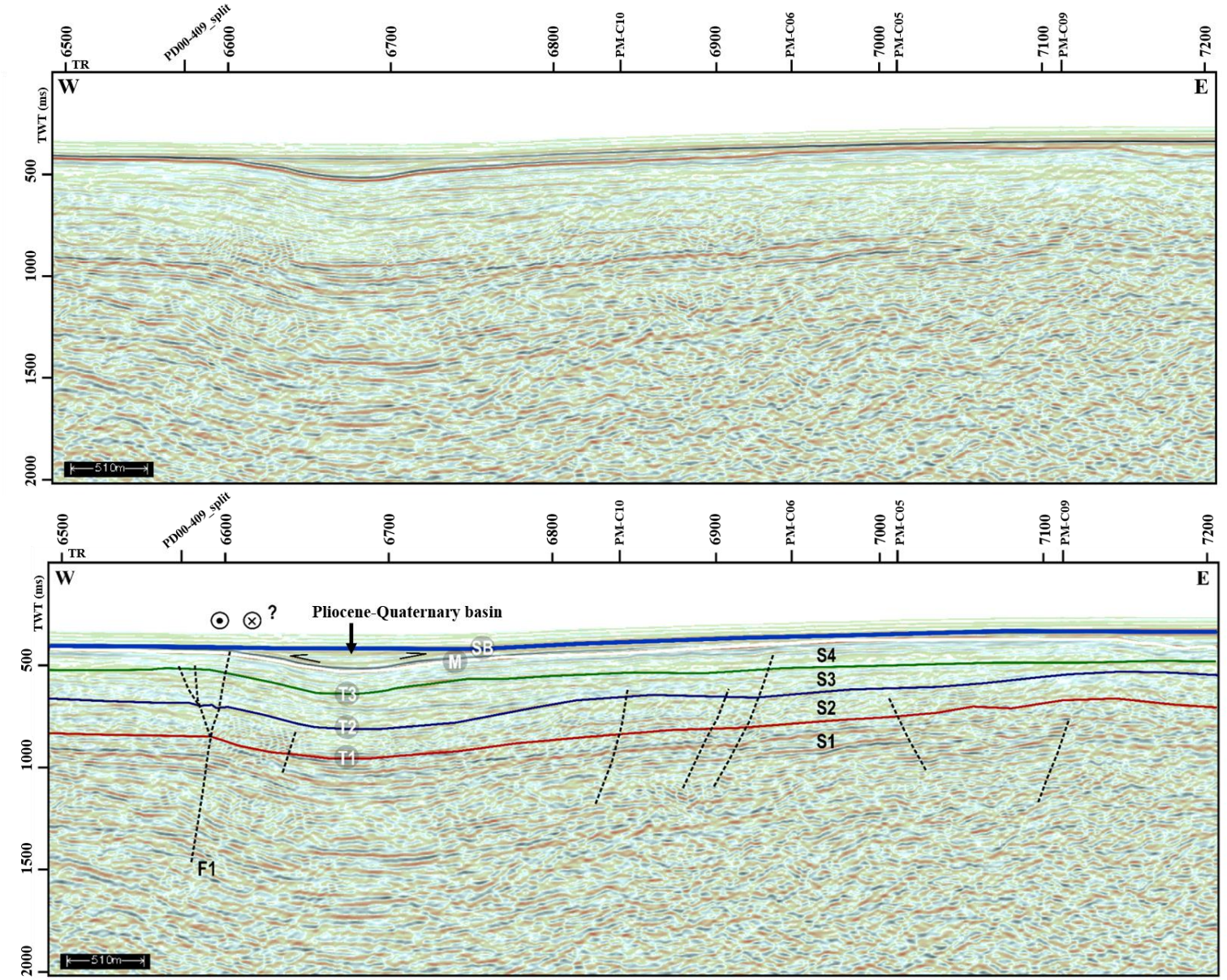

Figure 66 Interpretation of PD00-303. The location of this section if given in **Figure 64**. **SB** – Seafloor reflection; **M** – Miocene disconformity (the same observed in the PM seismic profiles); **T1**, **T2** and **T3** – seismic reflectors interpreted in the TGS-NOPEC seismic data, that separate four seismic units from Lower Jurassic to Middle Miocene (**S1** to **S4**). Location of this section if given in **Figure 64**.

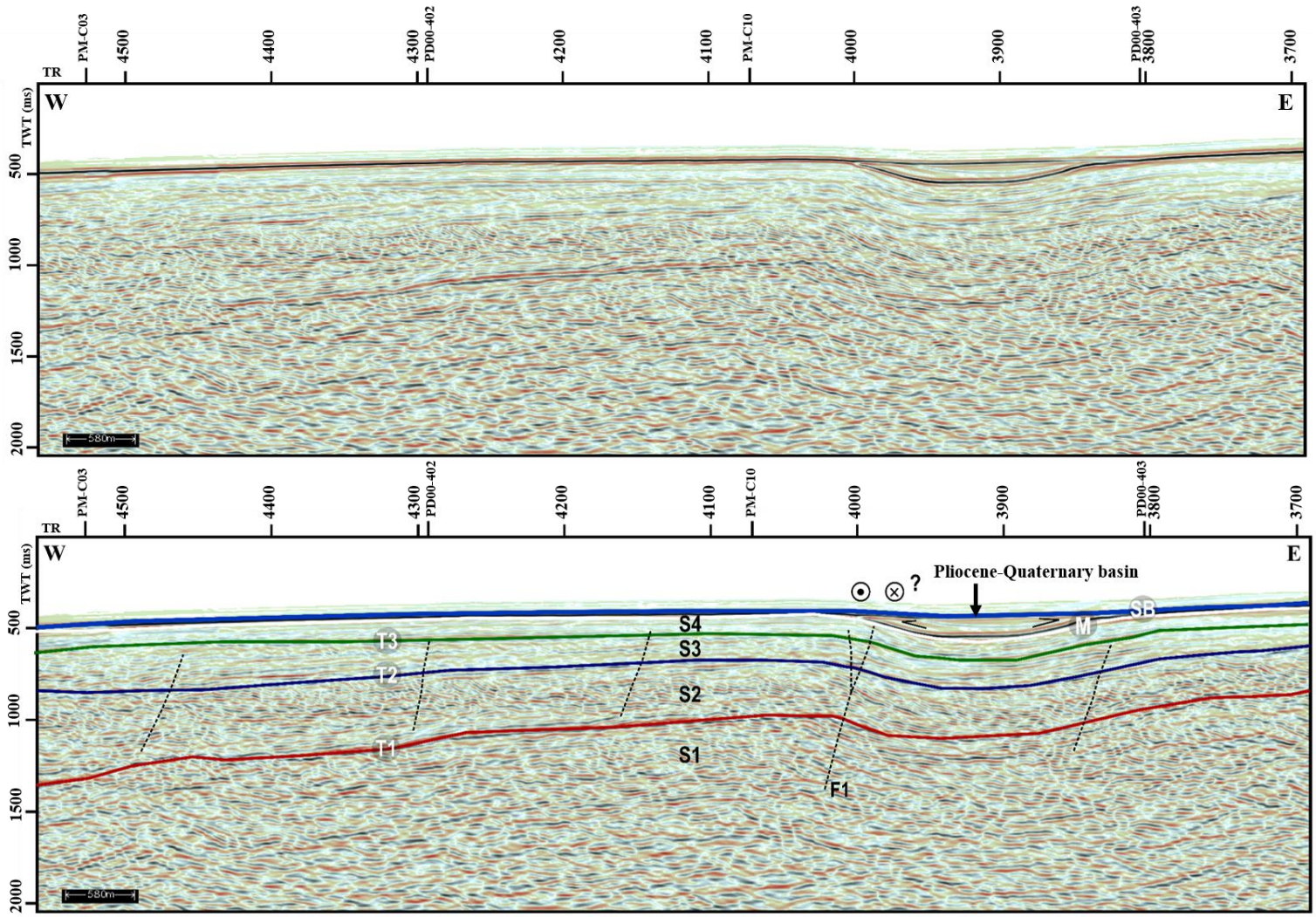

Figure 67 Interpretation of PD00-409_split seismic segment. The location of this section if given in **Figure 64**. **SB** – Seafloor reflection; **M** – Miocene disconformity (the same observed in the PM seismic profiles); **T1**, **T2** and **T3** – seismic reflectors interpreted in the TGS-NOPEC seismic data, that separate four seismic units from Lower Jurassic to Middle Miocene (**S1** to **S4**). Location of this section if given in **Figure 64**.

7.4 Isobaths and isopachs maps

After the picking of the horizons (M, H1, H2, H3, H4 and H5) in all the PACEMAKER seismic profiles, isobath surfaces were calculated for the base and the top of each seismic unit. Isobath and isopach maps were created using *Power View* for *SeisWorks* tool of the *Landmark* software, for all seismic units as well as for the complete Pliocene–Quaternary seismic sequence. The depth units in the isobaths and isopach maps are milliseconds in two-way travel-time (TWT ms). Contour lines were plotted to give a better perception of the values.

7.4.1 Isobath maps

The seismic horizons picked in the PACEMAKER dataset and the isobath maps, allow the visualization of the geometry and morphology of each horizon. In the following maps the blue color refers to deeper depths while the orange color represents zones where the horizons are located at shallower depths.

The isobath map for the top of the unit U1, discontinuity M (Figure 68), shows a close correspondence with the present-day bathymetry (Figure 36). It is possible to observe a depressed area with elongated in NE–SW direction, with a maximum depth of approximately 460 ms that corresponds to the axis of synform that folds of the basement unit (U1) observed in the seismic profiles (e.g. PM – C10;**Figure 63**). The northwestern and southeastern limits coincide with tectonic structures observed in the seismic sections and correspond to the faults (F1 and F2). The deeper part of the horizon M is found in the northern end of the map. The horizon M is shallower at southeast end of the map, reaching depths of about 330 ms and that gradually deepens northwestward with a constant slope. In the western area of the map there is another zone of high depths, being observed a circular area that reaches depths of 415 ms.

In the isobath maps of the seismic horizons H1, H2, H3 and H4 (Figure 69, Figure 70, Figure 71 and Figure 72) the observed structures and the morphologies are similar to the ones described for the horizon M. It is possible to notice the migration of the deeper region towards NW, accompanied by the advancement of the high region localized in the southeast area of the map, which suggests the migration of the depocenter through time (in total moved about 450 meters). This can be caused by the development of a progradant body through time, due to the lack of accumulation space for the newer units, causing their sedimentation to occur forward.

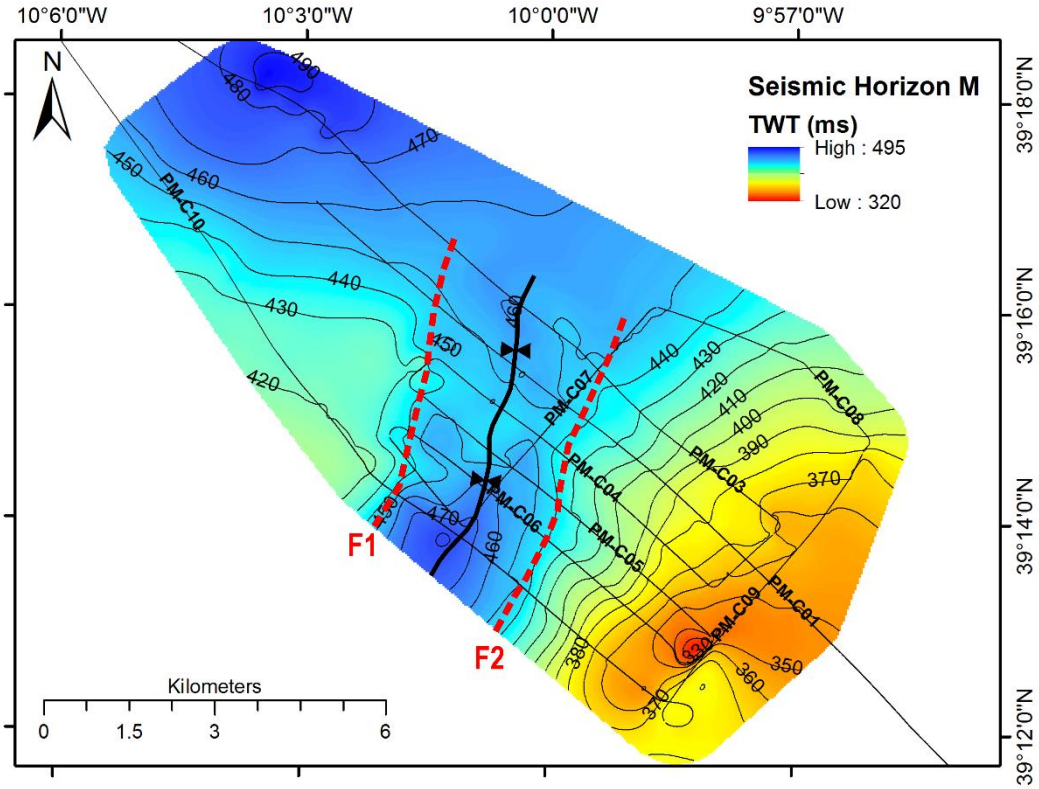

Figure 68 Isobath map for the seismic horizon M. **Black line:** synform axis; **Red dotted lines:** possible faults identified in the seismic data, F1 and F2. Equidistance: 10 ms.

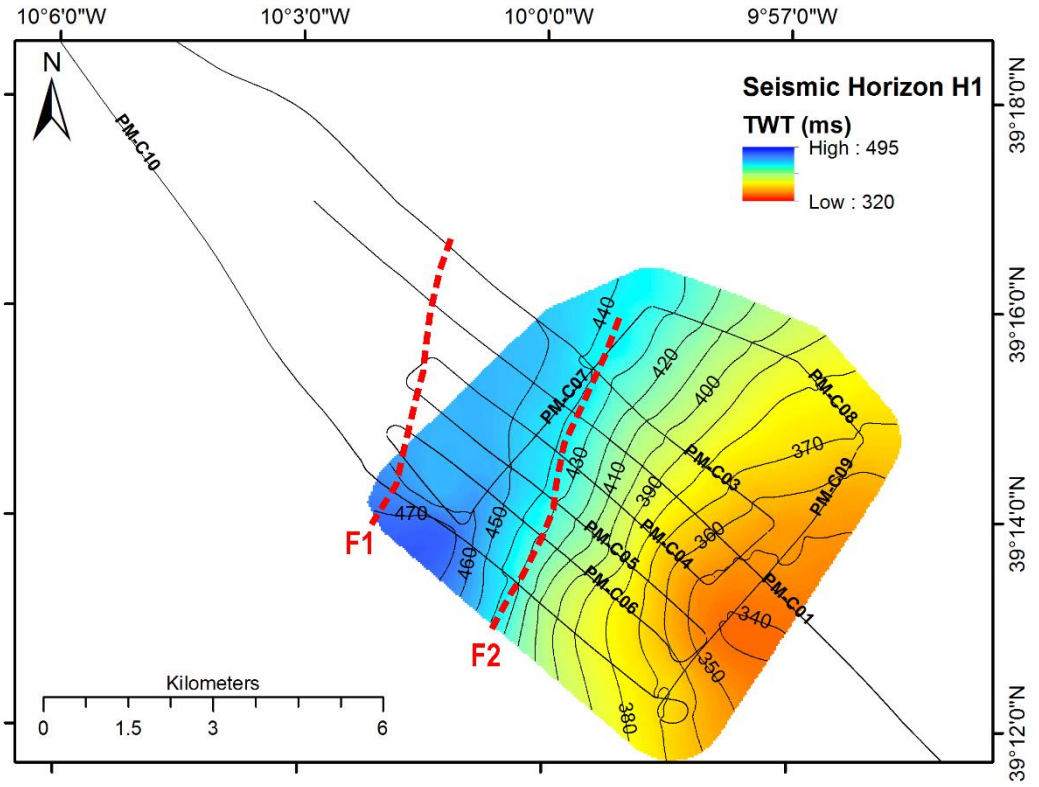

Figure 69 Isobath map for seismic horizon H1. **Red dotted lines:** possible faults identified in the seismic data, F1 and F2. Equidistance: 10 ms.

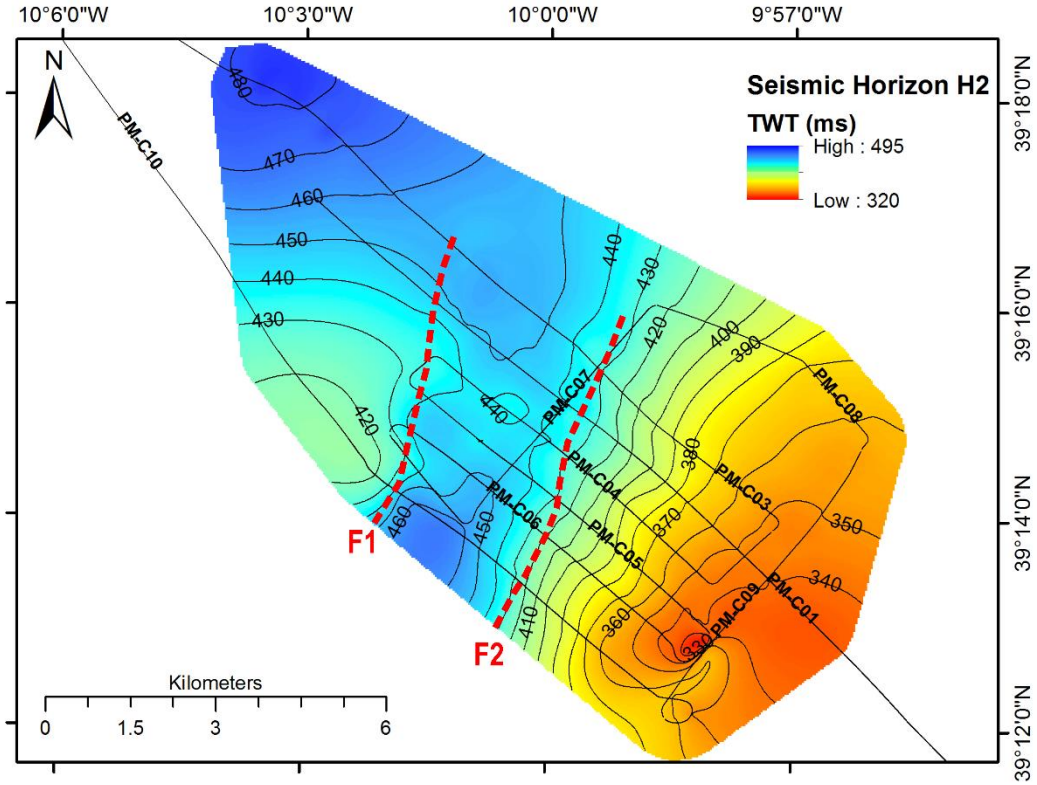

Figure 70 Isobath map for seismic horizon H2. **Red dotted lines:** possible faults identified in the seismic data, F1 and F2. Equidistance: 10 ms.

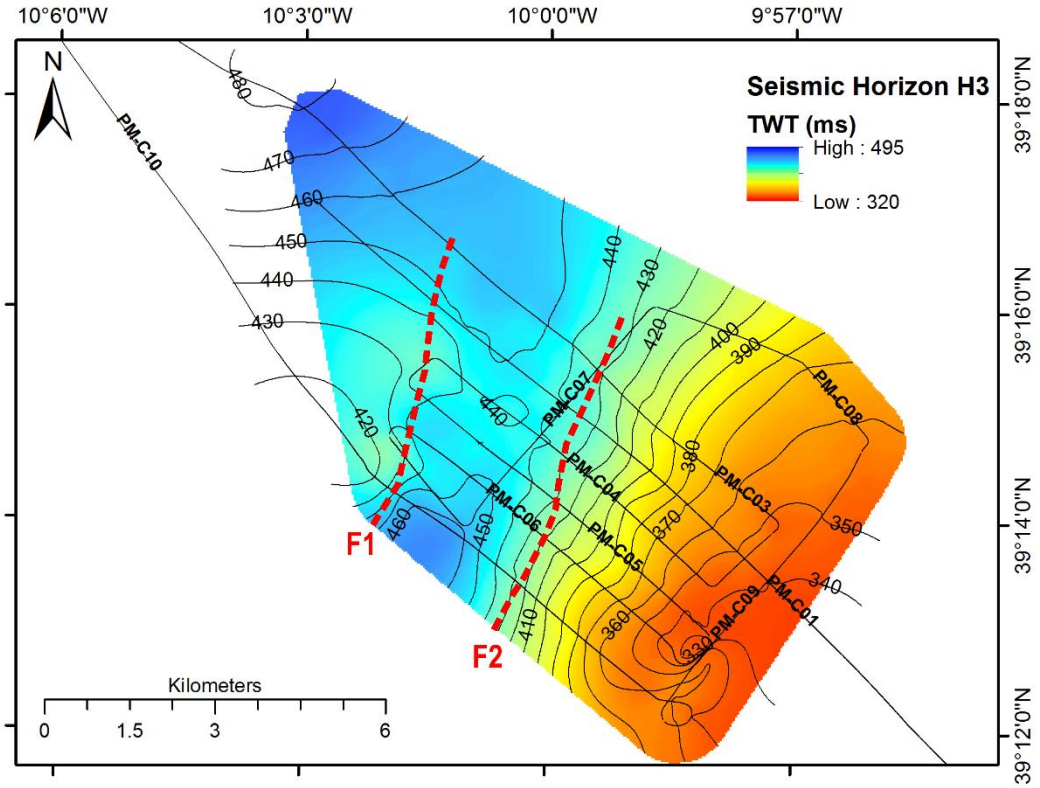

Figure 71 Isobath map for seismic horizon H3. **Red dotted lines:** possible faults identified in the seismic data, F1 and F2. Equidistance: 10 ms.

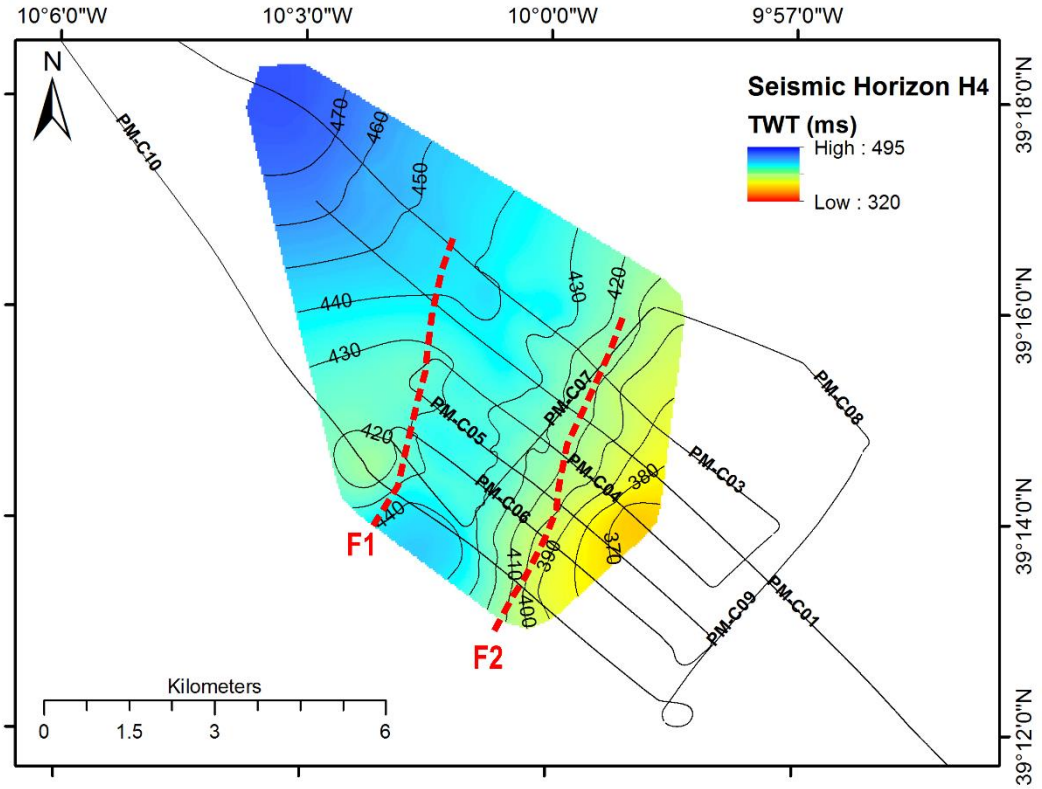

Figure 72 Isobath map for seismic horizon H4. **Red dotted lines:** possible faults identified in the seismic data, F1 and F2. Equidistance: 10 ms.

7.4.2 Isopach maps

The isopach maps illustrate the thickness of the several seismic units, defined as the time vertical distance between two horizons that delimit each seismic unit. These maps permit the location of depocenters, paleo-highs and paleo-depressions. The isopach maps for each seismic unit are based in the interpretation of the PACEMAKER seismic profiles and of the entire Pliocene-Quaternary sedimentary sequence. For the following maps, the blue color stands for the thicker zones and red color represents the thinner zones of the units. Artefacts due to the grid characteristics or to the small thickness of the units are observed in all the maps, especially when the units are thinner, such as in units U3 and U4 (Figure 74 and Figure 75).

The isopach map of unit U2 (M – H1) shows that its thickness varies from less than 1 ms to about 26 ms TWT (Figure 73). The unit presents the maximum thickness in the northeast region of the map. This indicates that when the deposition of U2 occurred, the depocentre of this small basin was located in the northeastern part of the map. Unit U3 (limited by horizons H1 – H2) has a maximum thickness of approximately 16 ms in the

central part of the map and a minimum of about 2 ms (Figure 74). The thickness of unit U4 (limited by horizons H2 – H3) varies from less than 1 ms to about 20 ms (Figure 75). In the isopach maps of this unit it is not clear the presence of a depocentre, and this unit is prone to the interpolation artifacts. The isopach map for unit U5 (limited by horizons H3 – H4; Figure 76) shows a minimum thickness of less than 1 ms and a its depocenter is located in the south and southeast region of the map, reaching a maximum thickness of approximately 20 ms. The isopach map of the top unit, U6 (limited by horizons H4 – FM) is thicker within an area with a NNE - SSW orientation, reaching a maximum thickness of about 20 ms in the southern part of this zone, where the depocentre is localized. The minimum thickness of this unit is less than 1 ms (Figure 77).

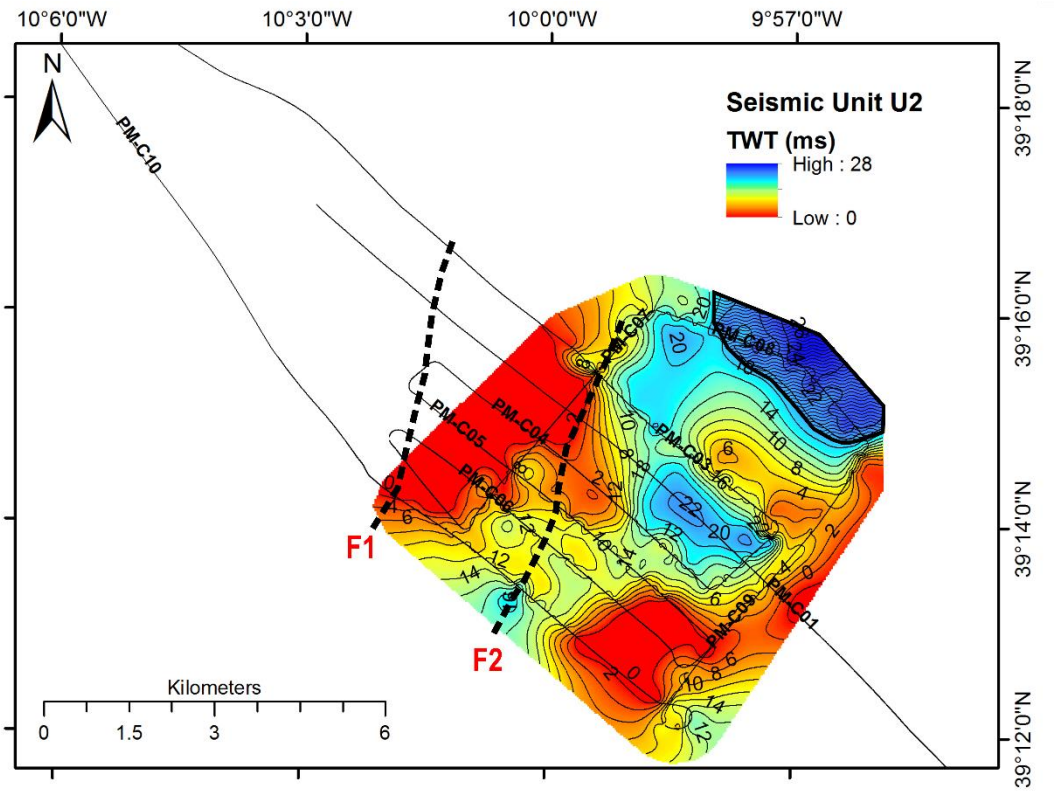

Figure 73 Isopach map for seismic unit U2 (M-H1). **Black dotted lines:** possible faults identified in the seismic data, F1 and F2. **Shaded region:** basin depocenter. Equidistance: 2 ms.

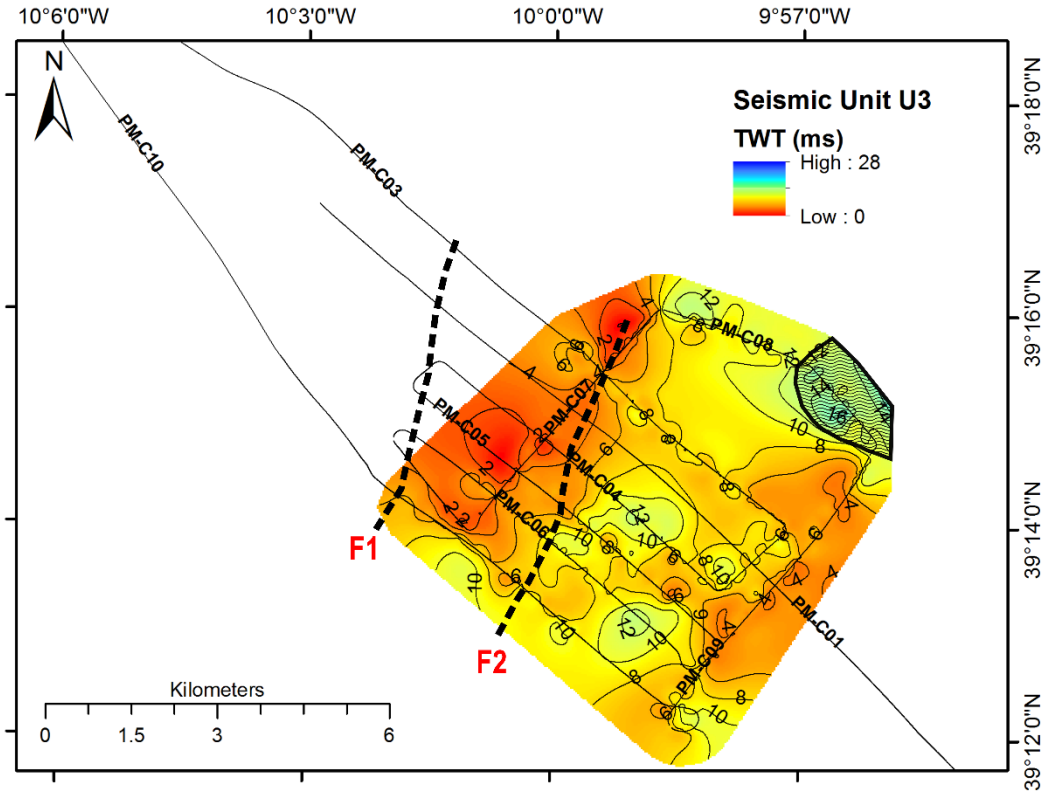

Figure 74 Isopach map for seismic unit U3 (H1-H2). **Black dotted lines:** major faults F1 and F2. **Shaded region:** basin depocenter. Equidistance: 2 ms.

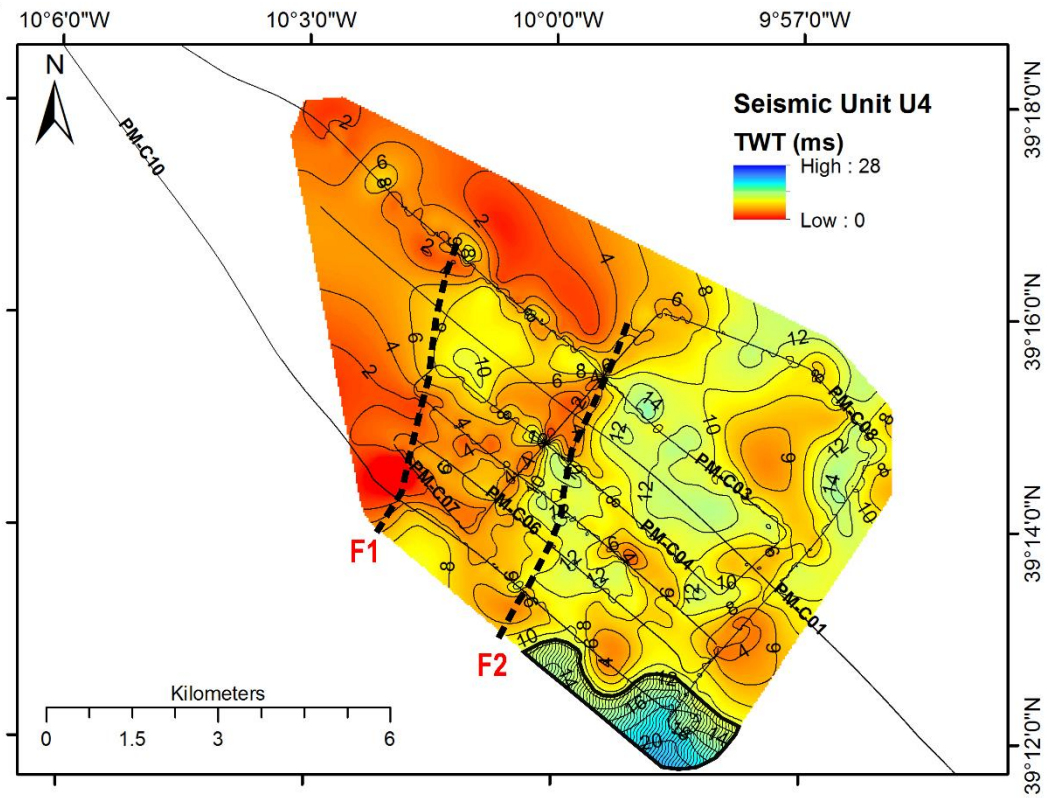

Figure 75 Isopach map for seismic unit U4 (H2-H3). **Black dotted lines:** major faults F1 and F2. **Shaded region:** basin depocenter. Equidistance: 2 ms.

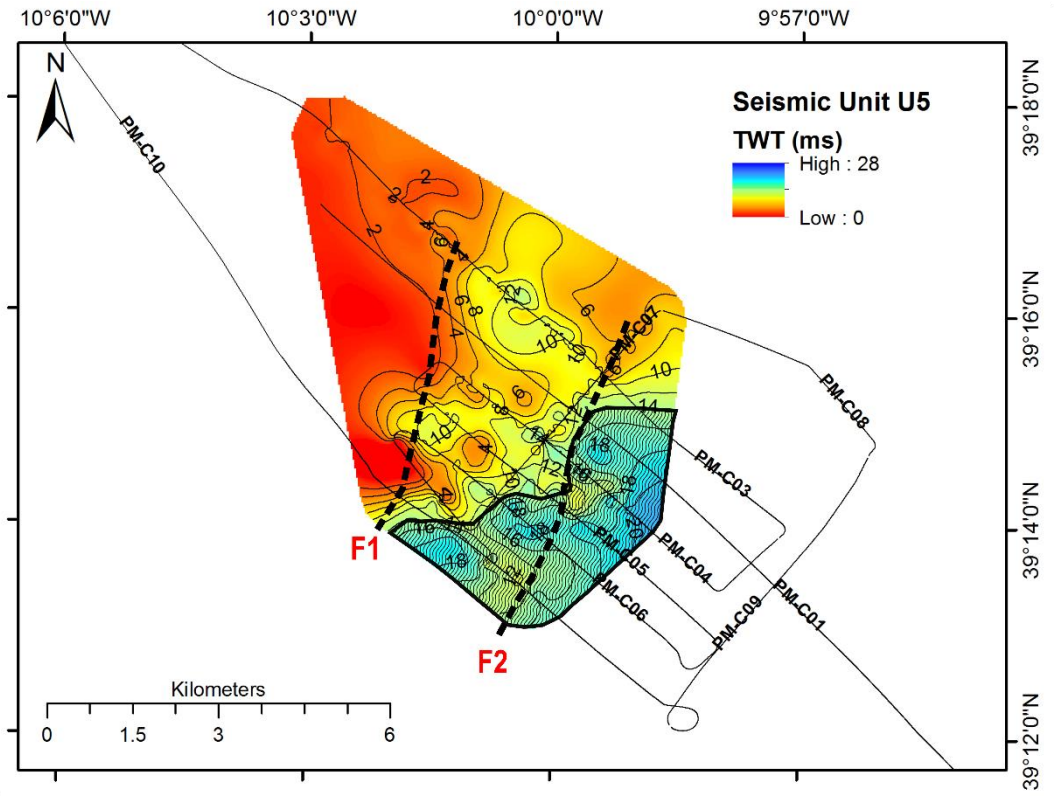

Figure 76 Isopach map for seismic unit U5 (H3-H4). **Black dotted lines:** major faults F1 and F2. **Shaded region:** basin depocenter. Equidistance: 2 ms.

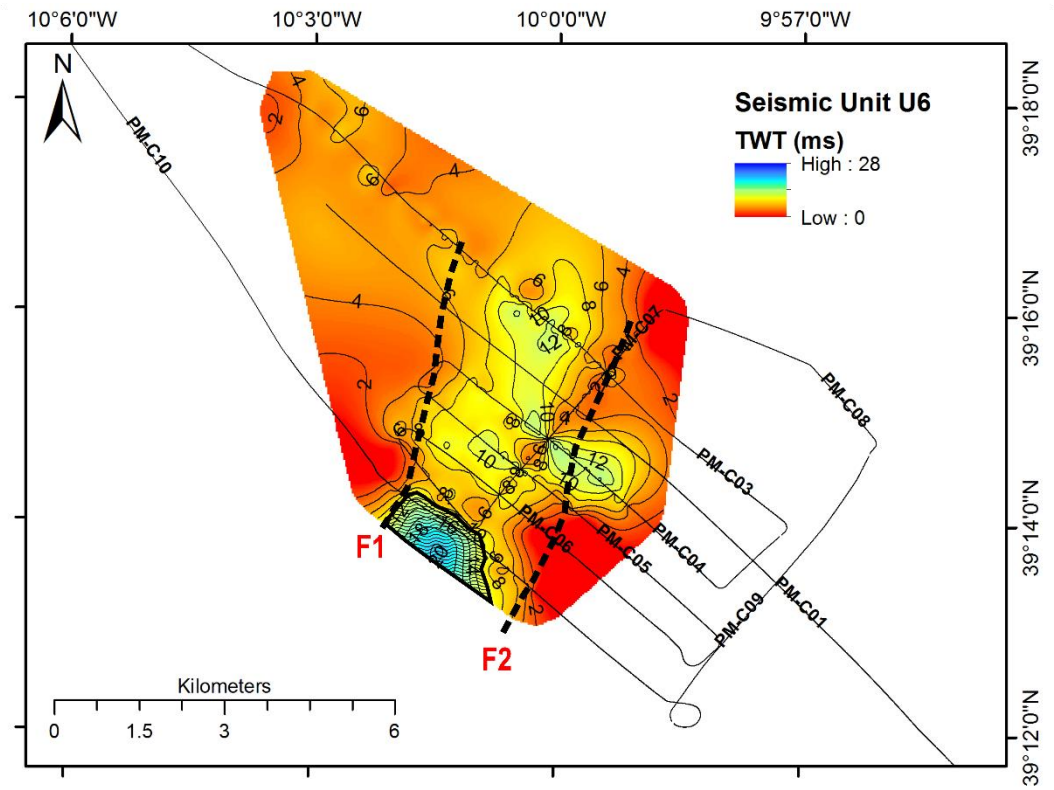

Figure 77 Isopach map for seismic unit U6 (H4-FM). **Black dotted lines:** major faults F1 and F2. **Shaded region:** basin depocenter. Equidistance: 2 ms.

The Pliocene-Quaternary sequence isopach map (Figure 78) shows the global tendency of deposition of all the units described in the Lourinhã monocline basin. The thickness of the Pliocene-Quaternary sucession varies from less than 5 ms up to 60 ms. The maximum thickness occurs within a region with a NE–SW orientation. There are two zones in which the thickness of the sequence is minimum (less than 5 ms): one in the northwest zone and another in the south of the map.

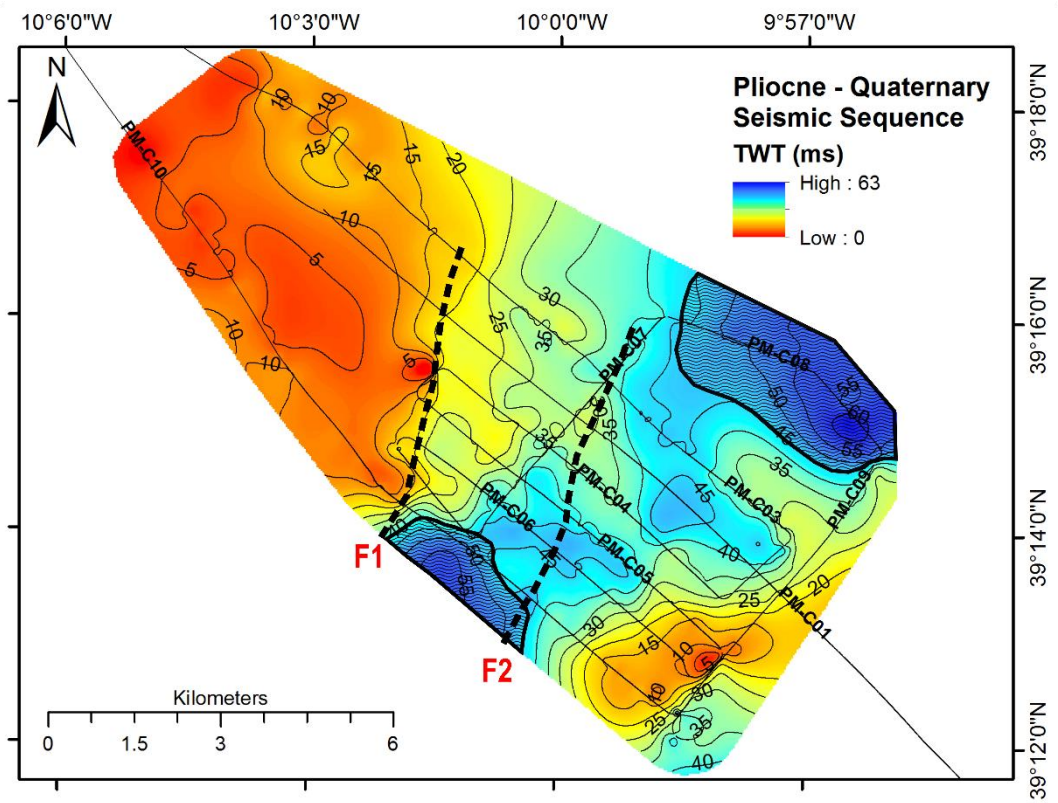

Figure 78 Isopach map for the Pliocene-Quaternary seismic sequence. **Black dotted lines:** major faults F1 and F2. **Shaded region:** basin depocenter. Equidistance: 2 ms.

From the interpretation of the isopach maps is possible to conclud that the Pliocene-Quaternary basin depocentre corresponds to the NE– SW synform area delineated in the isobath map of the horizon M (Figure 68). There are two regions were the thickness is maximum, the first at SW and the other at NE. During the deposition of the seismic units U2 and U3 the basin depocente was located at SW and later moved to the NW, were the variation of the basin depocentre was possibly caused by the decrease of the space disponible for the sediments to accumulate, which forced the depocenter migration to a region with more space to fill.

7.5 Seismic evidences of fluid flow

The acoustic evidences of fluids accumulation and seepage in the seismic profiles are expressed by the presence of migration pathways, acoustic transparency, acoustic turbidity and acoustic blanking. The occurrence of pockmarks at the seabed and buried is also an indicator of the presence of fluid flow in the subsurface.

7.5.1 Pockmarks

A series of "U" and "V" shaped depressions affecting the seafloor were identified on the PACEMAKER seismic profiles. The largest depression identified was found on seismic profile PM-C09 (Figure 79), and has a diameter of 147 meters and a depth of approximately 5 ms. These cone shaped depressions correspond to the depressions described in the results of the bathymetric analysis (in Chapter 5), that are characterized by high backscatter responses. Based on their dimensions and geometry, these features were interpreted as seafloor pockmarks produced by recent fluid seepage from the subsurface. The seafloor pockmarks are more frequent in the area of the Lourinhã monocline with higher slope angles (Area 3 in Figure 36 – Chapter 5) that corresponds to an area where U6 is absent (e.g. PM–C04 and PM–C05; Figure 57 and Figure 58).

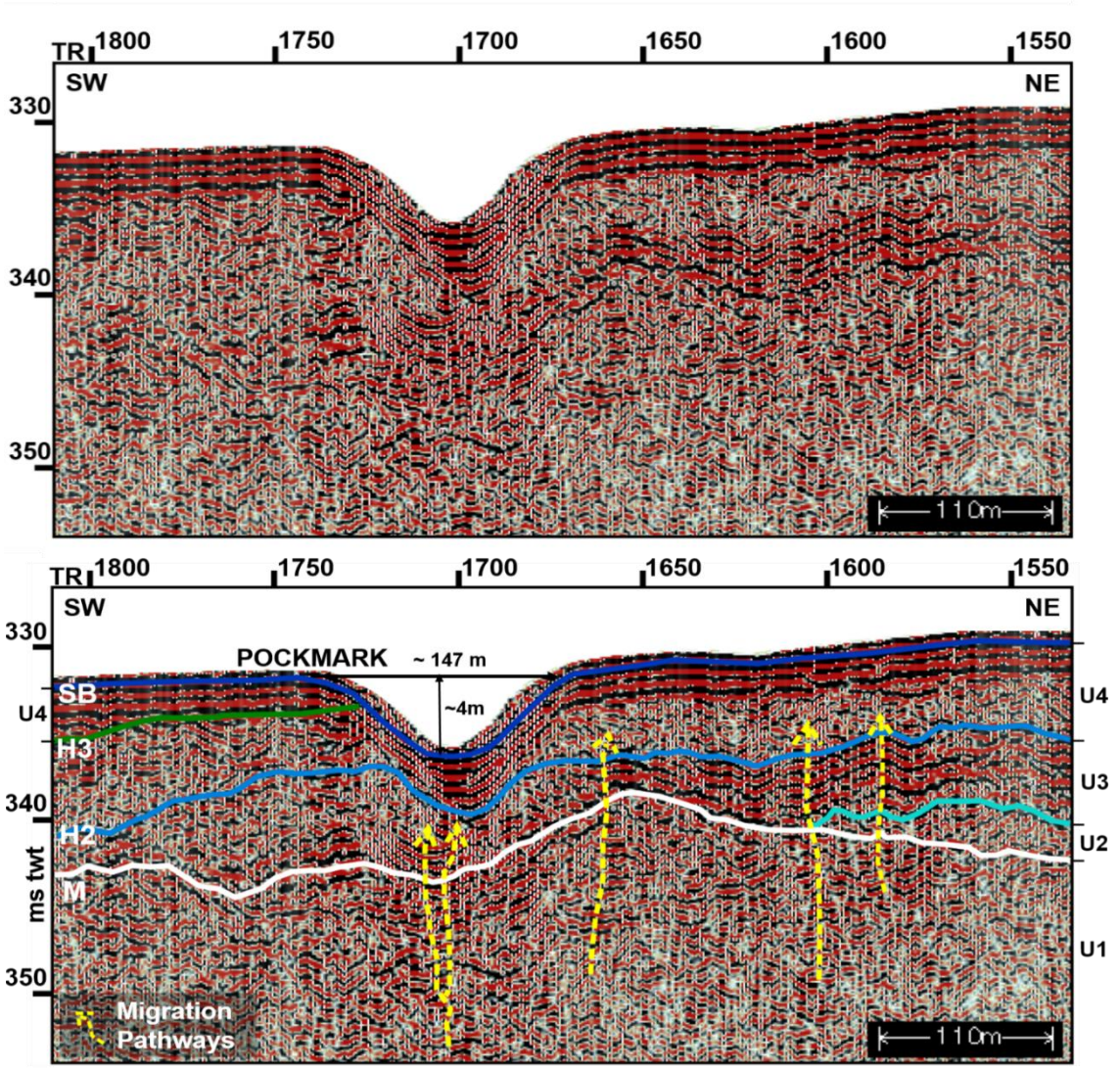

Figure 79 Detail of seismic profile PM–C09 showing a pockmark at the seabed (Figure 62 for location).

In the seismic records is also possible to observe buried pockmarks, located at various depths within the seismic unit U6. The geometry and size of these buried pockmarks are similar to the ones found on the seafloor (Figure 80 and Figure 82). These structures are currently inactive, since the pockmark is totally filled-up with sediments, which indicate that the fluid migration to the seabed is an episodic process.

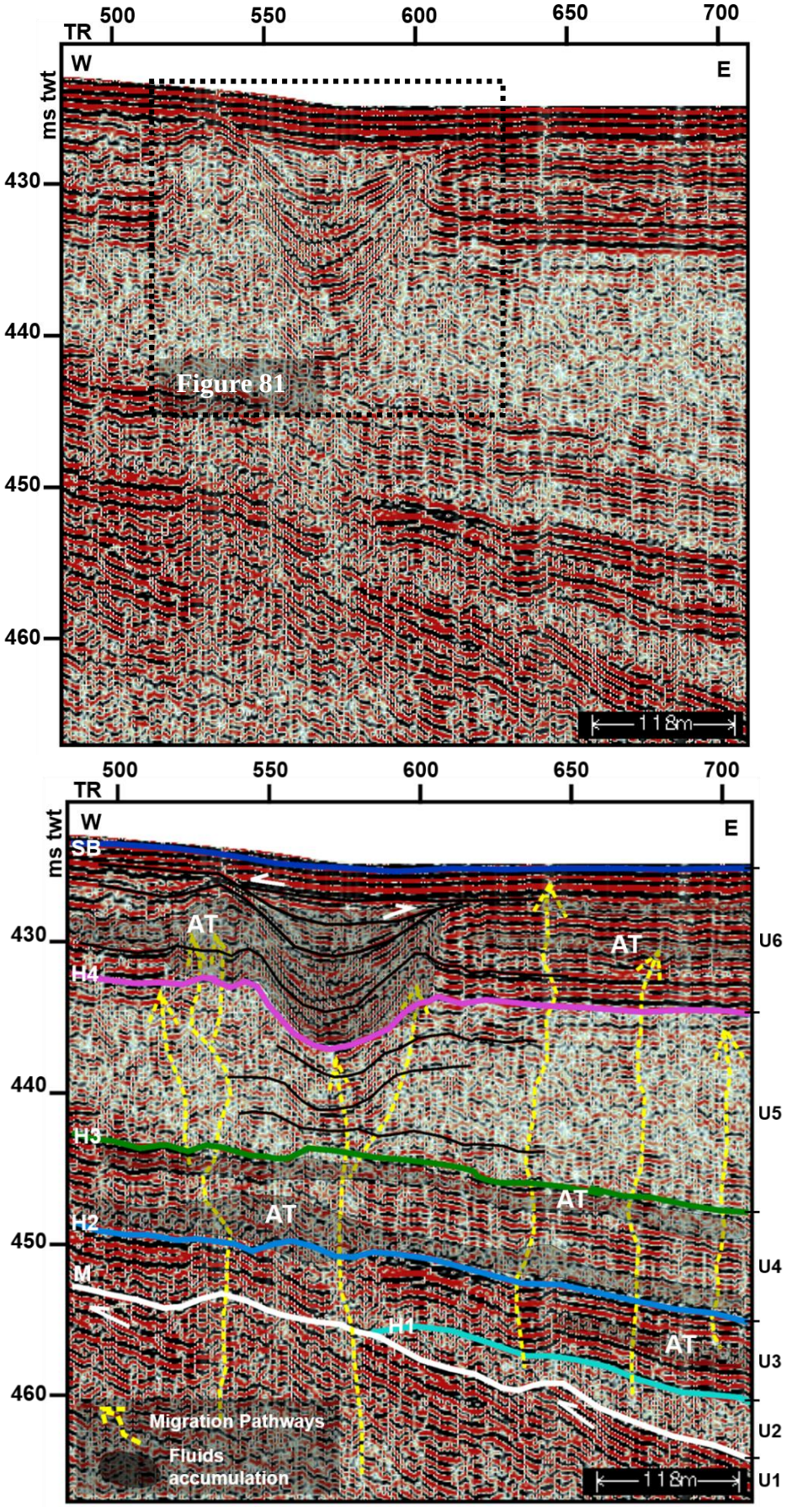

Figure 80 Detail of profile PM – C07 showing a buried pockmark and sub-seafloor evidences for fluid migration (see location of section in Figure 60). Layers with AT are interpreted as fluids reservoirs.

Figure 81 shows the details of the buried pockmark identified above (Figure 80). The base of his structure, which corresponds to horizon H4, is buried at approximately 12 ms below the seabed. The feature has a maximum diameter of 152 meters. The sedimentary infill appears greatly disrupted with a complex pattern, but it is possible to observe parallel reflections and onlap terminations against the depression walls and with toplap terminations against the overlying reflection.

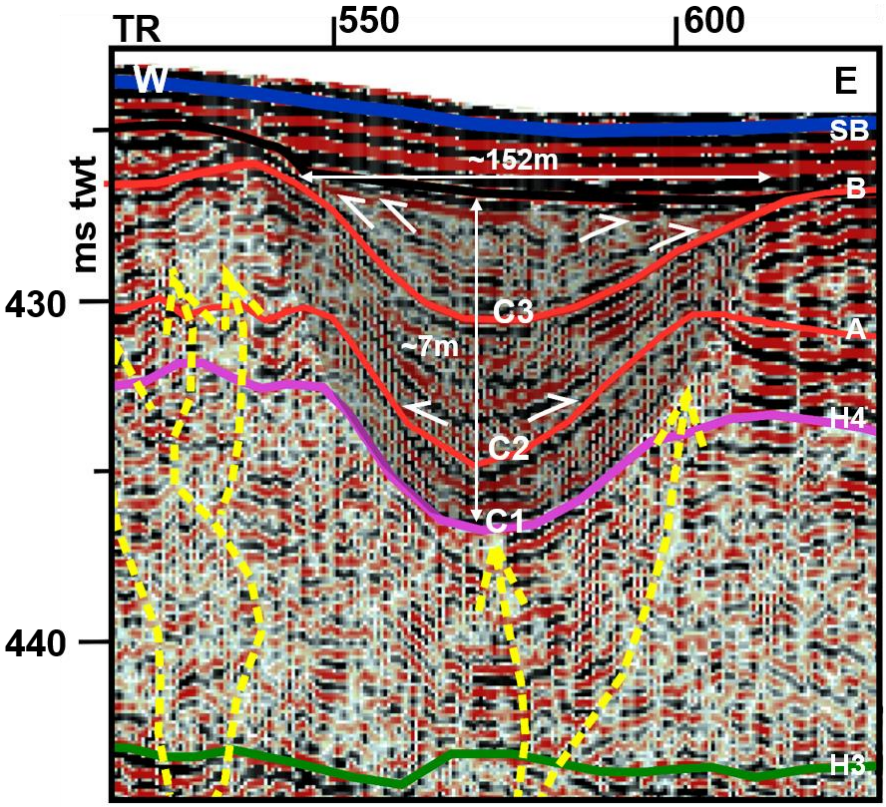

Figure 81 Detailed interpretation of a buried pockmark in profile PM–C07. Three phases of fluid expulsion causing deformation of the pockmark substract were identified (C1, C2 and C3) marking the paleo-depressions. The white arrows represent onlap and toplap terminations. Section location is given in Figure 80. Vertical exaggeration ~15x.

Based on the geometry of the sedimentary infill (lateral continuity, onlap and toplap terminations; Figure 81) three phases of intense fluid seepage at the paleo-seabed were interpreted: the horizon H4, and the A and B surfaces mark paleo-depressions (C1, C2 and C3, respectively) which are separated by the sediment packages: 1, 2 and 3. From horizon H4 to B fluids migration and seepage through the seabed was relatively constant, with periods of minor intensity that permitted the deposition of sediments. Between the horizon H4 and the surface a sedimentary package with a thickness of approximately 1 ms was deposited. The sedimentary package in between reflections A and B corresponds

of about 4.5 ms thick. The paleo-depression C3 was the last to form and above it occurred once more the deposition of sediments (approximately 3.5 ms), not being observed the formation of a new depression above them, which indicates that the pockmark became inactive.

Dubious evidence for possible pockmarks located deeper in the sedimentary sequence are also found within U5 (PM – C09; Figure 82). These evidences are beneath a pockmark (with a diameter of 165 m and depth of 7 ms) in the seabed two stacked structures with a morphology and dimensions that resemble the buried pockmarks. Both features have a diameter of about 110 m and depths of 6 ms. The three pockmarks appear to be separated by sediments infilling the corresponding depressions and sediments deposited in horizontal layers (with thickness of about 4 or 5 ms). The stacked pockmarks are underlying by a structure with an inverted cone shape (I, Figure 82; approximately 12 ms high), which will be discussed later on.

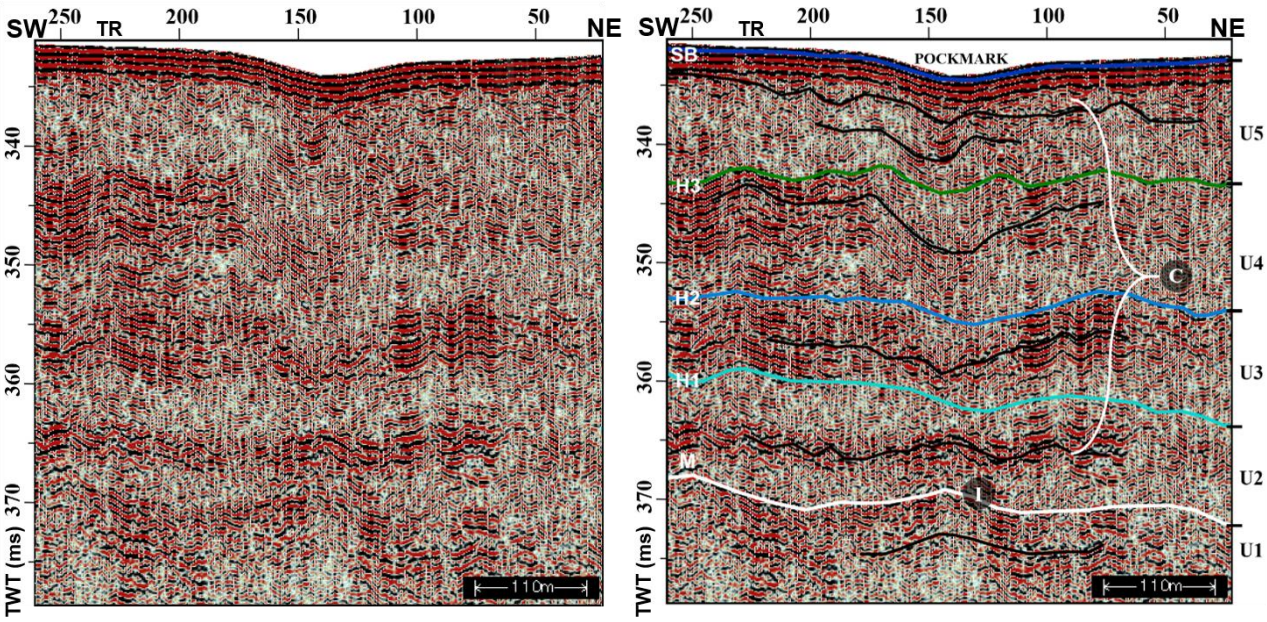

Figure 82 Detail of the northeast region of PM - C09 seismic line. A seabed pockmark stacked buried pockmarks. **C**: paleo-craters; **I**: inverted cone-shape. Location in Figure 62.

The region observed in Figure 82 was marked by acoustic turbidity (to be discussed below in this work) and lower amplitude reflections. The inverted cone structure (I) can be interpreted as related to a root zone of the fluids migration pathway, which were active during long periods of time, as it is observed a continuous pockmark formation above this structure location.

7.5.2 Mounds and tepee-shaped structures

In the northwestern sector of the study area, in the PM–C03 seismic profile (Figure 83) it is possible to identify a single mound structure, with 120 m wide, rising about 7.2 ms above the seabed. This structure is also observed in the bathymetry being characterized by a low backscatter acoustic signal. It seems to be an intrusive structure that cuts across the seismic sequence and whose nature is unknown.

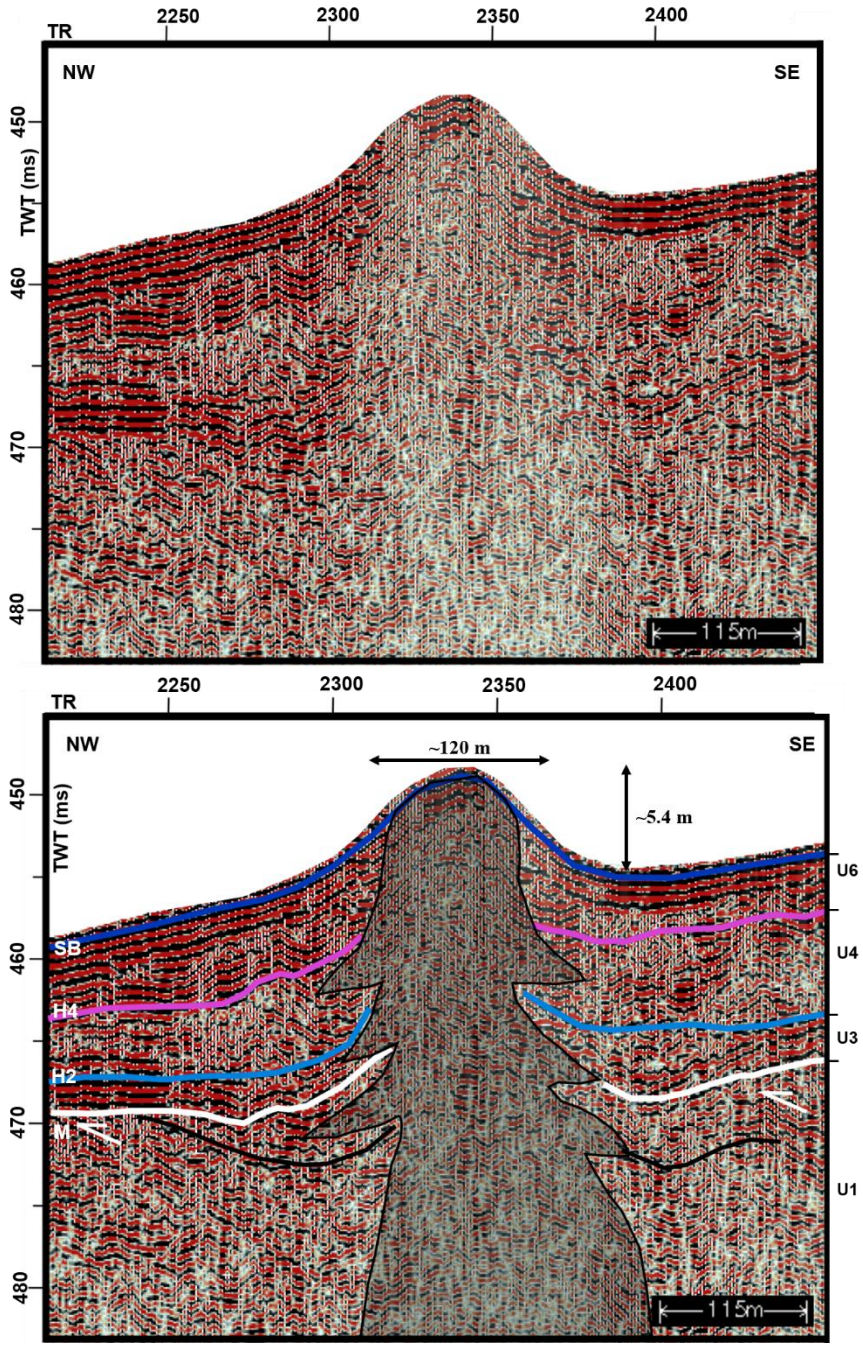

Figure 83 Mound like structure observed on the seismic profile PM–C03 (location in Figure 56). The lateral fluid intrusion interpretation is based on reflections terminations (cut offs). This structure may correspond to a mud volcano, diapir or carbonate mound, see text for discussion.

Mougenot (1989) and Badagola (2008) report the existence of several igneous intrusions in the Estremadura Spur, associated with the Upper Cretaceous volcanism. However, since the discovery of the evidences of fluid migration and seabed fluid extrusion in the Lourinhã Monocline region implies the consideration of alternative hypothesis on the nature of this structure, such as the hypothesis that this structure could be a shallow mud volcano, mud diapir or an seafloor doming due to an increase in the sediments pore pressure due to the presence (migration and accumulation) of fluids. This hypothesis is strengthened by two particular observations in the seismic data: (i) it is still possible to recognize inside the structure relics of the seismic horizons (something that is impossible in igneous intrusions, since they destroy the older structure); (ii) the observation of a christmas-tree structure, which is characteristic of subsurface mud volcanoes edifices. As the multibeam backscatter does not show any evidences of mud extrusive features, such as mud flows, this structure is probably a mud diapir or it is caused only by early stages of fluids accumulation.

In some seismic profiles (e.g. PM–C05 and PM–C06) inverted cone-shaped structures are also observed (Figure 84 and Figure 85) affecting the units U1 to U4, but with a greater expression in U2 and U3. These structures present a disturbed vertical zone (in U1) topped by reflections with higher amplitude and with 112-141 m wide and 2 to 5 ms high.
In some profiles (e.g. PM–C05; Figure 84) these structures appear to have formed post-sedimentation, since there was no evidence of a positive relief in the seabed, being interpreted as tepee structures constituted by complex carbonate rocks (Kauffman *et al.*, 1996; Kennedy *et al.,* 2001; Jiang *et al.*, 2003). And so it was interpreted that these

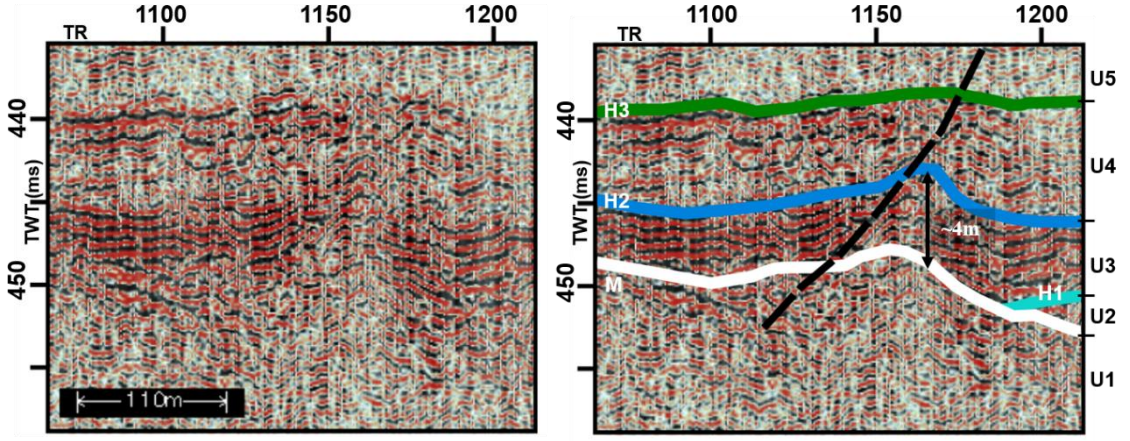

Figure 84 Inverted cone-shaped structure observed in PM-C05: tepee in U3. Location in Figure 58.

features were formed due to the upward migration of fluids that deformed the layers during the fluids upward migration.

However, in other seismic profiles (e.g. PM – C06; Figure 85) it is possible to observe a lateral thinning and onlap terminations of the overlying layers in these structures. This indicate long periods of development of these structures and suggest that they were formed at the seabed and then buried, which may indicate that they are carbonate mounds formed as the result of shallow sediments doming due to increased pore pressure during fluids migration and accumulation.

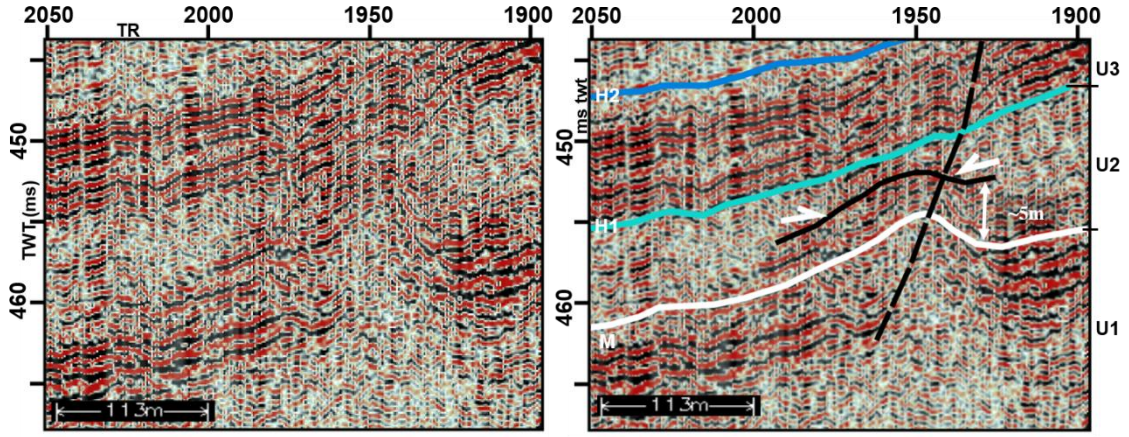

Figure 85 Inverted cone-shaped structure from PM-C06 (location in Figure 59). It is observed that the layers above this structure terminate *onlaping* against it (white arrows).

7.5.3. Acoustic evidences

In all the profiles vertical to sub-vertical columnar zones of acoustic wipe out (seismically transparent features) are observed, more commonly in the sector where the Pliocene-Quaternary sequence is thicker (the seismic profile PM-C07 cuts through this sector – Figure 60; isopach map of the seismic sequence in Figure 78). These features may be seismic artifacts that were not completely eliminated during the data processing or real structures caused by the circulation of fluids in the subsurface. Since they are observed throughout all the stages of the seismic processing (Chapter 6) were considered as real structures.

These structures commonly terminate at the seabed pockmarks, at buried pockmarks or at disturbed horizons and the majority of them seem to originate in unit U1 (e.g. Figure 80 and Figure 86), although some originate in the more recent units. Thereby, these features were interpreted as pipes or chimneys, formed by the upward migration of fluids.

Two types of wipe out zones were observed in the seismic profiles:

- The first group consists of sub-vertical narrow zones that are transparent or where the amplitude of the reflections is reduced. These features have approximately 10 m wide and seem to extend across the seismic sequence, as shown in Figure 86. The reflections of the host sedimentary package are usually offset or deformed close to these features. These observations suggest that these features are related to the upward migration of fluids along small faults or that the fluid overpressure caused fractures in the host strata;
- The second type, observed in Figure 86, comprises wider zones of disrupted or attenuated reflections with upward convex bending reflections that become narrow downwards. The reflections in the host strata appear to be bending upwards near to this features.

In the present work the first group of narrow structures are designated as pipes and the second group, with wider features, are referred as chimneys.

Throughout the seismic sections several disturbed reflections are observed where many of the fluid migration pipes begin or end. These disturbed zones are clearly identified in the seismic units characterized by continuous and coherent reflections (U3 in Figure 80; U4 and U6 in Figure 80 and Figure 86). These are interpreted as acoustic turbidity caused by fluid accumulation along these sediments. Vertical zones of acoustic anomaly that cross cut the seismic sequence, end near the seabed and are characterized by loss of lateral coherency and low amplitude of the reflections (Figure 86). These acoustic anomalous zones are observed in the seismic sections and interpreted as acoustic blanking zones, resulting from vertical migration and accumulation of fluids.

Seismic units U2 and U5 are characterized by chaotic to transparent facies although it is possible to follow coherent reflections with reduced amplitude. These characteristics can be due to the presence of fluids accumulated in the two units (Hovland, 1991; Hovland *et al* 1999), being observed variable degrees of disturbance (Figure 80 and Figure 86) most probably caused by different amounts of fluids in the pore-space of these seismic units. Since the disruption of the reflections is spread all over these units, it is not possible to clearly sustain that it is caused only by the presence and circulation of fluids, as alternatively it may be a consequence of lateral facies variations of these units.

Associated with the buried pockmarks it is frequently observed the presence of narrow pipes, approximately 10 m wide (Figure 80), through which occurs focalized fluid

migration. In general, the significant loss in the imaging accuracy with depth makes it difficult to define the root zones of these pipes. Nevertheless, it is possible to consider that some pipes are originated in seismic unit U1 or even in older sediments (traces between 525 and 600); and other pipes clearly originated, in seismic unit U2 (between traces 675 and 700). The upwards limit of these pipes is located bellow the seabed in acoustic turbidity horizontal layers and in buried pockmark. Seismic units U3, U4 and U6 are affected by acoustic turbidity, which suggest the accumulation of fluids within these units. The reflections observed on both sides of the buried pockmarks (in unit U6) have distinct characteristics. To the West of the buried pockmark (near trace 550 of the seismic profile PM-C07; Figure 80) the reflections appear disturbed, with low amplitude and that lose their lateral continuity. These characteristics are interpreted as acoustic turbidity. Contrariwise, the reflections to the East of the buried pockmark (traces from 600 to 700 of the seismic profile PM-C07; Figure 80) present good lateral continuity, being only observed two thin horizontal zones of acoustic turbidity, with 1 ms wide and some pipes, away from the buried pockmark boundary, that cross or terminate in these zones. This may indicate that after the pockmark was buried, fluid migration was still active and the system began to migrate along the buried pockmark west border, and accumulate in unit U6, perturbing stratabound layers of this seismic unit.

In Figure 86 are observed all the seismic units with exception of unit U2. Units U4 and U6 have stratabound like zones of acoustic turbidity, with 1.5 to 5 ms high, suggesting once more that fluids accumulate in these units. The seabed does not seem to be affected by fluid seepage, suggesting that the fluids do not migrate to the surface. Between traces 2450 and 2400 a vertical zone of acoustic anomaly affecting seismic units U4, U5 and U6 (near 16 ms high) is visible and interpreted as acoustic blanking. This feature ends 4 m below the seabed, and is connected with an acoustic turbidity zone in unit U4.

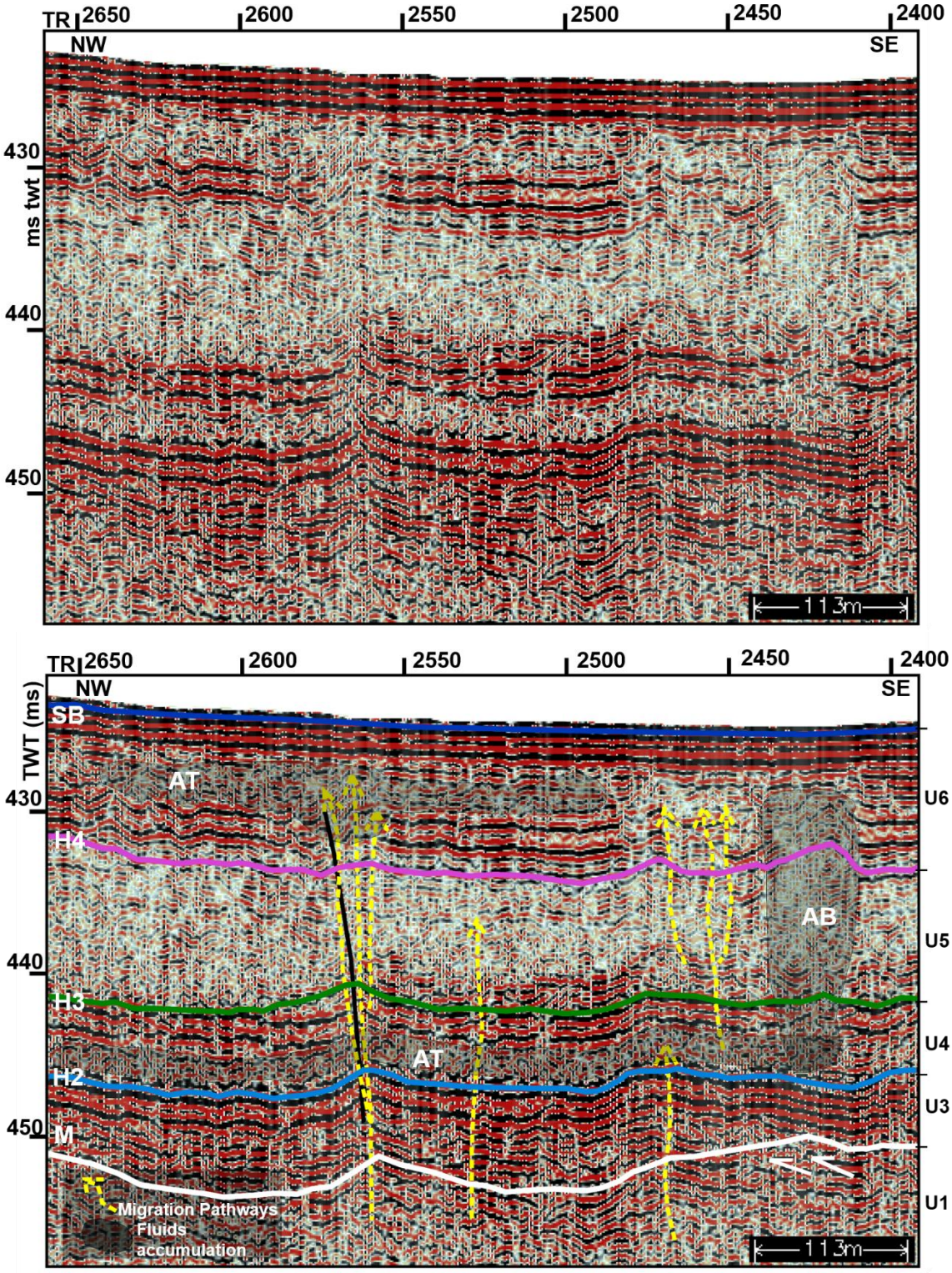

Figure 86 Detail of PM–C06: Seismic acoustic evidences for fluid accumulation and migration. AT: acoustic turbidity; AB: acoustic blanking (Figure 59).

In this section of PM–C06 the two types of localized migration pathways are observed, the chimneys and the pipes. Near trace 2550, it is possible to observe a chimney terminating in the acoustic turbidity zone of unit U6 with approximately 23 m wide. This

structure narrows downwards (to approximately 9 m in units U3 and U4). The host units internal reflections (U1, U3 and U4) are bending upwards near this migration pathway that appears to be rooted in unit U1 or older rocks. Fluid pipes are also observed, rooting in U1 or in stratabound acoustic turbidity zones in unit U4 and terminating in the chaotic unit U5 and in acoustic turbidity layers of units U4 and U6.

The chimneys, pipes and acoustic blanking perturbations point towards different types of fluid flow, focused fluid flow recorded as chimneys and pipes, and diffuse fluid flow recorded as acoustic blanking. In some cases both types of fluid flow are observed in close association. It is worthwhile to note that the deformation associated with the different types of fluid flow is also different. While, the diffuse flow (acoustic blanking) causes distributed deformation and the formation of localized folds and collapse structures (synclines), the localized flow (chimneys and pipes) profits from preexisting fractures and can become diffuse upwards.

CHAPTER 8

DISCUSSION

8.1 Lithostratigraphy and structure

A seismostratigraphic and tectonic map of the Lourinhã Monocline was done with the information gathered during the interpretation of the geomorphologic maps and seismic profiles of the PACEMAKER data (Figure 87). It is observed that only the seismic units U4, U5 and U6 of middle Pleistocene through Holocene age outcrop on the sea floor. There is a crude relation between distribution outcropping seismic units and their backscatter response, since the seismic unit U5 outcrops in the areas where the backscatter has a spotted pattern (SW of Area 1 and Area 3 in Figure 40) and the seismic unit U6 corresponds to monotonous low backscatter are with elongate moat-like depression (Area 2 in Figure 36 and Figure 40). Unit U4 only outcrops in a small circular area on the south limit of the map, corresponding to the region of Area 3 (Figure 40) were the backscatter pattern is constant and exhibit a facies with low response.

Four blind NNE-SSW to N-S striking, sub-vertical strike-slip faults were observed (Figure 87) in the Lourinhã Monocline both in the seismic profiles and backscatter image. The left-lateral kinematics are based on the present day approximate NW-SE orientation of the maximum horizontal stress (Ribeiro *et al*., 1998, Cunha *et al*., 2012). The position and kinematics of these faults agree with the interpretations resulting from study (Chapter 5) and are similar to the proposed by Badagola (2008). The tilting of the sequences shows tectonic deformation at a larger scale that encompasses the Lourinhã monocline (LM). Actually, the LM is bound by a roughly NNE-SSW trending extensional fault, probably a transtensional strike-slip fault, while the eastern part of the LM merges into the crest of an anticline. This indicates that active strike-slip tectonics has been occurring during the Pliocene and Quaternary, which is also in agreement with active seismicity in the Estremadura Spur. Custodio *et al*. (2015) have recently shown the existence of a West-East trending seismicity cluster just west of the study area. We can speculate that the observed N-S faults are associated as transfer faults to East-West thrusts.

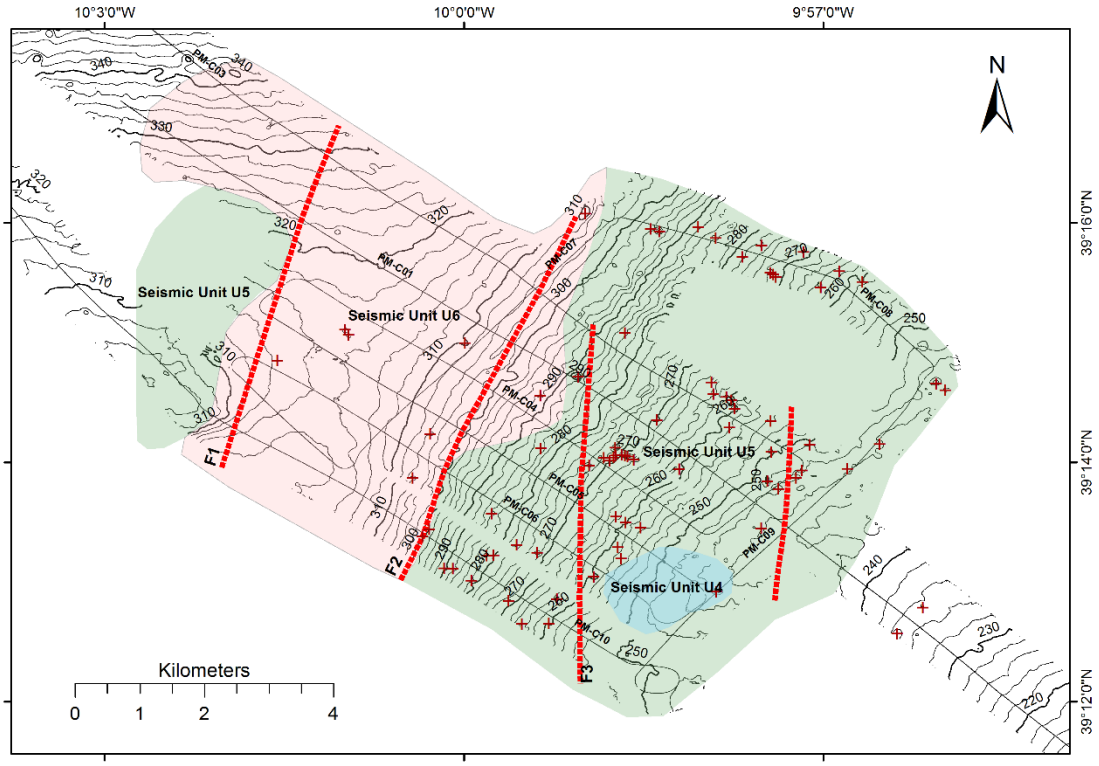

Figure 87 Sismostratigraphic and tectonic map of the Lourinhã Monocline. **Red dotted lines**: major faults identified in the LM; **Red crosses:** identified pockmarks.

8.2 Evidences for the presence and migration of fluids

Evidences of fluid migration and accumulation within the Estremadura Spur shelf sediments and fluids seepage at the seafloor were here presented and their geophysical signature was analysed (Chapter 5 and 7).

The occurrence of a large number of morphologic features interpreted as pockmarks from multibeam bathymetry and backscatter images of the seafloor (Figure 38 and Figure 40) was the first direct evidence of the presence of fluids seepage in this zone of the West Iberian margin. High-backscatter anomalies are commonly associated with recent seafloor seepage sites and suggest the presence of authigenic carbonates (Orange *et al.*, 2002; Klaucke *et al.*, 2006) that typically occur associated with active seepage sites. In order to investigate this hypothesis, visual observations made with the ROV Luso of three pockmarks were done, but showed that the high-backscatter depressed areas had no signs of active seepage at present (Figure 43 and Figure 44) and the pockmarks are recovered with sandy sediments.

The interpretation of the PACEMAKER seismic data also provided important indication for the presence of fluids trapped within the shelf sediments, but not for the occurrence of gas hydrates which are frequently found associated to the pockmarks in other regions

(e.g. Pinheiro *et al*, 2003; Judd and Hovland, 2007; Gay *et al*., 2006; 2007; Chand *et al*., 2008; Barnes et al., 2010). Fluid migration pathways (pipes and chimneys; Figure 79, Figure 80 and Figure 86) were observed as well as acoustically disturbed zones where the fluids accumulate (AT and AB in Figure 80 and Figure 86), mainly where the Pliocene-Quaternary sequence is thicker (Figure 88).

The pockmark field of the Estremadura Spur can be subdivided in two regions. The first is characterized by the preferential occurrence of buried pockmarks that corresponds to the basin depocentre area, where the seismic unit U6 outcrops (Figure 87; Area 2 in figure). The second region corresponds to the seismic unit U5 outcrops, where the Pliocene-Quaternary sedimentary package is normally thinner, and here most of the pockmarks occur at seafloor with a seabed expression (Figure 79). The pockmarks that occur at the seafloor or are buried near it (at less than 10 ms bsf) could have been formed during the same seepage event and then buried in the region where the sedimentary rate is higher.

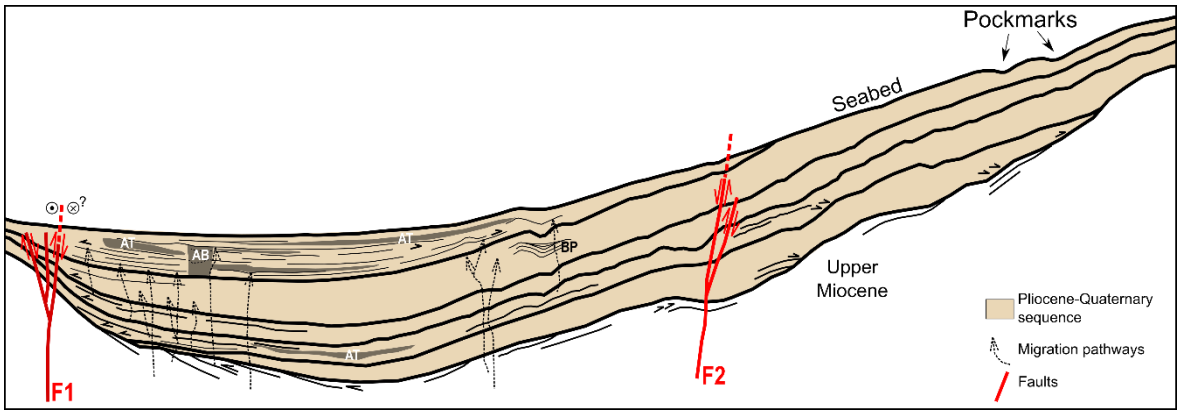

Figure 88 Conceptual model for fluid migration in the Estremadura Spur. Major faults are represented (F1 and F2). **AB** – acoustic blanking; **AT** – acoustic turbidity; **BP** – buried pockmark. **Dashed arrows** – principal migration pathways; **Black arrows** – onlap terminations (based on PM-C10).

The buried pockmarks are localized in the region where the Pliocene-Quaternary sequence is thicker, i.e. where the sedimentation rate is higher, leading to the faster burying of these features after their activity. The pockmarks that have expression in the seabed are located in the slope and less deeper zones of the studied area, where the sedimentation rate is lower or the erosion was more intense, allowing for their preservation instead of burial. Since this seismic unit is of Holocene age and many pockmarks are still marked on the seafloor, it is deduced that the fluid expulsion is occurring at present-day or has occurred recently.

8.3 Seepage activity during upper Pliocene and Quaternary

Cathles *et al*., 2010 suggest that pockmark craters form abruptly, when local accumulations of overpressured pore-water and gas erupt through the seafloor surface sediments, and they are thereafter maintained by slow pore-water and gas seepage. When the system that feeds the pockmarks becomes inactive the depressions are buried under the continuous deposition of sediments.

The presence of buried pockmarks along the Pliocene-Quaternary seismic unit (at various depths) indicates that the migration of fluids is intermittent and repeated periodically in the Estremadura Spur, at least since the upper Pliocene. This episodic occurrence of fluids seepage can be caused by several processes: by the cyclical sea-level changes, by seismologically driven periodical overpressure variations, or by periodically sub-basin pressure bluid-up and release triggered by unknown factors. It is also possible to recognize in the seismic data the accumulation of fluids in stratabound units (marked by acoustic turbidity; e.g.Figure 86) below the seafloor.

Based on the interpretation of the seismic profiles it can be interpreted that at present-day, the migration of fluids (probably a mixture of water and gas) does not reach the seafloor, since the system is in a dormant phase of vertical fluid migration and the fluids are accumulating within the seismic sedimentary sequence, as demonstrated by the seismic data (Figure 80 and Figure 86). This is consistent with the ROV images (Figure 43 and Figure 44), the structures observed during the dives were found to be covered with sandy sediments and no carbonates were found. Also, neither bubbling nor characteristic fauna were observed and the seafloor in these sites. Gay *et al*. (2007) sustains that seep sites, both active and recently active but currently inactive and buried under 10 m of sediments, may create anomalies on the backscatter signal (Figure 28).Therefore, the seepage in the Lourinhã Monocline pockmark field is possibly currently inactive although it has been active recently (probably during the Holocene).

Two possible evolution models are hereafter proposed to explain the fluid migration system that originate and control the Estremadura Spur pockmarks field: (i) seepage cyclic activity and (ii) MDAC system sealing.

8.3.1 Seepage cyclic activity

The fluids migration and expulsion at the seafloor occur in individual episodes intercalated with periods of dormancy (Figure 89). This model is sustained by the vertical stacked buried pockmarks that are observed the seismic profiles, as in profile PM–C09 (Figure 82). These features provide evidence for paleo-seepage activity, at least since the Pleistocene as the buried pockmarks are identified at various depths, being the oldest one in seismic unit U3. The stacked buried pockmarks appear to be separated by sediments infilling the corresponding depressions and sediments deposited in horizontal layers, which indicates that the seepage activity is not continuous.

A four phase cycle model is illustrated in Figure 89. Firstly, the occurrence of sub-surface pockets enriched in fluids (possibly accumulating in the seismic unit U1 or below) causes local deformation of the overlying sediments (doming as seen in PM–C09 figure, forming inverted cone-shaped structures). Due to the overpressuring the yield point of the sedimentary material is reached leading to an increase of percolation pathways and the vertical fluid migration throughout the seismic sequence (Figure 89–Stage 1). . If fluid flow is rapid and sudden then a pockmark forms at the seafloor (Figure 89–Stage 2), due to the remobilization of seabed fine sediments (Hovland *et al*., 2010). Fluid flow becomes slower or even stops after the pressure release event. In these phases of inactivity the pockmark depression is filled with sediments (Figure 89–Stage 3) until complete burial. Although the seafloor seepage is inactive, the fluid migration can still be active, with fluids migrating vertical or laterally through and/or along the sedimentary package and accumulate underneath impermeable layers. If the overpressure builds up again and overcomes the cohesion of the overlying cover, a new pockmark will form at the seafloor, caused by the new phase of rapid and abrupt fluid flux (Figure 89–Stage 4).

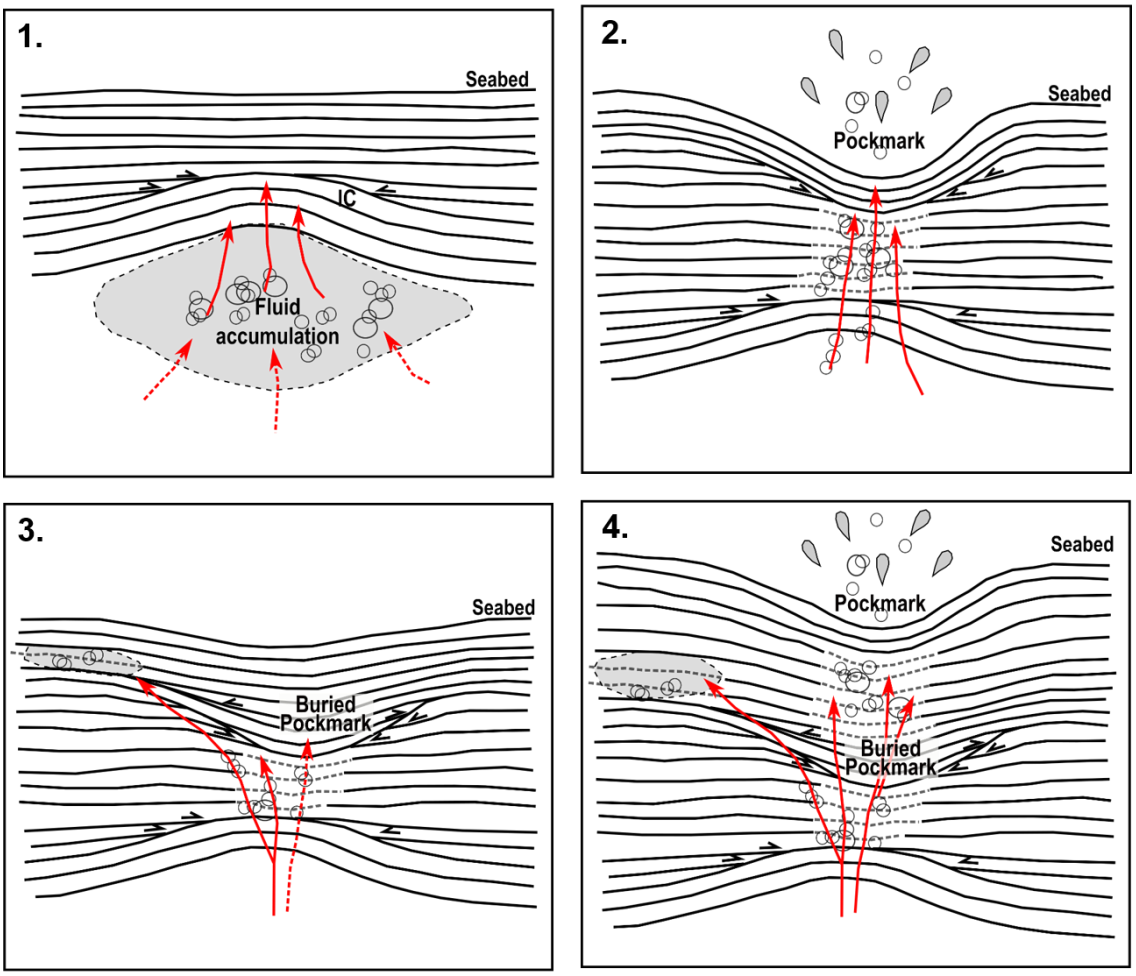

Figure 89 Seepage cyclic activity hypothesis. **1** – Start of the accumulation of fluids, causing the folding of the overlying sediments; **2** – Fluids overpressure is reached, causing its vertical migration and expulsion through the seafloor (pockmark formation); **3** – When the pressure decreases, the seafloor seepage ceases. The pockmark is buried by new sedimentation. The fluid continues to migrate through weak zones of the seismic sequence and accumulates within more permeable layers; **4** – With the increase of the pressure occurs other phase of fluid expulsion on the seafloor, creating a new pockmark depression over the buried one. **Red arrows**: migration pathways; **Red dashed arrows**: possible migration pathways; **Circles and drops**: fluid; **Dashed gray lines**: acoustically disturbed reflection; **Black arrows**: onlap terminations. Evidences for this model are observed in seismic profile PM-C09 (Figure 82).

Various reasons for the periodic interruption and reactivation of fluids seepage can be proposed, such as eustatic sea-level changes or earthquakes occurrence. This topic will is discussed elsewhere in this work.

8.3.2 MDAC system sealing

The precipitation of methane-derived authigenic carbonates (MDAC) inside the migration conduits (chimneys and pipes) that originate the pockmarks can seal the pathways for fluid flux (Hovland *et al.*, 2010 For this process to occur is necessary an anoxic environment, which is not common at shallow depths in porous sediments. The oxidation of migrating light hydrocarbons (such as methane), partly dissolved in advecting porewater and in a free gas phases, after some time causes the formation of anoxic conditions (Hovland, 2002). Thus, the required conditions for MDAC precipitation are formed. The MDAC precipitation forces the deactivation of the fluid migration pathways (and, consequently, the deactivation of the related pockmarks). Thereafter, new migration pathways will be formed laterally (Hovland *et al*., 2010), most probably in weak or more permeable zones of the seismic sequence. This model is supported by the observations done in seismic profiles such as line PM-C07 (Figure 80), in which is possible to recognize that a buried pockmark is completely sealed and a stratabound acoustically disturbed zone (acoustic turbidity), characteristic of the accumulation of fluids is formed laterally. This stratabound acoustically disturbed zone is interpreted as the result of migration of fluids through the border of the buried pockmark along a new conduit path after the pockmark sealing that is due to MDAC precipitation or as result of a stop of the fluids input and subsequent burial of the pockmark by impermeable sediments and then a subsequent sealing of the original migration pathway.

The occurrence of high backscatter facies inside pockmarks with seafloor morphologic expression also supports the existence of MDAC. It is likely that the areas with high backscatter are sealed and therefore no fluids seepage occurs where the MDAC seals the pockmark. The direct inspection of the seafloor using ROV did not show any evidence of MDAC hardgrounds in the two visited sites, but nevertheless it is possible that they were buried under the recent detritic sandy deposits (discussed in Chapter 5).

This evolution model is sub-divided in five phases, illustrated in Figure 89. The first two phases are similar to the ones described in the stacked pockmarks model (Figure 90– Stages 1 and 2). The third phase corresponds to the sealing of the migration pathways by the precipitation of MDAC (Figure 90–Stage 3). In this phase the fluid is still able to migrate upwards through fractures of the MDAC deposited in these conduits (Hovland *et al.*, 2010). When the migration pathways are completely sealed the pockmark becomes inactive. With the closure of the original migration pathways, the fluids open new

conduits in fragile zones of the sediment package (Figure 90–Stage 4), and the fluids migrate vertically until more permeable layers within the seismic unit U6 allow the accumulation of fluids near the seabed (Figure 90–Stage 5), this corresponds to the present-day state of the system.

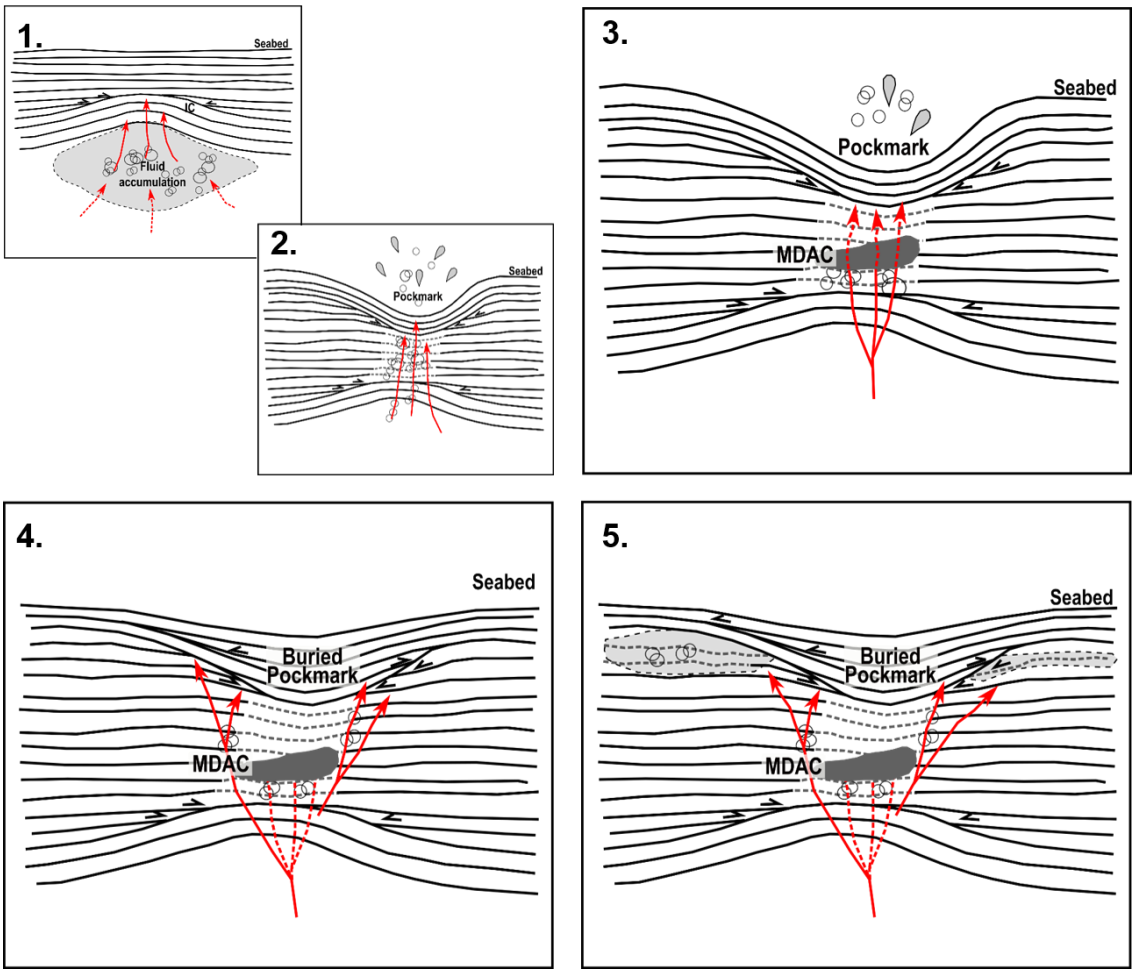

Figure 90 Metane-derived authigenic carbonates evolution model. **1** and **2** – With the start of the fluid accumulation, the overlying sediments are deformed and when the overpressure is reached these fluids start to migrate vertically and are expulsed through the seafloor to the water column, creating a pockmark (these two first phases are common two the two hypothesis); **3** – The subsurface formation of MDAC started to bloke the migration pathways that feed the pockmark, that will be eventually closed; **4** – with the migration pathways blocked the pockmark became inactive and is buried by new sediments. The fluid continues to migrate, opening new pathways through weaker zones of the seismic sequence; **5** – The fluid accumulates within permeable layers around the buried pockmark, not reaching the seafloor. **Red arrows**: migration pathways; **Red dashed arrows**: possible migration pathways; **Circles and drops**: fluid; **Dashed gray lines**: acoustically disturbed reflection; **Black arrows**: onlap terminations. In the seismic profiles is possible to observe evidences that confirms this evolutionary model, such as in PM-C07 (Figure 80).

Based on the interpretation of the available seismic data we can consider that these two evolution models can coexist in the Estremadura Spur pockmarks.

8.4 Geological control on fluid migration

Fluids tend to move towards lower hydraulic heads, i.e. towards locals of lower confining pressure. The fluids capacity to move upwards is controlled by the nature of the overlying sedimentary deposits and the availability of migration pathways. Typically, migration occurs by diffusion most readily through coarse and permeable sediments (Judd, 2001) and along fractures in a focused manner. Geological traps, i.e. impermeable layers or boundaries limit and control the direct fluid migration pathways. Thus, the fluid (water, gas or a mixture of both, which is believed to originate pockmarks) gets trapped below these impermeable layers, forming pore-water and gas pockets. The pressure at the base of the pocket is hydrostatic and at the top is much larger than the hydrostatic pressure, due to gas density being lower than the sediments'. As the thickness of the fluid pocket grows, the excess pressure increases and eventually becomes sufficient to crack the seal. When the yield point is reached the seal fails and the fluid is discharged through migration pathways (like chimneys and pipes), which propagate vertically through the sedimentary sequence (Cathles *et al*., 2010). These overpressured fluids gather along sedimentary discontinuities and favorable geologic structures, such as fault planes, anticline axes and preexisting deformations (Mazzini, 2009).

The fluid migration evidences in the Pliocene-Quaternary seismic sequence are clearly distinct from the migration evidences in the older and folded unit U1. The vertical fluid migration mostly takes place within the Pliocene-Quaternary sedimentary sequence, here it is better represented in the number of structures and their characteristics are more evident than in U1. In U1, the migration is essentially focused, occurring through fracture planes (which may be possibly opened during the folding event). This means that U1 is more compact and impermeable that the sequence that covers it (U2 to U6), where the upward movement of the fluid has a more diffuse character with many pathways that occur over large disturbed areas. In some units of the Pliocene-Quaternary sequence it is also observed lateral fluid migration suggesting that these rocks are relatively permeable and porous, allowing the accumulation of fluids that remain trapped by overlying seals of low permeability layers close to the seabed (Figure 80 and Figure 86).

There are several geological processes that may trigger vertical fluid migration and subsequent expulsion associated with excess pore-fluid pressure, such as tectonics, rapid sediment loading, earthquakes and sea-level changes (Kopf, 2001; Taluker, 2012).
From the observation of the sea-level variations through the last 3000 ka (De Boer *et al.*, 2010; Figure 91) it is possible to recognize that the differences between high-stands and low-stands are more accentuated during the last 1000 ka, being observed four high-stand important periods.

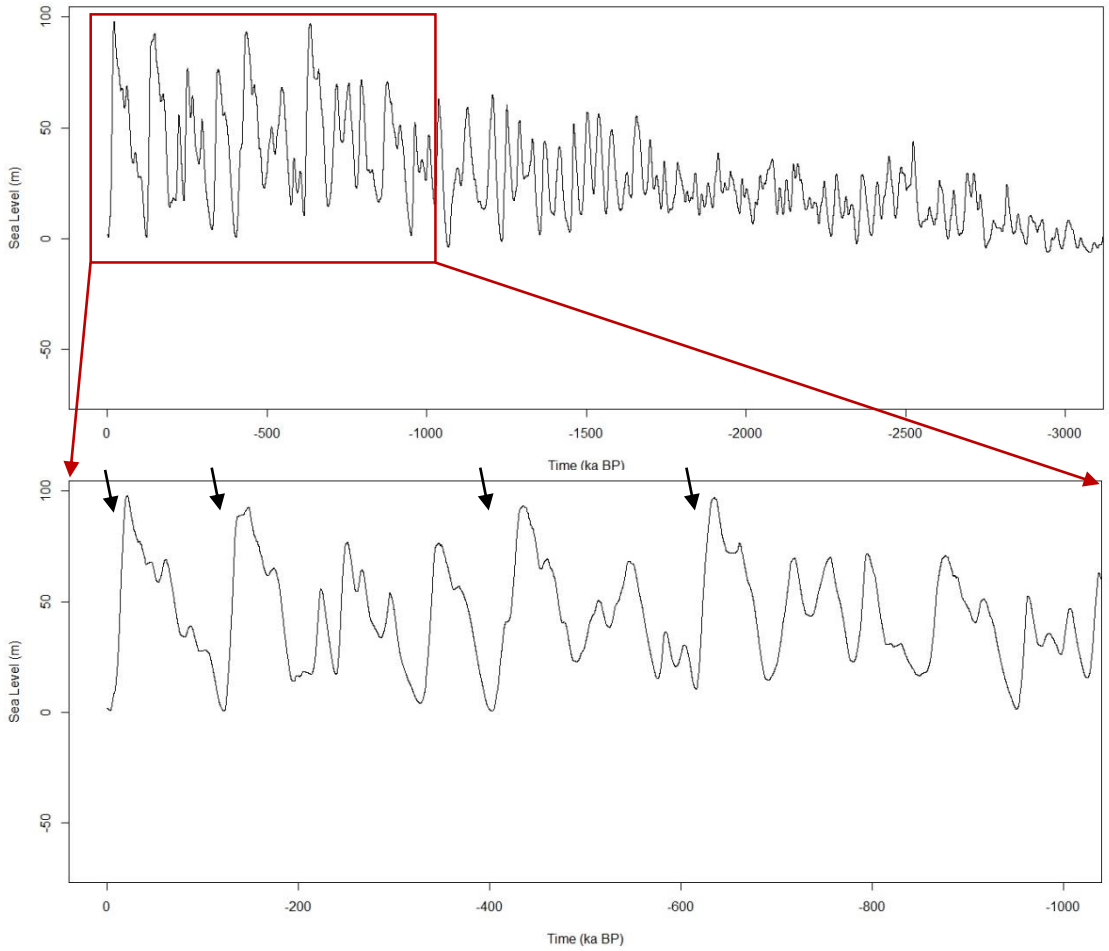

Figure 91 Sea-level changes in the last 3000 ka (from De Boer *et al.*, 2010). Four important low-stand peaks are observed during the Quaternary (black arrows).

During sea-level low-stands, hydrostatic pressure in the fluid reservoir decreases, causing the fluid migration and expulsion through the seabed, creating pockmarks. During the high-stand the water column is thicker and heavier, causing the increase of the hydrostatic pressure and consequently the decrease of the fluid expulsion (and the pockmarks become inactive).

Based on the stacked pockmarks model (Figure 89) the fluids accumulation and/or overpressure conditions at the Estremadura Spur suffers periodic variations. Therefore, the sea-level changes can be the trigger mechanism for seepage and pockmark formation. Despite being part of a passive margin, the Estremadura Spur is seismically active, so other possible trigger for cyclic seepage is the earthquake driven overpressure conditions. It was considered that the eustatic sea-level variations are more likely to have trigger the activation and interruption of the seepage, since it seems to be restricted to the Quaternary times. In Figure 82 is observed four stacked pockmarks, one is at the seafloor and the other three are buried. These structures affect the seismic units U3, U4 and U5 of lower to middle Pleistocene age. As referred, in Figure 91 are observed four low-stand important periods during the Pleistocene. This can be interpreted as the events that caused the fluid seepage at the seafloor and consequently the pockmarks.

No evidences or indications of the presence of gas hydrates in the sedimentary sequence were identified. This can be justified by the restricted thermodynamic conditions of their pressure/temperature stability domain. As gas hydrates (or methane hydrates, here we consider the gas composition of the hydrates as being methane) are stable at water depths of more than 300 m. Even, for water depths of 400 m (approximately the maximum water depth of the pockmark field area), gas hydrates to be stable require a seafloor temperature of less than 3°C. These conditions are not met in the Estremadura Spur continental shelf in the area of the pockmarks field where the average annual seabottom water temperature value, at 400 m water depth is of 11.7ºC and the minimum annual seabottom water temperature value is of 6.2ºC (Locarnini *et al*., 2013), therefore gas hydrates are not expected to be found in this area.

8.5 Origin of the fluids

The nature and origin of the fluids present in the Estremadura Spur is not fully understood, but it can be assumed that there is only one fluid circulation system.

The seismic interpretation allows the characterization of the fluids migration pathways, their shallow accumulations, and therefore permits to constrain a minimum depth of origin and infer their origin and age. Since the seismic image resolution diminishes with depth, the source and geometry (and hence tectonic/structural control) of migration pathways (pipes and chimneys; e.g. **Figure 86**) is limited. In addition, upward propagation

of these pathways may erase earlier evidences for pipe growth-arrest at intermediate stages (Cartwright *et al*., 2015).

The seismic observations presented in this work show various locations where the fluid migration pathways seem to be rooted below the Pliocene-Quaternary sediments (Figure 80 and Figure 86) in the older seismic unit U1. This is an indication that the fluids in the sedimentary cover of the Lourinhã Monocline originate, at least partially, in the Lower to Middle Miocene sediments or deeper. Since the seismic profiles do not allow the imaging of the Lourinhã Monocline subsurface under 500 ms (approx. 375 m), it is not possible to be sure that the fluids are not even older. This supports a deep-seated source for the fluid origin.

In the onshore part of the Lusitanian basin, equivalent to the Estremadura Spur (Estremanho Massif) several cases of oil and gas seepage in the Jurassic outcrops are referred (e.g. Montejunto Fm; Pena dos Reis and Pimentel, 2010; 2014), suggesting the existence of an deep sourced and at present day active hydrocarbon migration system. Pena dos Reis and Pimentel (2014) also suggest that the migration pathways efficiency was enhanced by the Late Miocene intense uplift, related with the Alpine compressive phase, which was responsible for the Estremadura Spur uplift. In the well 20B-1 (described in Chapter 3 of this thesis), localized about 40 km SE of the Lourinhã Monocline, a small gas occurrence in the Late Jurassic Coimbra Formation was reported. These two occurrences can indicate that the fluids that originated the pockmarks observed in the studied area formations have a deep origin, with a source-rock older than the Lower–Middle Miocene formations (seismic unit U1) and can be possibly related with the hydrocarbon system of Jurassic age. Thus, to better restrain the fluid age a more detailed characterization of the migration pathways geometry with high resolution and deep seismics and the analysis of the chemical nature of the fluids would be required.

However, with the available data, the presence of fluids formed at shallow depths within the Pliocene-Quaternary sequence cannot be discarded. It is not possible to determine the chemical nature of the fluids in the Lourinhã Monocline subsurface sediments just by using acoustic seismic data, it would be necessary to have geochemical data obtained through fluids, pore water and gases geochemical analysis of the near-bottom seawater and of the shallow sediments under the pockmarks crater or in an acoustic disturbed area (AB and AT zones; e.g. Figure 80).

CHAPTER 9

CONCLUSIONS

The main conclusions of this work can be summarized as follows:

i) The analysis of the PACEMAKER high-resolution seismic dataset allowed the identification of a sequence of six seismic units, disturbed by the migration and accumulation of fluids. The existence of N-S striking strike-slip faults cutting through the most recent seismic units is consistent with the instrumental seismic activity and NW-SE trending main horizontal stress.

ii) The NW region of the Estremadura Spur outer shelf has been affected by several episodes of fluid migration and fluid escape that are expressed by a vast number of seabed and buried pockmarks. It was concluded that the migration of fluids to the seabed occurred over the Pliocene-Quaternary, as indicated by the buried pockmarks at different depths. At present the pockmarks are mainly inactive, as the seabed pockmarks are recovered by recent sediments.

iii) The stacking of various pockmarks suggests a cyclical fluid flow activity that can passably be the result of the eustatic sea level variations and the subsequent changes of the hydrostatic pressure. An alternative hypothesis can be considered assuming the episodes of intense fluid flow as being associated with the local seismicity.

iv) Precipitation of methane-derived authigenic carbonates (MDAC) inside the migration conduits that originate pockmarks can force the deactivation of the fluid migration pathways and, consequently, the deactivation of the related pockmarks and creation of new migration pathways.

9.1 Future Work

This work was the starting point of the fluid expulsion structures occurring in the Estremadura Spur northwest outer shelf. Many questions still remain unanswered, such as the source-rocks of the fluid that originate the pockmark fields and the relation of this

field with the iceberg plug-mark evidences discovered during this work. Hence the need to continue the study of these structures. Some works are proposed to be realized in the future within the framework of the PES project:

- Microscopic characterization of the rock samples obtained during the EMEPC/PEPC/LUSO/2015 and roughly described in Chapter 5;
- New seismic surveys (high-resolution seismic) that complement the information that already exist and was interpreted in this study;
- More ROV dives for direct observations of the Estremadura Spur seafloor and other pockmark depressions and the single mound observed in the seismic data (in PM-C03) and;
- Geochemical analysis of the fluids (pore water and gases) of the near-bottom seawater and of the shallow sediments under the pockmarks crater.

BIBLIOGRAPHIC REFERENCES

Ali-Zade, A.; A., Shnyokov, E., Grigorianz, B., Aliev, A. and Rahmanov, R. (1984) – Geotectonic conditions of mud volcano manifestation on the Earth and their significance for oil and gas prospects. Proc. 27th World Geol. Congr. C13, 166–172 pp (in Russian).

Alves, T. M.; Gawthorpe, R. L.; Hunt, D. W. and Monteiro, J. H. (2003) – Cenozoic tectono-sedimentary evolution of the western Iberian Margin. Marine Geology, Vol. 195, 75-108 pp.

Alves, T. M.; Gawthorpe, R. L.; Hunt, D. W. and Monteiro, J. H. (2002) – Jurassic tectono-sedimentary evolution of the Northern Lusitanian Basin (offshore Portugal). Marine and Petroleum Geology, Vol. 19, 727-754 pp.

Alves, T. M.; Moita, C.; Sandes, F.; Cunha, C.; Monteiro, J. H. and Pinheiro, L. M. (2006) – Mesozoic-Cenozoic evolution of North Atlantic continental-slope basins: The Peniche basin, western Iberian margin. AAPG Bulletin, Vol. 90, no. 1, 31-60 pp.

Andeweg, B. (2002) – Cenozoic tectonic evolution of the Iberian Peninsula: effects and causes of changing stress fields. PhD thesis, University of Amsterdam. 178 pp.

Antonielli, B.; Monserrat, O.; Bonini, M.; Righini, G.; Sani, F.; Feyzullayev, A. A. and Aliyev, C. S. (2014) – Pre-eruptive ground deformation of Azerbaijan mud volcanoes detected through satellite radar interferometry (DInSAR). Tectonophysics, Vol. 637, 163-177 pp.

Badagola, A. P. L. (2008) – Evolução morfo-tectónica da plataforma continental do Esporão da Estremadura. Mestrado em Geologia Dinâmica (Área de Especialização em Geodinâmica). Tese de Mestrado, Departamento de Geologia da Faculdade de Ciências da Universidade de Lisboa. 171 pp.

Badagola, A.; Rodrigues, A.; Terrinha, P. and Veiga, L. (2006a) – Caracterização geomorfológica da plataforma continental do Esporão da Estremadura. Livro de resumos VII Congresso Nacional de Geologia, Vol. II, 377-380.

Badagola. A.; Rodrigues, A.; Terrinha, P. and Veiga, L. (2006b) – New insights on the Plio-Quaternary deposits of the Estremadura Spur shelf (West Iberian Margin). Abstract book of the 5th Symposium on the Iberian Atlantic Margin, Aveiro, 21-22.

Balsinha, M. (2008) – Sedimentary dynamics of Portuguese continental shelf between Nazaré submarine canyon and Ericeira. Master Thesis, University of Lisbon.

Balsinha, M.; Fernandes, C.; Oliveira, A.; Rodrigues, A. and Taborda, R. (2014) – Sediment transport patterns on the Estremadura Spur continental shelf: Insights from grain size trend analysis. Journal of Sea Research Vol. 93, 28-32 pp.

Baraza, J. and Ercilla, G. (1996) – Gas-charged sediment and large pockmark-like features on the Gulf of Cadiz slope (SW Spain). Marine and Petroleum Geology, Vol. 13, No. 2, 253-261 pp.

Barnes, P. M.; Lamarche, G.; Bialas, J.; Henrys, S.; Pecher, I.; Netzeband, G. L.; Greinert, J.; Mountjoy, J. J.; Pedley, K. and Crutchley, G. (2010) – Tectonic and Geological framework to gas hydrates and cold seeps on the Hikurangi subduction margin, New Zealand. Marine Geology, Vol. 272, 26-48 pp.

Berthou, P. Y. (1973) – Le Cénomanien de l' Estramadure Portugaise. Memórias dos Serviços Geológicos de Portugal Vol. 23.

Berthou, P. Y. (1984) – Résumé synthétique de la stratigraphie et de la paléogéographie du Crétacé moyen et supérieur du bassin occidental portugais. Geonovas 7, 99-120, Lisboa.

Berthou, P. Y. and Lauverjat, J. (1979) – Essai de synthèse paléogéographique et paléobiostratigraphique du bassin occidental Portugais au cours du Crétacé supérieur. Ciências da Terra Vol. 5, 121-144 pp.

Boillot, G.; Berthou, P. Y.; Dupeuble, P. A. and Muselec, P. (1972) – Géologie du plateau continental Portugais au nord du Cap Carvoeiro. La série stratigraphique. C. R. Acad. Sci. Ser. 2, 274:2748-2751.

Boillot, G.; Dupeuble, P.A. and Musellec, P. (1975) – Carte géologique du plateau continental nord-portugais. Bull. Soc. Geol. Fr. Vol. 17, 462-480 pp.

Boillot, G.; Malod, J. A. & Mougenot, D. (1979) – Évolution Géologique de la marge ouest-ibérique. Ciências da Terra 5, 215-222, Lisboa.

Bonini, M.; Tassi, F.; Feyzullayev, A. A.; Aliyev, C. S.; Capecchiacci, F. and Minissale, A. (2013) – Deep gaes discharged from mud volcanoes of Azerbaijan: New geochemical evidence. Marine and Petroleum Geology, Vol. 43, 450-463 pp.

Bünz, S.; Mienert, J. and Berndt, C. (2003) – Geological controls on the Storegga gas-hydrate system of the mid-Norwegian continental margin. Earth and Planetary Science Letters Vol. 209, 291-307 pp.

Cao, M.J.; Qin, K.Z.; Li, G.M.; Evans; N. J. and Jin, L.Y. (2014) – Abiogenic Fischer–Tropsch synthesis of methane at the Baogutu reduced porphyry copper deposit, western Junggar, NW-China. Geochimica et Cosmochimia Acta 141, 179-198 pp.

Caine, J. S.; Evans, J. P. and Forster, C. B. (1996) – Fault zone architecture and permeability structure. Geology 24, pp. 1025-1028.

Canérot, J., Rey, J., Baptista, R., Manuppella, G. and Peyberne's, B. (1995) – Nouvelle interprétation structurale et géodynamique de la marge atlantique portugaise dans le secteur de Caldas da Rainha (Portugal). C.R. Acad. Sci. Paris Ser. II, 320: 523-530.

Campbell, K. A.; Farmer, J. D. and Des Marais, D. (2002) – Ancient hydrocarbon seeps from Mesozoic convergent margin of California: carbonate geochemistry, fluids and paleoenvironments. Geofluids Vol. 2, 63-96 pp.

Cartwright, J.; Huuse, M. and Aplin, A. (2007) – Seal bypass systems. AAPG Bulletin Vol. 91, No. 8, 1141–1166 pp.

Cartwright, J. and Santamarina, C. (2015) – Seismic characteristics of fluid escape pipes in sedimentary basins: Implications for pipe genesis. Marine and Petroleum Geology Vol. 65, 126-140 pp.

Casas-Sainz, A.M. and De Vicente, G. (2009) – On the tectonic origin of Iberian topography. Tectonophysics, Volume 474, Issues 1-2, 214-235 pp.

Cathles, L. M.; Su, Z. and Chen, D. (2010) – The physics of gas chimney and pockmark formation, with implications for assessment of seafloor hazards and gas sequestration. Marine and Petroleum Geology, Vol. 27, 82-91 pp.

Chand, S. and Minshull, T. A. (2003) – Seismic constraints on the effects of gas hydrate on sediment physical properties and fluid flow: a review. Geofluids Vol. 3, 275-289 pp.

Chand, S.; Mienert, J.; Andreassen, K.; Knies, J.; Plassen, L. and Fotland, B. (2008) – Gas hydrate stability zone modelling in areas of salt tectonics and pockmarks of the Barents Sea suggests an active hydrocarbon venting system. Marine and Petroleum Geology Vol. 25, 625-636 pp.

Çifçi, G., Dondurur, D. and Ergun, M. (2003) – Deep and shallow structures of large pockmarks in the Turkish shelf, Eastern Black Sea. Geo-Marine Letters Vol. 23, 311-322 pp.

Clennell, M. B.; Hovland, M.; Booth, J. S.; Henry, P. and Winters, W. J. (1999) – Formation of natural hydrates in marine sediments. 1. Concenptual model of gas hydrate growth conditioned by host sediment properties. Journal of Geophysical Research Vol. 104, No. B10, 22.985-23.003 pp.

Cox, Michael J. G. (1999) – Static Corrections for Seismic Reflection Surveys. 9 Geophysical Reference Series. Society of Exploration Geophysicists.

Cukur, D.; Krastel, S.; Tomonaga, Y.; Çagatay, M. N.; Meydan, A. F. and The PaleoVan Science Team (2013) – Seismic evidence of shallow gas from Lake Van, eastern Turkey. Marine and Petroleum Geology Vol. 48, 341-353 pp.

Cunha, P. P. and Pena dos Reis, R. (1994) – Cretaceous sedimentar and tectonic evolution of the northern sector of the Lusitanian Basin (Portugal). Cretaceous Research Vol. 16, 155-170 pp.

Cunha, T. A.; Matias, L. M.; Terrinha, P.; Negredo, A. M.; Rosas, F.; Fernandes, R. M. S. and Pinheiro, L. M. (2012) – Neotectonics of the SW Iberia margin, Gulf of Cadiz and Alboran Sea: a reassessment including recent structural, seismic and geodetic data. Geophysics Journal International.

Custódio, S.; Dias, N. A.; Carrilho, F.; Góngora, E.; Rio, I.; Marreiros, C.; Morais, I.; Alves, P. and Matias, L. (2015) – Earthquakes in western Iberia: improving the understanding of lithospheric deformation in a slowly deforming region. Geophysical Journal International Vol. 203 (1), 127-145 pp.

De Boer, B.; Van de Wal, R. S. W.; Bintanja, R.; Lourens, L. J. and Tuenter, E. (2010) – Cenozoic global ice-volume and temperature simulations with 1-D ice-sheet models forced by benthic $\delta^{18}O$ records. Annals of Glaciology Vol. 51 (55), 23-33 pp.

De Vicente, G.; Cloetingh. S.; Van Wees, J. D. and Cunha, P. P. (2011) – Tectonic classification of Cenozoic Iberian foreland basins. Tectonophysics Vol. 502, 38–61 pp.

Dias, J. M. A. (1987) – Dinâmica Sedimentar e Evolução Recente da Plataforma Continental Portuguesa Setentrional. PhD Thesis, University of Lisbon. 384 pp.

Dias, J. M. A.,; Boski, T.; Rodrigues, A. and Magalhães, F. (2000) – Coast line evolution in Portugal since the Last Glacial Maximum until present – a synthesis. Marine Geology Vol. 170, 177-186pp.

Dias, J. M. A.; Monteiro, J. H. and Gaspar, L. C. (1980a) – Potencialidades em cascalhos e areias da plataforma continental portuguesa. Comunicações dos Serviços Geológicos de Portugal Vol. 66, 227-240 pp.

Dias, J. M. A.; Monteiro, J. H. and Gaspar, L. C (1980b) – Reconhecimento prévio dos depósitos de cascalho e areia a SW de Peniche. Comum. Serv. Geol. Portugal, 67: 65-83.

Dias, R.; Araújo, A.; Terrinha, P. and Kullberg, J. C. (eds) (2013a) – Geologia de Portugal. Volume I: Geologia Pré-mesozóica de Portugal. Escolar Editora, Lisboa. 807 pp.

Dias, R.; Araújo, A.; Terrinha, P. and Kullberg, J. C. (eds) (2013b) – Geologia de Portugal. Volume II: Geologia Meso-cenozóica de Portugal. Escolar Editora, Lisboa. 798 pp.

Dimitrov, L. I. (2002) – Mud volcanoes—the most important pathway for degassing deeply buried sediments. Earth-Science Reviews Vol. 59, 49-76 pp.

Dinis J.L.; Rey J.; Cunha P.P.; Callapez P. and Pena dos Reis R. (2008) – Stratigraphy and allogenic controls of the western Portugal Cretaceous: an update synthesis. Cretaceous Research Vol. 29, 772-780 pp.

Driscoll, N. W.; Hogg, J. R.; Christie-Blick, N. and Karner, G. D. (1995) – Extensional tectonics in the Jeanne d'Arc Basin, offshore Newfoundland: implications for the timing of break-up between Grand Banks and Iberia. From Scrutton, R. A.; Stoker, M. S.; Shimmield, G. B. and Tudhope, A. W. (eds), The Tectonics, Sedimentation and Paleoceanography of the North Atlantic Region. Geological Society Special Publication No. 90, pp. 1-28.

Duarte, H. (2009) – High-resolution seismic reflection investigation of gas accumulation and seepage in the tidal channels of the Ria of Aveiro barrier lagoon (Portugal). Doctoral Thesis, University of Aveiro, Aveiro, 166 pp.

Duarte, H.; Pinheiro, L. M. et al. (2007) – High-resolution seismic imaging of gas accumulations and seepage in the sediments of the Ria de Aveiro barrier lagoon (Portugal). Geo-Marine Letters Vol. 27(2-4), 115-126 pp.

Duarte, J. C.; Rosas, F. M.; Terrinha, P.; Schellart, W. P.; Boutelier, D.; Gutscher, M.-A. And Ribeiro, A. (2013) – Are subduction zones invading the Atlantic? Evidence from the southwest Iberia margin. Geology Vol. 41, 839-842 pp.

Estrutura de Missão para a Extensão da Plataforma Continental (EMEPC) (2015) – Scientific Cruise Report EMEPC/PEPC/LUSO/2015.

England, W. A.; MacKensie, A. S.; Mann, D. M. and Quigley, T. M. (1987) – The movement and entrapment of petroleum fluids in the subsurface. Journal of the Geological Society, London. Vol. 144, pp. 327-347.

GEO Marine Survey Systems Technical Manual, accessed January 2015 – Geo-Source 200 Light Weight. Marine Multi-Tip Sparker System. <www.geomarinesurveysystems.com>

Gay, A., Lopez, M., Berndt, C. and Seranne, M. (2007) – Geological controls on focused fluid flow associated with seafloor seeps in the Lower Congo Basin. Marine Geology Vol. 244, 68-92 pp.

Gay, A. ; Lopez, M.; Cochonat, P.; Séranne, M.; Devaché, D. and Sermondadaz, G. (2006) – Isolated seafloor pockmarks linked to BSRs, fluid chimneys, polygonal faults and

stacked Oligocene-Miocene turbiditic paleochannels in the Lower Congo Basin. Marine Geology Vol. 226(1-2), 25-40 pp.

Gay, A.; Lopez, M.; Ondreasc, H.; Charlouc, J.-L.; Sermondadaz, G. and Cochonat, P. (2005) – Seafloor facies related to upward methane flux within a Giant Pockmark of the Lower Congo Basin. Marine Geology Vol. 226(1-2), 81-95 pp.

Giammanco, S.; Parello, F.; Gambardella, B.; Schifano, R.; Pizzullo, S. and Galante, G. (2007) – Focused and diffuse effluxes of CO2 from mud volcanoes and mofettes south of Mt. Etna (Italy).

Gold, T. and Soter, S. (1985) – Fluid Ascent through the Solid Lithosphere and its Relation to Earthquakes. PAGEOPH, Vol. 122, 492-530 pp.

Gutscher, M.-A.; Dominguez, S.; Westbrook, G. K.; Le Roy, P.; Rosas, F.; Duarte, J. C.; Terrinha, P.; Miranda, J. M.; Graindorge, D.; Gailler, A.; Sallares, V. and Bartolome, R. (2012) – The Gilbraltar subduction: A decade of new geophysical data. Tectonophysics Vol. 574-575, 72-91 pp.

Gutscher, M.-A.; Malod, J.; Rehault, J.-P.; Contrucci, I.; Klingelhoefer, F.; Mendes-Victor, L. and Spakman, W. (2002) – Evidence for active subduction beneath Gilbraltar. Geology Vol. 30, No. 12, 1071-1074 pp.

Haq, B. U.; Hardenbol, J. and Vail, P. R. (1987) – Chronology of Fluctuating Sea Levels Since the Triassic. Science Vol. 235, 1156-1167 ppg.

Heller, C.; Blumenberg, M.; Hoppert, M.; Taviani, M. and Reitner, J. (2012) – Terrestrial mud volcanoes of the Salse di Nirano (Italy) as a window into deeply buried organic-rich shales of Plio-Pleistocene age. Sedimentary Geology Vol. 263-264, 202-209 pp.

Hindle, A. D. (1997) – Petroleum Migration Pathways and Charge Concentration: A Three-Dimensional Model. AAPG Bulletin Vol.81, No.9, 1451-1481 pp.

Hovland, M. (2002) – On the self-sealing nature of marine seeps. Continental Shelf Research Vol. 22, 2387-2396 pp.

Hovland, M. (2008) – Deep-water Coral Reefs: Unique Biodiversity Hot-Spots. Springer-Praxis, 254 pp.

Hovland, M.; Gardner, J. V. and Judd, A. G. (2002) – The significance of pockmarks to understanding fluid flow processes and geohazards. Geofluids Vol. 22, 127-136 pp. Blackwell Science Ltd.

Hovland, M.; Heggland, R.; De Vries, M. H. and tjelta, T. I. (2010) – Unit-pockmark and their potential significance for predicting fluid flow. Marine and Petroleum Geology, Volume 27, 1190-1199 pp.

Hovland, M. and Judd, A. (1988) – Seabed Pockmarks and Seepages: Impact on Geology, Biology and the Marine Environment. Graham & Trotman, London. 293 pp.

Hovland, M. (1991) – The effects of shallow gas in the Skagerrak surficial sediments. Marine and Petroleum Geology Vol. 8, 311-316 pp.

Holvand, M.; Løseth, H.; Børkum, P. A. ; Wensaas, L. and Arntsen, B. (1999) – Seismic detection of shallow high pore pressure zones: "Tifal pumping" pressurizes sediments. Offshore, 94-96 pp.

Hustoft, S.; Bünz, S. and Mienert, J. (2010) – Three-dimensional seismic analysis of the morphology and spatial distribution of chimneys beneath the Nyegga pockmark field, offshore mid-Norway. Basin Research 22, 465-480 pp.

Ivanov, M. K.; Limonov, A. F. and van Weering, T. C. E. (1996) – Comparative characteristics of the Black Sea and Mediterranean Ridge mud volcanoes. Marine Geology Vol. 132, 253-271 pp.

Instituto Hidrográfico (2010) – Folha 4 da Carta dos Sedimentos Superficiais da Plataforma Continental Portuguesa. Do Cabo Carvoeiro ao Cabo da Roca. 1:50 000.

Jakubov, A. A.; Ali-Zade, A. A. and Zeinalov, M. M. (1971) – Mud volcanoes of the Azerbaijan SSR: Atlas. Elm-Azerbaijan Acad. Of Sci. Pub. House, Baku.

Jiang, G.; Kennedy, M. J. and Cristie-Blick, N. (2003) – Stable isotopic evidence for methane seeps in Neoproterozoic postglacial cap carbonates. NATURE Vol. 426, 822-826 pp.

Joye, S. B.; Boetius, A.; Orcutt, B. N.; Montoya, J. P.; Schulz, H. N.; Erickson, M. J. and Lugo, S. K. (2004) – The anaerobic oxidation of methane and sulfate reduction in sediments from Gulf of Mexico cold seeps. Chemical Geology Vol. 205, 219-238.

Judd, A. G. (2001) – Pockmarks in the UK Sector of the North Sea. Technical Report TR_002 produced for Strategic Environmental Assessment – SEA2.

Judd, A. G. (2003) – The global importance and context of methane escape from the seabed. Geo-Marine Letters Vol. 23, 147-154.

Judd, A. and Hovland, M. (2007) – Seabed Fluid Flow, the Impact on Geology, Biology, and the Marine Environment. Cambridge University Press. 475 pp.

Kauffman, E.G.; Arthur, M.A.; Howe, B. and Scholle, P.A. (1996) – Widespread venting of methane-rich fluids in Late Cretaceous (Campanian) submarine springs (Tepee Buttes), Western Interior seaway, USA. Geology Vol. 24, 799–802 pp.

Kearey, P.; Brooks, M. and Hill, I. (2002) – An Introduction to Geophysical Exploration (Third Edition). Blackwell Science Ltd.

Kennedy, M. J.; Christie-Blick, N. and Sohl, L. E. (2001) – Are Proterozoic cap carbonates and isotopic excursions a record of gas hydrate destabilization following Earth's coldest intervals? Geology Vol. 29, No. 5, 443–446 pp. Geological Society of America.

Kim, J.-H & the shipboard scientific party (2011) – Report of cruise 64PE332 with RV Pelagia Texel-Lisbon. 09-31 March 2011.Royal Netherlands Institute for Sea Research, Texel.

King, L. H. and MacLean, B. (1970) – Pockmarks on the Scotian Shelf. Geological Society of America Bulletin Vol. 81, 3141-3148 pp.

Klaucke, I.; Sahling, H.; Weinrebe, W.; Blinova, V.; Bürk, D.; Lursmanashvili, N. and Bohrmann, G. (2006) – Acoustic investigation of cold seeps offshore Georgia, eastern Black Sea. Marine Geology Vol. 231, 51-67 pp.

Kongsberg Technical Manual (2003) – EM300: 30 kHz multibeam echo sounder for depths reaching 5000 meters.

Kongsberg Technical Manual (2014) – EM710: Multibeam echo sounder. High resolution seabed mapping system. 4 pp.

Kopf, A. J. (2002) – Significance of Mud Volcanism. Reviews of Geophysics 40, American Geophysical Union. 52 pp.

Kullberg, J. C. R. (2000) – Evolução Tectónica Mesozóica da Bacia Lusitaniana. Dissertação de Doutoramento, Universidade Nova de Lisboa. pp

Kullberg, J. C.; Rocha, R. B.; Soares, A. F.; Rey, J.; Terrinha, P.; Azerêdo, A. C.; Callapez, P.; Duarte, L. V.; Kullberg, M. C.; Martins, L.; Miranda, J. R.; Alves, C.; Mata, J.; Madeira, J.; Mateus, O.; Moreira, M. and Nogueira, C. R. (2013) - A Bacia Lusitaniana: Estratigrafia, Paleogeografia e Tectónica. In: Dias, R.; Araújo, A.; Terrinha, P. and Kullberg, J. C. (editors) (2013b) – Geologia de Portugal. Volume II: Geologia Meso-cenozóica de Portugal. Escolar Editora, Lisboa. 798 pp.

Kullberg, J. C.; Rocha, R. B.; Soares, A. F.; Terrinha, P.; Callapez, P. and Martins, L. (2006) – A Bacia Lusitaniana: Estratigrafia, Paleogeografia e Tectónica. In Geologia de Portugal no contexto da Ibéria (R. Dias, A. Araújo, P. Terrinha & J. C. Kullberg, Eds.). Univ. Évora, 317-368 pp.

León, R.; Somoza, L.; Medialdea, T.; Hernández-Molina, F. J.; Vázquez, J. T.; Díaz-del-Rio, V. and González, F. J. (2010) – Pockmarks, collapses and blind valleys in the Gulf of Cádiz. Geo-Marine Letters Vol. 30 (3–4), 231–247 pp.

Léon, R.; Somoza, L.; Medialdea, T.; Maestro, A.; Díaz-del-Río, V.; Fernández-Puga, M. d.-C. (2006) – Classification of sea-floor features associated with methane seeps along the Gulf of Cádiz continental margin. Deep-Sea Research II 53, 1464-1481.

Ligtenberg, H. (2005) – Detection of fluid migration pathways in seismic data: implications for fault seal analysis. Basin Research Vol. 17, 141-153 pp. Blackwell Publishing Ltd.

Locarnini, R. A.;. Mishonov, A. V.; Antonov, J. I. ; Boyer, T. P.; Garcia, H. E.; Baranova, O. K.; Zweng, M. M.; Paver, C. R.; Reagan, J. R.; Johnson, D. R.; Hamilton, M. and Seidov, D. (2013) – World Ocean Atlas 2013, Volume 1: Temperature. S. Levitus, Ed., A. Mishonov Technical Ed.; NOAA Atlas NESDIS 73, 40 pp.

Lollar, B. S.; Westgate, T. D.; Ward, J. A.; Slater, G. F. and Lacrampe-Couloume, G. (2002) – Abiogenic formation of alkanes in the Earth's crust as a minor source for global hydrocarbon reservoirs. Nature Vol. 416, 522-524 pp.

Lobo, F. J.; Durán, R.; Roque, C.; Ribó, M.; Carrara, G.; Mendes, I.; Ferrín, A.; Fernández-Salas, L. M.; García-Gil, S.; Galparsoro, I.; Rosa, F. and Bárcenas, P. (2015) – Shelves around the Iberian Peninsula (II): Evolutionary sedimentary patterns. In Geological processes in the Iberian continental margin: new developments and trends (Maestro, A.; Ercilla, G. and Hernández-Molina, F. J. Eds.), Edition 126 (2-3). Boletín Geológico y Minero, 377-408 pp.

Magalhães, V. H. da S. (2007) – Authigenic carbonates and fluid escape structures in the Gulf of Cadiz. Doctoral Thesis, University of Aveiro, Aveiro, 421 pp.

Magalhães, V. H.; Pinheiro, L. M.; Ivanov, M. K.; Kozlova, E.; Blinova, V.; Kolganova, J.; Vasconcelos, C.; McKenzie, J. A.; Bernasconi, S. M.; Kopf, A. J.; Díaz-del-Río, V.; González, F. J. and Somoza, L. (2012) – Formation processes of methane-derived authigenic carbonates from the Gulf of Cadiz. Sedimentary Geology Vol. 243-244, 155-168 pp.

Martínez-Carreño, N. and García-Gil, S. (2013) – The Holocene gas system of the Ría de Vigo (NW Spain): Factors controlling the location of gas accumulations, seeps and pockmarks. Marine Geology Vol. 344, 82-100 pp.

Mata, J.; Alves, C.F.; Martins, L.; Miranda, R.; Madeira, J.; Pimentel, N.; Martins, S.; Azevedo, M.R.; Youbi, N.; De Min, A.; Almeida, I.M.; Bensalah, M.K. and Terrinha, P. (2015) – $^{40}Ar/^{39}Ar$ ages and petrogenesis of the West Iberian Margin onshore magmatism at the Jurassic-Cretaceous transition: Geodynamic implications and assessment of open-system processes involving saline materials. Lithos Vol. 236-237, 156-172 pp.

Mazzini, A. (2009) – Mud Volcanism: Processes and Implications (Editorial). Marine and Petroleum Geology Vol. 26, 1677-1680 pp.

Mazzini, A.; Svensen, H.; Planke, S.; Guliyev, I.; Akhmanov, G. G.; Fallik, T. and Banks, D. (2009) – When mud volcanoes sleep: Insight from seep geochemistry at the Dashgil mud volcano, Azerbaijan. Marine and Petroleum Geology Vol. 26, 1704-1715 pp.

McGinnis, D. F.; Schmidt, M.; DelSontro, T.; Themann, S.; Rovelli, L.; Reitz, A. and Linke, P. (2011) – Discovery of a naturalCO2 seep in the German North Sea: Implications for shallow dissolved gas and seep detection. Journal of Geophysical Research, Vol. 116.

Medialdea, T.; Somoza, L.; Pinheiro, L. M.; Fernández-Puga, M. C.; Vásquez, J. T.; Léon, R.; Ivanov, M. K.; Magalhães, V.; Díaz-del-Río, V. and Vegas, R. (2009) – Tectonics and mud volcano development in the Gulf of Cádiz. Marine Geology Vol. 261, 48-63 pp.

Milkov, A. V. (2000) – Worldwide distribution of submarine mud volcanoes and associated gas hydrates. Marine Geology 167, 29-42 pp.

Miranda, R.; Valadares, V.; Terrinha, P.; Mata, J.; Azevedo, M. R.; Gaspar, M.; Kullberg, J. C. and Ribeiro, C. (2009) – Age constraints on the Late Cretaceous alkaline magmatism on the West Iberian Margin. Cretaceous Research 30, 575–586 pp.

Mitchum, R. M. Jr.; Vail, P. R.; Thompson III, S. (1977a) – Seismic stratigraphy and global changes of sea level, part 1: Overview. In: Seismic Stratigraphy-Applications to Hydrocarbon Exploration. Payton, C. E. (Ed.). Am. Ass. Petrol. Geol., Mem. 26, p. 51-52.

Mitchum, R. M. Jr.; Vail, P. R.; Thompson III, S. (1977b) – Seismic stratigraphy and global changes of sea level, part 2: The depositional sequence as a basic unit for stratigraphic analysis. In: Seismic Stratigraphy-Applications to Hydrocarbon Exploration. Payton, C. E. (Ed.). Am. Ass. Petrol. Geol., Mem. 26, p. 53-62.

Mitchum, R. M. Jr.; Vail, P. R.; Sangree, J. B. (1977c) – Seismic stratigraphy and global changes of sea level, part 6: Stratigraphic interpretation of seismic reflection patterns in depositional sequences. In: Seismic Stratigraphy-Applications to Hydrocarbon Exploration. Payton, C. E. (Ed.). Am. Ass. Petrol. Geol., Mem. 26, p. 117-133.

Moore, C. H. and Wade, W. J. (2013) – Carbonate Reservoirs Porosity and Diagenesis in a Sequence Stratigraphic Framework. In: Loon, A. J. v. (Ed.), Developments in sedimentology. Second Edition. Elsevier. 374 pp.

Mougenot, D. (1989) – Geologia da Margem Portuguesa. Documento Técnico Nº32, Instituto Hidrográfico, 259p.

Mougenot, D. (1976) – Géologie du plateau continental portugaise (entre le cap Carvoeiro et le cap de Sines). Fascicule 1 et 2. Thèse 3ème cycle. Univ. Rennes, 76p. (not published)

Musselec, P. (1974) – Géologie du plateau continental portugaise au Nord du Cap Carvoeiro. Thèse 3ème cycle. Univ. Rennes, 170p. (not published)

Natural Methane Seepage is Widespread on the U.S. Atlantic Ocean Margin, USGS, accessed March 2015 <http://soundwaves.usgs.gov/2014/10/>

Naudts, L.; Greinert, J.; Artemov, Y.; Beaubien, S. E.; Borowski, C. and De Batist, M. (2008) – Anomalous sea-floor backscatter patterns in methane venting areas, Dnepr paleo-delta, NW Black Sea. Marine Geology Vol. 251, 253–267 pp.

Neres, M.; Bouchez, J. L.; Terrinha, P. ; Font, E.; Moreira, M. ; Miranda, R.; Launeau, P. and Carvallo, C. (2014) – Magnetic fabric in a Cretaceous sill (Foz da Fonte, Portugal): flow model and implications for regional magmatism. Geophysics Journal International Vol. 199, 78-101 pp.

Niemann, H.; Duarte, J.; Hensen, C.; Omoregie, E.; Magalhães, V. H.; Elvert, M. ; Pinheiro, L. M.; Kopf, A. And Boetius, A. (2006) – Microbial methane turnover at mud volcanoes of the Gulf of Cadiz. Geochimica et Cosmochimica Acta 70, 5336–5355 pp.

Orange, D. L.; Yuna, J.; Maherb, N.; Barry, J. and Greene, G. (2002) – Tracking California seafloor seeps with bathymetry, backscatter and ROVs. Continental Shelf Research Vol. 22, 2273–2290 pp.

Ostanin, I.; Anka, Z.; di Primio, R and Bernal, A. (2012) – Identification of a large Upper Cretaceous polygonal fault network in the Hammerfest basin: Implications on the reactivation of regional faulting and gas leakage dynamics, SW Barents Sea. Marine Geology Vol. 332-334, 109-125 pp.

Pais. J. (2002) – The Neogene of the Lower Tagus Basin (Portugal). Revista Española de Paleontología, Vol. 19 (2), 229-242 pp.

Pais, J.; Cunha, P. P.; Pereira, D.; Legoinha, P.; Dias, R.; Moura, D.; Brum da Silveira, A.; Kullberg, J. C. and González-Delgado, J. A. (2012) – The Paleogene and Neogene of Western Iberia (Portugal). A Cenozoic Record in the European Atlantic Domain. Springer. 158 pp.

Palomino, D.; López-González, N.; Vázquez, J. T.; Fernández-Salas, L. M.; Rueda, J. L.; Sánchez-Leal, R. and Días-del-Río, V. (2015) – Multidisciplinary study of Mud Volcanoes and Diapirs and their relationship to seepages and bottom currents in the Gulf of Cádiz continental slope (Northeastern sector).

Parallel Geoscience Corporation (2014) – SPW3 Manual Rev. 7: Seismic Processing WorkshopTM Manual V 3.2 October 2014. Parallel Geoscience Corporation, PO Box 5989. Incline Village, NV 89450. *http://www.parallelgeo.com*

Pena dos Reis, R. B. and Mayer, R. (1982) – Sédimentation continental du Crétacé terminal au Miocéne dans the Bassin de Coimbra-Leiria (Portugal). Actions tectoniques et climatiques (silicification). Comptes Rendus de l'Académie des Sciences Vol. 294, 741-744 pp.

Pena dos Reis, R. and Pimentel, N. (2010) – A evolução da Bacia Lusitânica (Portugal) and its associated petroleum systems. VIII Congresso Nacional de Geologia, GEOTIC – Sociedade Geológica de Portugal. Revista Electrónica de Ciências da Terra. Vol. 19, No 4, 4 pp.

Pena dos Reis, R. and Pimentel, N. (2014) – Analysis of the Petroleum Systems of the Lusitanian Basin (Western Iberian Margin) – A Tool forDeep Offshore Exploration. Bob Perkins Conference, "Sedimentary Basins: Origin, Depositional Histories and Petroleum Systems". GCSSEPM, Houston, Texas.

Pinheiro, L. M.; Ivanov, M. K.; Sautkin, A.; Akhmanov, G.; Magalhães, V. H.; Volkonskaya, A.; Monteiro, J. H.; Somoza, L.; Gardner, J.; Hamouni, N. and Cunha, M. R. (2003) – Mud volcanism in the Gulf of Cadiz: results from the TTR-10 cruise. Marine Geology 195, 131-151 pp.

Pinheiro, L. M.; Wilson, R. C. L.; Pena dos Reis, R.; Whitmarsh, R. B. and Ribeiro, A. (1996) – The Western Iberia Margin: A Geophysical and Geological overview. In Whitmarsh, R. B.; Sawyer, D. S.; Klaus, A. and Masson, D. G. (Eds.) Proceedings of the Ocean Drilling Program, Scientific Results, Vol. 149.

Potter, J.; Rankin, A. H. and Treloar, P. J. (2004) – Abiogenic Fischer–Tropsch synthesis of hydrocarbons in alkaline igneous rocks; fluid inclusion, textural and isotopic evidence from the Lovozero complex, N.W. Russia. Lithos Vol. 75, 311-330 pp.

Potter, J.; Salvi, S. and Longstaffe, F. J. (2013) – Abiogenic hydrocarbon isotopic signatures in granitic rocks: Identifying pathways of formation. Lithos Vol. 182-183, 114-124 pp.

Rainone, M. L.; Rusi, S. and Torrese, P. (2015) – Mud volcanoes in central Italy: Subsoil characterization through a multidisciplinary approach. Geomorphology Vol. 234, 228-242 pp.

Rasmussen, Erik S.; Lomholt, Steen; Andersen, Claus & Vejbæ k, Ole V. (1998) – Aspects of the structural evolution of the Lusitanian Basin in Portugal and the shelf and slope area offshore Portugal. Tectonophysics Vol. 300, 199-225 pp.

Rey, J. (1979) – Le crétacé inférieur de la marge atlantique portugaise : biostratigraphie, organisation séquentielle, évolution paléogéographique. Ciências da Terra Vol. 5, 97-120 pp. Lisboa.

Ribeiro, A. (2013a) – Evolução geodinâmica de Portugal; os ciclos ante-mesozóicos. In: Dias, R.; Araújo, A.; Terrinha, P. and Kullberg, J. C. (editors) (2013a) – Geologia de Portugal. Volume I: Geologia Pré-mesozóica de Portugal. Escolar Editora, Lisboa. 807 pp.

Ribeiro, A. (2013b) – Evolução geodinâmica de Portugal; os ciclos Meso-Cenozóicos. In: Dias, R.; Araújo, A.; Terrinha, P. and Kullberg, J. C. (editors) (2013b) – Geologia de Portugal. Volume II: Geologia Meso-cenozóica de Portugal. Escolar Editora, Lisboa. 798 pp.

Ribeiro, A.; Cabral, J.; Baptista, R. and Matias, L. (1996) – Stress pattern in Portugal mainland and the adjacent Atlantic region, West Iberia. Tectonics Vol. 15, No. 2, 641-659 pp.

Roberts, H. H. and Aharon, P. (1994) – Hydrocarbon-derived carbonate buildups of the northern Gulf of Mexico continental slope: A review of submersible investigations. Geo-Marine Letters 14, 135-148.

Roberts, S. J. and Nunn, J. A. (1995) – Episodic fluid expulsion from geopressured sediments. Marine and Petroleum Geology 12, 195-204. Elsevier Science Limited.

Rodrigues, A.; Dias, J. A. and Ribeiro, A. (2000) – The North Portuguese shelf during the last Glacial Maximum and Younger Dryas. 3rd Symposium on the Iberian Atlantic Margin, Faro. 209-210 pp.

Rønhovde, A. (1999) – High Resolution Beamforming of SIMRAD EM3000 Bathymetric Multibeam Sonar Data. Cand Scient thesis, Department of Informatics, University Of Oslo.

Roque, C. (2007) – Tectonostratigrafia do Cenozóico das margens continentais sul e sudoeste portuguesas: um modelo de correlação sismostratigráfica. PhD thesis, Universidade de Lisboa, Lisbon, 348 pp.

Shell Prospex Portuguesa, S.A. (1976a) – 17 C-1 Well Completion Report. (Not published)

Shell Prospex Portuguesa, S.A. (1976b) – 20 B-1 Well Completion Report. (Not published)

Sheriff, Robert E. & Geldart, Lloyd P. (1995) – Exploration Seismology (Second Edition). Cambridge University Press, Cambridge, United Kingdom, 592 pp.

Sibuet, J.-C.; Srivastava, S. and Manatschal, G. (2007) – Exhumed mantle-forming transitional crust in the Newfoundland-Iberia rift and associated magnetic anomalies. Journal of Geophysical Research Vol. 112, 23 pp.

Sloan, E. D. and Koh, C. A. (2007) – Clathrate Hydrates of Natural Gases. Third Edition. Chemical Industries Series. CRC Press, Taylor & Francis Group, New York. 721 pp.

Soares, D. M.; Alves, T. M. and Terrinha, P. (2012) – The breakup sequence and associated lithospheric breakup surface: Their significance in the context of rifted continental margins (West Iberia and Newfoundland margins, North Atlantic). Earth and Planetary Science Letters Vol. 355-356, 311-326 pp.

Somoza, L.; Díaz-del-Río, V.; León, R.; Ivanov, M.; Fernández-Puga, M. C.; Gardner, J. M.; Hernández-Molina, F. J.; Pinheiro, L. M.; Rodero, J.; Lobato, A.; Maestro, A.; Vázquez, J. T.; Medialdea, T. and Fernández-Salas, L. M. (2003) – Seabed morphology and hydrocarbon seepage in the Gulf of Cádiz mud volcano area: Acoustic imagery, multibeam and ultra-high resolution seismic data. Marine Geology 195, 153-176 pp.

Stadnitskaia, A.; Ivanov, M. K.; Poludetkina, E. N.; Kreulen, R. and van Weering, T. C. E. (2008) – Sources of hydrocarbon gases in mud volcanoes from the Sorokin Trough, NE Black Sea, based on molecular and carbon isotopic compositions. Marine and Petroleum Geology Vol. 25, Issue 10, 1040-1057 pp.

Stoker, M. S.; Pheasant, J. B. and Josenhans, H. (1997) – Seismic Methods and Interpretation. In: Davies, T. A.; Bell, T.; Cooper, A. K.; Josenhans, H.; Polyak, L.; Solheim, A.; Stoker, M. S. and Stravers, J. A. (eds.) Glaciated Continental Margins: An Atlas of Acoustic Images. Springer Netherlands.

Tabela de Mares do Instituto Hidrográfico, acessed January 2015 < www.hidrografico.pt/previsao-mares.php>

Talukder, A. R. (2012) – Review of submarine cold seep plumbing systems: leakage to seepage and venting. Terra Nova Vol 24, No. 4, 255-272 pp.

Tassi, F.; Fiebig, J.; Vaselii, O. and Nocentini, M. (2012) – Origins of methane discharging from volcanic-hydrothermal, geothermal and cold emissions in Italy. Chemical Geology Vol. 310-311, 36-48 pp.

Telford, W. M.; Gekdart, L. P. & Sheriff, R. E. (1990) – Applied Geophysics (Second Edition). Cambrigde University Press.

Terrinha, P.; Matias, L.; Vicente, J.; Duarte, J.; Luís, J.; Pinheiro, L.; Lourenço, N.; Diez, S.; Rosas, F.; Magalhães, V.; Valadares, V.; Zitellini, N.; Roque, C.; Mendes Víctor, L. and the MATESPRO Team (2009) – Morphotectonics and strain partitioning at the Iberia–Africa plate boundary from multibeam and seismic reflection data. Marine Geology Vol. 267, 156-174 pp.

Terrinha, P.; Ribeiro, C.; Kullberg, J. C.; Lopes, C.; Rocha, R. and Ribeiro, A. (2002) – Compressive Episodes and Faunal Isolation during Rifting, Southwest Iberia. The Journal of Geology Vo. 110, 101-113 pp.

Vanneste, M.; Guidard, S. and Mienert, J. (2005) – Bottom-simulating reflections and geothermal gradients across the western Svalbard margin. Terra Nova Vol. 17, No. 6, 510-516 pp.

Vanney, J.-R- and Mougenot, D. (1981) – La Plate-forme Continentale du Portugal et les Provinces adjacentes: Analyse Geomorphologique. Memórias dos Serviços Geológicos de Portugal, número 28. Direcção Geral de Geologia e Minas, Lisboa. 145p.

Vanney, J.-R and Mougenot, D. (1990) – Un canyon sous-marin du type «gouf » : le Canhão da Nazaré (Portugal). Oceanologia Acta 1990. Vol. 13, Nº 1.

Wilson, R. C. L. (1988) – Mesozoic Development of the Lusitanian Basin, Portugal. Rev. Soc. Geol. España, 1, 3-4, 393-407.

Xing, J. and Spiess, V. (2015) – Shallow gas transport and reservoirs in the vicinity of deeply rooted mud volcanoes in the central Black Sea. Marine Geology Vol. 369, 67-78 pp.

Ylmaz, Öz (2001) – Seismic Data Analysis: Processing, Inversion and Interpretation of Seismic Data. Volume 1. Investigations in Geophysics No. 10. Society of Exploration Geophysicists. Tulsa, Oklahoma, USA. 2027 pp.

Ylmaz, Öz (2001) – Seismic Data Analysis: Processing, Inversion and Interpretation of Seismic Data. Volume 2. Investigations in Geophysics No. 10. Society of Exploration Geophysicists. Tulsa, Oklahoma, USA. 2027 pp.

Zitellini, N.; Gràcia, E.; Matias, L.; Terrinha, P.; Abreu , M.A.; DeAlteriis, G.; Henriet, J.P.; Dañobeitia, J.J.; Masson, D.G.; Mulder, T.; Ramella, R.; Somoza, L. and Diez, S. (2009) – The quest for the Africa-Eurasia plate boundary west of the Strait of Gilbraltar. Earth and Planeraty Science Letters Vol. 280 (1-4), 13-50 pp.